WIM-Based Live Load Model for Bridges

by

Olga Iatsko

A dissertation submitted to the Graduate Faculty of
Auburn University
in partial fulfillment of the
requirements for the Degree of
Doctor of Philosophy

Auburn, Alabama
May 5, 2018

Keywords: bridge live load, weigh-in-motion, permit load, load effect, design point, reliability index

Approved by

Andrzej S. Nowak, Chair, Elton and Lois G. Huff Professor of Civil Engineering
J. Michael Stallings, Co-Chair, Professor of Civil Engineering
Rod E. Turochy, James M. Hunnicutt Professor of Traffic Engineering
J. Brian Anderson, Associate Professor of Geotechnical Engineering
Roy Hartfield, Professor of Aerospace Engineering

Abstract

The knowledge of the actual live load is essential for a rational management of highway structures. Overloaded vehicles can cause damage including concrete cracking, potholes, excessive vibration and deflection, and even a catastrophic collapse. The design live load HL-93 in AASHTO LRFD Code was developed in the 1990's based on the truck survey from Ontario (Canada) as the US data was not available. In the meantime, an extensive weigh-in-motion (WIM) database has been collected and provided a rational basis for verification of the live load model. The analyzed WIM database includes over 200 million records, about 1-2 million per year for each location. The economic life of a bridge in the AASHTO code is 75 years. Therefore, the maximum 75-years live load effects, i.e., moments and shear forces are determined using extrapolation and Monte Carlo simulation. A design live load representative for the whole country is proposed.

Prediction of live load involves consideration of three groups of vehicles: legal, permit and illegally overloaded vehicles. Therefore, it is essential to identify these three groups in the WIM data. Vehicles that require permits in the WIM database are sorted out using the parameters of issued permits to identify which vehicles have permits. The remaining vehicles can be considered as illegal traffic. The procedure of separation of permit traffic and illegally overloaded vehicles is tested and demonstrated on the example of recorded WIM data and issued-permit data in Alabama.

There has been considerable progress in the reliability-based code development procedures. The load and resistance factors in the AASHTO bridge design code were determined using the statistical parameters from the 1970's and early 1980's. Therefore, the original calibration was revisited and the load and resistance factors as coordinates of the so-called "design point" were calculated. The analysis is performed for the same types of girder bridges, i.e., reinforced concrete T-beams, prestressed concrete girders and steel girders as in the original calibration presented in NCHRP Report 368. The recommended new load and resistance factors provide consistent reliability and a reasonable safety margin.

Acknowledgements

I dedicate my dissertation to my family, my husband Pavel and daughter Sofia, who kept me motivated to accomplish this study. I also dedicate it to my grandfather Oleksiy Sulima, who supported my life changing decision to achieve a Doctoral degree in Auburn University.

The completion of this research could not have been possible without assistance and guidance from my mentor, Dr. Andrzej S. Nowak. The knowledge and expertise he generously shared led me through this program, and I have learned a lot from him. I would also like to thank Dr. J. Michael Stallings for his wise advice and encouragement during my work on this dissertation. Thanks are also due to my committee members, Dr. Rod Turochy and Dr. Brian J. Anderson, for their comments and review of my dissertation.

I would also like to offer my thanks to my colleagues at Auburn University. Firstly to Anjan Babu for cooperation during work on permit identification and secondly to Patryk Wolert and Marek Kolodziejczyk, for their help in the development of the reliability analysis procedure.

The presented research is co-sponsored by the Alabama Department of Transportation, which is gratefully acknowledged. The authors thank the ALDOT technical staff for their advice, discussion, and constructive comments. Special thanks are due to Randy Braden and Kevin Perdue for providing access to the WIM and permit databases.

I also gained from experience related to involvement in SHRP2 R19B and NCHRP 12-83. In particular, I benefited from the discussions with John M. Kulicki, Hani Nassif and Wagdy Wassef.

Table of Contents

List of Tables

List of Illustrations

List of Abbreviations

WIM – Weigh-in-Motion

GVW – Gross vehicle weight

PDF – Probability density function

CDF – Cumulative density function

CLT – Central limit theorem

ULS – Ultimate limit state

SLS – Serviceability limit state

FLS – Fatigue limit state

GDF – Girder distribution factor

LLDF – Live load distribution factor

DLF – Dynamic load factor

Introduction

1.1. Problem Statement

Transportation structures such as roads and bridges are exposed to moving traffic loads. Excessive static and dynamic live load effects can cause damage or even collapse of structural components or whole structures. According to the Federal Highway Administration (Federal Highway Administration 2015), from 11% (Minnesota) to 52% (Massachusetts) of all bridges in the United States are structurally deficient or functionally obsolete. In particular, 3,608 of the 16,078 (22.4%) in Alabama are in an unsatisfactory condition. At the same time, over 188 million trips are occuring daily in the US through structurally deficient bridges (*ASCE's 2017 Infrastructure Report Card* n.d.).

The oversized and overloaded vehicle's load is often called the most severe factor of damage to the roads and bridges. The overloaded vehicles are usually transporting the abnormal (e.g., cranes, agricultural or military machinery) or illegal cargo. The threatening effect caused by these trucks can be quite considerable, especially for aged bridges that are often in poor condition and located in rural areas.

To prevent failures, it is important to provide an adequate safety margin in the design, i.e., load effects are overestimated, and load carrying capacity (resistance) is underestimated. In the new generation of design codes, safety reserve is provided with load and resistance factors that are determined in the reliability-based calibration process (Nowak and Collins 2012). The

acceptance criterion is closeness to the target reliability index. The code calibration requires the knowledge of statistical parameters of load and resistance; in particular, this applies to live load. The basis for the current AASHTO LRFD Code (AASHTO 2014) was developed in the 1980's (Agarwal and Wolkowicz 1976), (Nowak 1999). There is an enormous weigh-in-motion (WIM) database collected by state DOT's for various locations, practically covering the whole nation. However, it is often underutilized by bridge engineers and not employed in current AASHTO LRFD Bridge Design Specifications. There is a need to develop the national live load model to reflect changes in current traffic loads and derive the optimum load and resistance factors AASHTO LRFD Bridge Design Specifications. It is also necessary to provide recommendations for the more accurate estimation of the traffic load for bridge evaluation, design, fatigue analysis, and more efficient law enforcement.

1.2. Objectives of the Research

The primary objective of this dissertation is to process and validate the available WIM data collected from 45 WIM sites in 20 states around the US (SHRP 2 Research Reports 2015), (Ghosn et al. 2011), develop statistical parameters for live load effects in bridges and verify if the current code-specified live load HL-93 is representative of the actual traffic. The load and resistance factors, that reflect the recent changes in load and resistance parameters have to be developed using reliability-based procedure. Another objective of this study is to develop a procedure to determine the portion of illegal or unauthorized traffic load.

The research involved the following tasks:

1. Review of the WIM databases available from FHWA WIM data, NCHRP Report 683 (Ghosn et al. 2011) and Alabama DOT.

2. Process the available WIM data to obtain the statistical parameters. The statistical parameters were also determined for various WIM stations and groups of trucks.
3. Develop the statistical parameters for live load effects, i.e., moment and shear for Strength I Limit State in AASHTO (2014).
4. Re-visit the design tandem (HL-93 Loading) to adequately reflect the recent changes in truck configuration.
5. Analyze the available database of the permits issued for Alabama and develop the procedure to separate illegal traffic from legal and permitted vehicles.
6. Determine the load and resistance factors corresponding to the "design point."

This study is focused on load effects for simply supported bridges with the span length from 30 to 200ft as it covers the majority of US bridges. Proposed load and resistance factors are developed using the reliability-based calibration procedure (Nowak 1999),(Nowak and Iatsko 2017), available WIM live load data and resistance statistics from 368 NCHRP Report (Nowak 1999), (Nowak and Szerszen 2003), and (Szerszen and Nowak 2003).

1.3. Prior Investigations

Weigh-in-motion data is an important source of information about the actual traffic load in a particular region or state, including frequency and configuration of vehicles. A number of researchers applied the traffic records, collected using the WIM systems, for efficient bridge design (Nowak 1999), (Nowak and Iatsko 2017), evaluation (Nowak and Tharmabala 1988), (Nowak A. S. and Hong Y.K., 1991), (Sivakumar 2007), (Sivakumar et al. 2011) and fatigue analysis (Fisher et al. 1983), (Laman and Nowak 1996), (SHRP 2 Research Reports 2015).

The original calibration of AASHTO LRFD Bridge Design Specifications was carried out as part of the NCHRP 12-33. The calibration procedure and results are documented 368 NCHRP Report (Nowak 1999). The live load model was based on the traffic survey from Ontario (Canada) that consisted of 9,250 selected trucks since U.S. data was not available (Agarwal and Wolkowicz 1976). In the meantime, an extensive weigh-in-motion (WIM) database has been collected by State DOTs, FHWA and as part of other NCHRP studies. New data is based on weigh-in-motion (WIM) measurements collected by FHWA and state DOTs, and it is documented by Allen et al. (2005), Ghosn et al. (2010), Kwon et al. (2010), Ghosn et al. (2011), Nowak et al., (2012), Nowak et al. (2012), SHRP 2 Research Reports (2015), Nowak and Iatsko (2017).

The first application of the reliability-based calibration procedure for bridge design was presented by Nowak and Lind (1979). This concept was then applied for the development of load and resistant factors for an original calibration of AASHTO LRFD Bridge Design Specifications (Nowak 1999). Statistical parameters of live load were obtained using extrapolation method based on the extreme value theory introduced by Castillo (1988) and Coles (2001).

California and Missouri DOTs conducted state-specific studies to verify the current load factors in AASHTO LRFD for Strength and Fatigue limit state based on locally collected WIM data and bridge types. Caltrans' project is entitled "California Permit and Fatigue Truck Load Development and Calibration" n.d.) (in progress). Missouri University of Science and Technology used the state-specific WIM data to verify the validity of the live load factor for Strength I Limit State.

Use of WIM data for evaluation of existing bridges was considered by Nowak and Hong (1991), Moses (2001), Sivakumar (2007), and it served as a basis for load factors in AASHTO Guide

Manual for Condition Evaluation and Load and Resistance Factor Rating (AASHTO LRFR 2011). The changes in the truck traffic volume, weight, and configuration during recent decades were reviewed by Ghosn et al. (2011) and Treacy and Brühwiler (2012). A set of protocols and techniques for collection and analysis of the WIM data along with the methods for calibration of the live load factors for LRFD design are presented in the report (Ghosn et al. 2011). WIM records collected from 26 sites in 2005-2006 in California, Texas, Florida, Indiana, and Mississippi were considered in this research.

The problem of unrestricted operation of the short trucks with GVW below 80kips was considered by (Sivakumar 2007) using much larger WIM database collected from 18 states during 2001-2003. The consequences of permit violators to the infrastructure were estimated by (Luskin and Walton 2001) with different scenarios of changing the permit regulations.

The benefits of using WIM data for permit and illegal traffic separation are shown by Caprani et al. (2008). In Wisconsin, individual vehicle records were used to evaluate the state-specific standard permit vehicles based on statistical analysis of the load effects caused by the heaviest 5% of trucks in each class (Zhao and Tabatabai 2012). Similarly, both European and US WIM databases were analyzed to identify permit vehicles based on the state regulations and to produce equivalent permit truck traffic using Monte-Carlo simulation (Enright et al. 2016). Fiorillo and Ghosn (2014) proposed a sorting procedure to define the proportions of illegally overloaded and permitted traffic based on WIM data collected by New York DOT. However, there is still no exact method developed to distinguish permit and illegal vehicles in the collected WIM dataset (Enright et al. 2016).

1.4. Organization of Dissertation

The Dissertation is organized in 7 Chapters and Appendix A and B.

0 presents the introduction, problem statement, objective and scope of the research of the dissertation and the literature review in the subject area.

0 introduces the basic concepts of statistics and reliability theory employed in this study. The concepts of a random variable, distribution function, limit state function, and reliability index are defined, and different types of distribution functions are presented. These functions can possibly be used for the development of structural reliability models.

0 presents an overview of the currently available weigh-in-motion (WIM) technologies, as well as the practice of WIM data collection, analysis, and implementation. WIM databases utilized in this study are also introduced and summarized herein. The results of data mining are presented as probability plots and analyzed.

0 discusses various methods to predict the maximum expected live load effect for a specified period. The statistical live load parameters for Strength I Limit State were determined by using linear extrapolation (Nowak and Hong 1991) and Monte Carlo simulation. The HL-93 design tandem from the current AASHTO LRFD was evaluated, and the new live load combination for short spans was developed based on recent WIM data and proposed.

0 considers the live load from different groups of vehicles: legal, permit and illegally overloaded vehicles. The algorithm of identification of illegally overloaded vehicles in the WIM database is presented. The illegal traffic loads, as well as load effects, are presented and discussed. The procedure is demonstrated on the example of WIM and issued-permit data in Alabama.

0 describes the concept of the reliability-based procedure used for development of the current AASHTO LRFD Bridge Design Specification. The contemporary methods of structural reliability and updated statistical models of load and resistance are also introduced herein. The re-calibrated load and resistance factors for Strength I limit state are presented for different spans and types of girder bridges: i.e., reinforced concrete T-beams, prestressed concrete girders, and steel girders. The effect of changing the HL-93 tandem load case is analyzed and discussed.

0 contains the conclusions of the current study and discussions of future research in the area.

Reliability Analysis Procedures

2.1. Summary

Contemporary design codes are often developed using principles of structural reliability. It became necessary due to multiple sources of uncertainty that are inevitably involved in the structural design. Unlike the traditional approach that considers all parameters of load and resistance as deterministic quantities, reliability-based design criteria take into account the variability associated with geometry, fabrication errors, natural unpredictability, human factor, material properties, etc. Thus, zero probability of failure cannot be practically achieved, but can be reduced to an optimum safety level. The detailed statistical models for load and resistance parameters are utilized to assess the reliability of structural performance.

2.2. Probability Paper

Most parameters of load and resistance can be treated as random variables. The cumulative distribution function (CDF) can be developed for both discrete and continuous random variables for better representation. For a discrete random variable *X*, *F(x)* is the probability that *X* is lower or equal to *x* (the lower limit of *x* - $\boldsymbol{F_X(x) = P(X \leq x)}$ Equation 0-1). As an example, the GVW (kips) measured at WIM site (Ex.: ALDOT-911 in 2014) is treated as a discrete random variable *X* and the cumulative distribution function (CDF) is developed in Table 0-1, and resultant CDF is plotted in Figure 0-1a.

$$\boldsymbol{F_X(x) = P(X \leq x)} \qquad \textbf{Equation 0-1}$$

Large number of measurements with a high precision (Ex.: GVW, kips - WIM site ALDOT-911 in 2014) can be also treated as a continuous type of random variables (Stern et al. 2000), (Nowak and Collins 2012). Although, such a data set is technically discrete, the random variable X can take on any value within an interval from the minimum to maximum measured weight. Visually, discrete variables can be plotted as points on a chart, and continuous random variable can be represented as a linear function as it is shown in Figure 0-1.

Table 0-1. Outcome of Measuring GVW for Cumulative Distribution Function

Event #	Criteria	Number of occurrences	Cumulative number of occurrence	Probability	Cumulative probability
1	0-20	0	0	0	0.000
2	20-40	132,645	132,645	0.4599	0.4599
3	40-60	65,704	198,349	0.2278	0.6878
4	60-80	64,579	262,928	0.2239	0.9117
5	80-100	24,690	287,618	0.0856	0.9973
6	100-120	609	288,227	0.0021	0.9994
7	120-140	109	288,336	0.0004	0.9998
8	140-160	55	288,391	0.0002	1.0000

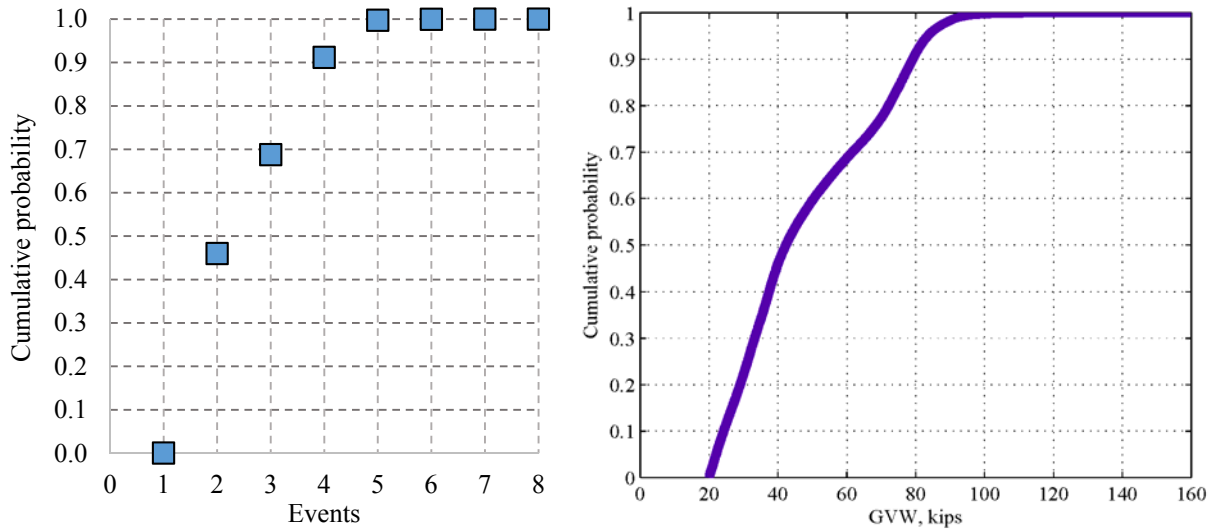

Figure 0-1. Cumulative Distribution Function (CDF) for GVW as a Discrete (a) and Continuous (b) Random Variable

Some research requires presenting data in more user-friendly format. Once the upper or lower tail of CDF requires more precise consideration, the statistical data can be presented in the normal probability paper. The construction and use of the normal probability paper are described in textbooks e.g., Benjamin (1970), Nowak and Collins (2012).

Normal probability paper is a special scale for the presentation of the cumulative distribution function. It is built up based on the standard normal non-decreasing CDF (S-shape function). The CDF of GVW collected in WIM site ALDOT-911 in 2014 is plotted on the normal probability paper as it is shown in Figure 0-2Figure 0-1. However, for each value of GVW, the corresponding value on the vertical left-hand side axis represents the probability that this value of GVW will not be exceeded. For example, the probability that GVW is less than 80 kips is 0.92, and less than 100 kips is 0.99. This interpretation is too complex to render using a traditional plot (Figure 0-2).

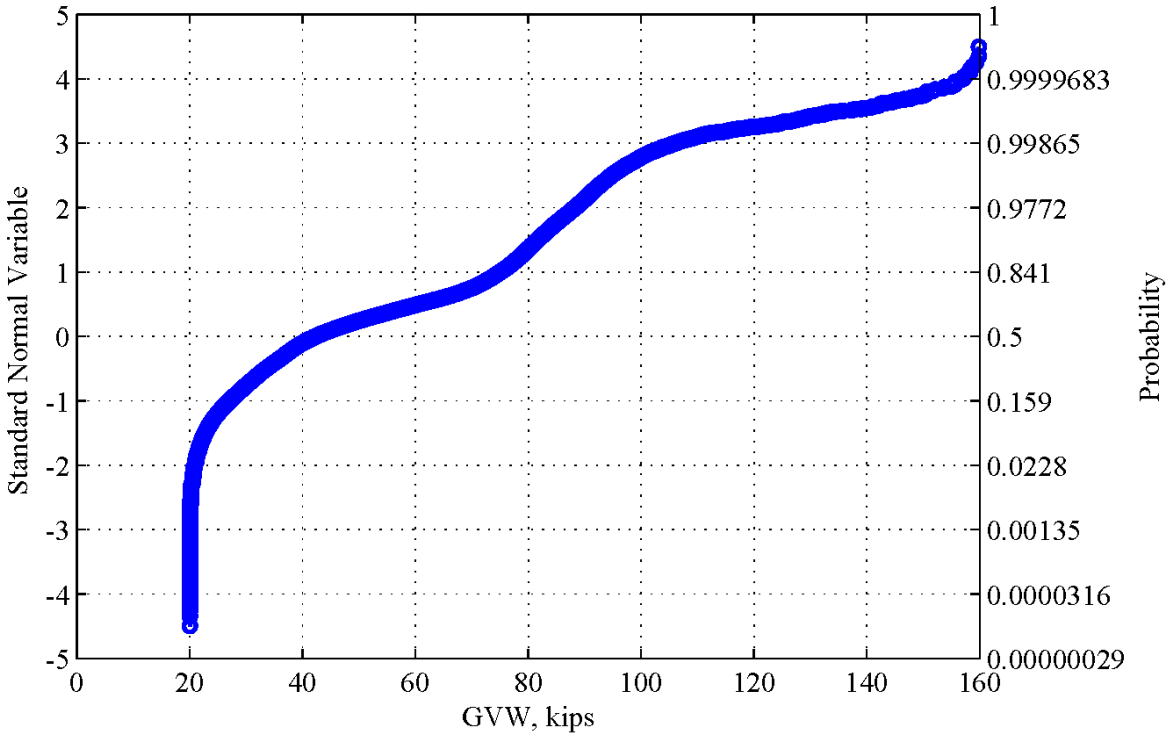

Figure 0-2. Cumulative Distribution Function for GVW Plotted on Probability Paper

A standard normal variable scale can also replace the vertical probability scale on the normal probability paper (0, +/-1, +/2 …), as shown in Table 0-2. This regular scale is also shown on the left-hand side in Figure 0-2. The linear relationship between the standardized variable and the corresponding probability is defined through the function below:

$$\boldsymbol{\Phi^{-1}(p) = z = \left(\frac{1}{\sigma_X}\right) x + \left(\frac{-\mu_X}{\sigma_X}\right)} \qquad \textbf{Equation 0-2}$$

Where: Φ^{1} – inverse standard normal function.

The shape of CDF on the normal probability paper can help to determine the type of distribution. The structure of the most common types of probability functions are is considered in more detail in Section 2.3.

Table 0-2: Vertical Scale and Corresponding Probabilities

x	*Φ(x)*
5.0	0.999999713
4.0	0.9999683
3.0	0.99865
2.0	0.9772
1.0	0.841
0.0	0.5
-1.0	0.159
-2.0	0.0228
-3.0	0.00135
-4.0	0.0000316
-5.0	0.00000029

2.3. Distribution Functions for Random Variables

There is a number of standard distribution functions defined by the specific statistical properties. It is important to determine the type of distribution while analyzing the raw data and fitting the data with the correct distribution function. The most common functions of continuous random variables in structural reliability are uniform, normal, lognormal, exponential, gamma, beta, extreme value type I, II and III.

The normal (or Gaussian) distribution function approximates binomially distributed events. It is the most important type of continuous probability distribution statistics and structural reliability since a large number of random variables are normally distributed. Also, the Gaussian distribution function is applicable if the number of events is substantial using a central limit theorem (CLT). It states that a sum of independent random variables in most cases follow Gaussian distribution if the number of events approaches infinity, even if each of them is not distributed normally.

A random variable X follows a normal distribution with parameters μ_X and σ_X if the probability density function (PDF) is:

$$f_X(x) = \frac{1}{\sigma_X\sqrt{2\pi}} exp\left[-\frac{1}{2}\left(\frac{x-\mu_X}{\sigma_X}\right)^2\right] \qquad \textbf{Equation 0-3}$$

Where: x is distributed from $-\infty$ to ∞

There is no closed-form solution for cumulative distribution function for a normal random variable for most cases. However, if μ_X=0 and σ_X=1 then X is called standard normal variable z, and CDF can be denoted by $\Phi(z)$:

$$\Phi(z) = \int_{\infty}^{\infty} \frac{1}{\sqrt{2\pi}} exp\left(-\frac{z^2}{2}\right) dz \qquad \textbf{Equation 0-4}$$

Thus, the standard normal variable and cumulative probability are inversely related through the function Φ ($\Phi - \mathbf{1}(\boldsymbol{p}) = \boldsymbol{z} = \left(\frac{\mathbf{1}}{\sigma_X}\right)\boldsymbol{x} + \left(\frac{-\mu_X}{\sigma_X}\right)$ Equation 0-2

and $\Phi(\boldsymbol{z}) = \int_{\infty}^{\infty} \frac{\mathbf{1}}{\sqrt{2\pi}} \boldsymbol{exp}\left(-\frac{\boldsymbol{z^2}}{\mathbf{2}}\right) \boldsymbol{dz}$ Equation 0-4) as it is summarized in Table 0-2 and shown in Figure 0-2.

The important aspect of using a normal probability scale is a possibility to identify the normal probability distribution by its shape. If a straight line on the probability plot represents the CDF, the variable can be considered as normal. The general shape of the PDF and CDF plotted on the normal probability paper are shown in Figure 0-3 and Figure 0-4.

The normal distribution is the most common for randomly generated variables, and the function is often used for statistical analysis. However, the real data sets may not follow the normal distribution and require alternative distribution function to be used for fitting. The lognormal distribution function is commonly used in structural reliability analysis to represent the distribution of the load components. In particular, the live load effect caused by the passing trucks can be more accurately estimated using lognormal distribution function.

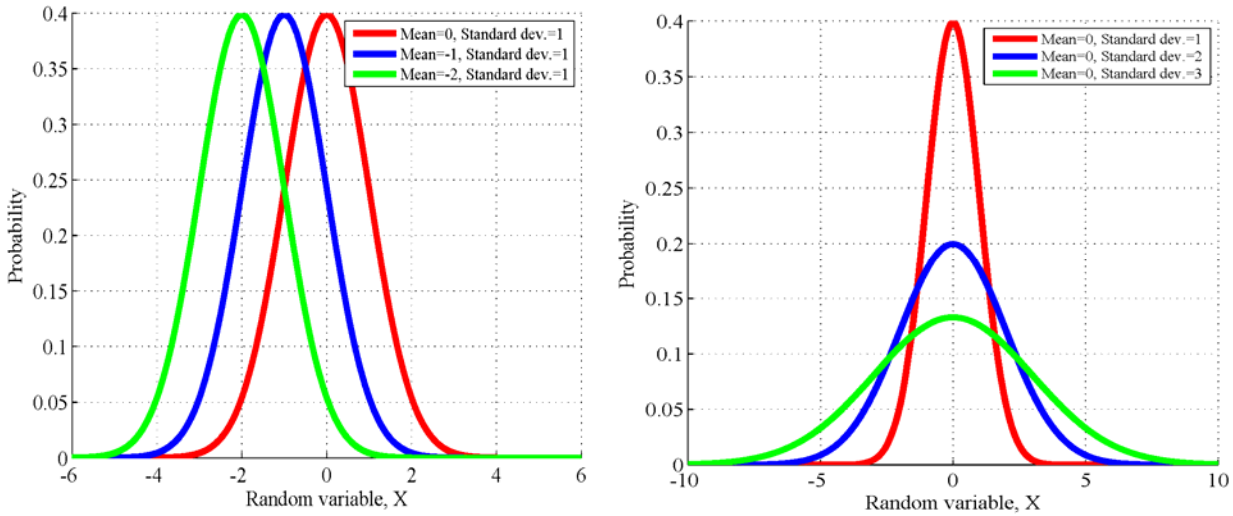

a) b)

Figure 0-3. PDF's of the Normal Distribution X with Different Values of μ_X (a) and σ_X (b)

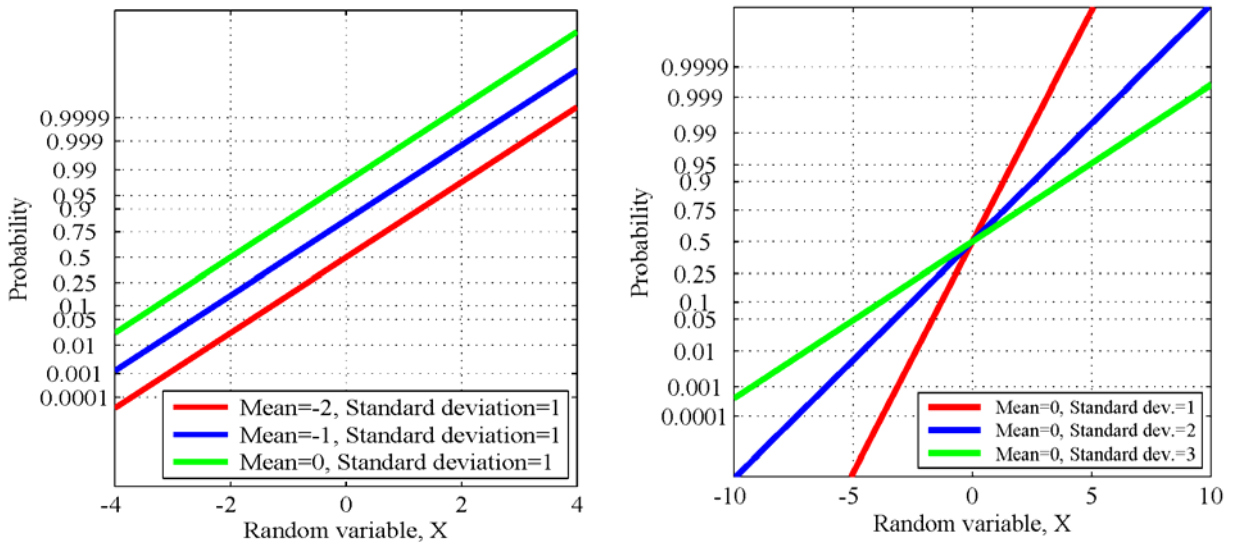

a) b)

Figure 0-4. CDF's of the Normal Distribution X with Different Values of μ_X (a) and σ_X (b)

Plotted on the Normal Probability Paper

A lognormal distribution (Gulton distribution) function is a continuous probability of a positive random variable X when $Y=ln(X)$ distributed normally. Thus, the cumulative distribution function can be defined through the standard normal function:

$$\boldsymbol{F_X(x) = F_Y(y) = \Phi\left(\frac{y-\mu_Y}{\sigma_Y}\right)} \qquad \textbf{Equation 0-5}$$

Where: $y=ln(x)$

μ_Y – mean value of variable X in logarithmic scale, $ln(x)$

σ_Y – standard deviation of variable X in logarithmic scale, $ln(x)$

Both can be determined using the following equations:

$$\boldsymbol{\sigma_Y^2 = \sigma_{ln_X}^2 = ln\left(V_X^2 + 1\right)} \qquad \textbf{Equation 0-6}$$

$$\boldsymbol{\mu_Y = \mu_{ln_X} = ln(\mu_X) - \frac{1}{2}\sigma_{ln_X}^2} \qquad \textbf{Equation 0-7}$$

Where: V_X– coefficient of variation of X

If X is a continuous random variable, the probability density function is the first derivative of the cumulative density function. Thus, the PDF can be determined as follows:

$$\boldsymbol{f_X(x) = \frac{dF_X(x)}{dx} = \frac{1}{x\sigma_{ln_{(X)}}}\phi\left(\frac{\ln(x)-\mu_{ln_{(X)}}}{\sigma_{ln_{(X)}}}\right)} \qquad \textbf{Equation 0-8}$$

The general shape of the PDF and corresponding CDF of lognormal distribution plotted on probability paper are shown in Figure 0-5 and Figure 0-6.

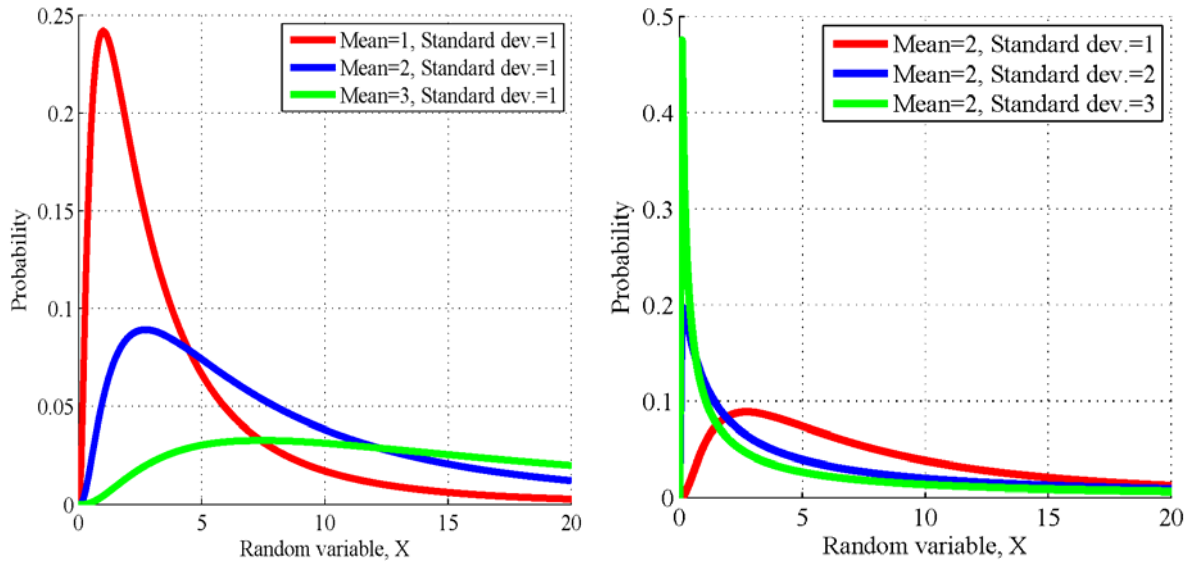

a) b)

Figure 0-5. PDF's of the Lognormal Distribution *X* with Different Values of μ_X (a) and σ_X (b)

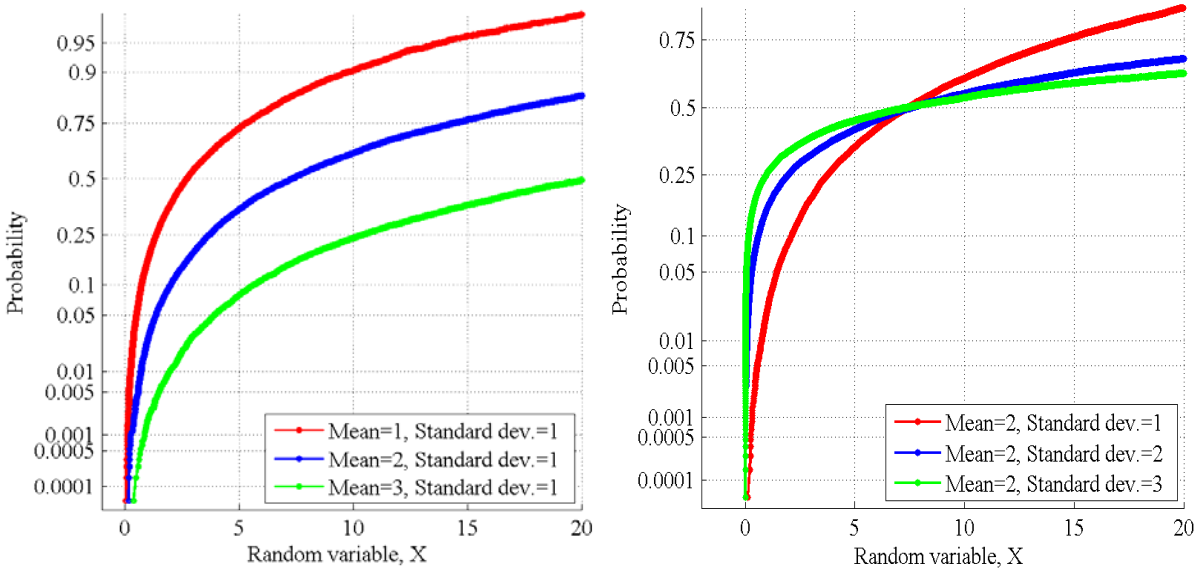

a) b)

Figure 0-6. CDF's of the Lognormal Distribution *X* with Different Values of μ_X (a) and σ_X (b) Plotted on the Normal Probability Paper

In some cases, it is useful to apply a distribution function with customary adjustable distribution parameters, such as Gamma distribution. This type of distribution function is also applicable to

simulate various load components (Ex.: sustainable dead load - (Nowak and Collins 2012). It belongs to a family of two-parameter continuous random variables. The shapes of PDF and CDF of Gamma distribution functions are defined by the shape parameter *a*, and scale parameter *b*, where both *a* and *b* are positive real numbers. The PDF of the Gamma distribution function can be defined as:

$$f_X(x) = \frac{a(ax)^{b-1}e^{-ax}}{\Gamma(b)} \qquad \textbf{Equation 0-9}$$

Where:

$$\Gamma(b) = \int_0^\infty e^{-u}u^{b-1}du \qquad \textbf{Equation 0-10}$$

The general shapes of the PDF and corresponding CDF of Gamma distribution plotted on probability paper are shown in Figure 0-7 and Figure 0-8.

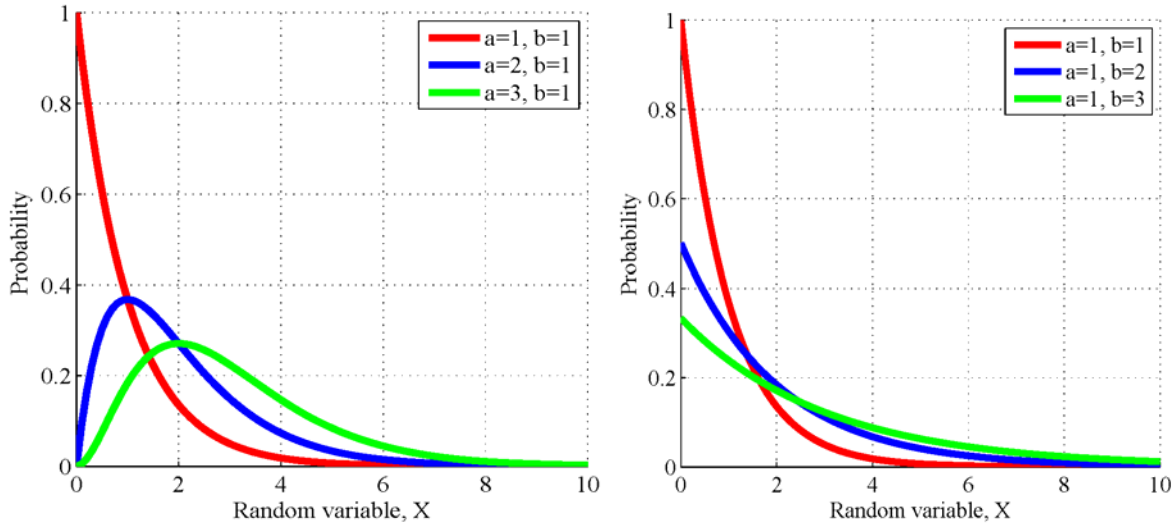

a) b)

Figure 0-7. PDF's of the Gamma Distribution *X* with Different Values of *a* (a) and *b* (b)

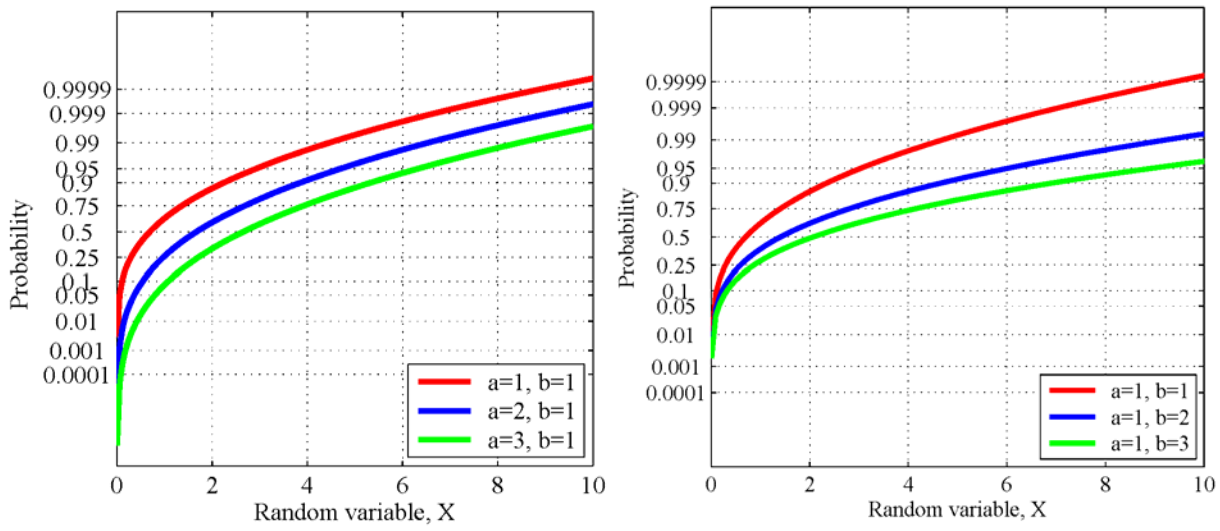

a) b)

Figure 0-8. CDF's of the Gamma Distribution X with Different Values of a (a) and b (b) Plotted on the Normal Probability Paper

Except for the shape of distribution, some data sets are distributed within a specific range. For example, the records of axle loads mostly follow a normal distribution but cannot have negative values, as well as cannot exceed carrying capacity of the truck axle. At the same time, most of the distribution functions for continuous random variables are distributed from -∞ to +∞ (Gaussian distribution) or from 0 to +∞ (Lognormal distribution). Thus, there are only a few options to create boundaries to a distribution with infinite tails: "truncating" a probability distribution object with upper and lower thresholds or using a probability distribution function with shape and boundaries to be defined, such as Beta distribution.

The Beta distribution function belongs to the family of continuous probability distributions with defined range and real positive shape parameters, often denoted as *a* and *b* (Beyer 1987). If *X* is

distributed within domain [x_{min}, x_{max}], the probability density function can be obtained using

$$f_X(x) = \frac{1}{B(a,b)} \frac{(x-x_{min})^{a-1}(x_{max}-x)^{b-1}}{(x_{max}+x_{min})^{a+b-1}}$$ Equation 0-11 :

$$f_X(x) = \frac{1}{B(a,b)} \frac{(x-x_{min})^{a-1}(x_{max}-x)^{b-1}}{(x_{max}+x_{min})^{a+b-1}}$$ **Equation 0-11**

Since PDF is a first derivative of the cumulative distribution function, the CDF can be calculated by:

$$F_X(x) = \int_0^x \frac{1}{B(a,b)} \frac{(x-x_{min})^{a-1}(x_{max}-x)^{b-1}}{(x_{max}+x_{min})^{a+b-1}} dx$$ **Equation 0-12**

Where: B – is a Beta function that can be obtained using Gamma distribution, Γ(z):

$$B(a,b) = \frac{\Gamma(a)\Gamma(b)}{\Gamma(a+b)}$$ **Equation 0-13**

The general shape of the PDF and CDF of random variable *X* distributed with Beta distribution within domain [0, 10] are plotted on probability paper are shown in Figure 0-9 and Figure 0-10.

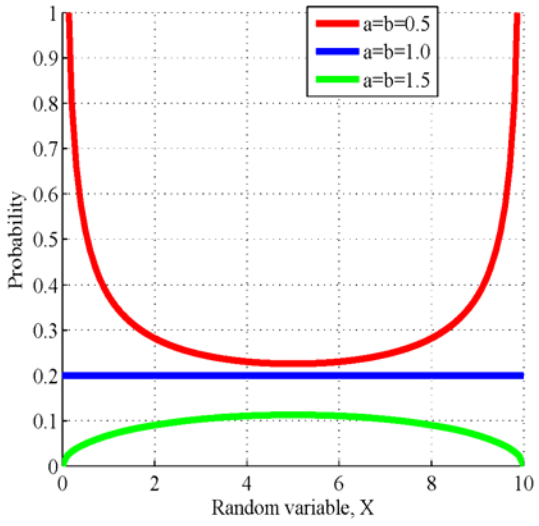

a)

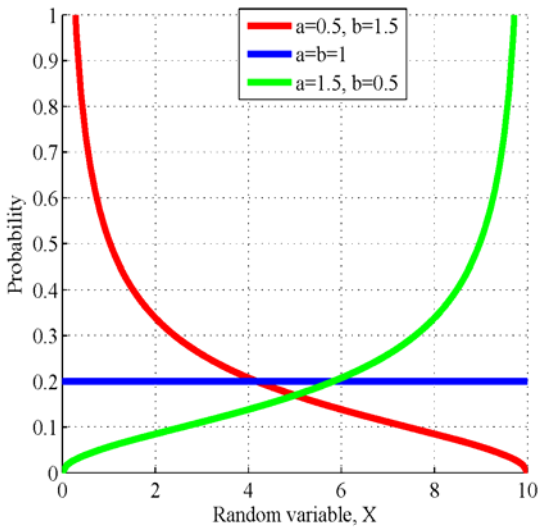

b)

Figure 0-9. PDF's of the Beta Distribution *X* with Different Values of *a* (a) and *b* (b)

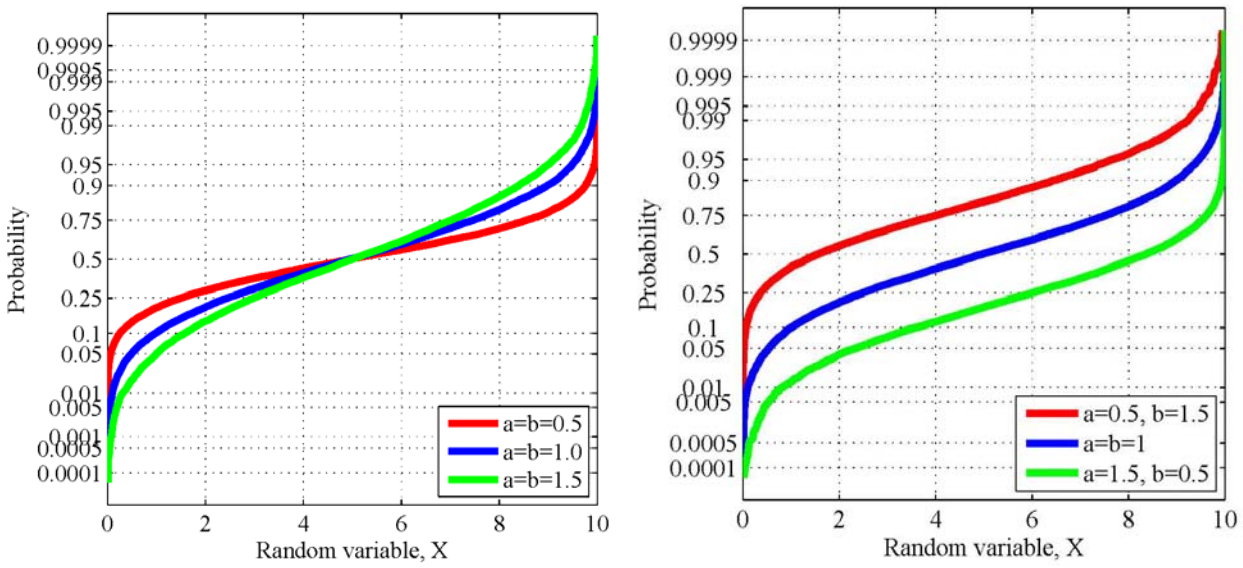

a) b)

Figure 0-10.CDF's of the Beta Distribution X with Different Values of a (a) and b (b) Plotted on the Normal Probability Paper

There are more distribution functions of continuous random variables, such as exponential, Logistic, Log-logistic, Rician, Pareto, etc. Some of them can be alternatively used for fitting and simulation of variable load and resistance parameters in the reliability-based analysis.

2.4. Concept of Limit State

The concept of limit state design is often referred to a boundary between safe performance and structural failure. In particular, the term “limit state” describes the conditions of potential failure when the structure no longer fulfills the required design criteria. There are three distinct types of limit states in structural reliability analysis:

- Ultimate limit states (ULSs) – conditions when the excessive deformations inevitably lead to a collapse of a structural component or entire structure (Ex.: Plastic hinge formation, local or global buckling of the steel components, crushing of concrete in compression controlled elements). In some cases, the ULS conditions are related to specific pre-agreed criteria, which represent the engineering demand and may not match the actual failure conditions.
- Serviceability limit states (SLSs) are related to an ability of the structure to remain functional under routine load conditional. For example, cracking, excessive vibrations, temporary or permanent deformations may cause the occupants/users discomfort or lead to progressive deterioration.
- Fatigue limit states (FLSs) consider the conditions of losing carrying capacity as a result of accumulated damage due to repeated load-unload cycles. The eventual failure usually occurs under the stress conditions less severe than defined by the ultimate limit state. Thus, both the magnitude of stress and frequency are critical in fatigue analysis and design. Structures made of or containing ductile materials are mostly prompt to accumulate the damage once the plastic limit was repeatedly exceeded.

The limit state function or performance function describes the criteria of failure for a particular design case. It consists of two components representing the load effect and resistance (carrying capacity of the structure). Each limit state can be described with a particular function. In general form, a performance function is:

$$\boldsymbol{g(R, Q) = R - Q} \qquad \textbf{Equation 0-14}$$

Or

$$g(R,Q) = \frac{R}{Q} - 1 \qquad \textbf{Equation 0-15}$$

Structural performance is then evaluated by resultant *g(R, Q)*:

- $g(R,Q) > 0$ – the structure performs within its safety limits
- $g(R,Q) = 0$ – boundary between acceptable and unacceptable limit
- $g(R,Q) < 0$ – structural failure

From the previous statement, the probability of failure P_f can be defined as follows:

$$P_f = P(g < 0) \qquad \textbf{Equation 0-16}$$

From the previous limit state function, $g = R - Q$, the probability of failure, P_f, can be derived considering the PDF's of R and Q as continuous random variables (Figure 0-11).

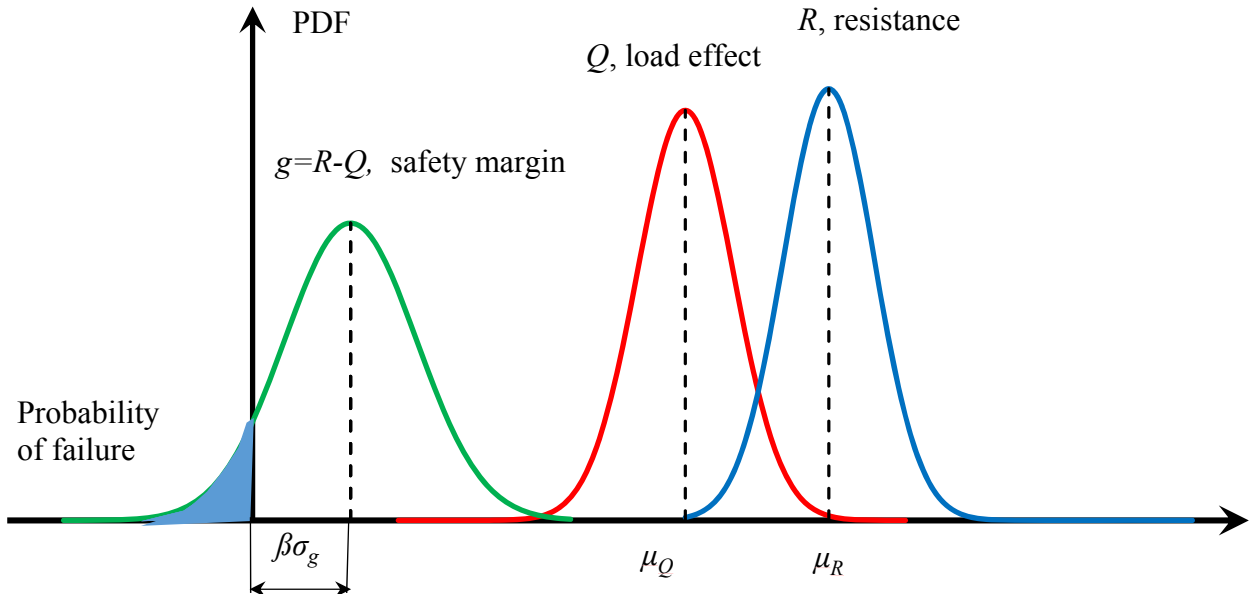

Figure 0-11. PDFs of Load, Resistance, and Safety Margin

The resultant of *R-Q* is also a continuous random variable representing the safety margin. The probability of failure is shown as a shaded area of PDF of *g(R, Q)*. For this case, the actual

probability of failure P_f can be computed as an integral of the joint PDF (shaded area in Figure 0-11, volume within the "failure domain" in Figure 0-12) over the values of load and resistance that create a negative part of a performance function *g(R, Q)*:

$$\boldsymbol{P_f = \int_{-\infty}^{\infty} f_Q(q) F_R(q) dq} \qquad \textbf{Equation 0-17}$$

Where: F_R – cumulative distribution function of resistance

f_Q – probability density function of load.

The general structure of the joint probability function for the limit state function ($\boldsymbol{g(R, Q) = R - Q}$ Equation 0-14 is shown in Figure 0-12.

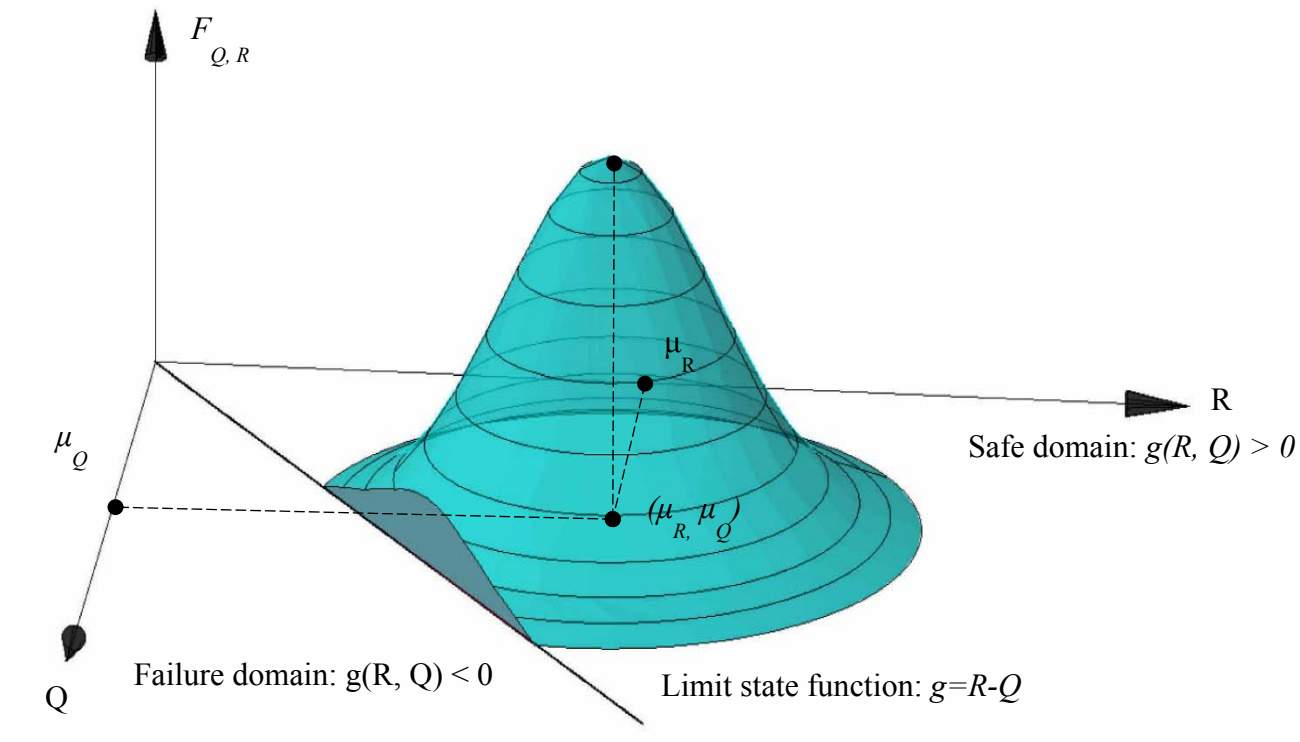

Figure 0-12. General 3D Joint Probability Density Function for Random Variables *R* and *Q*

In a particular design case, the performance function can be complicated. The load and resistance usually include several components and associated factors. There is also a lack of statistical data to define the distribution of each component. Altogether, they make computing the probability of failure P_f a convoluted process. Thus, it becomes handier to calculate the probability of failure using the concept of reliability index.

2.5. Concept of the "Design point"

Each design provision/formula can be evaluated using the reliability analysis. Therefore, the level of safety is expressed with the reliability index, denoted with, β (the concept of reliability index is introduced in 0.6 of this study). Additionally, the result of reliability analysis can be coordinates of the "design point". The concept of the "design point" was first introduced in 1974 by (Hasofer and Lind 1974) as a location at the failure surface, $g(R, Q)=0$, where the limit state function can be evaluated, instead of mean values.

For the linear limit state function and normally distributed load and resistance components, the Hasofer-Lind reliability index can be calculated using the First-order, second-moment reliability method ($\boldsymbol{\beta} = \frac{\mu_R - \mu_Q}{\sqrt{\sigma_R^2 + \sigma_Q^2}}$ Equation 0-24). The corresponding "design point" is located at the coordinates of factored load Q^* (Figure 0-1) and factored resistance R^* (Figure 0-2). In three-dimensional representation, the location of the design point is shown in Figure 0-14.

$\boldsymbol{=R-Q}$ Equation 0-14, the design point is a point in two-dimensional space, denoted by Q and R, the highest probability of failure, $P(g<0)$, is at the coordinates of Q^*

$\mu R-\mu Q\sigma R2+\sigma Q2$ Equation 0-24 the coordinates of the design point can be determinate as:

$$R^*=\mu_R-\frac{\beta\sigma_R^2}{\sqrt{\sigma_R^2+\sigma_Q^2}} \quad \textbf{Equation 0-18}$$

$$Q^*=\mu_Q+\frac{\beta\sigma_Q^2}{\sqrt{\sigma_R^2+\sigma_Q^2}} \quad \textbf{Equation 0-19}$$

Where: μ_R – mean value of resistance

σ_R – standard deviation of resistance

μ_Q – mean value of load

σ_Q – standard deviation of resistance

β – reliability index

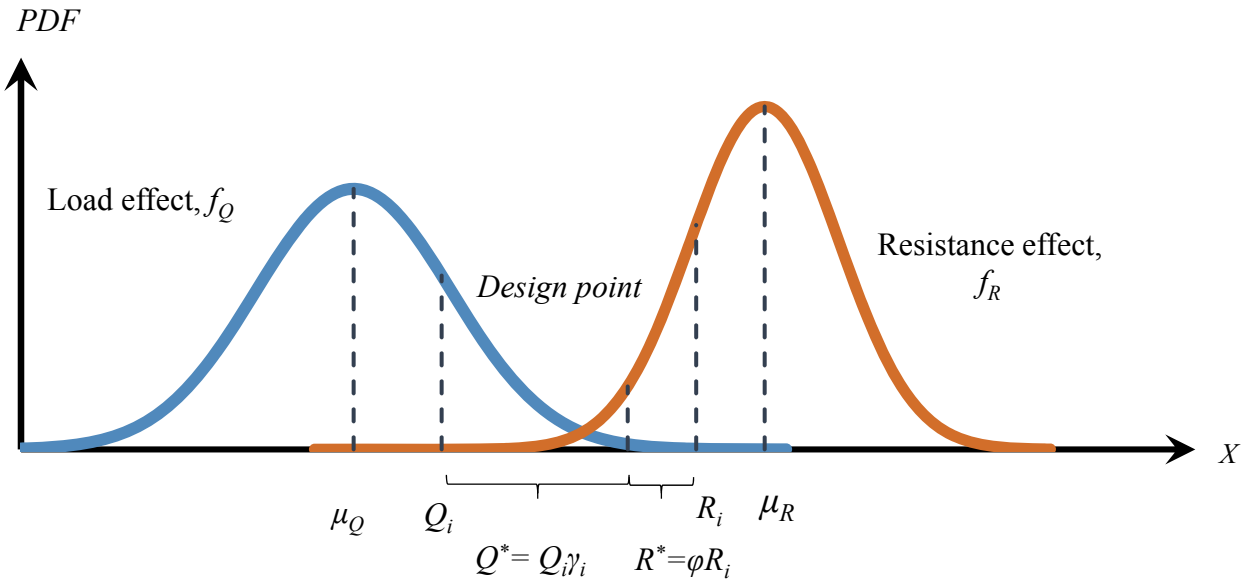

Figure 0-13. Design Point on PDFs of Load and Resistance for Linear Function *g(R, Q)=R-Q*

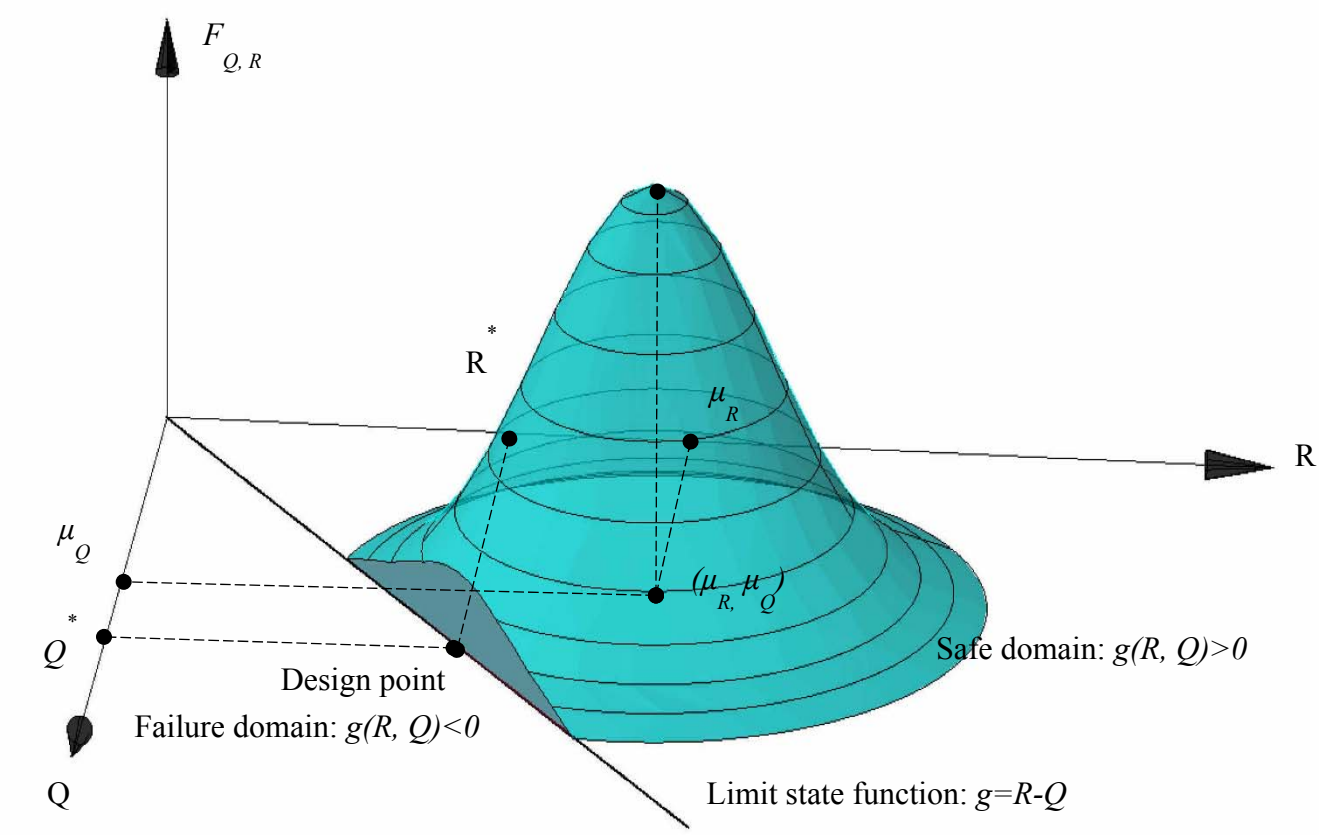

Figure 0-14. Design Point at the Failure Boundary for Linear Function *g(R, Q) = R-Q*

In most cases the position of the design point is unknown. Thus, the iterative Rackwitz and Fiessler procedure (Rackwitz and Flessler 1978) can be applied to determine coordinates of the "design point". Since a relatively wide range of design point coordinates corresponds to the same value of reliability index, in practice, $R^*=\mu_R-\frac{\beta\,\sigma_R^2}{\sqrt{\sigma_R^2+\sigma_Q^2}}$ Equation 0-18

and $Q^*=\mu_Q+\frac{\beta\,\sigma_Q^2}{\sqrt{\sigma_R^2+\sigma_Q^2}}$ Equation 0-19 can be used even for non-normal distributions.

2.6. Reliability Index

In reliability theory, the term "reliability index" or Cornell safety index (Cornell 1967), denoted as β, defines the level of structural safety while the probability of failure (P_f) is a measure of failure. These two terms are inversely related and if the limit state function is normal:

$$\boldsymbol{P_f = P(g < 0) = \Phi\left(\frac{\mu_g}{\sigma_g}\right) = \Phi(-\beta) = 1 - \Phi(\beta)} \qquad \textbf{Equation 0-20}$$

Where: Φ^{-1} – the inverse standard normal distribution function

μ_g – mean value of g

σ_g – standard deviation of g

Thus, the corresponding reliability index can be computed as follows:

$$\boldsymbol{\beta = -\Phi^{-1}(P_f)} \qquad \textbf{Equation 0-21}$$

This measure is not as accurate as probability of failure, since majority of cases $P_f \neq 1 - \Phi(\beta)$. However, it is more computationally appropriate when the value of P_f is relatively large or, there is no sufficient statistical data to access P_f.

Further on, Hasofer and Lind introduced an improved version of the Cornell safety index in terms of standard form random variables (Hasofer-Lind reliability index). It can be graphically presented as a shortest distance from the origin to the intersection with the limit state function in a reduced variable scale, $g(Z_R, Z_Q)$ (Hasofer and Lind 1974) as it is shown in Figure 0-15.

The non-dimensional "standard form" of random variables or reduced variables can be determined using the statistics of the basic variables:

$$Z_R = \frac{R-\mu_R}{\sigma_R} \qquad \textbf{Equation 0-22}$$

$$Z_Q = \frac{Q-\mu_Q}{\sigma_Q} \qquad \textbf{Equation 0-23}$$

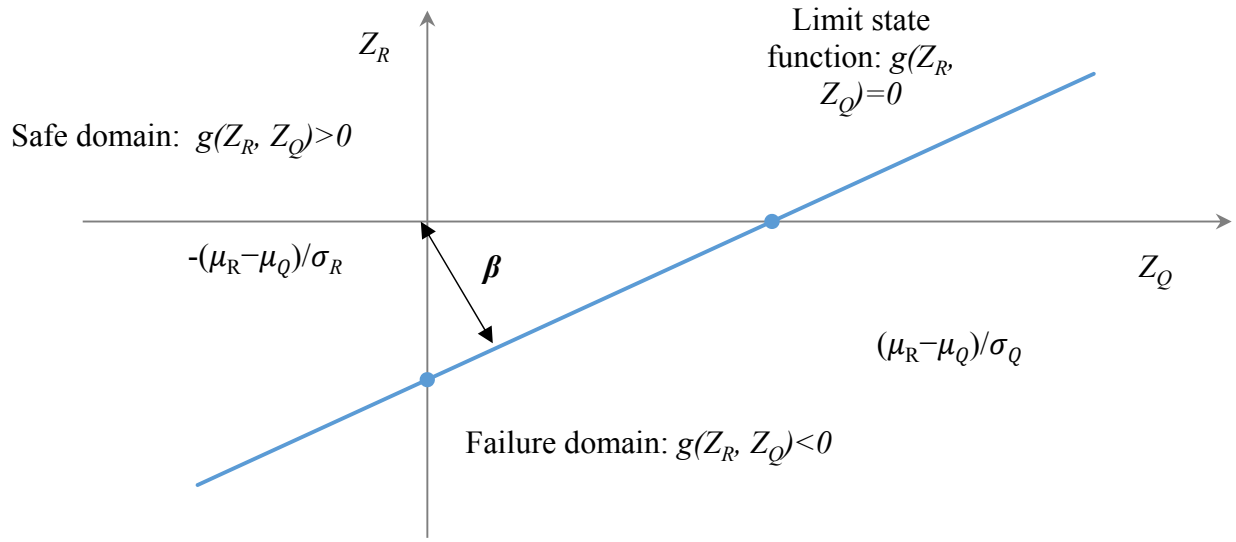

Figure 0-15. Reliability Index (Hasofer and Lind 1974)

Using graphical representation of reliability index and basic geometry β can be determined as:

$$\beta = \frac{\mu_R-\mu_Q}{\sqrt{\sigma_R^2+\sigma_Q^2}} \qquad \textbf{Equation 0-24}$$

This expression also corresponds to the inverse of COV for function $g(R, Q)$ when R and Q are uncorrelated normally distributed random variables. In this case, the First-order, second-moment reliability method (Nowak and Collins 2012) is appropriate and defines the exact value of the reliability index. The "second-moment" stands for the first two moments of random variable g (1st moment is expected value $E(g)=\mu_g$ and the second moment $E(g^2)=\sigma_g$) that are required in order to calculate the reliability index.

Otherwise, this method is highly approximate and involves considerable errors since "normalization" excludes the upper and lower tails (including extremums) and affect the variance of the actual distribution function (Ellingwood 1980), (Nowak and Collins 2012)). Thus, the corresponding P_f is commonly referred as "notional" probability of failure implying the imprecise relationship of P_f and β. However, there is a number of methods and techniques to calculate the reliability index that takes into account the type of distribution function, non-linearity of the limit state function and correlation between variances (Hasofer and Lind 1974), (Rackwitz and Flessler 1978), (Rackwitz 2001), (Nowak and Collins 2012). Some of them will be considered in this study.

2.6.1. Rackwitz-Fiessler Method

A simplified technique, considered in the previous chapter, requires determining the statistical parameters for the random variables involved in the limit state function, In structural analysis and design, it is common that the load and resistance components are not normally distributed, but can be fitted with a primary known distribution function. The knowledge of the approximate type of distribution can substantially increase the accuracy of computing the reliability index, once the iterative Rackwitz-Fiessler method is applied (Rackwitz and Flessler 1978). This technique is based on the idea to "normalize" the random variable into so-called "equivalent normal variable." It is done by approximating the actual distribution function with the normal linear function at the "design point" as it is shown in Figure 0-16. The concept of the design point was discussed in Section 2.5.

For any non-normal random variable *X,* the CDF and PDF "normalized" at the design point, x^* assumed in the first iteration can be defined using $\boldsymbol{F_X(x^*) = \Phi\left(\frac{x^* - \mu_X^e}{\sigma_X^e}\right)}$ Equation 0-25 and $\boldsymbol{f_X(x^*) = \frac{1}{\sigma_X^e}\phi\left(\frac{x^* - \mu_X^e}{\sigma_X^e}\right)}$ Equation 0-26 respectively.

$$\boldsymbol{F_X(x^*) = \Phi\left(\frac{x^* - \mu_X^e}{\sigma_X^e}\right)} \qquad \textbf{Equation 0-25}$$

$$\boldsymbol{f_X(x^*) = \frac{1}{\sigma_X^e}\phi\left(\frac{x^* - \mu_X^e}{\sigma_X^e}\right)} \qquad \textbf{Equation 0-26}$$

Where: Φ – is a CDF for a standard normal distribution

ϕ – is a PDF of a standard normal distribution

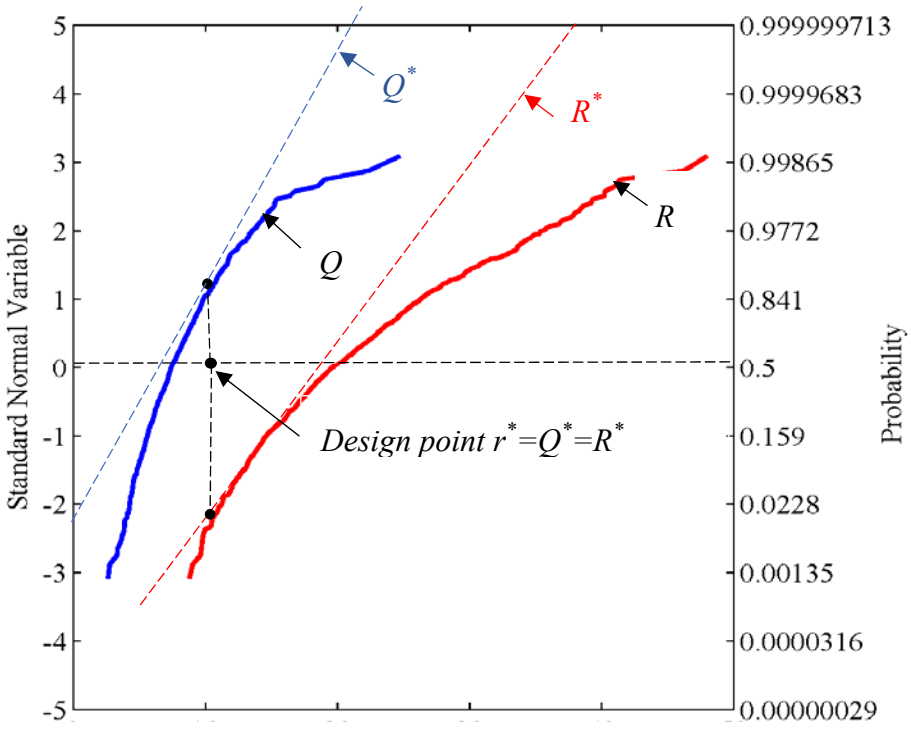

Figure 0-16. Graphical Representation of Rackwitz-Fiesler Method

The corresponding equivalent normal parameters of X (mean μ_X^e, and standard deviation σ_X^e)

$FXx*=\Phi x*-\mu Xe\sigma Xe$ Equation 0-25 $fXx*=1\sigma Xe\phi x*-\mu Xe\sigma Xe$

Equation 0-26 as follows:

$$\mu_X^e = x^* - \sigma_X^e[\Phi^{-1}(F_X(x^*))] \quad \textbf{Equation 0-27}$$

$$\sigma_X^e = \frac{1}{f_X(x^*)}\phi\left(\frac{x^*-\mu_X^e}{\sigma_X^e}\right) \quad \textbf{Equation 0-28}$$

For a fundamental case, previously expressed by $g(R,Q) = R - Q$

Equation 0-14, the 1st iteration reliability index at the point $r^*=R^*=Q^*$ can be determined as:

$$\beta = \frac{\mu_R^e-\mu_Q^e}{\sqrt{(\sigma_R^e)^2+(\mu_Q^e)^2}} \quad \textbf{Equation 0-29}$$

Where: μ^e_R – equivalent normal mean value of resistance at $r^*=R^*=Q^*$

σ^e_R – equivalent normal standard deviation of resistance at $r^*=R^*=Q^*$

μ^e_Q – equivalent normal mean value of load at $r^*=R^*=Q^*$

σ^e_Q – equivalent normal standard deviation of resistance at $r^*=R^*=Q^*$

β – reliability index at the 1st iteration

At the next iteration the location of the new design point can be calculated as follows

$$R^*=\mu_R^e-\frac{\beta(\sigma_R^e)^2}{\sqrt{(\sigma_R^e)^2+(\sigma_Q^e)^2}} \quad \textbf{Equation 0-30}$$

$$Q^*=\mu_Q^e+\frac{\beta(\sigma_Q^e)^2}{\sqrt{(\sigma_R^e)^2+(\sigma_Q^e)^2}} \quad \textbf{Equation 0-31}$$

The iteration has to be continued until an acceptable convergence of β and r^* is achieved. Graphically this method is presented in Figure 0-16.

2.6.2. Monte Carlo Simulation

The Monte Carlo simulation method is often referred to as an effective tool to simulate an unlimited number, *N*, of test results, based on the information from the limited number, *n*, of conducted tests (Thoft-Christensen and Baker 1982), (Enright & OBrien, 2012), (Nowak and Collins 2012). This technique is primarily based on applying the specific statistical parameters obtained from the test results to a range of simulated random or semi-random numbers.

It is widely used to solve complex numerical problems without a simplified close-form solution, where a number of random variables are related through non-linear functions. It is suitable for the tasks involving time-consuming non-linear finite element analysis, expensive or unavailable full-scale proof load testing, and prediction of the result over a time period. This method is commonly applied to simulate the traffic condition in a certain return period, since otherwise it requires decades of a data collection (Jacoboni and Reggiani 1983), (Enright and OBrien 2012), (Enright et al. 2016), etc.).

The important step in Monte Carlo simulation is generation of *N* random numbers, u_i ($i=1 \dots N$), uniformly distributed from 0 to 1. These numbers plays a key role in further simulation process by defining the random locations of virtual test results on the probability scale (Figure 0-17).

The next step in this procedure is to generate the inverse standard normal variables, z_i. As it was mentioned above, the random numbers generated within domain [0, 1] represent the probabilities of simulated test results occurrence. Therefore, the approximate conversion can be made using the $\boldsymbol{z_i = \Phi^{-1}(u_i)}$ Equation 0-32:

$$\boldsymbol{z_i = \Phi^{-1}(u_i)} \qquad \textbf{Equation 0-32}$$

Where: Φ^{-1} – the inverse of the standard normal cumulative distribution function.

Then, the variable of interest, X, can be generated for every N^{th} case knowing the statistical parameters of the actual data set (type of distribution, mean value μ_X and standard deviation σ_X). If X is normally distributed, i^{th} virtual result can be generated as:

$$x_i = \mu_X + z_i \sigma_X \qquad \textbf{Equation 0-33}$$

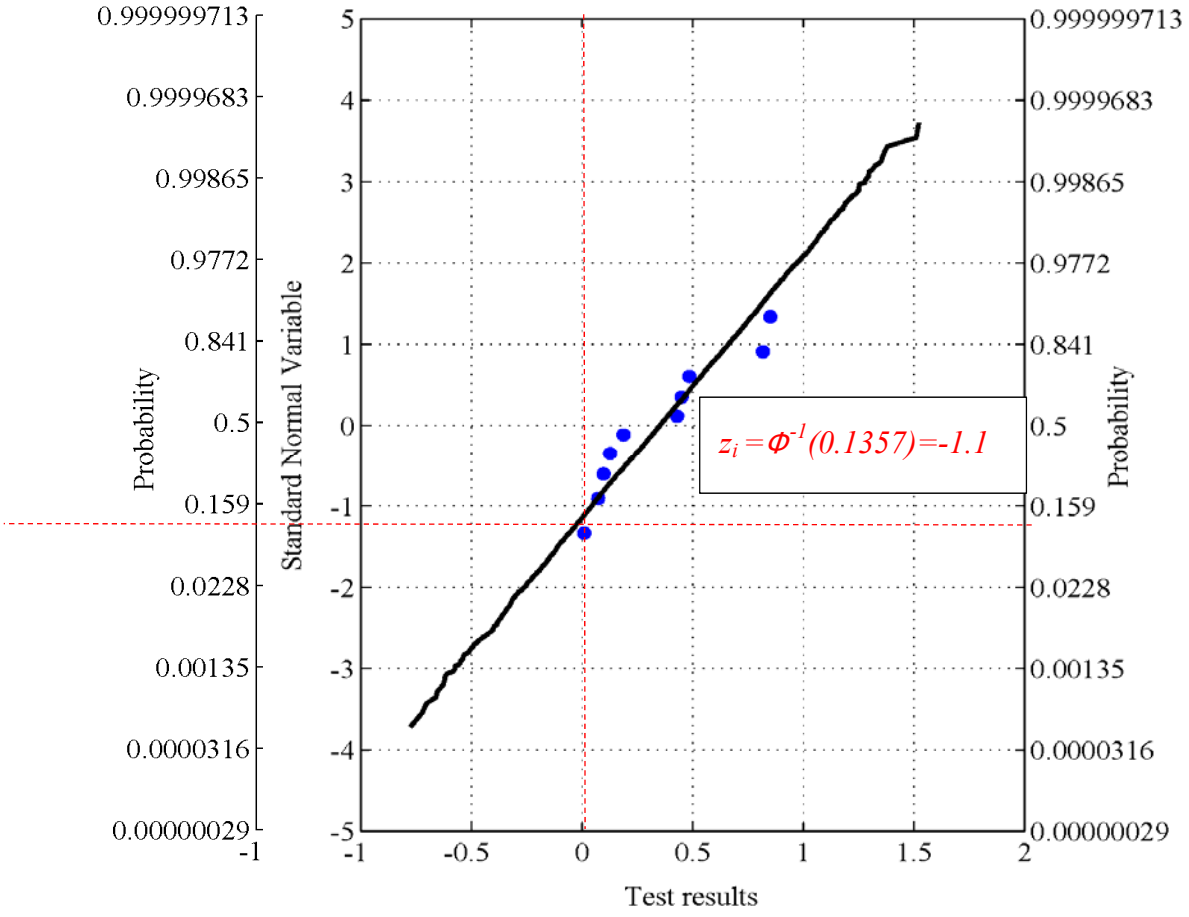

Figure 0-17. Simulation of Test Results using Monte Carlo Method

Except of simulating the test results, Monte Carlo method can be successfully used to predict the probability of failure. If $P_f = P_{(g(x)<0)}$, then using a simulation technique the probability of failure can be assessed as a ratio of the number of cases, n, when failure occurred ($g<0$) and the total number of simulations, N:

$$P_f = \frac{n}{N} = \frac{total\ number\ of\ cases\ when\ g<0}{total\ number\ of\ simmulated\ cases} \qquad \textbf{Equation 0-34}$$

It is worth to noting, that using simulation techniques, the accuracy of the result can be significantly improved by increasing the number of simulations, *N*.

Live Load Data

3.1. Summary

A considerable amount of weigh-in-motion (WIM) data is now available for most of the states. The truck data was collected at 13 WIM sites in Alabama and 32 WIM sites across the US since 2005. The quality control procedure, which consists of a set of filtering criteria was applied to the available WIM database to ensure the accuracy of the data and eliminate the errors that can affect the analysis. To calculate the load effects such as moment and shear force, the vehicles from the WIM database were "run" over influence lines. The resulting load spectra are presented in the form of cumulative distribution functions (CDF) on the normal probability paper for an easier interpretation. A preliminary analysis of the WIM data indicates that live loads have changed with respect to traffic volume, mix, and weight.

3.2. Weigh-in-Motion Systems

There is a variety of Weigh-in-Motion technologies available for permanent or temporary traffic data collection. Usually, WIM sites across the US are equipped with the following types of weigh-in-motion (WIM) systems: piezoelectric sensor, bending plate and load cell (McCall and Vodrazka 1997). Almost all of the WIM data used in this study was collected using these devices. In only one WIM site, located on Alabama state road US-231, the measurements were accumulated using a Bridge-WIM system, that used the bridge as a scale (*SiWIM Bridge Weigh-in-Motion Manual: 4th Edition* 2011), (O'Brien; et al. 1999). Recently one of the ALDOT WIM

sites located near Montgomery has been upgraded to a Virtual Weigh Station (Office of Freight Management and Operations 2017). This technology has additional features such as capturing images of the vehicles along with the license numbers and USDOT ID numbers.

Most of the WIM systems can record over 15,000 trucks a day and collect raw data continuously for about 30 days (Quinley 2010). Traffic Volume Trends (TVT) system is used to process the continuous traffic volume data and produce the monthly Traffic Volume Trends report in the FHWA's Traffic Monitoring Guide Card Format (*Traffic Monitoring Guide* 2001). The WIM database obtained by combining TVT monthly reports is mostly considered in this study.

Almost all WIM stations in Alabama except one were equipped with permanent bending plate systems consisting of two scales and inductive loops for vehicle count as shown in **Error! Reference source not found.**. The central principle is based on using strain gauges attached to the weigh pads and re-computing the axle loads from the strains measured. These systems were designed for long-term (over ten years) monitoring of traffic, moving with speed from 3 to 124 mph. Calibration of these weighing systems was performed using test trucks according to (ASTM E1318 - 09 2009). The expected accuracy of measurement for Type I WIM sensors is 10% for GVW and 25% for axle load and axle spacing group (Table 3.3, McCall and Vodrazka 1997). However, according to ALDOT WIM calibration reports, the accuracy of GVW measurement reaches 3-5% for vehicles moving with an average highway speed.

Figure 0-1. Bending Plate Systems in WIM Location 965 (Shorter, I-85)

Piezoelectric WIM sensors can be divided into three basic types based on piezoelectric material: piezoceramic sensors, piezopolymer sensors, and piezoquartz sensors. The first two types are highly temperature dependent and mostly used for vehicle count and classification (Al-Qadi et al. 2016). Piezoquartz WIM sensors are widely used in the regions prompt to frequent freeze-and-thaw cycles due to the low sensitivity to temperature fluctuations (White et al. 2006). They also belong to the ASTM E1318 Type I WIM systems and, thus, can be used for measuring vehicle weight with the sufficient accuracy(10% for GVW and 25% for axle load and spacing). A principle of piezoelectric sensor operation is based on the difference in voltage due to the applied force. Calibration procedure determines the force-voltage relationship. However, this type of system is only accurate in case of dynamic load, while for static or slow-motion speed measurements it produces a substantial error.

Load cell-based WIM systems utilize a similar mechanism as bending plates. The weight sensor is usually a strain-gauge type, which converts the applied force into the proportional electrical

signal. The load cell WIM systems are commonly used in conjunction with the inductance loops to eliminate incorrect records and activate the principle system (Al-Qadi et al. 2016).

The B-WIM system installed on US-231 is built base on a combination of strain gauges, attached to the bottom surface of the main longitudinal members, and axle detectors as shown in **Error! Reference source not found.**, according to *SiWIM Bridge Weigh-in-Motion Manual: 4th Edition* (2011). The principle of B-WIM system performance is based on the comparison of measured and modeled bending moments. The bending moments are calculated from the recorded strains and mechanical properties of structural members. The accuracy of the system was checked and verified by the European WIM Specifications – "COST | Weighing in motion of road vehicles" (1999). The calibration procedure was performed using trucks that were weighed by stationary scales, including axle loads and axle spacing. Random traffic was not used in B-WIM system calibration.

According to SiWIM Bridge Weigh-in-Motion Manual, Class A(5) accuracy of B-WIM systems measurement is achievable for a very smooth pavement surface. It means that approximately 95 % of the gross vehicle weight (GVW) results can be expected between ±5 % from the true static value, single axle loads – in the interval of ±15 % and group axles – in the interval of ±12 %. However, calibration for bridges with a very rough wearing surface may result in class D(25) accuracy – Table 2-8 of *SiWIM Bridge Weigh-in-Motion Manual: 4th Edition* (2011).

Virtual Weight Stations utilize practically the same WIM scale systems along with the digital cameras and software to process the visual information in real time. These systems can recognize the characters on vehicle license plates and analyze this information along with the GVW, axle weight, and vehicle class, obtained from the traditional sensors, such as listed above.

Figure 0-2. Placement of SiWIM Strain Transducers - Bridge Weigh-in-Motion

There are several factors, which can affect the accuracy of measurements collected by any type of WIM system, such as pavement roughness (causing bouncing axle movement or dynamic impact) and temperature effects. However, the dynamic portion of load is usually pre-evaluated and eliminated in the final measurements.

3.3. Weigh-in-Motion Data Collection

WIM data collection provides a powerful tool for the traffic load estimation. One of the first WIM systems was developed in 1952 by the United States Bureau of Public Roads (predecessor of FHWA), (Norman and Hopkins 1952). It was just a reinforced concrete platform instrumented with resistance wire strain gauges. The vehicle weight was calculated manually by making use of output from the oscilloscope attached to strain gauges. Contemporary WIM systems are very different from the sensors developed in the 1960's. They enabled a user, in addition to axle loads, to determine the vehicle type, process and transmit the recorded data (AASHTO 2014).

Bridge-WIM technology (utilized in US231 in Alabama) was developed by researchers led by Dr. Fred Moses in 1979 and became widely employed in Australia for instrumenting culverts. In the 1990's, an improved and upgraded version of the system was applied in Slovenia, Ireland, and France ("COST | Weighing in motion of road vehicles" 1999), (O'Brien; et al. 1999).

Recently, FHWA along with State DOTs have collected a substantial weigh-in-motion (WIM) database. As of 2011, WIM systems have been in operation for more than 20 years in most states in the U.S. Over 700 portable and permanent WIM stations are currently in operation around the country (Ghosn et al. 2011).

Each traffic record collected at the WIM site includes a detailed description of the vehicle configuration (*Traffic Monitoring Guide* 2001). The information recorded for each vehicle in the WIM database includes the exact time and date, lane and direction code, speed, GVW, speed, individual axle loads, individual axle spacing and class of vehicle based on FHWA Classification scheme (Cambridge Systematics, Inc. 2007). Routine monitoring of the traffic in each lane is also performed to determine the Average Daily Traffic (ADT) and Average Daily Truck Traffic (ADTT) that are necessary for fatigue life and load capacity computation. This data are widely used for traffic monitoring and analysis, pavement safety evaluation, bridge structures design, and enforcement.

Despite the advantages of WIM technologies, a decrease in WIM research has been observed since 2000 (Pigman et al. 2012). One of the reasons is that the setting of permanent WIM devices, as well as following service, is quite costly. Therefore, the WIM systems are usually installed on busy state roads or interstate highways.

3.4. Available WIM Databases

3.4.1. Ontario Truck Survey

Since US traffic data was not available, the design live load, HL-93, in the AASHTO LRFD Specifications (*AASHTO LRFD* 2014) was developed based on a truck survey conducted by the Ontario (Canada) Ministry of Transportation (Agarwal and Wolkowicz 1976). This survey collected the configurations of 9,250 selected heavy vehicles (approximately every tenth truck in the traffic flow) from different regions in the Province of Ontario. In the 1980's, the Ontario traffic load and the population were comparable and applicable to the US (Nowak 1999). The collected database included truck configuration (axle load distribution and axle spacing configuration) and weight (GVW). This database was used in the current study to compare with the contemporary WIM data and to track the changes in truckload over time.

3.4.2. SHRP2 R19B WIM Database

Two primary sources were used to obtain the WIM data for the present study: NCHRP Project 12-76 (Sivakumar 2007) and FHWA files. WIM data collected from 32 WIM sites cover 18 states for the years 2005 to 2008 over the US. This data was previously used for SHRP 2 Research Reports (2015). States, where WIM data is available are marked orange and shown in Figure 0-3. The years, months and the number of vehicles recorded in each state are summarized in Table 0-1. In case of multilane WIM site in FHWA and NCHRP data, the lane with maximum ADTT is listed.

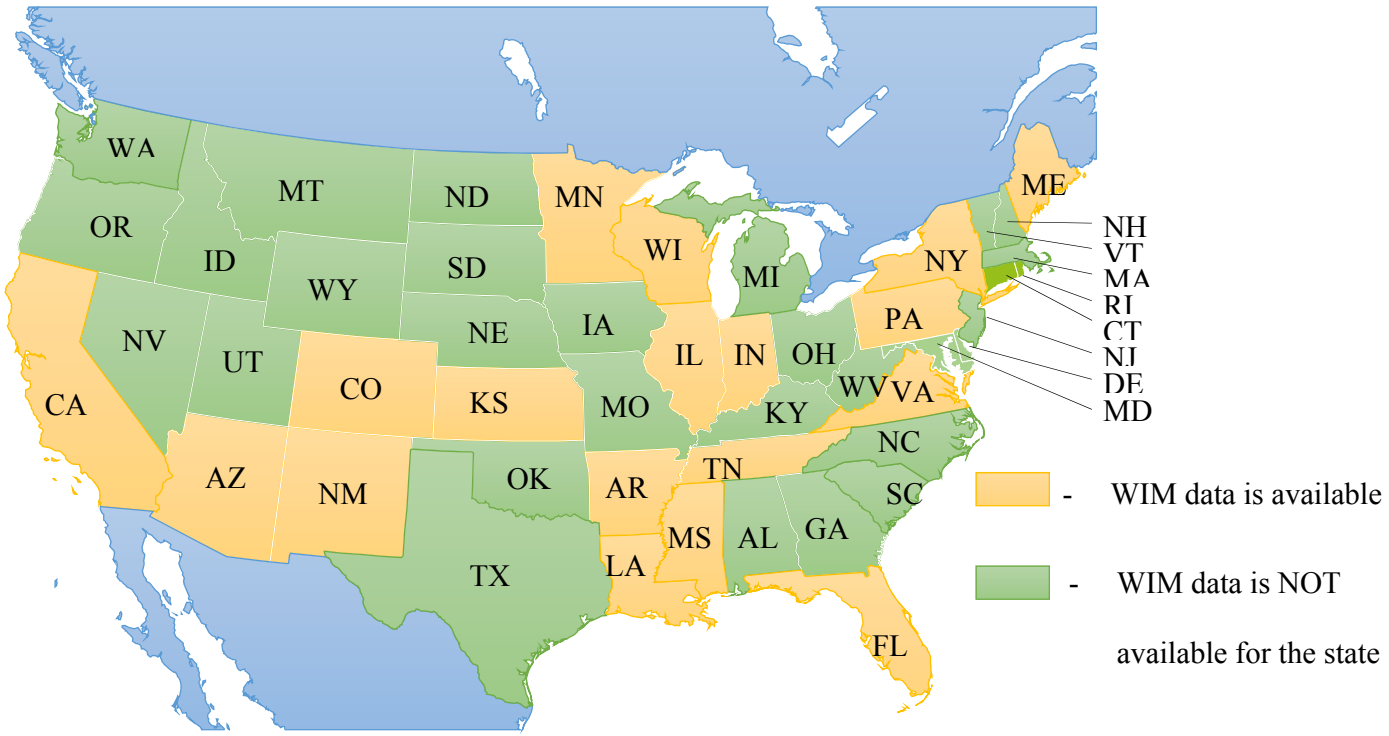

Figure 0-3. WIM data availability in the United States (based on FHWA and NCHRP 12-76)

Table 0-1. WIM States and Number of Records (NCHRP 12-76, FHWA data) – 2005-2008

#	State	# of records	ADTT	2005												2006											
				1	2	3	4	5	6	7	8	9	10	11	12	1	2	3	4	5	6	7	8	9	10	11	12
1	MS	5,914,950	2,967*													x	x	x	x	x	x	x	x	x	x	x	x
2	CA	13,458,818	8,366*																x	x	x	x	x	x	x	x	x
3	FL	4,143,162	2,558*	x	x	x	x	x	x	x	x	x	x	x	x	x	x	x									
4	AR	1,675,349	3,919																								
5	AZ	1,466,033	4590																								
6	CO	343,603	941																								
7	DE	201,677	553																								
8	IL	854,075	2340																								
9	IN	185,267	508																								
10	LA	477,922	1309																								
11	MD	328,778	235																								
12	ME	183,576	503																								
13	MN	55,572	450																								
14	NM	725,382	1,667																								
15	PA	1,495,741	4098																								
16	TN	1,622,320	4445																								
17	VA	259,190	710																								
18	WI	226,943	622																								

Table 0-1 continued

#	State	# of records	ADTT	2005												2006											
				1	2	3	4	5	6	7	8	9	10	11	12	1	2	3	4	5	6	7	8	9	10	11	12
1	MS	5,914,950	2,967*																								
2	CA	13,458,818	8,366*	x	x	x																					
3	FL	4,143,162	2,558*																								
4	AR	1,675,349	3,919													x	x	x	x	x	x	x	x	x	x	x	x
5	AZ	1,466,033	4590													x	x	x	x	x	x	x	x	x	x	x	x
6	CO	343,603	941													x	x	x	x	x	x	x	x	x	x	x	x
7	DE	201,677	553													x	x	x	x	x	x	x	x	x	x	x	x
8	IL	854,075	2340													x	x	x	x	x	x	x	x	x	x	x	x
9	IN	185,267	508													x	x	x	x	x	x	x	x	x	x	x	x
10	LA	477,922	1309													x	x	x	x	x	x	x	x	x	x	x	x
11	MD	328,778	235													x	x	x	x	x	x	x	x	x	x	x	x
12	ME	183,576	503													x	x	x	x	x	x	x	x	x	x	x	x
13	MN	55,572	450													x	x	x	x	x	x	x	x	x	x	x	x
14	NM	725,382	1,667													x	x	x	x	x	x	x	x	x	x	x	x
15	PA	1,495,741	4098													x	x	x	x	x	x	x	x	x	x	x	x
16	TN	1,622,320	4445													x	x	x	x	x	x	x	x	x	x	x	x
17	VA	259,190	710													x	x	x	x	x	x	x	x	x	x	x	x
18	WI	226,943	622													x	x	x	x	x	x	x	x	x	x	x	x

* NCHRP data is for multilane cases, lane with maximum ADTT is listed

Originally, the WIM database from NCHRP and FHWA consisted of more than 65 million vehicles. Later, the WIM database from New York (about 8 million vehicles) was removed because of a considerable number of extremely heavy vehicles, which may significantly affect statistical parameters of live load for the US. A part of the WIM database from Indiana (about 13 million vehicles) was removed as well because of the different format of the recorded data.

3.4.3. ALDOT WIM Database

A considerable amount of WIM data was also obtained from the Alabama DOT within the project ALDOT 930-870 “WIM-Based Live Load for Alabama Bridges”. It was collected from 13 locations around the State (Figure 0-4). Initially, WIM database covered the period from 2009 until 2014. Further, it was completed with data recorded at the same WIM stations during 2006

to 2008. Previously, these records were used in the project "Development of Alabama Traffic Factors for Use in Mechanistic-Empirical Pavement Design" (Turochy et al. 2015). In 2016, this database was supplemented with the traffic records collected from 2014 until 2017 for project ALDOT-930-947 "Application of WIM and Permit Data."

The following information from each particular site was also specified: time of record, the direction of travel code, gross vehicle weight (GVW), vehicle type, axle spacing, axle loads, and vehicle speed. A summary of all the available records is presented in Table 0-2,

Table 0-3, Table 0-4, Table 0-5, Table 0-6 andTable 0-7 for each location identified with a station code, name, and year.

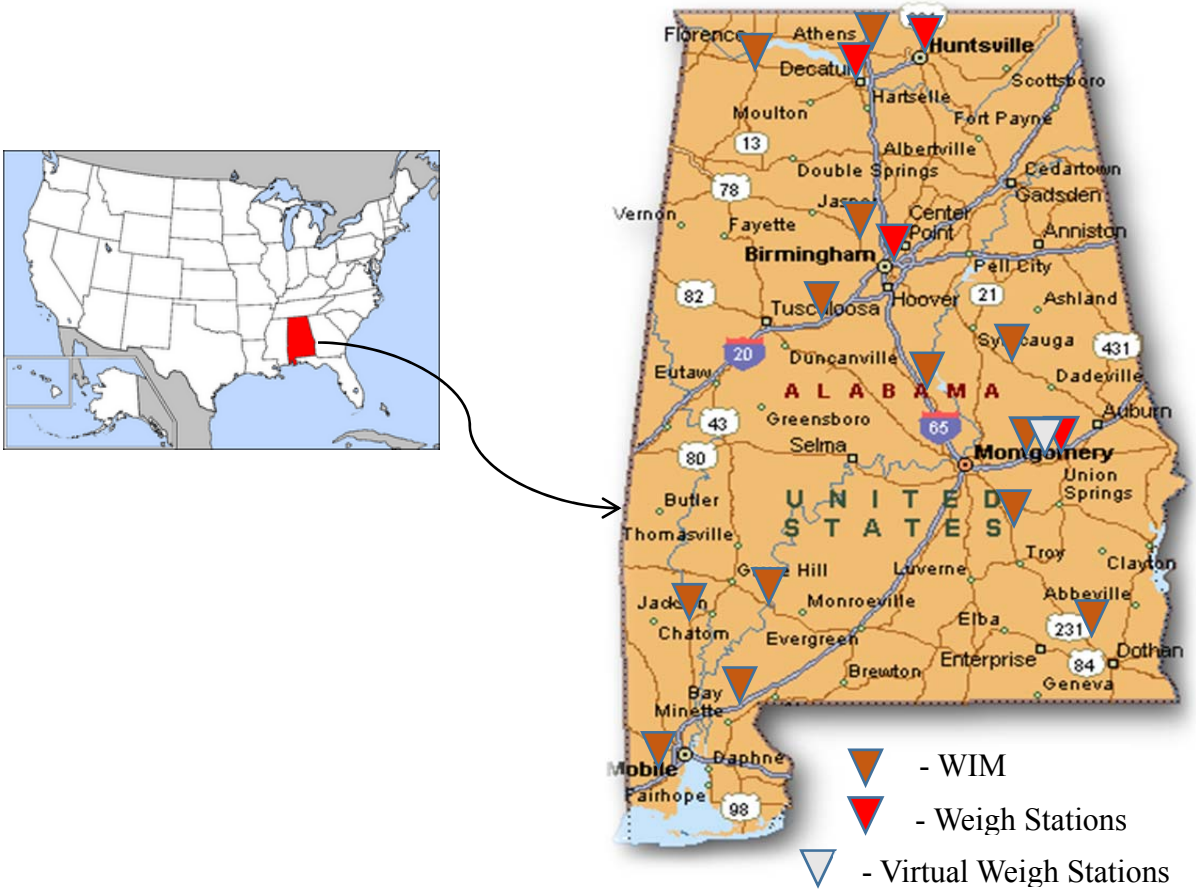

Figure 0-4.Locations of Traffic Data Recording Stations in Alabama

It was observed that some data points were recorded incorrectly. In particular, there are some monthly files, which are empty, containing corrupted records or data from different locations mixed together. There are also gaps in records due to planned maintenance or recalibration when the WIM systems are off. For example, WIM data from location 918 (Bucksville) which was corrupted for years 2009-2014, was later received undamaged for years 2006-2008 and processed (
Table 0-2 -Table 0-7). Later on, the traffic monitoring was terminated due to a system malfunction. For the rest of WIM sites, records were taken smoothly until January 2008 and then the data collection became terminated until January 2013.

Initial processing of available database was based on ensuring proper format and quality of records. Specially developed MATLAB (*MATLAB* 2014) routines were used to convert the original records in the TMG (*Traffic Monitoring Guide* 2001a) weigh format to MATLAB tables suitable for further analysis. The years and months covered are summarized in Table 0-2,

Table 0-3, Table 0-4, Table 0-5, Table 0-6 andTable 0-7.

Table 0-2. Summary of ALDOT WIM Data Used for Years 2006-2007

Station code	# of records	ADTT	2006												2007											
			1	2	3	4	5	6	7	8	9	10	11	12	1	2	3	4	5	6	7	8	9	10	11	12
911	1,487,440	928*	x	x	x	x	x	x	x	x	x	x	x	x	x	x	x	x	x	x	x	x	x	x	x	x
915	1,184,912	715*	x	x	x	x	x	x	x	x	x	x	x	x	x	x	x	x	x	x	x	x	x	x	x	x
918	7,614,736	5,563*	x	x	x	x	x	x	x	x	x	x	x	x	x	x	x	x	x	x	x	x	x	x	x	x
931	2,675,726	3,366*	x	x	x										x	x	x	x	x	x	x	x	x	x	x	x
933	2,448,277	2,051*	x	x	x	x	x	x	x	x	x	x	x	x	x	x	x	x	x	x						x
934	4,216,706	3,871*	x	x	x	x	x	x	x	x	x	x	x	x	x	x	x	x	x	x	x	x	x	x	x	x
942	2,894,247	2,354*	x	x	x	x	x	x	x	x	x	x	x	x	x	x	x	x	x	x	x	x	x	x	x	x
960	1,399,739	986*	x	x	x	x	x	x	x	x	x	x	x	x	x	x	x	x	x	x	x	x	x	x	x	x
961	4,145,031	3,361*	x	x	x	x	x	x	x	x	x	x	x	x	x	x	x	x	x	x	x	x	x	x	x	x
963	7,877,010	4,652*	x	x	x	x	x	x	x	x	x	x	x	x	x	x	x	x	x	x	x	x	x	x	x	x
964	1,056,145	867*	x	x	x	x	x	x	x	x	x	x	x	x	x	x	x	x	x	x						x
965	5,637,415	4,532*	x	x	x	x	x	x	x	x	x	x	x	x	x	x	x	x	x	x	x	x	x	x	x	x
US231	0	-																								
Total	42,637,384																									

*ALDOT data multilane cases, lane with maximum ADTT is listed

Table 0-3. Summary of ALDOT WIM Data Used for Years 2008-2009

Station code	# of records	ADTT	2008												2009											
			1	2	3	4	5	6	7	8	9	10	11	12	1	2	3	4	5	6	7	8	9	10	11	12
911	651,465	841*	x	x	x	x	x	x	x	x	x	x	x	x												
915	672,752	779*	x	x	x	x	x	x	x	x	x	x	x	x												
918	3,977,030	5,361*	x	x	x	x	x	x	x	x	x	x	x	x												
931	4,523,937	2,969*	x	x	x	x	x	x	x	x	x	x	x	x	x	x	x	x	x	x	x	x	x	x	x	x
933	2,732,737	1,404*	x	x	x	x	x	x	x	x	x	x	x	x	x	x	x	x	x	x	x	x	x	x	x	x
934	678,764	736*	x	x	x	x	x	x	x	x	x	x	x	x												
942	724,325	1,224*	x	x	x	x	x	x	x	x	x	x	x	x												
960	517,375	885*	x	x	x	x	x	x	x	x	x	x	x	x												
961	2,428,785	3,000*	x	x	x	x	x	x	x	x	x	x	x	x												
963	3,508,336	3,833*	x	x	x	x	x	x	x	x	x	x	x	x												
964	1,998,947	761*	x	x	x	x	x	x	x	x	x	x	x	x	x	x	x	x	x	x	x	x	x	x	x	x
965	2,491,993	4,235*	x	x	x	x	x	x	x	x	x	x	x	x												
US231	0	-																								
Total	24,906,446																									

*ALDOT data multilane cases, lane with maximum ADTT is listed

Table 0-4. Summary of ALDOT WIM Data Used for Years 2010-2011

Station code	# of records	ADTT	2010												2011											
			1	2	3	4	5	6	7	8	9	10	11	12	1	2	3	4	5	6	7	8	9	10	11	12
911	0	-																								
915	960,772	326*						x	x	x	x	x	x	x	x	x	x	x	x	x	x	x	x	x	x	x
918	0	-																								
931	5,403,914	2,104*	x	x	x	x	x	x	x	x	x	x	x	x	x	x	x	x	x	x	x	x	x	x	x	x
933	3,145,779	894*	x	x	x	x	x	x	x	x	x	x	x	x	x	x	x	x	x	x	x	x	x	x	x	x
934	0	-																								
942	0	-																								
960	0	-																								
961	0	-																								
963	0	-																								
964	2,420,485	813*	x	x	x	x	x	x	x	x	x	x	x	x	x	x	x	x	x	x	x	x	x	x	x	x
965	0	-																								
US231	0	-																								

Total	11,930,950																							

*ALDOT data multilane cases, lane with maximum ADTT is listed

Table 0-5. Summary of ALDOT WIM Data Used for Years 2012-2013

Station code	# of records	ADTT	2012												2013											
			1	2	3	4	5	6	7	8	9	10	11	12	1	2	3	4	5	6	7	8	9	10	11	12
911	353,633	-					x	x	x	x	x	x	x	x	x	x	x	x	x	x	x	x	x			x
915	366,051	354*	x	x											x	x	x	x	x	x	x	x	x			x
918	0	-	x	x	x	x	x	x	x	x	x	x	x	x												
931	0	-													x	x	x	x	x	x	x	x	x			x
933	630,507	751*													x	x	x	x	x	x	x	x	x			x
934	210,097	257*													x	x	x	x	x	x	x	x	x			
942	691,034	1,054*	x	x	x										x	x	x	x	x	x	x	x	x			x
960	328,867	414*	x	x		x	x	x							x	x	x	x	x	x	x	x	x			x
961	1,332,267	1,884*													x	x	x	x	x		x	x	x			x
963	2,981,883	1,251*	x	x	x	x	x	x	x	x	x	x	x	x			x	x	x	x	x	x	x			x
964	600,608	778*													x	x	x	x	x	x	x	x	x			x
965	106,269	-	x	x	x	x	x	x	x	x																x
US231	1,461,687	890*											x	x	x	x	x	x	x	x	x	x	x	x	x	x
Total	9,062,903																									

*ALDOT data multilane cases, lane with maximum ADTT is listed

Table 0-6. Summary of ALDOT WIM Data Used for Years 2014-2015

Station code	# of records	ADTT	2014												2015											
			1	2	3	4	5	6	7	8	9	10	11	12	1	2	3	4	5	6	7	8	9	10	11	12
911	1,956,343	483*	x	x	x	x	x	x	x	x	x	x	x	x	x	x	x	x	x	x	x	x	x	x	x	x
915	1,329,292	398*	x	x	x	x	x	x	x	x	x	x	x	x	x	x	x	x	x	x	x	x	x	x	x	x
918	1,283,147	821*	x	x	x	x	x	x	x	x	x	x	x	x	x	x	x	x	x							
931	7,680,440	2,011*	x	x	x	x	x	x	x	x	x	x	x	x	x	x	x	x	x	x	x	x	x	x	x	x
933	1,909,397	755*	x	x	x	x	x	x	x	x	x	x	x	x	x	x	x	x	x	x	x	x	x	x	x	x
934	1,204,983	236*	x	x	x	x	x	x	x	x	x	x	x	x	x	x	x	x	x	x	x	x	x	x	x	x
942	2,337,129	1,096*	x	x	x	x	x	x	x	x	x	x	x	x	x	x	x	x	x	x	x	x	x	x	x	x
960	1,030,981	443*	x	x	x	x	x	x	x	x	x	x	x	x	x	x	x	x	x	x	x	x	x	x	x	x
961	2,327,861	1,915*	x	x	x	x	x	x	x	x	x	x														x
963	13,591,823	2,636*	x	x	x	x	x	x	x	x	x	x	x	x	x	x	x	x	x	x	x	x	x	x	x	x
964	1,495,707	806*	x	x	x	x	x	x	x	x	x	x	x	x	x	x	x									x
965	4199160	2,480*	x	x	x	x	x	x	x	x	x	x	x	x	x	x	x	x	x	x	x					x
US231	0	-																								
Total	40,346,263																									

*ALDOT data multilane cases, lane with maximum ADTT is listed

Table 0-7. Summary of ALDOT WIM Data Used for Years 2016-2017

Station code	# of records	ADTT	2016												2017											
			1	2	3	4	5	6	7	8	9	10	11	12	1	2	3	4	5	6	7	8	9	10	11	12
911	1,714,002	557*	x	x	x	x	x	x	x	x	x	x	x	x	x	x	x									
915	975,224	417*	x	x	x	x	x	x	x	x	x	x	x	x	x	x	x									
918	0	-																								
931	5,195,995	2,008*	x	x	x	x	x	x	x	x	x	x	x	x	x	x	x									
933	1,029,090	670*	x	x	x	x	x	x	x	x	x	x	x	x	x	x	x									
934	787,864	228*	x	x	x	x	x	x	x	x	x	x	x	x	x	x	x									
942	1,464,460	1,162*	x	x	x	x	x	x	x	x	x	x	x	x	x	x	x									
960	695,249	431*	x	x	x	x	x	x	x	x	x	x	x	x	x	x	x									
961	2,432,085	2,113*	x	x	x	x	x	x	x	x	x	x	x	x	x	x	x									
963	3,406,241	3,169*	x	x	x	x	x																			
964	1,513,268	882*	x	x	x	x	x	x	x	x	x	x	x	x	x	x	x									
965	3,235,939	2,783*	x	x	x	x	x	x	x	x	x	x	x	x	x	x	x									
US231	0	-																								
Total	22,449,417																									

*ALDOT data multilane cases, lane with maximum ADTT is listed

3.5.Quality Control Procedure

Most of the time, WIM records are used by State DOTs to screen weight violators and to conduct statistical analysis of the traffic mix. A significant number of incorrectly recorded vehicles that create high load effects may lead to over-conservative design or unrealistically high estimated fatigue damage. There is a need to assure the high quality of recorded information since it is irregularly recorded and also due to various errors occurring during the recording process. Therefore, the development of the detailed quality control procedure was an essential step in this study.

A correctly installed and maintained WIM system can produce the high quality traffic data that bridge and transportation engineers can use for analysis (Pigman et al. 2012), (Quinley 2010). However, the raw data generated by any WIM system has to be validated and processed to exclude errors and incorrect records. There is a number of case studies related to traffic data quality checks that are analyzed and employed by many state agencies in the US (Turochy et al. 2015), (Elkins and Higgins 2008), (Southgate 1990), (Ramachandran et al. 2011), (Qu et al. 1997), (Quinley 2010), (SHRP 2 Research Reports 2015), Sivakumar et al. (2011), etc.). At the same time, there is no documented state-specific quality control (QC) procedure employed by Alabama DOT.

There are two types of errors occurring in long-term WIM data collection: random and systematic errors. Random errors always occur without a particular pattern, and they cannot be replicated by repeating the experiment. Systematic errors are constant and repeatable. This type of errors is usually associated with the malfunctioning of the WIM system, misrecording, non-typical vehicle configuration, or vehicle position with regard to the sensor, and other causes. As a result, the recorded database contains unrealistic vehicle configuration, zero GVW or axle load. Thus, the quality control (QC) algorithm has been developed to improve the quality of the data, to identify systematic errors and to increase the accuracy of the WIM measurements (*Traffic Monitoring Guide* 2016).

Selection and systematization of the quality control criteria are critical to ensure the accuracy of the data and eliminate the errors that can affect the further analysis. The first set of filtering criteria, so-called "logical" was developed based on the common practice reported in the literature (Hellenbeck 1994), (Buch et al. 2009), (Middleton et al. 2012), (Fiorillo and Ghosn

2016). These requirements can be applied instantly once a vehicle record is delivered to the database, as well as when a specific database has been accumulated. Special Matlab (*MATLAB* 2014) routine was developed to run the available database through the filtering algorithm summarized in Table 0-8.

Table 0-8. Quality Control Criteria for Available WIM Database

#	Filtering criterion	Reference
1	FHWA Class of vehicle less than 3 or larger than 14	(Systematics 2007), (SHRP 2 Research Reports 2015)
2	Individual axle weight less than 1kip	(Qu et al. 1997)
3	Individual axle weight and greater than 70kips	(SHRP 2 Research Reports 2015)
4	Individual axle spacing less than 3.3ft	Bridge Formula Weights- FHWA Freight Management and Operations" n.d.
5	Number of Axles = Number of Axle Spaces + 1	Ramachandran et al. (2011)
6	Sum of axle weights ≠GVW (± 10%)	Pelphrey et al. (2008)
7	Speed less than 10mph	(SHRP 2 Research Reports 2015)
8	Speed greater than 100mph	(SHRP 2 Research Reports 2015)
9	Minimum first axle spacing is less than 6ft for vehicle classes 4-13, (Systematics 2007)	Pelphrey et al. (2008)
10	Record in which the sum of the axle spacing lengths was less than 7ft	Pelphrey et al. (2008)
11	Sum of axle spacing ≠ wheelbase of truck (±1ft)	Sivakumar et al. (2011)
12	Sum of the axle spacing lengths was greater than 220ft	Sivakumar et al. (2011)
13	Records with identical records(rows)	

Vehicles with gross vehicle weight (GVW) less than 20 kips were also eliminated from further consideration as cars and lightweight traffic. The records that do not satisfy the criteria above were eliminated from analyzed WIM database (SHRP and ALDOT databases).

Initially, the obtained data included over 200 million records during 2005-2017. About 10 million records were filtered out from SHRP database (SHRP 2 Research Reports 2015) because of errors in reading. The remaining SHRP database consists of 34 million vehicles. The Alabama DOT (ALDOT) WIM database included over 151 million vehicles (Table 0-2, Table 0-3, Table 0-4, Table 0-5Table 0-6 and Table 0-7). Then, about 73 million vehicles with the lightweight or questionable configuration of axle loading were filtered out using the QC criteria (Table 0-8). Also, records collected from locations 918, 963 and US-231 were eliminated due to significant (over 70%) number of errors and different truck traffic statistics. Thus, the remaining ALDOT WIM database consists of 58 million vehicles. A summary of the WIM database after the filtering is shown in Table 0-9.

Besides incorrect records, all datasets also include legal, permit, and illegally overloaded vehicles. Thus, the remaining database was analyzed to determine trucks representing normal service traffic, which belongs to Strength I live load (AASHTO 2014). This group of traffic includes legal trucks, "grandfathered" exceptions, routine permits (Permits that do not require advanced individual routing) and illegally overloaded (Sivakumar et al. (2011), (Commernet, 2011 n.d.). To determine routine permit vehicles the algorithm based on state-specific regulation was developed and applied similarly to the Comprehensive Truck Size and Weight Study (Abowd et al. 1999). Apparently, each state Department of Transportation has a set of requirements limiting axle weight and total GVW to assure not exceedance of HL-93 design load by routinely permitted vehicles.

While legal, "grandfathered" and routinely permitted vehicles can be easily detected in the traffic flow based on state-specific weight regulations, it is still a complicated process to identify

illegally overloaded trucks that belong to the live load for Strength I without comprehensive study and cooperation with State DOTs.

There are a few approaches applied and described in the literature (Abowd et al. 1999), (Sivakumar et al. 2011), (A. O'Connor & Enevoldsen, 2009) and (OBrien et al. 2016).

Table 0-9. Number of Recorded Vehicles (NCHRP 12-76, FHWA and ALDOT data)

#	State	Station code	Total Number of Truck Records, N
1	Arizona	AZ SPS-1	35,572
		AZ SPS-2	1,430,461
2	Arkansas	AR SPS-2	1,675,349
3	Colorado	CO SPS-2	343,603
4	Delaware	DE SPS-1	201,677
5	Illinois	IL SPS-6	854,075
6	Indiana	IN SPS-6	185,267
7	Kansas	KS SPS-2	477,922
8	Louisiana	LA SPS-1	85,702
9	Maine	ME SPS-5	183,576
10	Maryland	MD SPS-5	164,389
11	Minnesota	MN SPS-5	55,572
12	New Mexico	NM SPS-1	117,102
		NM SPS-5	608,280
13	Pennsylvania	PA SPS-6	1,495,741
14	Tennessee	TN SPS-6	1,622,320
15	Virginia	VA SPS-1	259,190
16	Wisconsin	WI SPS-1	226,943
17	California	CA Antelope EB	837,667
		CA Antelope WB	943,147
		CA Bowman	651,090
		CA LA-710 NB	4,092,484
		CA LA-710 SB	4,661,287
		CA Lodi	3,298,499
18	Florida	FL I-10	1,641,480
		FL I-95	2,112,518
		FL US-29	389,164
19	Mississippi	MS I-10	1,965,022
		MS I-55U	1,232,223
		MS I-55R	1,333,268
		MS US-49	1,225,138
		MS US-61	159,299

20	Alabama	AL 911	2,354,130
		AL 915	2,415,890
		AL 931	12,839,543
		AL 933	6,040,557
		AL 934	3,703,494
		AL 942	5,263,320
		AL 960	2,229,743
		AL 961	7,060,813
	Total		95,415, 068

The second set of filtering criteria based on SHRP 2 Research Reports (2015) and "Super load" state permit regulation is summarized in **Error! Not a valid bookmark self-reference.**. In this chapter, vehicles fitting the gap between routine permits and trucks detected by the second set of filtering criteria are considered illegally overloaded and included in Strength I live load group. These records were identified and separated from the remaining data that represents Strength II traffic load. More detailed analysis of the load spectra produced by illegally overloaded vehicles is presented in Chapter 5.

Table 0-10. Filtering criteria for Strength I vehicular load

#	Filtering criterion	Reference
1	Total number of axles is less than 3, and GVW is more than 220kN (50kips)	(SHRP 2 Research Reports 2015)
2	Steering axle weight is more than 150kN (35kips)	
3	Individual axle weight is more than 200kN (50kips)	
4	Total GVW exceeds the state-restricted limit for "Superload."	

Finally, the WIM database accepted for the next steps of this study, representing Strength I limit state, consists of about 100 million records from 20 states, including legal trucks, "grandfathered" exceptions, routine permits, and illegally overloaded vehicles.

3.6. WIM Data Analysis

3.6.1. Vehicle Class Distribution

One or a few types of vehicles can control the live load model. The distribution of GVW and live load effects for each WIM site strongly depends on traffic mix, in particular, the dominating vehicle types. The configurations of vehicle classes are specified by the FHWA (Cambridge Systematics, Inc. 2007) as shown in Figure 0-5.

Vehicle classification is primarily based on the axle spacing configuration. Typically, WIM systems installed in the majority of locations process input data based on Scheme F (*Traffic Monitoring Guide* 2001), (Cambridge Systematics, Inc. 2007). The main principle is a comparison of the measured axial spacing with the corresponding values for individual vehicle classes. Then, vehicle class is verified based on the expected GVW and reclassified if needed.

The traffic mix composition for vehicles with GVW $\geq$ 20 kips was reviewed for each state, summarized in Table 0-11 and shown in Figure 0-6. It can be concluded, that vehicle class 9 (five-axle, single trailer truck - Figure 0-5) is the most common for many available locations in the US WIM database. However, in some states, vehicles of the other classes create a substantial portion of the traffic mix. Thus, class 5 (single unit, 2-axle trucks) is from 10 to 30 % of a total number of trucks in Delaware, Maryland, Florida, Mississippi and Virginia. Similarly, class 6 (single unit, 3-axle trucks) is 10% of a total number of trucks in Delaware and California, and class 10 (single trailer, 6 or more axle trucks) is 20% in Maryland (Table 0-11 and Figure 0-6).

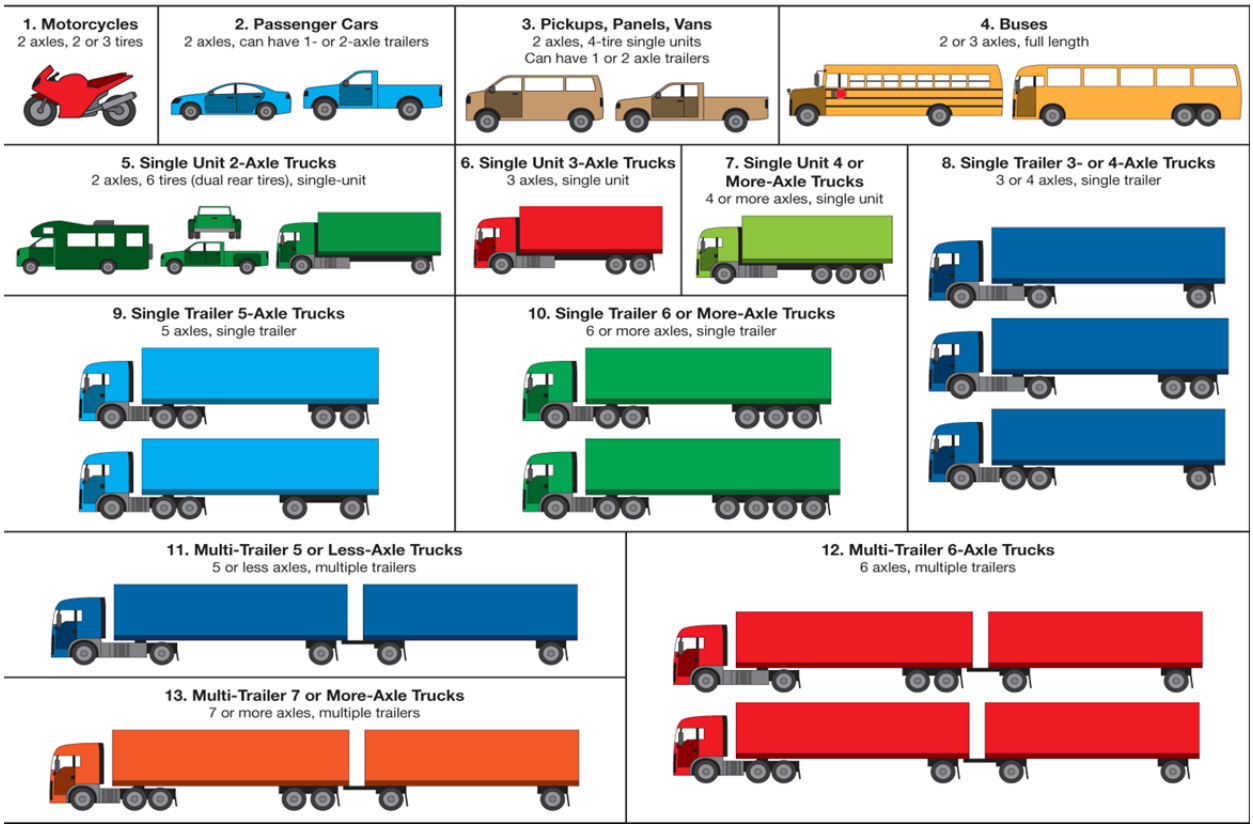

Figure 0-5. FHWA Vehicle Classification Scheme (Cambridge Systematics, Inc. 2007)

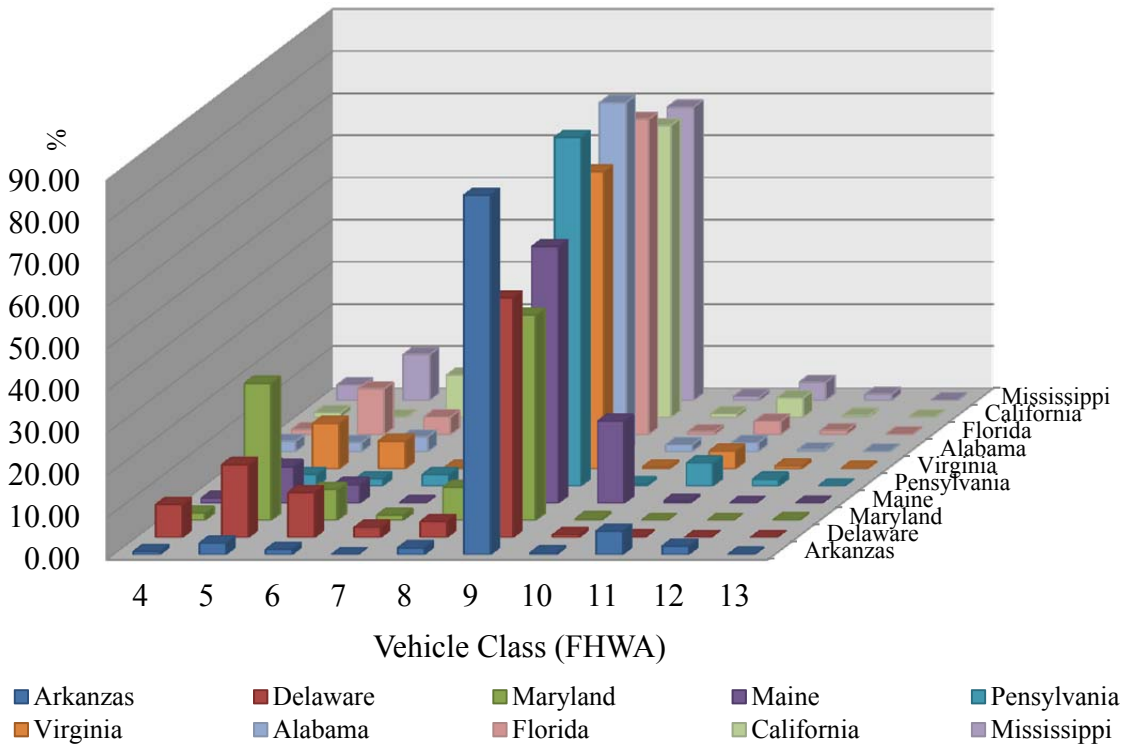

Figure 0-6: Percentage of Each Vehicle Class in the United States

Table 0-11. Percentage of Vehicles (GVW ≥ 20 kips) in Each Class for WIM Locations in the United States

	AR	DE	MD	ME	PA	VA	AL	FL	CA	MS
	2008	2008	2007-2009	2008	2008	2008	2006-2014	2005-2006	2006-2007	2006
4	0.75	7.85	1.74	1.16	0.83	0.86	2.46	1.25	1.15	3.62
5	2.76	17.36	32.56	8.72	2.73	10.75	2.20	10.84	0.15	10.81
6	1.23	10.71	7.33	4.43	1.83	6.65	3.59	4.17	10.04	3.78
7	0.07	2.42	1.28	0.14	2.72	0.37	0.58	0.47	0.17	0.04
8	1.65	3.83	7.84	4.53	1.46	5.36	3.91	3.58	3.08	5.44
9	85.3	56.88	48.67	60.9	82.68	70.45	82.80	74.77	69.29	69.56
10	0.45	0.66	0.38	19.47	0.59	0.56	1.65	0.71	0.89	0.88
11	5.63	0.19	0.01	0.58	5.46	4.21	2.15	3.15	4.64	4.30
12	2.04	0.04	0.01	0.04	1.63	0.68	0.51	0.95	0.56	1.47
13	0.12	0.05	0.18	0.08	0.07	0.10	0.15	0.12	0.15	0.09

3.6.1. Gross Vehicle Weight

The normal probability paper is used in this chapter to facilitate the interpretation of the results. The use of probability paper is presented in the available textbooks (Nowak and Collins 2012) and discussed in Subchapter **Error! Reference source not found.**. The difference in GVW distribution depends on vehicle configuration, level of loading and weight distribution.

The CDF's of GVW are plotted on the normal probability paper as shown in **Error! Reference source not found.**, Figure 0-8 and Figure 0-9 for each state and location in FHWA, NCHRP and ALDOT WIM databases respectively. Since the WIM data were collected from 45 WIM sites in the US, each of the 45 curves represents a different location and state. From **Error! Reference source not found.**,Figure 0-8 and Figure 0-9 it is evident, that GVW of the recorded traffic is not normally distributed, except the upper tails representing 1% maximum. The uneven shape of CDF's is a result of different types of vehicles in the WIM data. For example, a sharp almost vertical segment of each CDF curve at the level of 80 kips corresponds to the US legal load limit and relatively high population trucks carrying the maximum legal load ("Bridge Formula Weights- FHWA Freight Management and Operations" n.d.).

For comparison, the CDF of GVW of the vehicles in the Ontario truck survey (Agarwal and Wolkowicz 1976) is also shown in **Error! Reference source not found.**, Figure 0-8 and Figure 0-9. The relative position of the Ontario curve is a result of the intentional selection of seemingly heavy vehicles, albeit based solely on the appearance of the vehicles.

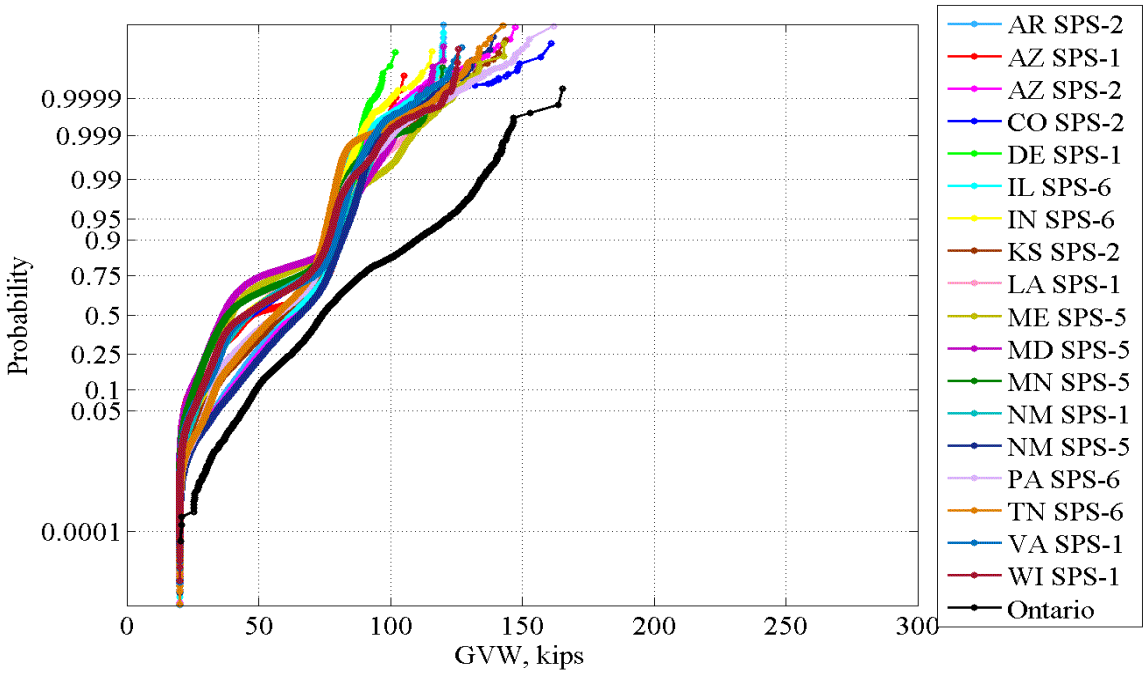

Figure 0-7.CDF's of GVW for all WIM Locations in FHWA Database

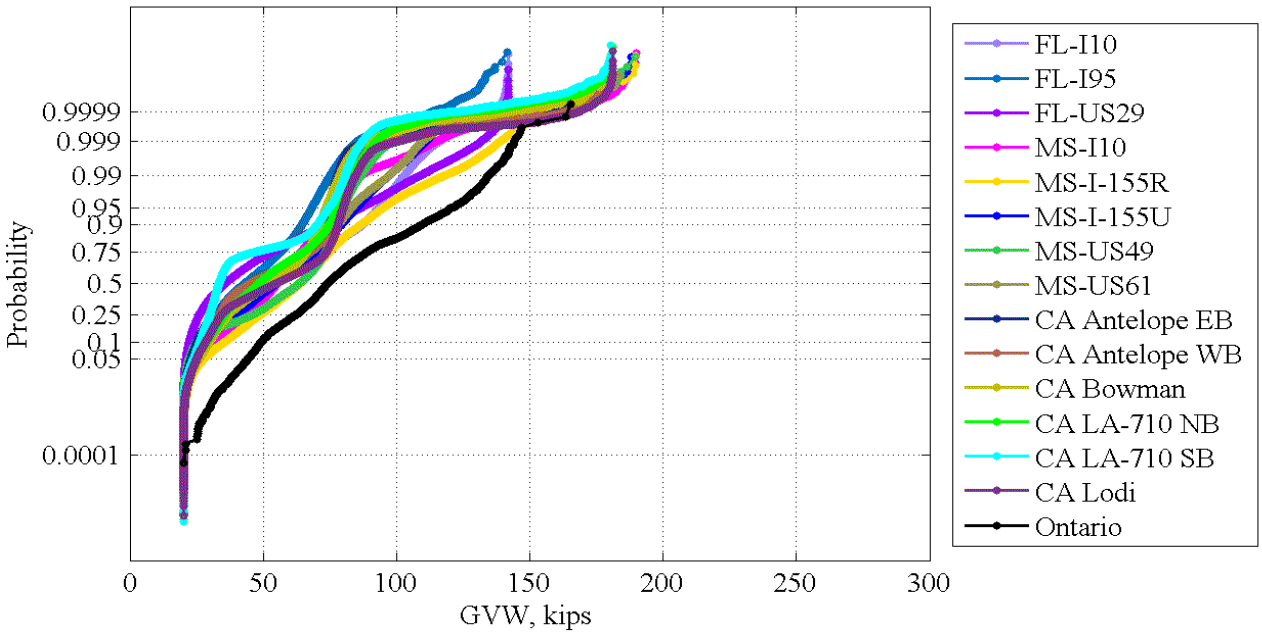

Figure 0-8. CDF's of GVW for all WIM Locations in NCHRP Database

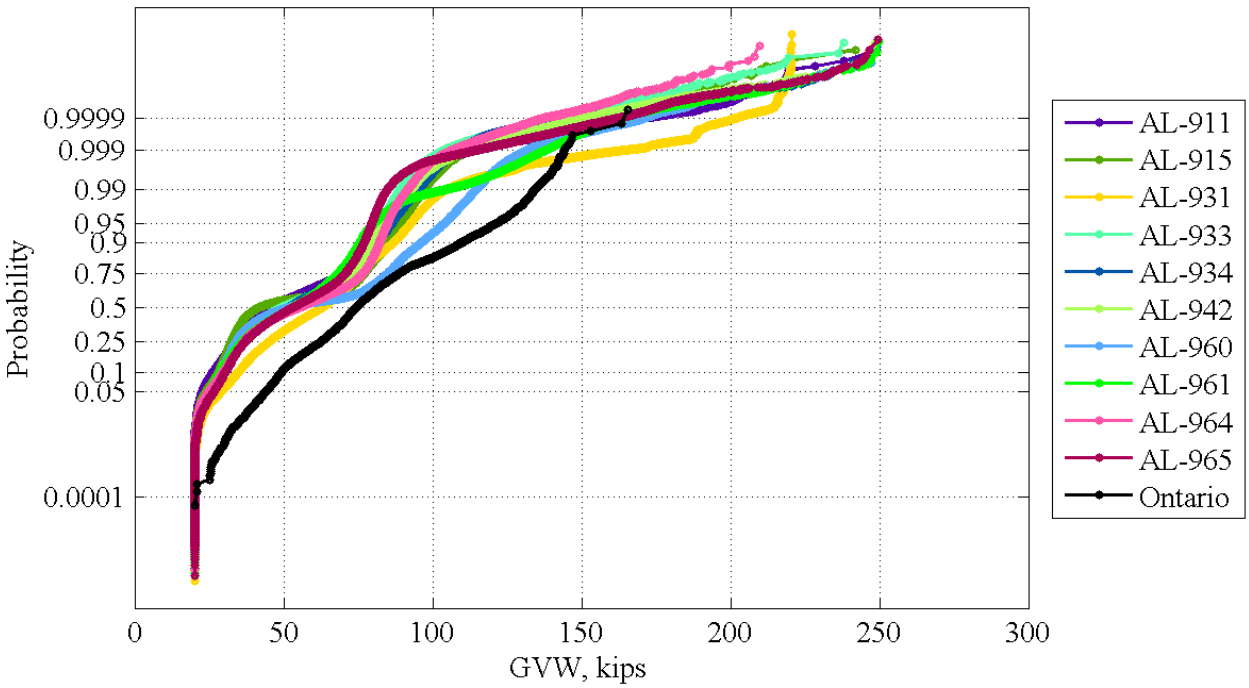

Figure 0-9. CDF's of GVW for all WIM Locations in ALDOT Database

The analysis of the plotted data indicates that the shape of the distribution is similar for almost all considered locations except the upper tails of CDF's. The statistical parameters, such as mean value, standard deviation, and coefficient of variation can be read directly from probability plot for each curve. The mean values range from 20 kips to 65 kips. All CDF's have also a vertical part, which corresponds to 20kips cut-off according to the filtering criteria. From 60 to 95 % of all trucks are lighter than 80 kips, about 15% are between 80kips and 150kips, and less than 1% are above 150kips. The slope of upper tails of the CDF's are similar, but the maximum values vary depending on the state permit regulations and truck traffic mix. For comparison, the maximum GVW for Ontario database is 160kips, while the mean value is 80kips.

The heaviest truck in ALDOT WIM database with GVW 300kips was recorded in location 960 (Whatley, US-84). Such vehicles belong to a "Super load" category of permits ("Title 32. Motor

Vehicles and Traffic" 2015) and thus, is not considered for the Strength I live load model. The configuration of the heaviest vehicle (Class 13 of FHWA Vehicle Classification Scheme) is shown in Figure 0-10.

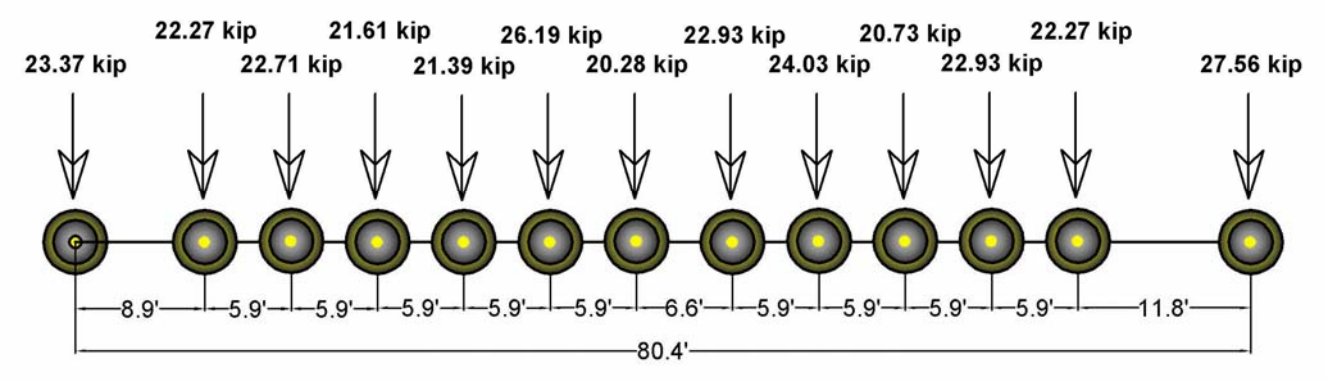

Figure 0-10. The heaviest vehicle in "Regular Traffic" category WIM database for Alabama (vehicle class 13, GVW-298 kips)

Although the WIM data from New York was not considered, the configuration of the heaviest recorded vehicle from that state is shown in Figure 0-11. GVW, total length, and configuration of axles indicate that it was a permitted vehicle. The WIM recording system categorizes those vehicles as Class 13 and 14 (Cambridge Systematics, Inc. 2007).

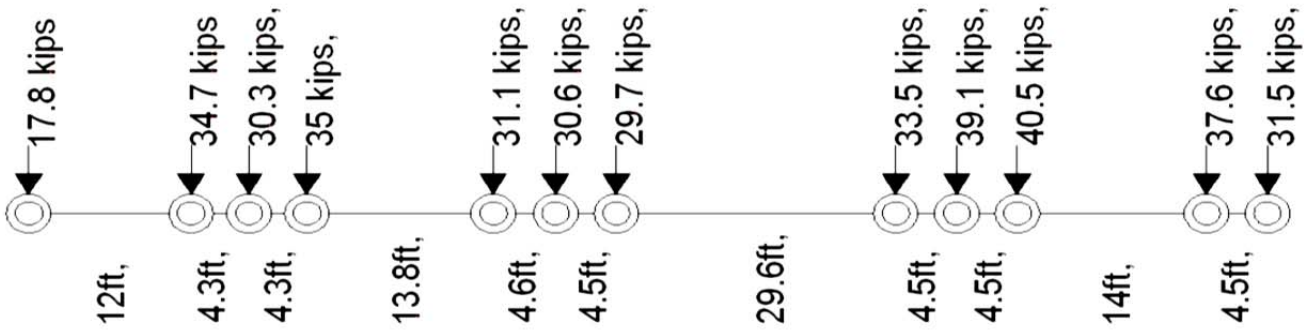

Figure 0-11: The Heaviest Vehicle in FHWA Database (Port Jervis, NY) – GVW 391 kips, L=100 ft

3.6.2. Live Load Effects

This subchapter is focused on the load effects, such as bending moment ratios. Statistical parameters for live load effects were calculated using the available WIM database described in Section 3.5. For each truck, a specially developed code(*MATLAB* 2014) was used to find the maximum value of the bending moment. The trucks from the WIM data were run over influence lines and for each vehicle, the maximum moment was computed. The calculations were performed for simply supported spans of 30, 60, 90, 120, and 200 ft. For an easier interpretation of the results, the obtained moments and shear forces were divided by the corresponding code-specified values, i.e., HL-93 live load effects (AASHTO LRFD, 2014). Two cases of HL-93 loading were considered: Design Tandem + Design Lane (Figure 0-12a); Design Truck + Design Lane (Figure 0-12b). The load combination, which creates the maximum moment for specific span length, controlled.

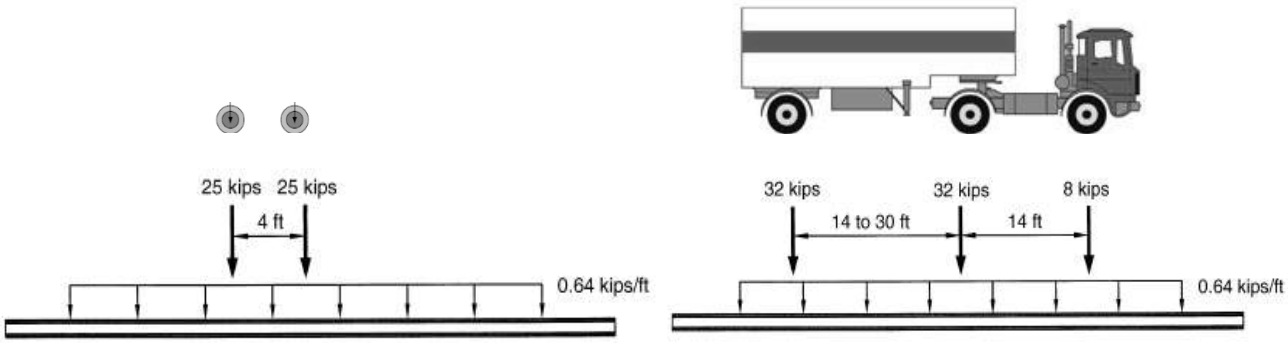

a) b)

Figure 0-12. HL-93 Loading Cases for Flexure (AASHTO LRFD, 2014)

Shear forces were calculated by running each recorded WIM truck over influence lines using the same MATLAB routine as for moments. The same span lengths were chosen for computing the

shear forces. Maximum in the envelope shear forces caused by each WIM truck was divided by the corresponding tabulated shear forces caused by HL-93 loading (AASHTO LRFD, 2014). Unlike in the case of bending moment, only one case of HL-93 loading is considered for all span lengths: Design Truck + Design Lane (Figure 0-13).

The CDF's of the computed non-dimensional ratios for moments and shear forces were plotted on the normal probability paper for each location and year. The CDF's of resultant 30ft span moment ratios are shown in Figure 0-14, Figure 0-16 and

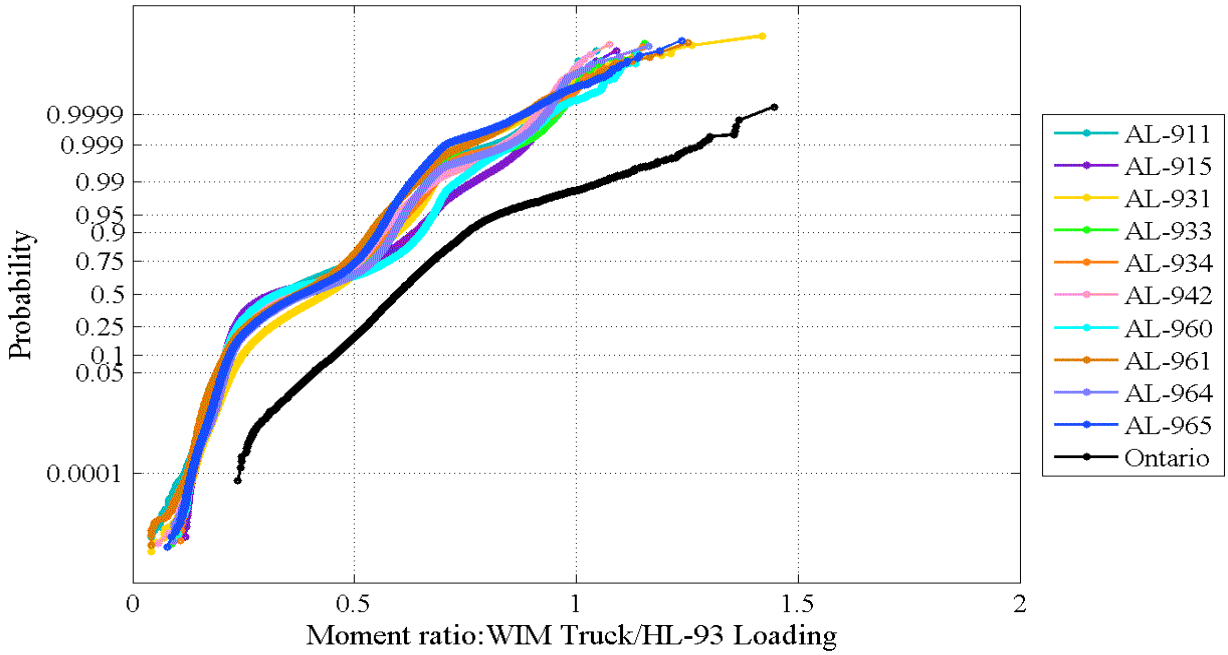

Figure 0-18 calculated for FHWA, NCHRP and ALDOT WIM database respectively. Similarly, moment ratios for long spans (200ft) were calculated for all available data and plotted on probability paper as it is shown in Figure 0-15, Figure 0-17 and Figure 0-19. For comparison, the cumulative distribution function of live load effect ratios calculated for the Ontario trucks for the same span lengths and plotted on Figure 0-14 -Figure 0-19. The FHWA and NCHRP 12-76 WIM data mostly contains records from only one location in each state and covering up to one year.

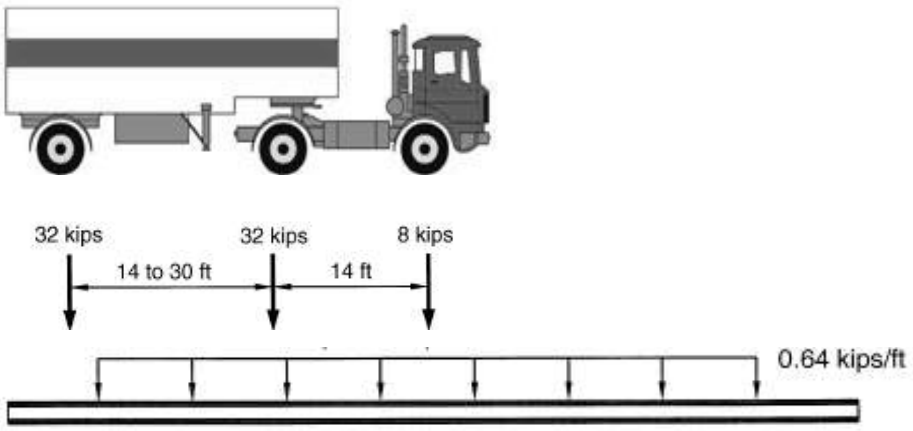

Figure 0-13: HL-93 Loading Case for Shear Force (*AASHTO LRFD* 2014)

The shape of CDF curves is similar for each location but the maximum value depends on the number of records. The larger is number of recorded vehicles, the larger probability of having a very large moment ratio. The shear force ratios are distributed similarly to the corresponding moment ratios for short (30ft) (Figure 0-20, Figure 0-22 and

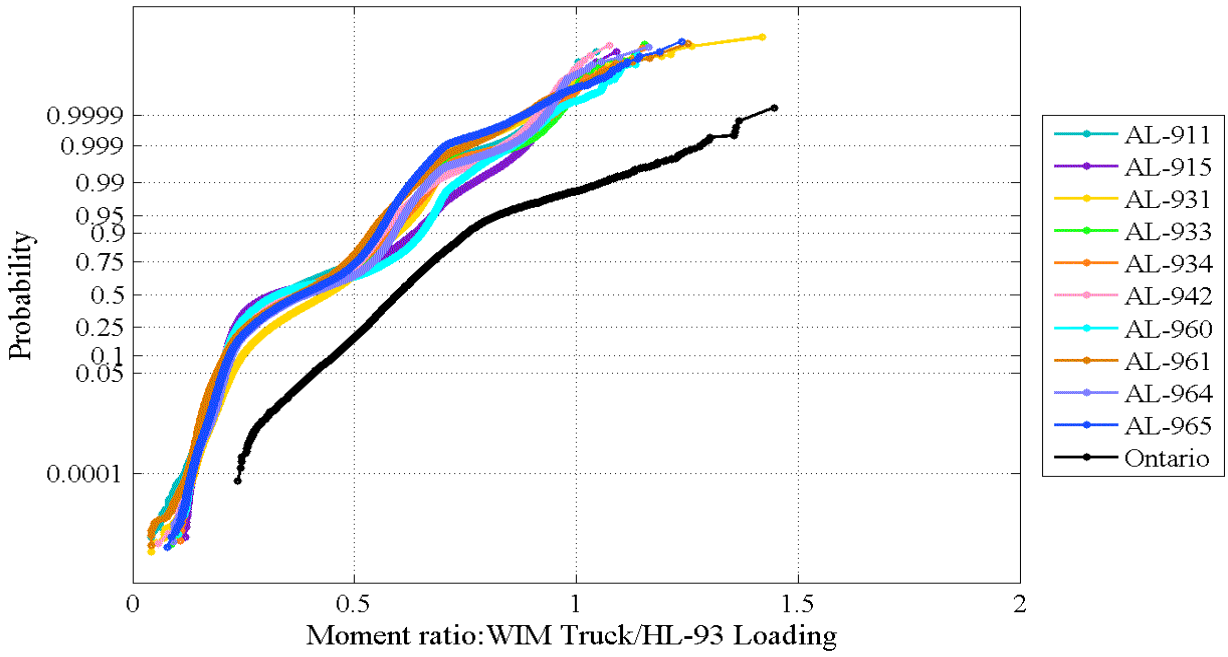

Figure 0-24) and long (200ft) (Figure 0-21, Figure 0-23 and Figure 0-25) span lengths.

The mean values for the moment and shear force ratio varies from 0.3 to 0.5 for all considered span lengths for FHWA, NCHRP and ALDOT WIM databases. The maximum value for each moment ratio is 1.0 to 1.5 for most cases. It also can be observed, that the mean value of the ratio for both moment and shear force gradually decreases for longer spans in most cases. At the same time, the of CDFs of Ontario moment ratios significantly outlies from the rest of the data.

For each location, the shape of the obtained CDF curves is very similar to that of GVW. However, live load parameters are very sensitive to the span length and axial configuration of the vehicle. For example, in some cases (CA-Lodi, CA LA-710SB – NCHRP data) the maximum values of moment ratios for long spans (200ft) are higher than for short spans (30ft). The heaviest vehicles in these locations mostly belong to class 13 (multi-trailer, 7 or more – axle truck) 14 or 15 (undefined by FHWA classification – Figure 0-5) with uniformly distributed GVW over the multiple axles. The short span moment ratios reflect mostly the effects caused by short vehicles or closely spaced axial loads (such as tandems and tridems). These vehicles control the upper tail of CDFs in Alabama data for recent years 2013-2017.

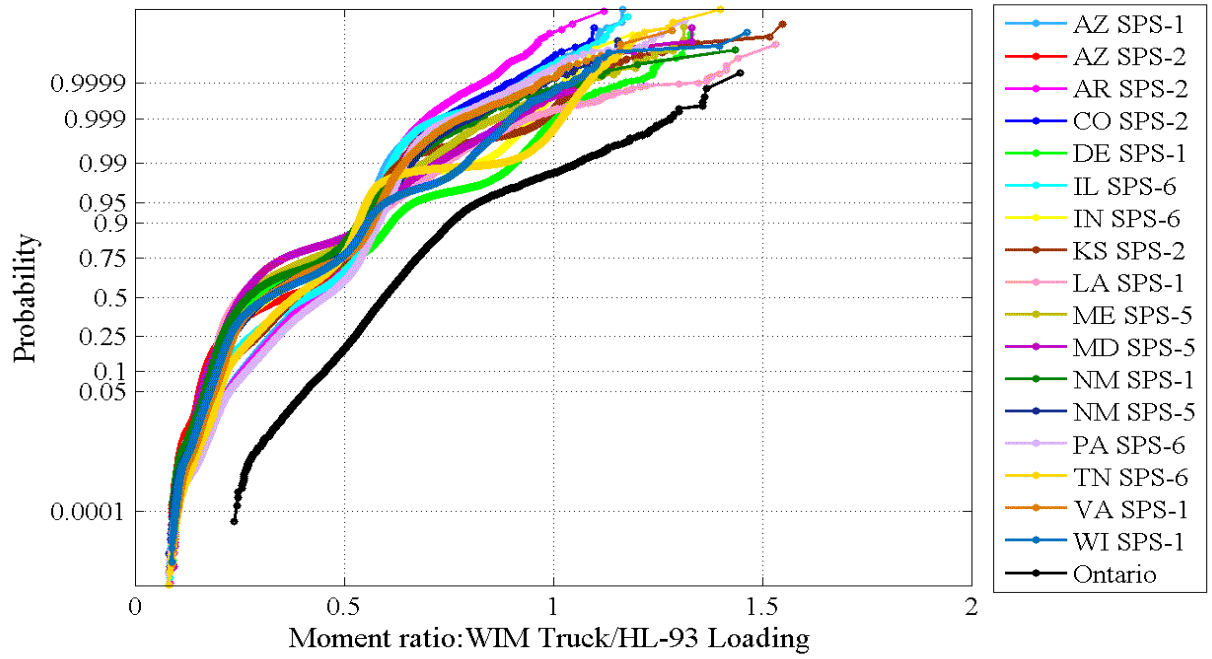

Figure 0-14. CDF plot for FHWA WIM Database Moment Ratio for 30ft Span for all Available WIM Sites

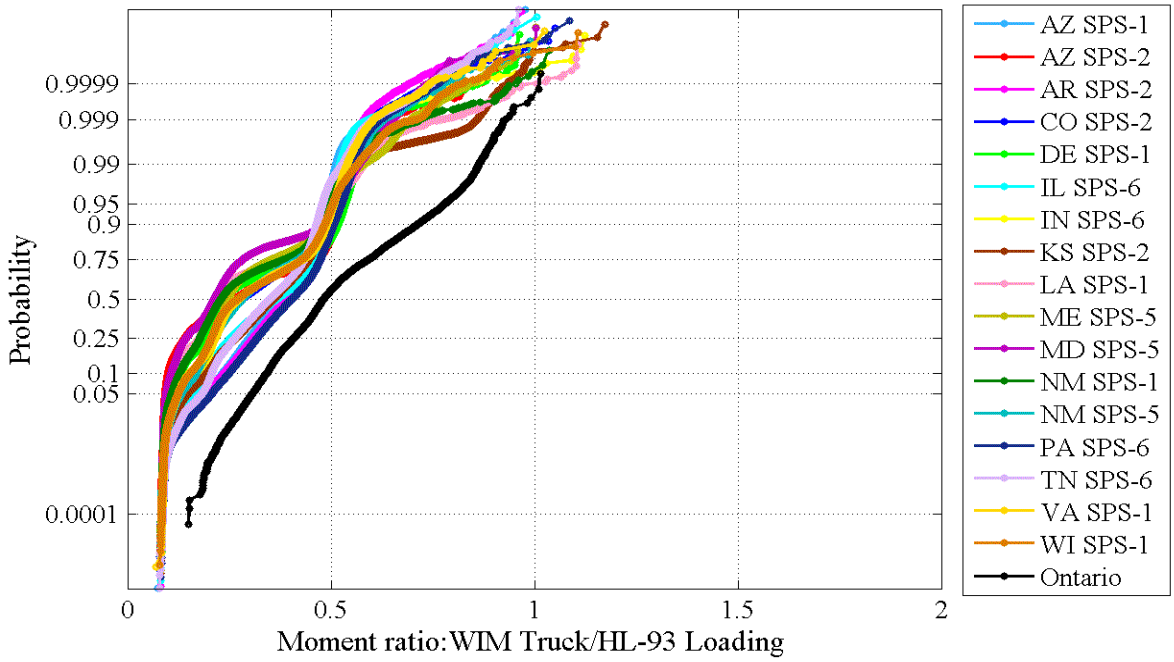

Figure 0-15. CDF Plot for FHWA WIM Database Moment Ratio for 200ft Span for all Available WIM Sites

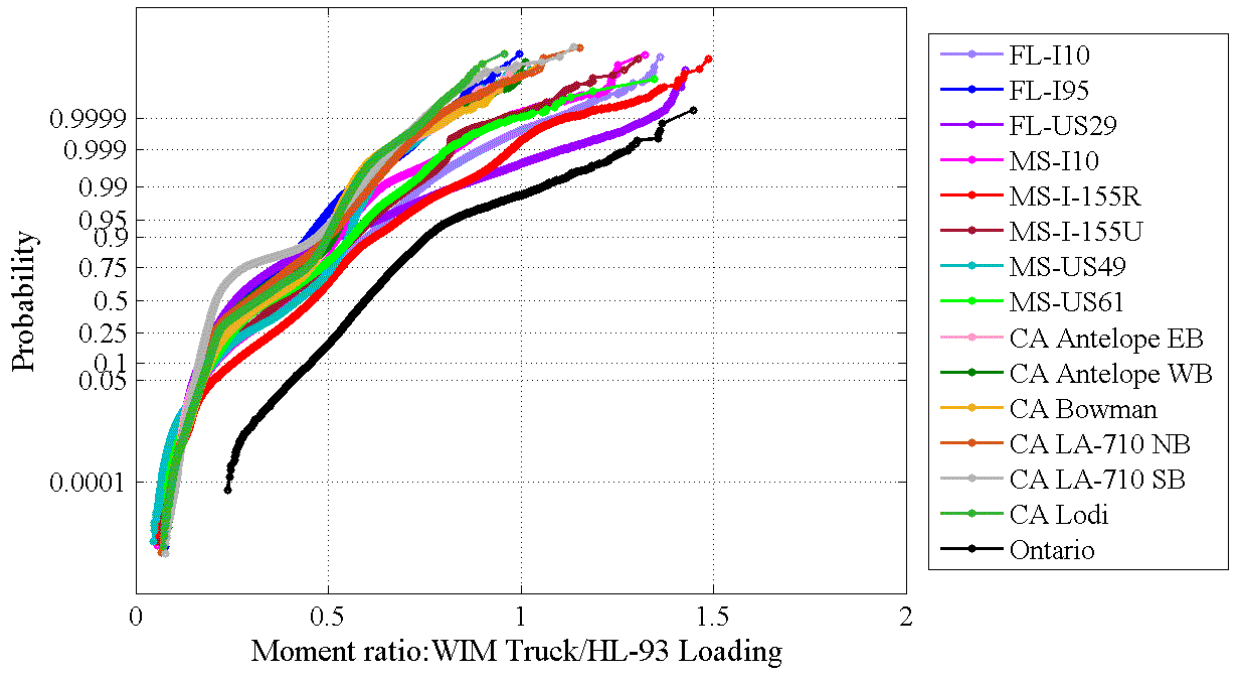

Figure 0-16. CDF Plot for NCHRP WIM Database Moment Ratio for 30ft Span for All Available WIM Sites

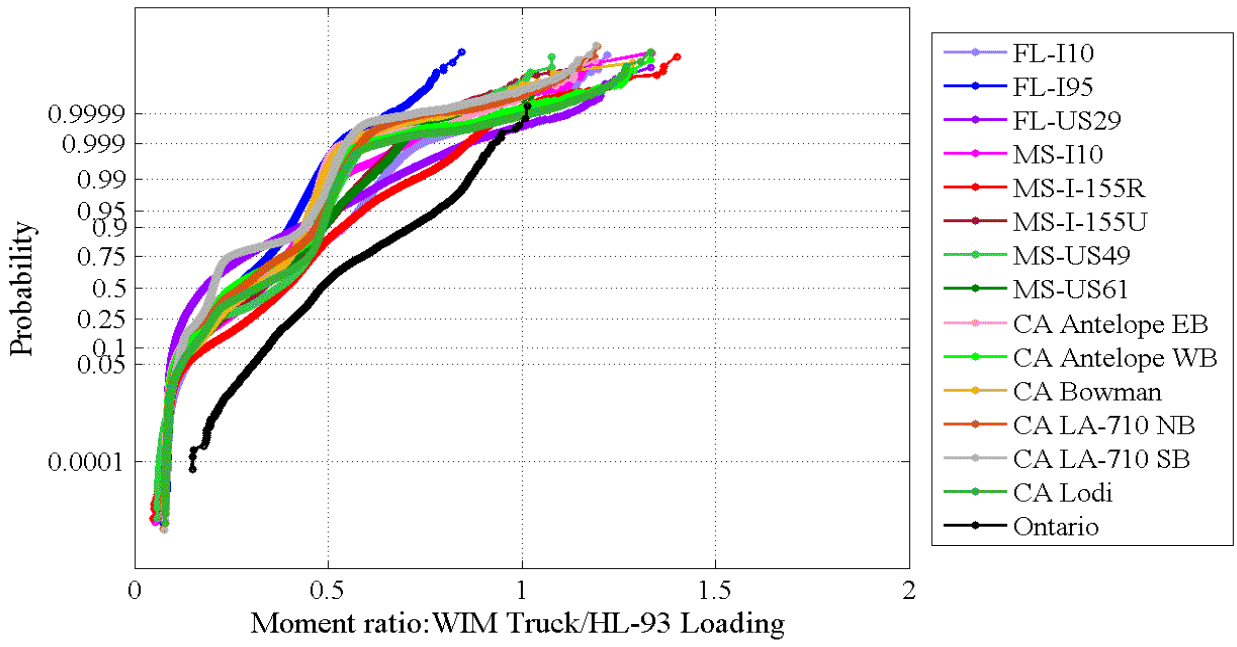

Figure 0-17. CDF Plot for NCHRP WIM Database Moment Ratio for 200ft Span for All Available WIM Sites

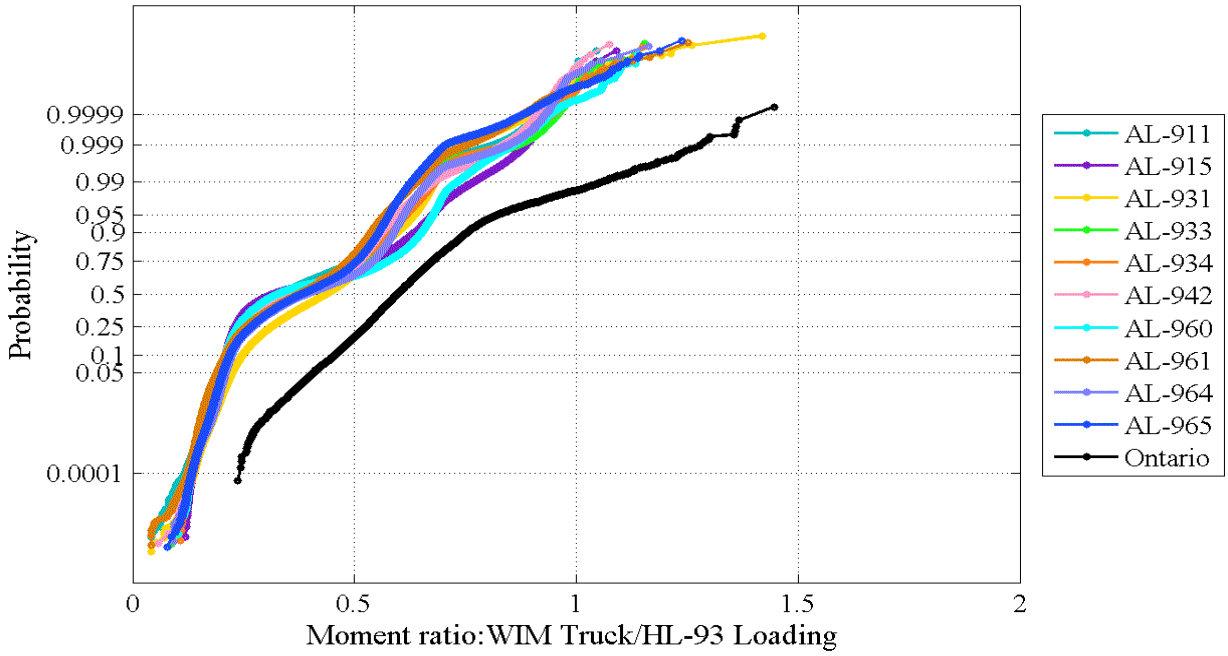

Figure 0-18. CDF Plot for ALDOT WIM Database Moment Ratio for 30ft Span for All Available WIM Sites

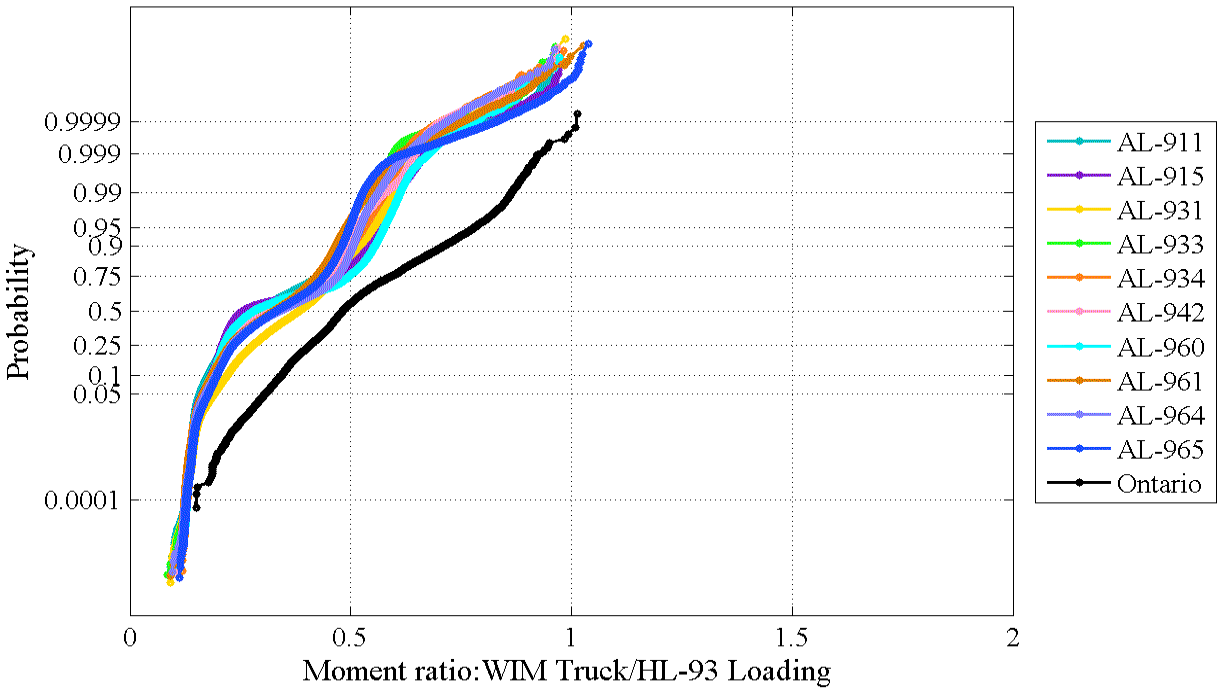

Figure 0-19. CDF Plot for NCHRP WIM Database Moment Ratio for 200ft Span for All Available WIM Sites

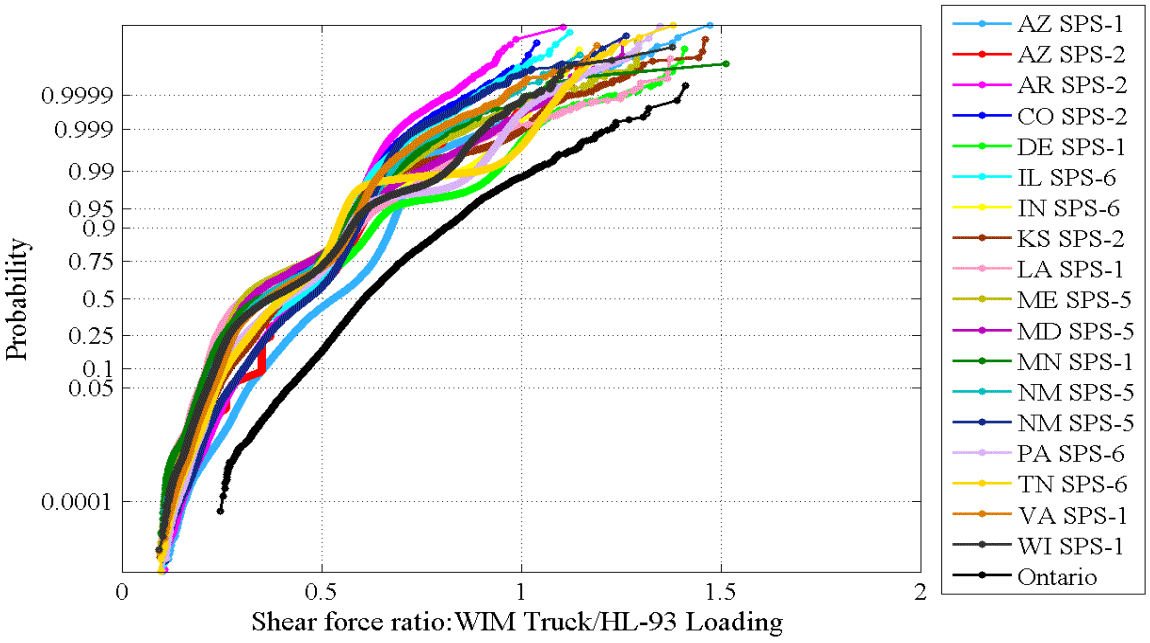

Figure 0-20. CDF Plot for FHWA WIM Database Shear Force Ratio for 30ft Span for All Available WIM Sites

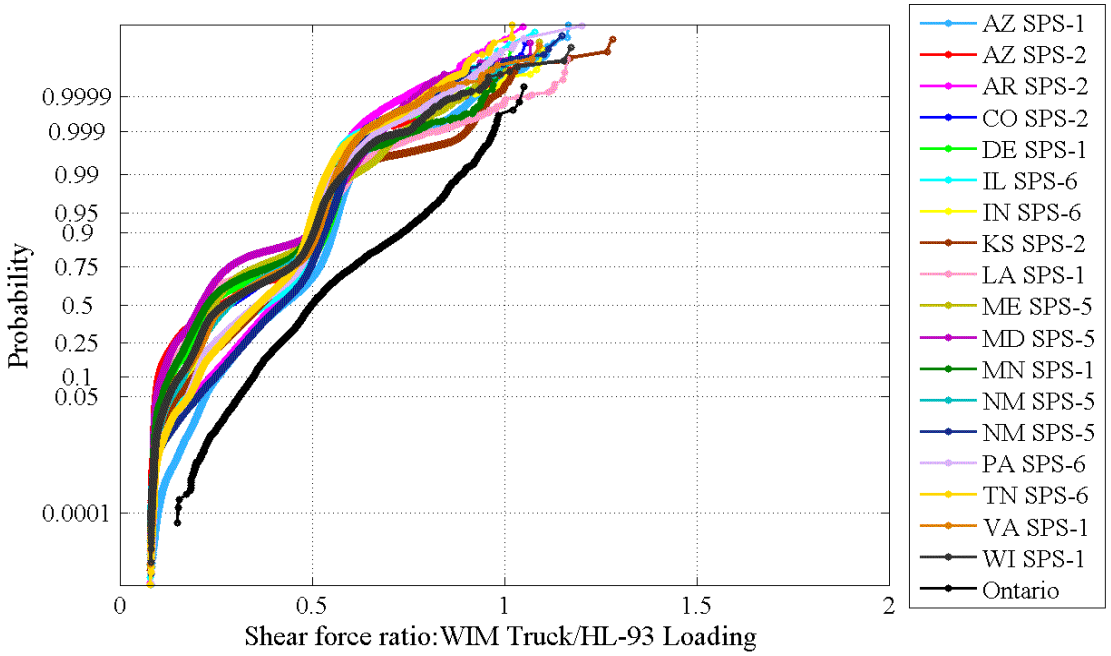

Figure 0-21. CDF Plot for FHWA WIM Database Shear Force Ratio for 200ft Span for All Available WIM Sites

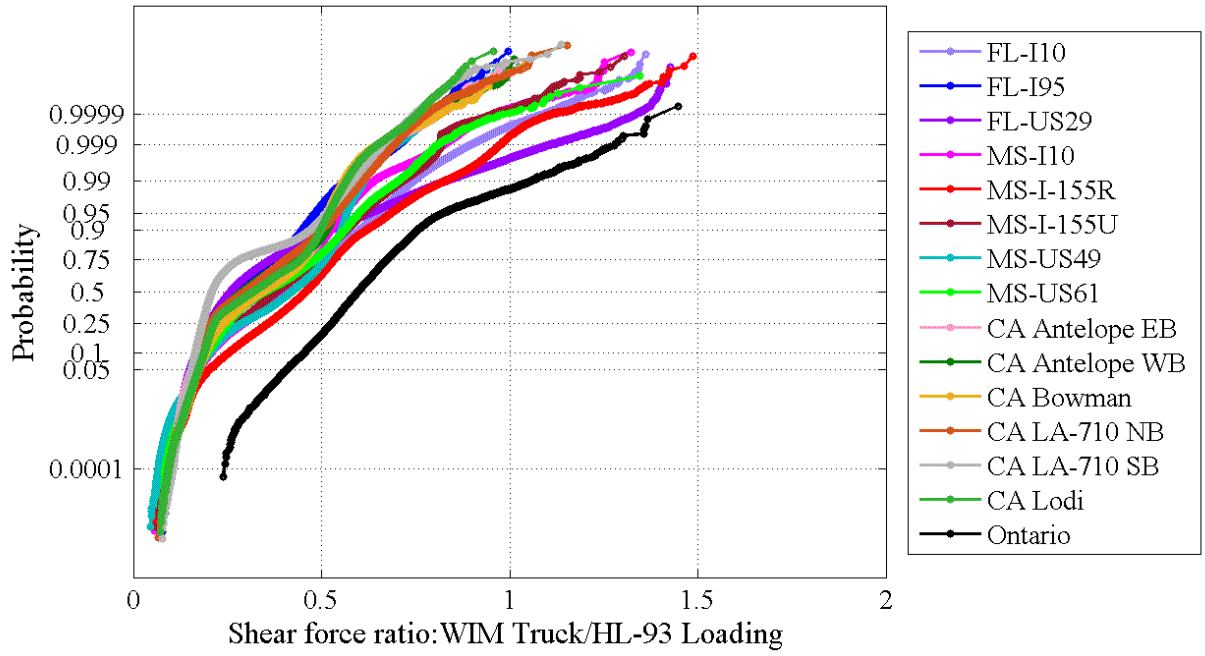

Figure 0-22. CDF Plot for NCHRP WIM Database Shear Force Ratio for 30ft Span for All Available WIM Sites

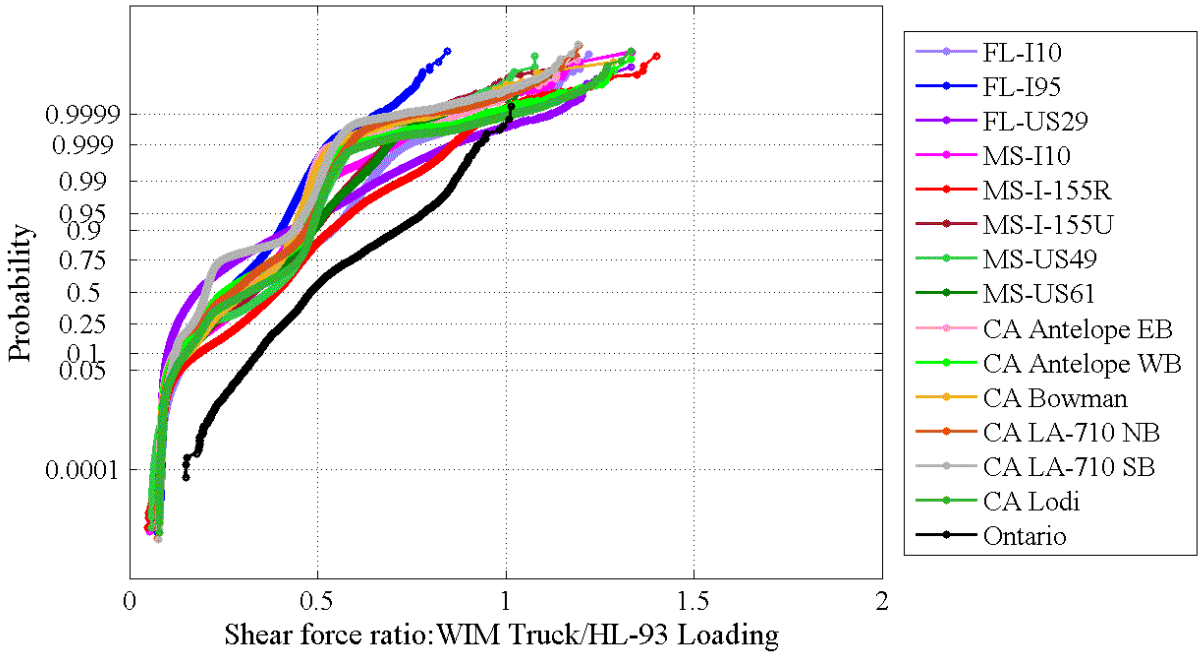

Figure 0-23. CDF Plot for NCHRP WIM Database Shear Force Ratio for 200ft Span for All Available WIM Sites

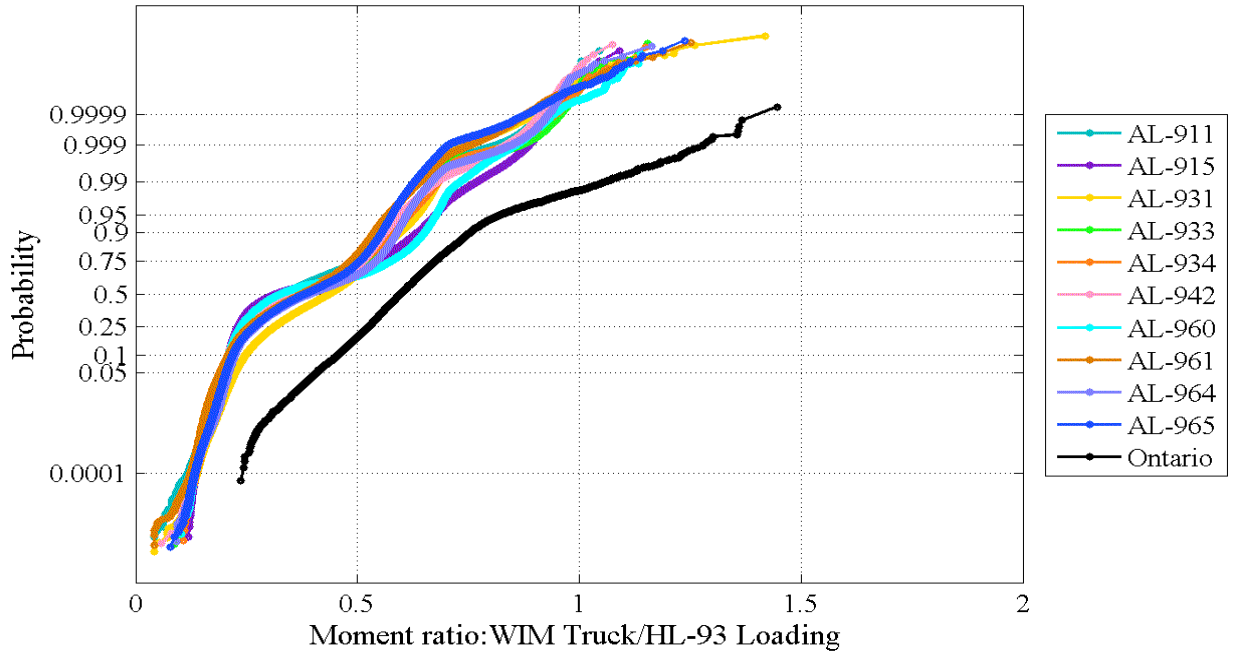

Figure 0-24. CDF Plot for ALDOT WIM Database Shear Force Ratio for 30ft Span for All Available WIM Sites

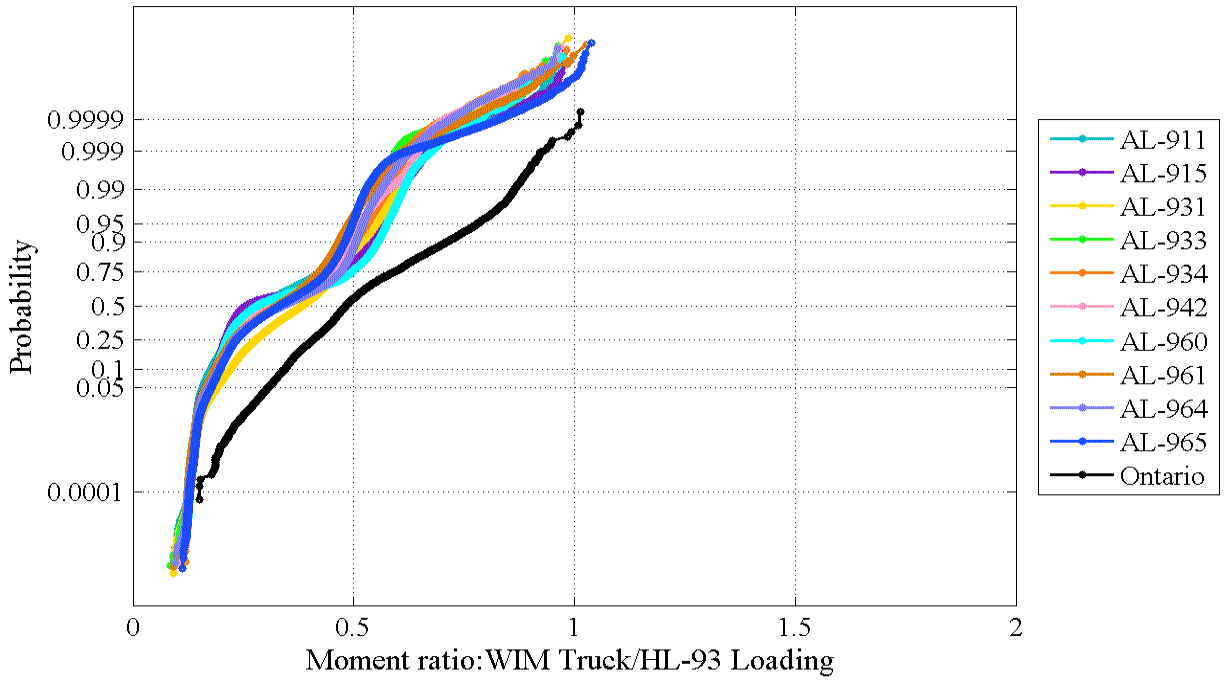

Figure 0-25. CDF Plot for NCHRP WIM Database Shear Force Ratio for 200ft Span for All Available WIM Sites

Statistical Live Load Model

4.1. Summary

Accurate design of bridges requires an adequate prediction of expected live load spectra for service period. It depends on the limit state considered. Since the present study is focused on live load for Strength I Limit State; the maximum expected live load is considered for 75-years economic lifetime of a bridge (AASHTO 2014). The objective of this chapter is to derive the maximum expected live load effects for periods from one day to 75 years. Usually, the live load for bridges consists of two components: static (*LL*) and dynamic (*I*) load (Nowak 1993). Since most of WIM systems are designed to eliminate the dynamic impact, only the static component is considered in this study. As a result, statistical parameters for a design live load representative for the whole country are proposed.

4.2.Review of Available Extrapolation Methods

Although there are substantial traffic databases collected for the recent decades, it is still insufficient to determine the maximum live load that the bridge may experience during the entire service period. Thus, there is a need for an efficient and reliable technique to predict the extreme load effect.

4.2.1. Exponential Extrapolation Model

There are few methods developed to assess the maximum expected live load effect for a given period. Nowak and Lind (Nowak and Lind 1979) introduce one of them to determine a 50- years maximum bending moment for the *Calibration of the Ontario Highway Bridge Design Code 1991 Edition* (1994). The truck survey conducted by the Ontario Ministry of Transportation (Agarwal and Wolkowicz 1976) was taken as a basis to obtain the live load effects statistics.

It was observed that the upper tail of the bending moment can be fit with a straight line on an exponential scale. Thus, it can be extrapolated up to the required probability ordinate using exponential function ($\boldsymbol{F_{50}(x) = 1 - exp(-x)}$ Equation 0-1), (Nowak and Grouni 1994).

$$\boldsymbol{F_{50}(x) = 1 - exp(-x)} \qquad \textbf{Equation 0-1}$$

The maximum mid-span bending moment was determined for the heaviest trucks in the survey. The simple span lengths varied from 10 to 200 ft. Then each moment was divided by corresponding nominal the OHBDC truck moment (Nowak and Grouni 1994). As example the moment ratios calculated for Florida I-10 WIM site are extrapolated is shown in Figure 0-1. The non-dimensional moment ratios were plotted using a logarithmic scale, where the vertical scale represented the natural logarithm of the number of trucks per given period. The distributions of moment ratio for each span were plotted in ascending order, with the maximum value corresponding to a zero at the vertical scale (log(1)=0).

The maximum expected moment for 50 years return period, LL_{50}, was assessed by using exponential extrapolation function from the largest values of the moment ratio. The expected

population of trucks passing a bridge during 50 years was assumed to be 600 times larger than the number of surveyed trucks.

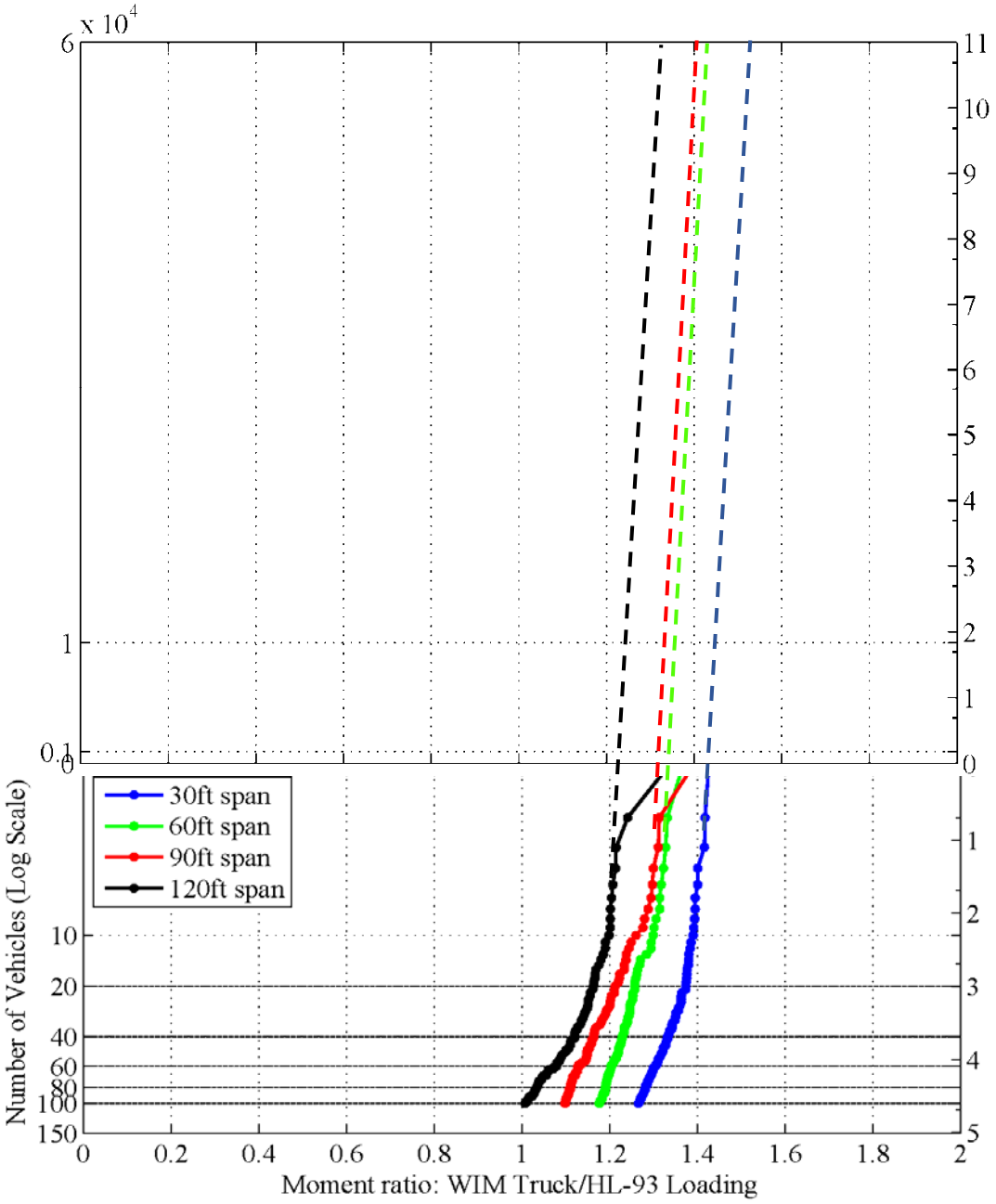

Figure 0-1. Exponential extrapolation of the upper tail (Nowak and Lind 1979)

This approach was further modified by revisiting the concept of extreme trucks. The importance of including the heaviest trucks in the database was verified by applying the sensitivity analysis. It was concluded, that the maximum GVW is not necessarily corresponded to the maximum load effect and therefore can not determine the maximum expected 50-years ratio.

4.2.2. Linear Extrapolation Model

Further on, this method was improved by Nowak and Hong (Nowak and Hong 1991) using the same 1975 Ontario truck survey database(Agarwal and Wolkowicz 1976). The authors made numerous assumptions related to the truck multiple presence statistics, involving different levels of correlation between the truck configurations. If there was no correlation between truck moving side-by-side, the Turksta's rule (Turkstra 1970) was utilized to determine the most severe load combination in 50-years period.

In this model, the cumulative distribution function of the live load effect was plotted on probability paper and analyzed, as it is shown in Figure 0-2. Instead of probability scale, the corresponding inverse standard normal variable scale was used for the vertical axis. The distribution function for 50-years maximum live load effect was derived from the primary equation for the maximum value in cumulative distribution function:

$$\boldsymbol{F_n(x) = [F(x)]^n} \qquad \textbf{Equation 0-2}$$

Where: *n* – is a number of values in a sample field.

Similarly, the expected load effect for 50-year service life can be determined as:

$$\boldsymbol{F_{50}(x) = [F_{ave}(x)]^n} \qquad \textbf{Equation 0-3}$$

Where: F_{ave} – CDF of the arbitrary-point-in-time load effect.

It was also concluded that the upper tail of the CDF of load effect (bending moment ratio) approaches the Gaussian distribution with the increase of the number of records. At the same time, the rest of the data may not be distributed normally or follow any known distribution function (Nowak 1994). Thus, the upper tail of the cumulative distribution function can be extrapolated with any type of a linear regression model (Figure 0-2).

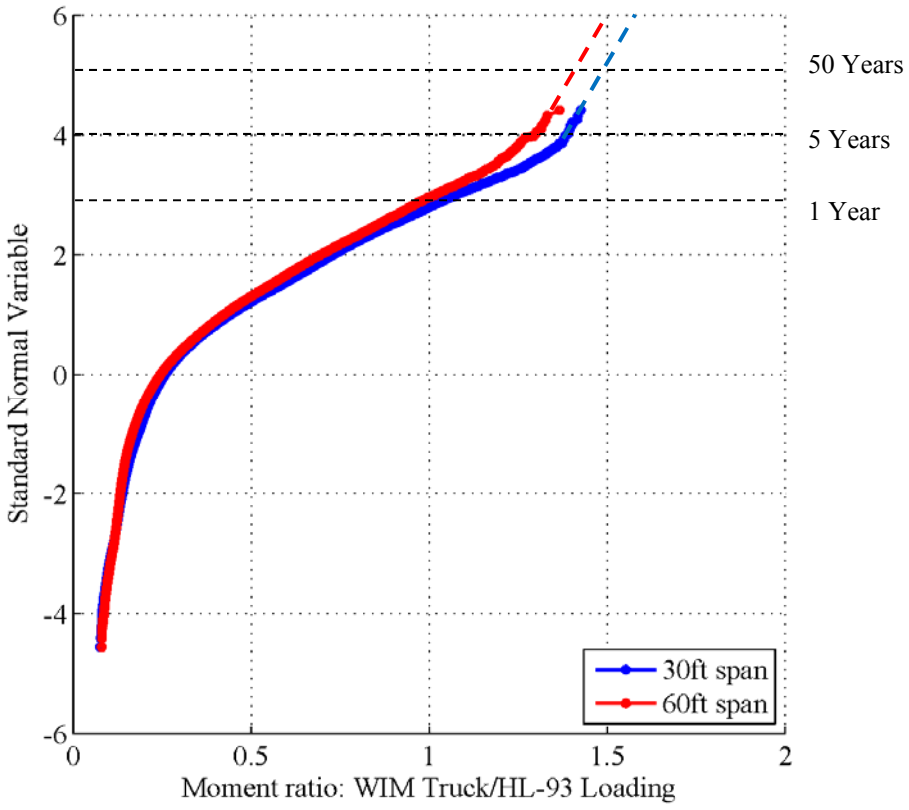

Figure 0-2. Linear extrapolation of the upper tail of the CDF of the moment ratio (A. Nowak & Hong, 1991)

In this study (Nowak and Hong 1991), it was assumed that the available truck survey data represent the 2-week maximum live load effect. Therefore, the database needed to determine the

50-years maxima has to be 1000 times larger. The analysis was performed for different classes of highway (A, B, C1, C2 - (*Ontario Highway Bridge Design Code* 1983) with regard to the traffic population.

This method was further applied to develop the statistical live load model for the current AASHTO LRFD (Nowak 1999). Later, to evaluate the HL-93 design load model using the recently collected WIM data, Nowak and Hong's linear extrapolation model was used in the SHRP Project (SHRP 2 Research Reports 2015).

4.2.3. Ghosn and Moses' Model

Ghosn and Moses applied the multi-dimensional stochastic approach to developing a live load model based on WIM data collected in Ohio (Ghosn and Moses 1984). This method takes into consideration the critical factors directly affecting the expected bridge live load, such as multi-lane distribution, multiple presence, girder distribution, and future traffic growth factors.

According to Ghosn and Moses the maximum live load effect for 50-years return period can be determined as:

$$\boldsymbol{LL_{50} = a\, m\, H\, W_{0.95}} \qquad \textbf{Equation 0-4}$$

Where: LL_{50} – maximum live load effect expected during 50-years bridge service life.

a – factor that depends on truck configuration and span length.

H – headway factor.

W_{95} – 95% of dominating truck weight.

To estimate the maximum live load effect (bending moment) acting on a single girder during a 50-year period, the following equation can be applied:

$$LL_{50_G} = LL_{50}\, g\, G_r \qquad \textbf{Equation 0-5}$$

Where: g – girder distribution factor.

G_r – future traffic load growth factor.

This technique was further recommended for

The application and comparison of the last two methods introduced in this chapter were performed by Tabsh (Tabsh 1990) to estimate the live load distribution for girder bridges (Table 0-1).

Table 0-1. Comparison of Bias Factors for Moment Ratios (Survey Truck/OHBDC Truck) (Tabsh 1990)

Span length, ft	40	60	80	100
Nowak and Hong's Linear	1.283	1.381	1.405	1.507
Ghosn and Moses' Model	1.134	1.035	1.130	1.218

As reported, the resultant bias ratios and mean

4.2.4. Live Load Modeling Using Monte Carlo Simulation

All the methods described above are purely

An alternative approach based on traffic

Summarizing the review, it was decided to apply the

4.3.Maximum Expected 75-years Load Effect Using Linear Extrapolation

The present study is focused on live load for

The maximum moment is considered as a random

The total number of vehicles *N* expected during

To meet the objectives of this study, the maximum mean moment for different time periods (one day, two weeks, one month, two months, six months, one year, five years, 50 years, 75 years and 100 years were determined. The number of recorded vehicles for each location is given in Table 0-9. The WIM data was collected over different time periods (Table 0-1Table 0-7). In most cases, the WIM data is available for about one year, but there is an exception: ALDOT WIM data cover about 13 years (Table 0-2Table 0-7). The number of vehicles is also different due to the different ADTT. Each CDF curve representing moment ratio includes the number of data points equal to the corresponding number of vehicles, *N*. These CDFs served as a basis for a linear extrapolation of the live load effect.

The shapes of CDF curves are similar regardless of the number of records and actual ADTT at the location. Only upper tails of each CDF representing the maximum values vary depending on the number of recorded vehicles. Thus, for each CDF (each location) the maximum moment (Z_{max}) can be determined by the vertical (probability axis) coordinate depending on selected ADTT Zmax=-Φ-1$(\frac{1}{N})$ Equation 0-6):

$$Z_{max}=-\Phi^{-1}(\frac{1}{N}) \qquad \textbf{Equation 0-6}$$

where: $-\Phi^{-1}$ – is the inverse standard normal distribution function

N – the number of records for the period T (in days) and certain $ADTT$ ($N=(T)(ADTT)$ Equation 0-7).

$$N=(T)(ADTT) \qquad \textbf{Equation 0-7}$$

In in this study, the following ADTT's are considered 250, 1,000, 2,500, 5,000, and 10,000. The calculations were performed separately for each ADTT. First, the vertical coordinates are found, using an inverse random variable scale, to determine the mean maximum moments corresponding to the considered return periods.

For example, if ADTT = 250, the number of trucks per 1 day is 250 and the vertical coordinate of the mean maximum 1-day moment, Z_{max}, is:

$$Z_{max}=-\Phi^{-1}\left(\frac{1}{250}\right)=2.65 \qquad \textbf{Equation 0-8}$$

Similarly, since the number of trucks per 2 weeks is (250 trucks) (14 days) = 3,500 trucks, the mean maximum 2-week moment Z_{max} is given by $Zmax=-\Phi^{-1}\left(\frac{1}{250}\right)=2.65$ Equation 0-8).

$$Z_{max}=-\Phi^{-1}\left(\frac{1}{3500}\right)=3.44 \qquad \textbf{Equation 0-9}$$

Finally, since the number of trucks per 100 years is (250 trucks) (365 days) (100 years) = 9,125,000 trucks, the mean maximum 100-years moment, Z_{max}, is:

$$Z_{max}=-\Phi^{-1}\left(\frac{1}{9,125,000}\right)=5.18 \qquad \textbf{Equation 0-10}$$

Values of vertical coordinates corresponding to the considered return periods one day to 100 years are summarized in Table 0-2.

There are 45 WIM locations and, therefore, 45 curves in each plot, representing CDFs of WIM moment. The mean maximum moment can be obtained directly from the graph by reading the moment ratio (horizontal axis) corresponding to the vertical coordinate representing the considered period. For example, the mean maximum one-day moment ratio for FL-I10 is 0.76, and the mean maximum one-year moment ratio is 1.15 (Figure 0-3).

In the results for each ADTT and span length, there are 45 values of the maximum one-day moment, 45 values of the mean maximum two week moment, and so on. For a more easy review and comparison, cumulative distribution functions of these 45 values obtained from Figure 0-3, are plotted on the normal probability paper as it is shown in Figure 0-4 (ADTT=1,000).

Table 0-2. Vertical Coordinates for the Mean Maximum Moment

Time Period	ADTT				
	250	**1000**	**2500**	**5000**	**10000**
1 Day	2.65	3.09	3.35	3.54	3.72
2 Weeks	3.44	3.8	4.02	4.18	4.33
1 Month	3.65	4.00	4.20	4.35	4.50
2 Months	3.82	4.15	4.35	4.50	4.65
6 Months	4.09	4.39	4.59	4.73	4.87
1 Year	4.24	4.55	4.73	4.87	5.01
5 Years	4.59	4.87	5.05	5.18	5.31
50 Years	5.05	5.31	5.47	5.60	5.72
75 Years	5.13	5.38	5.55	5.67	5.78
100 Years	5.18	5.44	5.60	5.72	5.83

The values located on the intersection of extrapolated CDFs and corresponding ordinates (Table 0-2) are bias factors (λ), which are the ratios of mean-to-nominal value (nominal load effect is bending moment created by HL-93 loading combination). From Figure 0-4 it is evident, that the obtained CDFs are almost parallel, in particular, this applies to the upper linear part. Because of

regularity, it is easier to determine the statistical parameters, such as a mean value (μ) and coefficient of variation, V, which are summarized in Table 0-3

Table 0-4, Table 0-5, **Error! Reference source not found.** and **Error! Reference source not found.** for ADTT from 250 to 10,000.

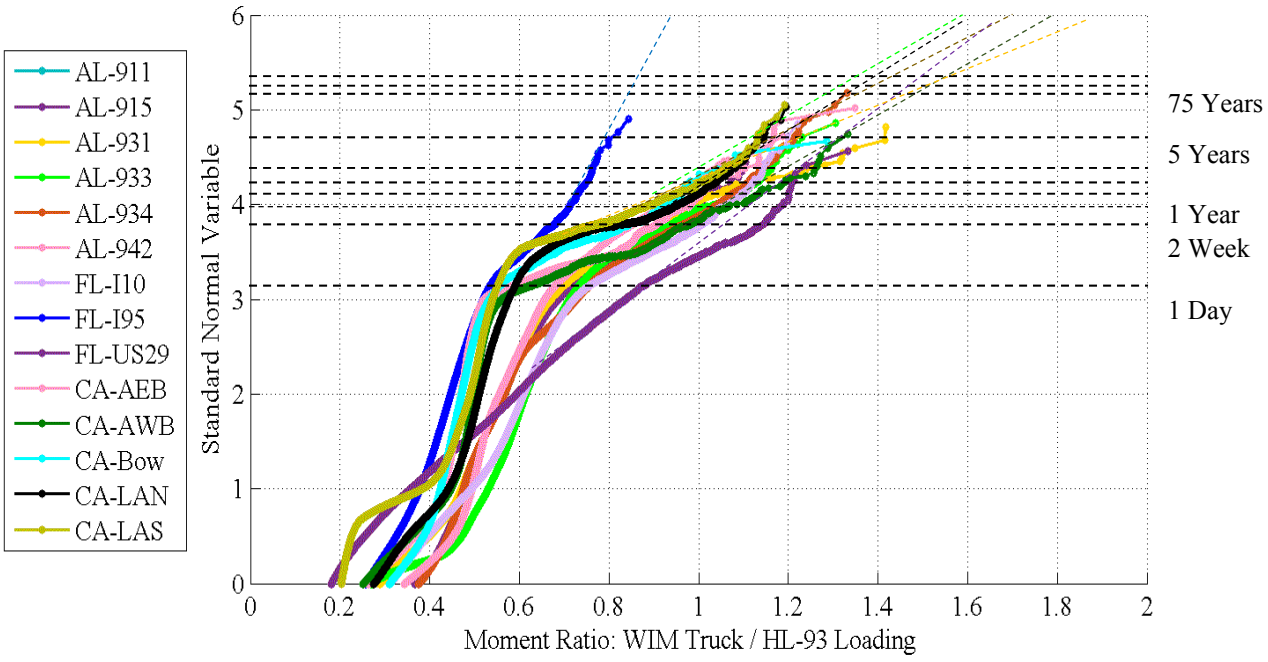

Figure 0-3. Vertical Coordinates for Different Time Periods for ADTT =1,000 and Span=30ft.

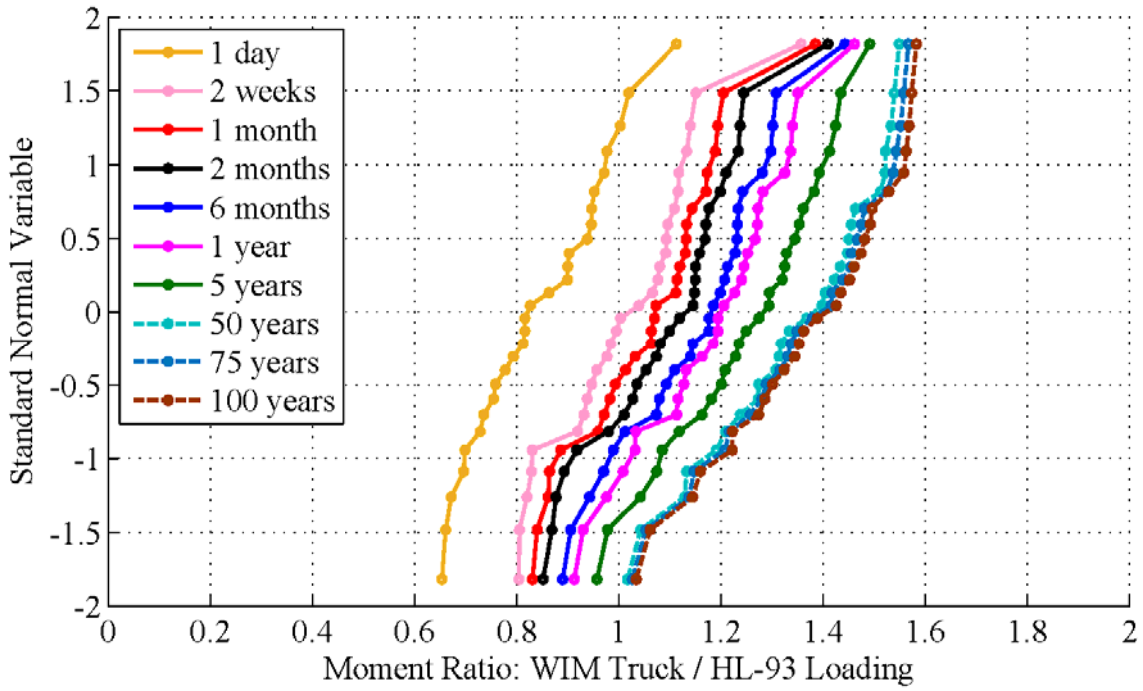

Figure 0-4. CDFs of Mean Maximum Moment Ratios for ADTT=1,000 and 30ft Span

The bias factors for shear force ratio, determined the same way as moment ratios, are summarized in Table 0-8,

Table 0-9, Table 0-10,

Table 0-11 and Table 0-12 for ADTT=250, …, 10,000. The corresponding mean values, μ, and coefficients of variation, V, are also presented herein.

Table 0-3. Statistical Parameters of Live Load Moments for ADTT=250

ADTT 250															
Span	30 ft			60 ft			90 ft			120 ft			200 ft		
	λ	μ	V	λ	μ	V	λ	μ	V	λ	μ	V	λ	μ	V
1 Day	1.04	0.81	0.19	0.95	0.74	0.19	0.86	0.71	0.15	0.86	0.68	0.16	0.78	0.61	0.14
2 Weeks	1.25	0.99	0.16	1.14	0.91	0.17	1.09	0.87	0.16	1.07	0.86	0.15	0.95	0.79	0.14
1 Month	1.30	1.04	0.16	1.21	0.95	0.16	1.15	0.92	0.15	1.13	0.91	0.14	1.00	0.84	0.14
2 Months	1.34	1.08	0.15	1.25	0.99	0.15	1.20	0.96	0.14	1.18	0.95	0.13	1.09	0.88	0.14
6 Months	1.39	1.14	0.14	1.30	1.05	0.15	1.27	1.02	0.13	1.28	1.02	0.13	1.18	0.95	0.14

1 Year	1.40	1.17	0.13	1.33	1.08	0.14	1.30	1.05	0.13	1.32	1.05	0.12	1.24	0.99	0.14
5 Years	1.47	1.25	0.13	1.39	1.15	0.13	1.37	1.12	0.12	1.38	1.13	0.11	1.35	1.07	0.14
50 Years	1.55	1.34	0.12	1.46	1.24	0.12	1.45	1.21	0.12	1.44	1.23	0.10	1.41	1.16	0.13
75 Years	1.56	1.36	0.12	1.47	1.25	0.12	1.46	1.22	0.12	1.45	1.24	0.10	1.42	1.18	0.12
100 Years	1.57	1.37	0.12	1.47	1.26	0.11	1.47	1.23	0.12	1.46	1.25	0.10	1.43	1.19	0.12

Table 0-4. Statistical Parameters of Live Load Moments for ADTT=1000

ADTT 1000															
Span	30 ft			60 ft			90 ft			120 ft			200 ft		
	λ	μ	V	λ	μ	V	λ	μ	V	λ	μ	V	λ	μ	V
1 Day	1.18	0.91	0.18	1.07	0.83	0.18	0.98	0.79	0.16	0.96	0.77	0.16	0.86	0.69	0.16
2 Weeks	1.33	1.08	0.15	1.25	0.99	0.16	1.19	0.96	0.14	1.17	0.95	0.14	1.07	0.88	0.14
1 Month	1.37	1.12	0.14	1.29	1.03	0.15	1.25	1.00	0.14	1.24	1.00	0.13	1.15	0.93	0.13
2 Months	1.40	1.15	0.14	1.32	1.07	0.14	1.28	1.03	0.13	1.30	1.03	0.12	1.20	0.96	0.14
6 Months	1.40	1.20	0.12	1.35	1.11	0.13	1.34	1.08	0.13	1.35	1.08	0.11	1.29	1.03	0.14
1 Year	1.45	1.23	0.12	1.38	1.14	0.13	1.37	1.11	0.12	1.38	1.12	0.11	1.34	1.06	0.14
5 Years	1.52	1.31	0.12	1.43	1.20	0.12	1.43	1.17	0.12	1.41	1.19	0.10	1.39	1.13	0.13
50 Years	1.59	1.39	0.11	1.49	1.29	0.11	1.49	1.26	0.12	1.47	1.28	0.10	1.44	1.22	0.12
75 Years	1.60	1.41	0.11	1.50	1.30	0.11	1.50	1.27	0.12	1.48	1.30	0.09	1.45	1.23	0.12
100 Years	1.61	1.42	0.11	1.51	1.31	0.11	1.50	1.28	0.12	1.49	1.31	0.09	1.46	1.24	0.12

Table 0-5. Statistical Parameters of Live Load Moments for ADTT=2500

ADTT 2500															
Span	30 ft			60 ft			90 ft			120 ft			200 ft		
	λ	μ	V	λ	μ	V	λ	μ	V	λ	μ	V	λ	μ	V
1 Day	1.23	0.97	0.17	1.12	0.88	0.17	1.07	0.85	0.16	1.04	0.83	0.15	0.93	0.76	0.15
2 Weeks	1.37	1.13	0.14	1.29	1.04	0.15	1.25	1.00	0.14	1.25	1.00	0.13	1.16	0.93	0.13
1 Month	1.38	1.16	0.13	1.32	1.08	0.14	1.29	1.04	0.13	1.31	1.04	0.12	1.23	0.98	0.14
2 Months	1.41	1.20	0.13	1.35	1.10	0.14	1.33	1.07	0.13	1.34	1.08	0.12	1.29	1.01	0.14
6 Months	1.47	1.25	0.13	1.39	1.15	0.13	1.37	1.12	0.12	1.38	1.13	0.11	1.35	1.07	0.14
1 Year	1.50	1.28	0.12	1.41	1.18	0.12	1.40	1.15	0.12	1.40	1.16	0.10	1.37	1.10	0.13
5 Years	1.55	1.34	0.12	1.46	1.24	0.12	1.45	1.21	0.12	1.44	1.23	0.10	1.41	1.16	0.13

50 Years	1.61	1.42	0.11	1.52	1.32	0.11	1.51	1.29	0.12	1.50	1.31	0.09	1.46	1.25	0.12
75 Years	1.63	1.44	0.11	1.53	1.33	0.11	1.53	1.30	0.12	1.51	1.33	0.09	1.47	1.26	0.12
100 Years	1.63	1.45	0.11	1.54	1.34	0.11	1.54	1.31	0.12	1.52	1.34	0.09	1.48	1.27	0.12

Table 0-6. Statistical Parameters of Live Load Moments for ADTT=5000

ADTT 5000															
Span	30 ft			60 ft			90 ft			120 ft			200 ft		
	λ	μ	V	λ	μ	V	λ	μ	V	λ	μ	V	λ	μ	V
1 Day	1.28	1.02	0.16	1.17	0.93	0.16	1.11	0.90	0.15	1.10	0.89	0.14	0.97	0.81	0.14
2 Weeks	1.40	1.16	0.14	1.32	1.07	0.14	1.29	1.03	0.13	1.30	1.04	0.12	1.22	0.97	0.13
1 Month	1.41	1.20	0.13	1.35	1.10	0.14	1.33	1.07	0.13	1.34	1.08	0.12	1.29	1.01	0.14
2 Months	1.46	1.23	0.12	1.37	1.13	0.13	1.36	1.10	0.12	1.37	1.11	0.11	1.33	1.05	0.14
6 Months	1.50	1.28	0.12	1.41	1.18	0.12	1.40	1.15	0.12	1.40	1.16	0.10	1.37	1.10	0.13
1 Year	1.52	1.31	0.12	1.43	1.20	0.12	1.43	1.17	0.12	1.41	1.19	0.10	1.39	1.13	0.13
5 Years	1.57	1.37	0.12	1.47	1.26	0.11	1.47	1.23	0.12	1.46	1.25	0.10	1.43	1.19	0.12
50 Years	1.63	1.45	0.11	1.54	1.34	0.11	1.54	1.31	0.12	1.52	1.34	0.09	1.48	1.27	0.12
75 Years	1.65	1.46	0.11	1.55	1.35	0.11	1.55	1.33	0.12	1.53	1.36	0.10	1.49	1.29	0.12
100 Years	1.66	1.47	0.11	1.55	1.36	0.11	1.56	1.34	0.12	1.55	1.37	0.10	1.50	1.30	0.12

Table 0-7. Statistical Parameters of Live Load Moments for ADTT=10,000

ADTT 10,000															
Span	30 ft			60 ft			90 ft			120 ft			200 ft		
	λ	μ	V	λ	μ	V	λ	μ	V	λ	μ	V	λ	μ	V
1 Day	1.32	1.06	0.15	1.23	0.97	0.16	1.16	0.93	0.14	1.15	0.93	0.14	1.04	0.85	0.14
2 Weeks	1.41	1.19	0.13	1.35	1.10	0.14	1.32	1.07	0.13	1.34	1.07	0.12	1.28	1.01	0.14
1 Month	1.46	1.23	0.12	1.37	1.13	0.13	1.36	1.10	0.12	1.37	1.11	0.11	1.33	1.05	0.14
2 Months	1.47	1.26	0.12	1.40	1.16	0.13	1.39	1.13	0.12	1.39	1.14	0.11	1.36	1.08	0.13
6 Months	1.52	1.31	0.12	1.43	1.20	0.12	1.43	1.17	0.12	1.41	1.19	0.10	1.39	1.13	0.13
1 Year	1.54	1.33	0.12	1.45	1.23	0.12	1.45	1.20	0.12	1.43	1.22	0.10	1.41	1.15	0.13
5 Years	1.59	1.39	0.11	1.49	1.29	0.11	1.49	1.26	0.12	1.47	1.28	0.10	1.44	1.22	0.12

50 Years	1.66	1.47	0.11	1.55	1.36	0.11	1.56	1.34	0.12	1.55	1.37	0.10	1.50	1.30	0.12
75 Years	1.68	1.48	0.11	1.56	1.37	0.11	1.58	1.35	0.12	1.58	1.38	0.10	1.51	1.31	0.12
100 Years	1.70	1.49	0.11	1.57	1.38	0.11	1.59	1.36	0.12	1.59	1.39	0.10	1.52	1.32	0.12

Table 0-8. Statistical Parameters of Live Load Shear Forces for ADTT=250

ADTT 250															
Span	30 ft			60 ft			90 ft			120 ft			200 ft		
	λ	μ	V	λ	μ	V	λ	μ	V	λ	μ	V	λ	μ	V
1 Day	1.02	0.83	0.14	0.85	0.70	0.14	0.87	0.69	0.12	0.85	0.68	0.13	0.73	0.61	0.13
2 Weeks	1.17	1.00	0.12	1.03	0.87	0.11	1.07	0.89	0.12	1.05	0.86	0.12	0.97	0.80	0.14
1 Month	1.21	1.04	0.11	1.08	0.91	0.11	1.13	0.95	0.12	1.10	0.91	0.12	1.06	0.88	0.14
2 Months	1.25	1.08	0.11	1.12	0.95	0.12	1.19	0.99	0.12	1.15	0.95	0.12	1.12	0.92	0.14
6 Months	1.31	1.14	0.11	1.19	1.01	0.12	1.24	1.07	0.13	1.22	1.02	0.13	1.18	0.97	0.14
1 Year	1.34	1.17	0.11	1.23	1.04	0.12	1.27	1.11	0.13	1.25	1.05	0.13	1.22	1.01	0.14
5 Years	1.42	1.24	0.11	1.32	1.12	0.13	1.36	1.20	0.13	1.33	1.13	0.14	1.35	1.11	0.14
50 Years	1.53	1.34	0.11	1.43	1.21	0.13	1.47	1.31	0.13	1.45	1.23	0.15	1.45	1.18	0.15
75 Years	1.54	1.36	0.11	1.45	1.23	0.13	1.50	1.33	0.13	1.49	1.24	0.15	1.46	1.19	0.15
100 Years	1.55	1.37	0.11	1.47	1.24	0.13	1.51	1.35	0.13	1.48	1.26	0.15	1.47	1.20	0.15

Table 0-9. Statistical Parameters of Live Load Shear Forces for ADTT=1000

ADTT 1000															
Span	30 ft			60 ft			90 ft			120 ft			200 ft		
	λ	μ	V	λ	μ	V	λ	μ	V	λ	μ	V	λ	μ	V
1 Day	1.12	0.93	0.13	0.92	0.79	0.11	0.98	0.80	0.11	0.96	0.77	0.12	0.84	0.70	0.13
2 Weeks	1.25	1.08	0.11	1.09	0.94	0.11	1.16	0.99	0.11	1.15	0.94	0.12	1.09	0.91	0.13
1 Month	1.29	1.12	0.11	1.13	0.99	0.11	1.21	1.04	0.11	1.21	0.99	0.12	1.17	0.97	0.13
2 Months	1.32	1.15	0.11	1.16	1.02	0.11	1.25	1.08	0.12	1.23	1.03	0.13	1.22	1.01	0.14
6 Months	1.38	1.20	0.11	1.21	1.07	0.12	1.30	1.14	0.13	1.28	1.08	0.13	1.28	1.05	0.14
1 Year	1.41	1.23	0.11	1.26	1.10	0.12	1.33	1.18	0.12	1.32	1.12	0.14	1.32	1.09	0.14

5 Years	1.49	1.30	0.11	1.34	1.17	0.12	1.41	1.26	0.12	1.40	1.19	0.14	1.38	1.14	0.14
50 Years	1.58	1.40	0.11	1.47	1.26	0.13	1.54	1.37	0.13	1.51	1.28	0.15	1.47	1.20	0.15
75 Years	1.60	1.41	0.11	1.49	1.27	0.13	1.55	1.39	0.13	1.53	1.30	0.15	1.48	1.21	0.15
100 Years	1.61	1.42	0.11	1.50	1.29	0.13	1.57	1.40	0.13	1.55	1.31	0.16	1.49	1.22	0.15

Table 0-10. Statistical Parameters of Live Load Shear Forces for ADTT=2500

ADTT 2500															
Span	30 ft			60 ft			90 ft			120 ft			200 ft		
	λ	μ	V	λ	μ	V	λ	μ	V	λ	μ	V	λ	μ	V
1 Day	1.16	0.98	0.12	0.98	0.85	0.11	1.05	0.87	0.12	1.02	0.84	0.12	0.93	0.78	0.13
2 Weeks	1.30	1.12	0.11	1.14	0.99	0.11	1.21	1.04	0.12	1.21	1.00	0.13	1.19	0.99	0.13
1 Month	1.34	1.16	0.11	1.17	1.03	0.11	1.26	1.09	0.12	1.24	1.04	0.13	1.23	1.02	0.14
2 Months	1.37	1.19	0.11	1.20	1.06	0.12	1.29	1.13	0.13	1.27	1.07	0.13	1.29	1.06	0.14
6 Months	1.42	1.24	0.11	1.27	1.11	0.12	1.34	1.19	0.13	1.33	1.13	0.14	1.33	1.09	0.15
1 Year	1.45	1.28	0.11	1.31	1.14	0.12	1.37	1.23	0.13	1.37	1.16	0.14	1.38	1.12	0.15
5 Years	1.53	1.34	0.11	1.39	1.21	0.13	1.47	1.30	0.13	1.45	1.23	0.15	1.43	1.17	0.15
50 Years	1.62	1.43	0.11	1.51	1.29	0.13	1.58	1.41	0.13	1.55	1.32	0.16	1.50	1.21	0.16
75 Years	1.64	1.45	0.11	1.54	1.31	0.13	1.60	1.43	0.13	1.57	1.34	0.16	1.51	1.22	0.16
100 Years	1.65	1.46	0.11	1.55	1.32	0.14	1.61	1.44	0.13	1.59	1.35	0.16	1.51	1.23	0.16

Table 0-11. Statistical Parameters of Live Load Shear Forces for ADTT=5000

ADTT 5000															
Span	30 ft			60 ft			90 ft			120 ft			200 ft		
	λ	μ	V	λ	μ	V	λ	μ	V	λ	μ	V	λ	μ	V
1 Day	1.19	1.02	0.11	1.03	0.89	0.11	1.09	0.92	0.13	1.07	0.88	0.12	1.02	0.84	0.14
2 Weeks	1.33	1.16	0.11	1.17	1.02	0.11	1.25	1.09	0.13	1.24	1.04	0.13	1.26	1.03	0.15
1 Month	1.37	1.19	0.11	1.20	1.06	0.12	1.29	1.13	0.13	1.27	1.07	0.13	1.30	1.06	0.15
2 Months	1.40	1.22	0.11	1.24	1.09	0.12	1.32	1.17	0.13	1.31	1.11	0.14	1.33	1.09	0.15
6 Months	1.45	1.28	0.11	1.31	1.14	0.12	1.37	1.23	0.13	1.37	1.16	0.14	1.39	1.13	0.15
1 Year	1.49	1.30	0.11	1.34	1.17	0.12	1.41	1.26	0.13	1.40	1.19	0.14	1.41	1.15	0.15

5 Years	1.55	1.37	0.11	1.43	1.23	0.13	1.50	1.34	0.12	1.48	1.26	0.15	1.46	1.19	0.15
50 Years	1.65	1.46	0.11	1.55	1.32	0.14	1.61	1.44	0.12	1.59	1.35	0.16	1.52	1.23	0.15
75 Years	1.66	1.47	0.11	1.57	1.33	0.14	1.63	1.46	0.12	1.60	1.36	0.16	1.53	1.24	0.15
100 Years	1.68	1.48	0.11	1.59	1.34	0.14	1.64	1.47	0.12	1.62	1.37	0.16	1.53	1.25	0.15

Table 0-12. Statistical Parameters of Live Load Shear Forces for ADTT=10,000

ADTT 10,000															
Span	30 ft			60 ft			90 ft			120 ft			200 ft		
	λ	μ	V	λ	μ	V	λ	μ	V	λ	μ	V	λ	μ	V
1 Day	1.23	1.06	0.11	1.08	0.93	0.11	1.14	0.97	0.13	1.12	0.93	0.12	1.11	0.91	0.14
2 Weeks	1.36	1.19	0.11	1.20	1.06	0.12	1.29	1.13	0.13	1.27	1.07	0.13	1.31	1.07	0.15
1 Month	1.40	1.22	0.11	1.24	1.09	0.12	1.32	1.17	0.13	1.31	1.11	0.14	1.36	1.1	0.15
2 Months	1.44	1.26	0.11	1.28	1.12	0.12	1.35	1.21	0.12	1.35	1.14	0.14	1.39	1.13	0.15
6 Months	1.49	1.30	0.11	1.34	1.17	0.12	1.41	1.26	0.12	1.40	1.19	0.14	1.41	1.15	0.15
1 Year	1.52	1.33	0.11	1.38	1.20	0.13	1.45	1.29	0.12	1.44	1.22	0.15	1.44	1.17	0.15
5 Years	1.58	1.40	0.11	1.47	1.26	0.13	1.54	1.37	0.12	1.51	1.28	0.15	1.49	1.22	0.15
50 Years	1.68	1.48	0.11	1.59	1.34	0.14	1.64	1.47	0.13	1.62	1.37	0.16	1.54	1.25	0.15
75 Years	1.69	1.50	0.12	1.61	1.36	0.14	1.65	1.48	0.12	1.63	1.39	0.16	1.55	1.26	0.15
100 Years	1.71	1.51	0.12	1.62	1.37	0.14	1.67	1.50	0.12	1.64	1.40	0.16	1.55	1.27	0.15

For most considered locations, the 75-years maximum moment ratios ($\lambda_{75years}$) range from about 1.39-1.67 of HL-93 for various span length and ADTT. It is mostly similar for span length 60-120 ft but outlies for 30 and 200ft. The latter is shifted by 0.1 due to a more significant difference in span length (80ft), while 30ft moment ratio can be an outlier due to a different nominal live load model (Figure 0-12). The average coefficient of variation is 0.12. It tends to decrease with the increase of the return period (Table 0-3,

Table 0-4, Table 0-5, **Error! Reference source not found.** and **Error! Reference source not found.**).

The CDFs of 75-years bias factors of bending moment ratio obtained using linear extrapolation are shown in **Error! Reference source not found.**,

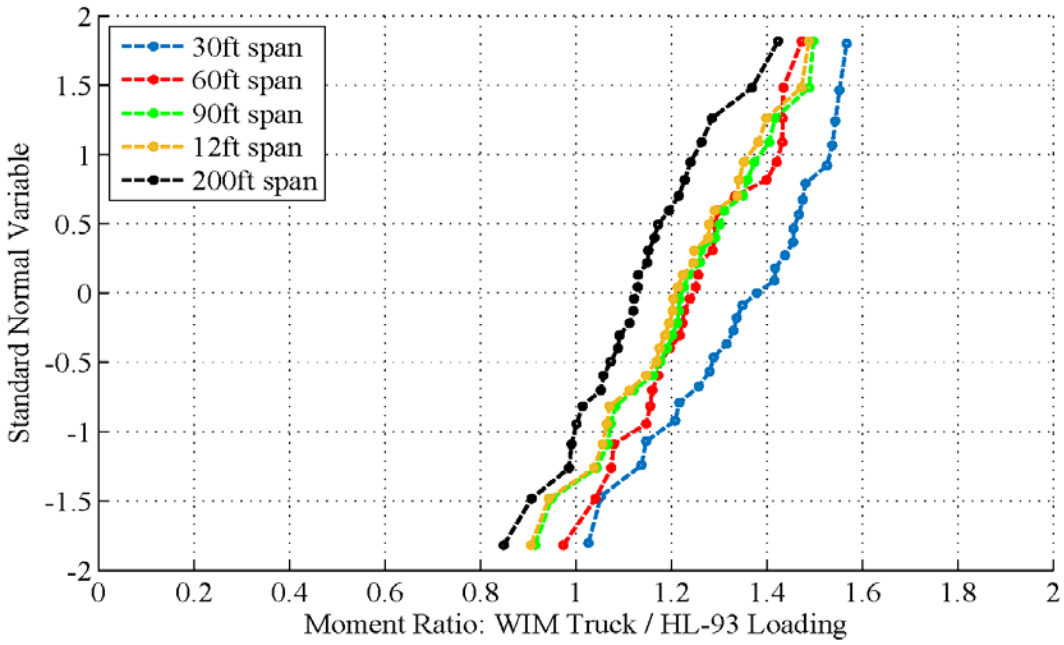

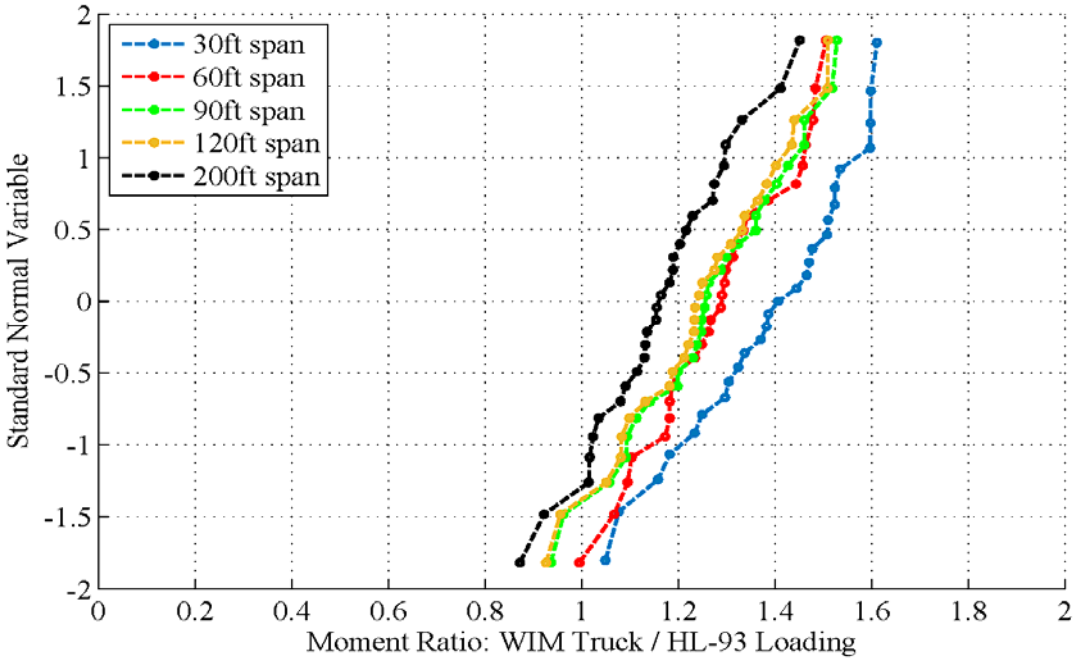

,

Figure 0-7, Figure 0-8 and Figure 0-9 for ADTT equal to 250, 1000, 2500, 5000 and 10000 respectively. To summarize, the bias factors for live load moment and shear ratio are plotted versus simple span lengths in Figure 0-10 and Figure 0-11, respectively, for the average daily truck traffic from 250 to 10,000.

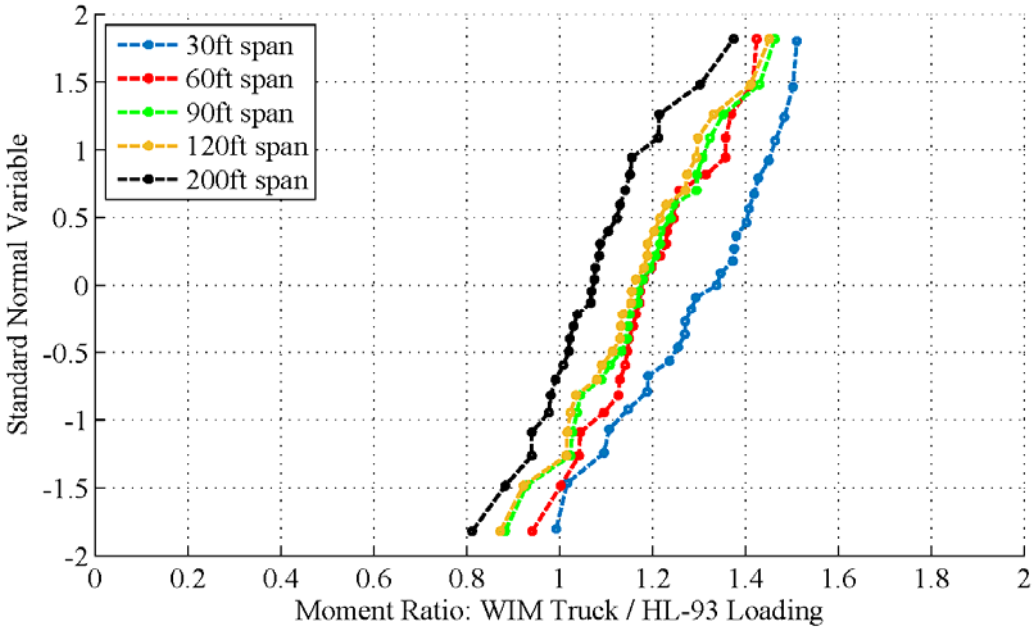

Figure 0-5. CDFs of 75-years Maximum Bias Factors for Bending Moment vs. Simple Span for ADTT=250

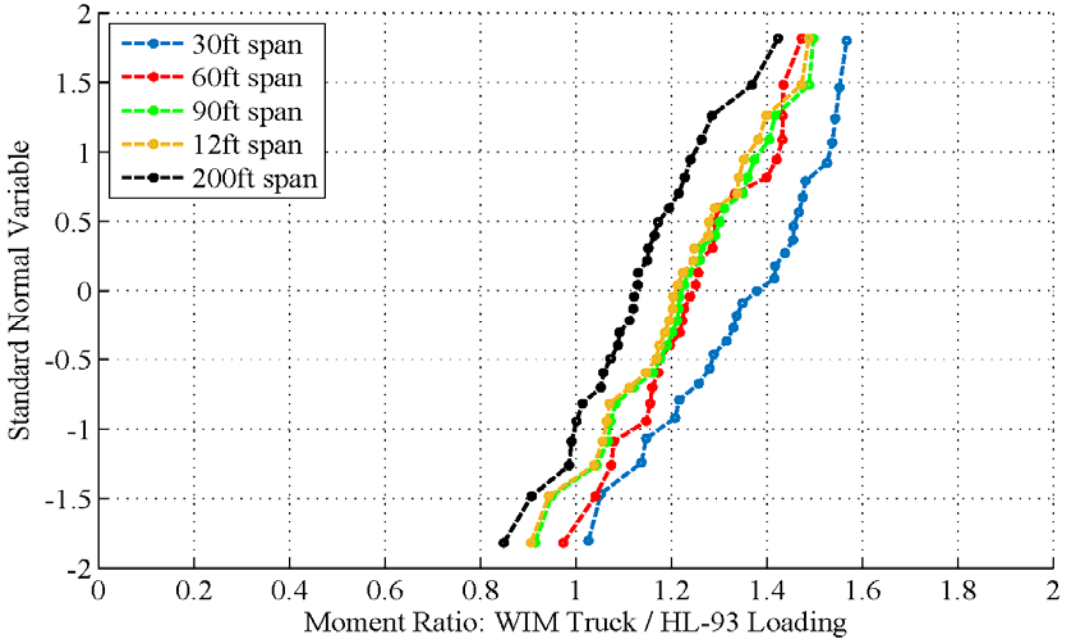

Figure 0-6. CDFs of 75-years Maximum Bias Factors for Bending moment vs. Simple Span for ADTT=1000

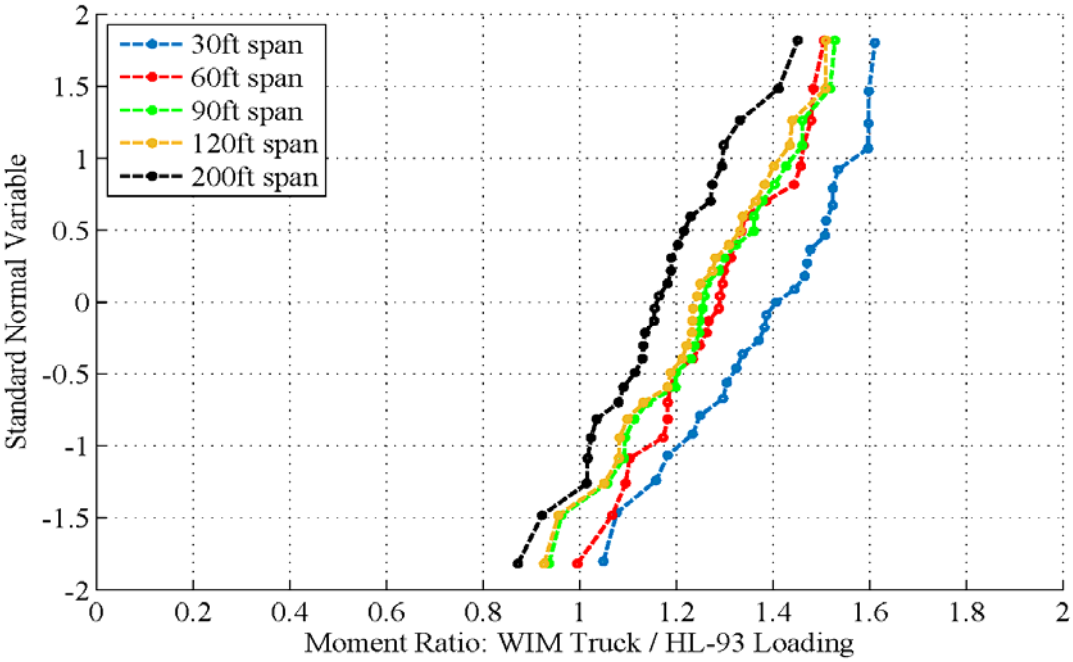

Figure 0-7. CDFs of 75-years Maximum Bias Factors for Bending Moment vs. Simple Span for ADTT=2500

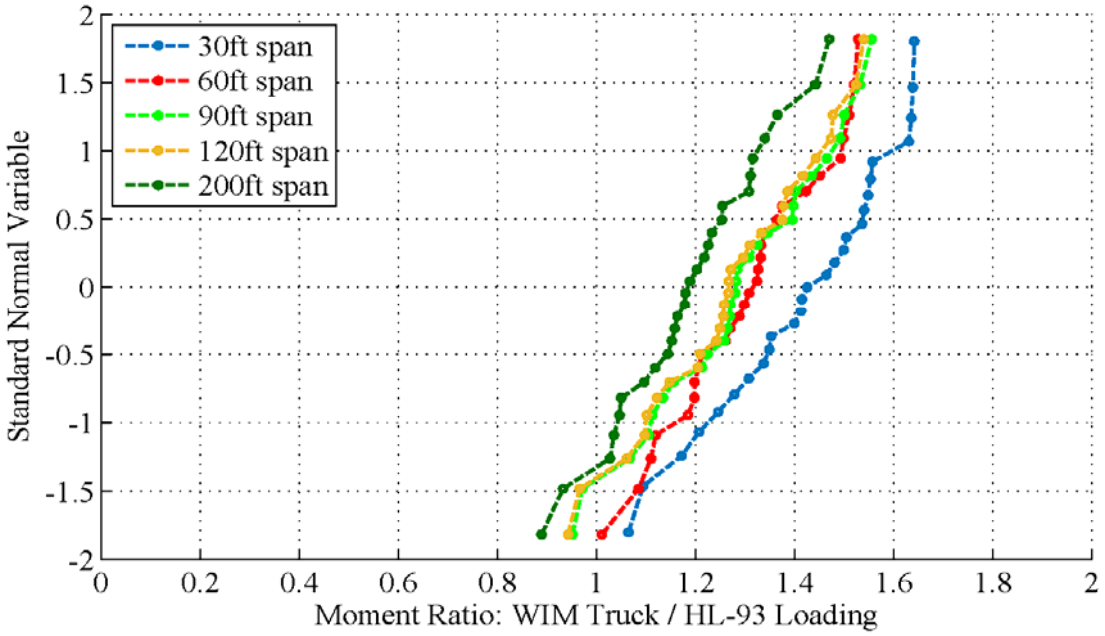

Figure 0-8. CDFs of 75-years Maximum Bias Factor for Bending Moment vs. Simple Span for ADTT=5000

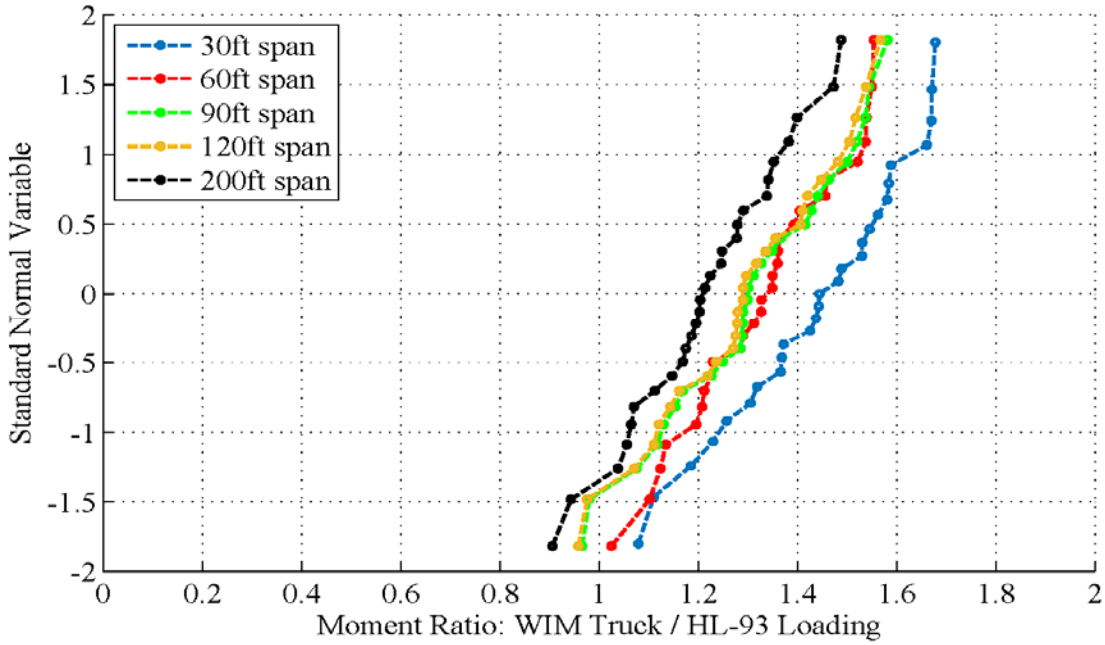

Figure 0-9. CDFs of 75-years Maximum Bias Factors for Bending Moment vs. Simple Span for ADTT=10,000

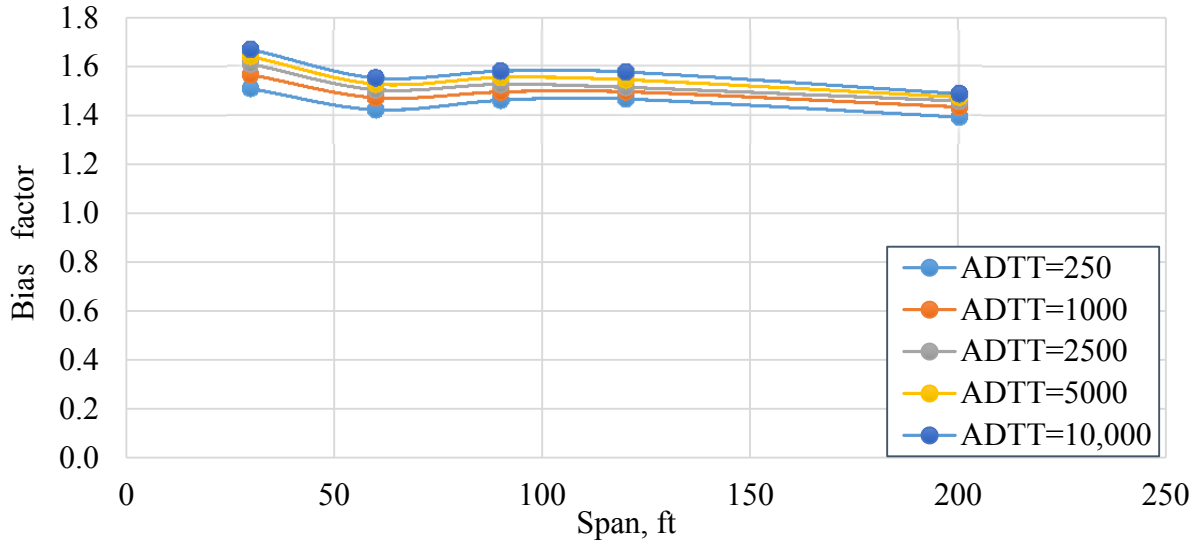

Figure 0-10. Bias Factors for Moment vs. Span Length for the Maximum 75 years

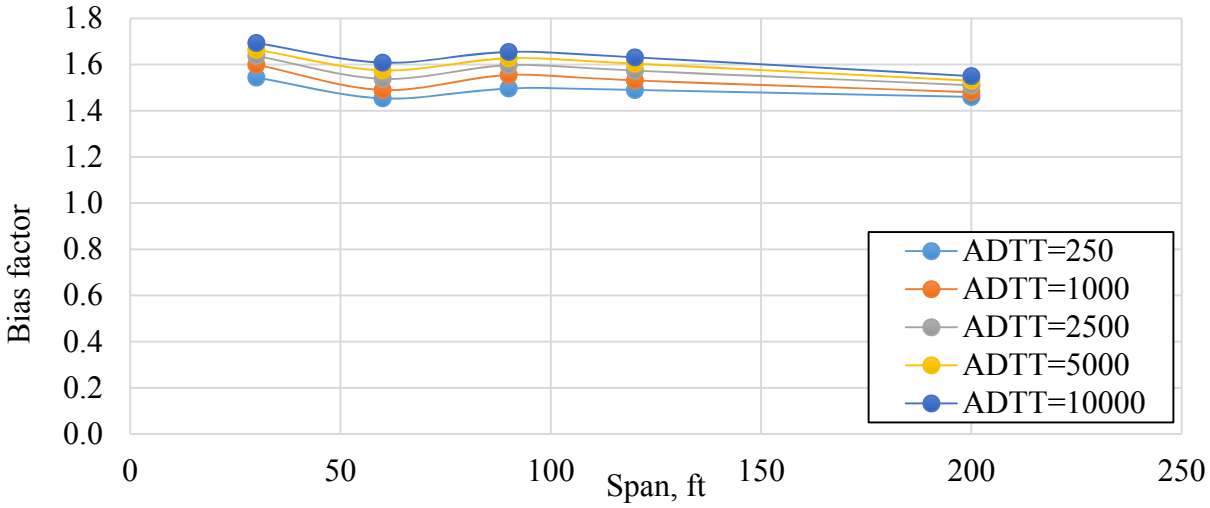

Figure 0-11. Bias factor for shear force vs. span length for the maximum 75 years

The live load parameters used in the original calibration of AASHTO LRFD (Nowak 1999) were based on the Ontario truck survey data (Agarwal and Wolkowicz 1976). Thus, for comparison, the 75-years moment and shear maxima for ADTT=1000 is shown in Figure 0-12 and Figure 0-13 respectively, along with the corresponding factors developed based on the Ontario truck survey, (Nowak 1999). The plot shows 15-20% increase in the truck load effect since the 1980's.

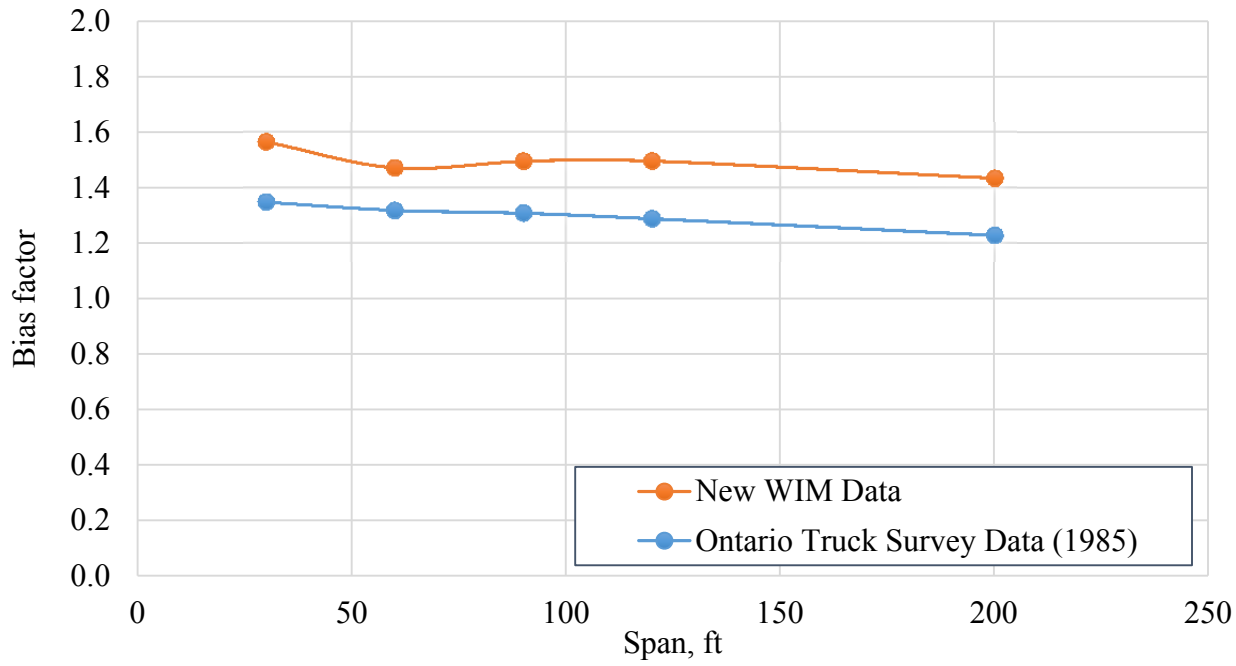

Figure 0-12. 75-years Maximum Moments vs. Span Length for Newly Available WIM Data and Ontario Truck Survey (ADTT=1000)

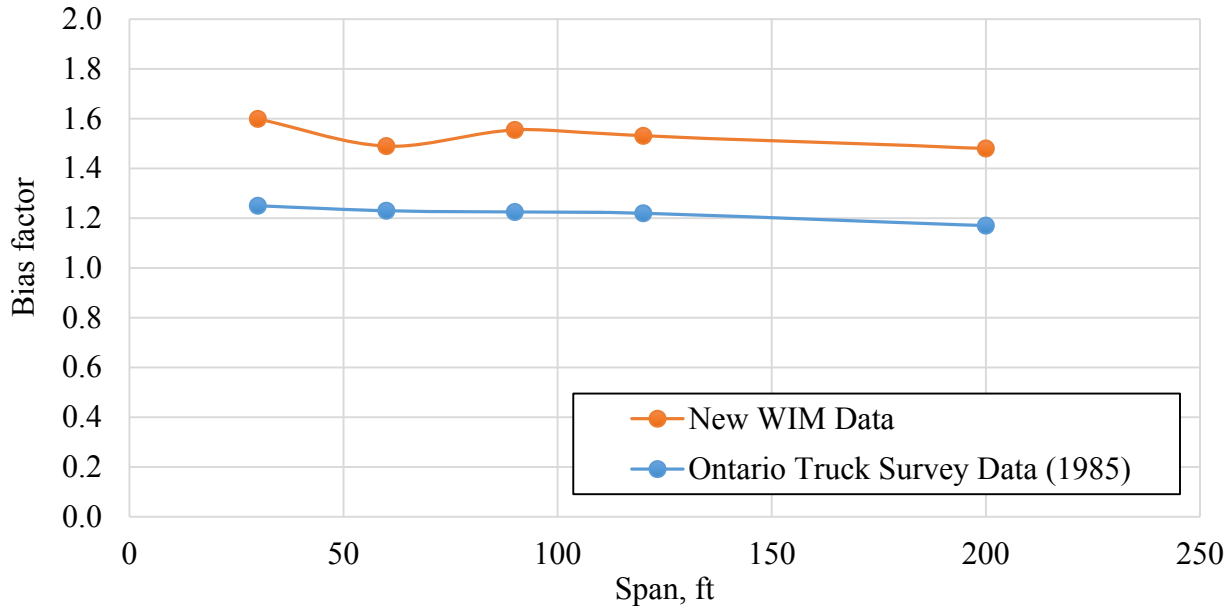

Figure 0-13. 75-years Maximum Shear Force vs. Span Length for Newly Available WIM Data and Ontario Truck Survey (ADTT=1000)

4.4. Maximum Expected 75-years Load Effects Using Traffic Simulation

The previous chapters discussed methods based on fitting the calculated load effect with an appropriate statistical distribution. However, the lifetime maximum live load effect estimated using such techniques does not correspond to realistic truck configurations. The alternative family of methods is based on simulation of the actual traffic using Monte Carlo method (Bailey and Bez 1999),(O'Brien et al. 2006), (O'Connor and O'Brien 2005) (Enright and OBrien 2012). This technique is discussed in more detail in Chapter 2.6.2

Moments strongly depend on truck axle configuration and total load distribution on axles rather than on magnitude of the GVW itself. To determine the maximum load effect for a given return period the parameters of each truck, such as axle loads and spacing, can be generated using the statistics obtained from the available WIM measurements. The number of simulated vehicles depends on the period *(T)* in days and *ADTT*. Therefore, the total number of simulations, (*N*), is equal to $T \times ADTT$, similar to the approach discussed in the previous chapter. The proposed technique is based on the same approach as the extrapolation method (Nowak and Hong 1991). The location of the maximum expected live load effect is at the intersection of its CDF with the ordinate on the standard inverse variable scale that corresponds to the desired period. However, the size of the problem can become too large for a conventional desktop computer. The result depends on the number of simulated vehicle configurations and assumptions made to simplify the process. The following can be assumed:

- The maximum live load effect for a given period *(T),* is created only by a small percent of the permit or illegally overload vehicles (OBrien et al. 2016)

- The statistical parameters for simulation are taken for the trucks that create 1% of the upper tail of the CDF's of moment and shear force ratio.
- Axle spacing and axle loads of each particular vehicle are considered as random variables with the defined types of distribution, mean values and standard deviations.

The number of simulated vehicles is calculated for each of 45 locations in the database. For a particular location, the required number of generated vehicle configurations, N_{req} can be determined as follows:

$$\boldsymbol{N_{req} = 0.01(N)(T)(ADTT)} \qquad \textbf{Equation 0-11}$$

Where: N – Total number of WIM records collected from a particular location

T – Period T (in days). Since AASHTO LRFD (*AASHTO LRFD* 2014) specifies bridge service life equal to 75, years $T=27,375$.

The statistical parameters (mean, standard deviation and type of distribution) can be different for different vehicle classes (Cambridge Systematics, Inc., 2007). Configurations of vehicle classes specified by FHWA are used in this study. The database of N_{req} is then divided depending on class they belong to (Ex.: $N_{req_{class7}}, N_{req_{class8}}, N_{req_{class10}}$, etc.). Since it is assumed that the traffic mix remains the same during the service life of the bridge, the statistical parameters are determined for each vehicle class and corresponding vehicle configurations generated.

The type of distribution of axle load and spacing was determined using already developed Matlab function 'ALLFITDIST' ("Mike Sheppard - MATLAB Central" n.d.), which fits CDF of each axle load and spacing with all valid continuous parametric probability distributions (Beta, Exponential, Extreme value, Gamma, Lognormal, etc.). The most common probability distribution functions are described in Chapter 0. The best fit is selected based on Bayesian

information criterion (Schwarz 1978) and Akaike information criterion (Akaike 1973). The examples of fitting the distribution of particular axle load and axle spacing are shown in Figure 0-14 and Figure 0-15.

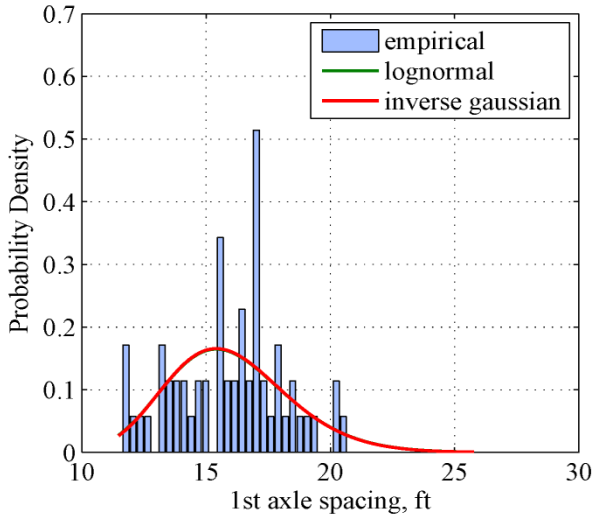

a) b)

Figure 0-14. Fitting Statistical Distribution Function for a) PDF and b) CDF of 1st Axle Spacing (Class 10, FL-I10)

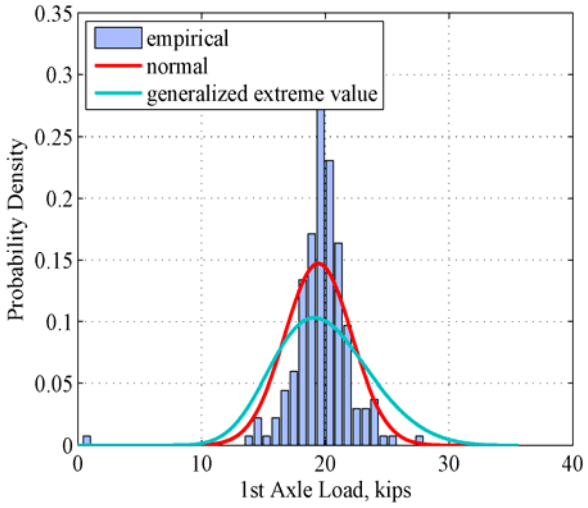

a) b)

Figure 0-15. Fitting Statistical Distribution Function for a) PDF and b) CDF 1st Axle Load (Class 10, FL-I10)

Mostly all values of axle spacing are distributed

After the required number of vehicle configurations was generated, the corresponding load and shears were calculated by running each simulated truck over the influence lines for the same simple spans as recorded WIM trucks (30, 60, 90, 120 and 200ft). The number of generated configurations is determined for a particular return period (T) and ADTT. Therefore, the maximum load effect for a particular span length is equal to the maximum effect a bridge can experience within the service life. The resultant maximum moments and shear ratios are summarized in Figure 0-16 and Figure 0-17 respectively.

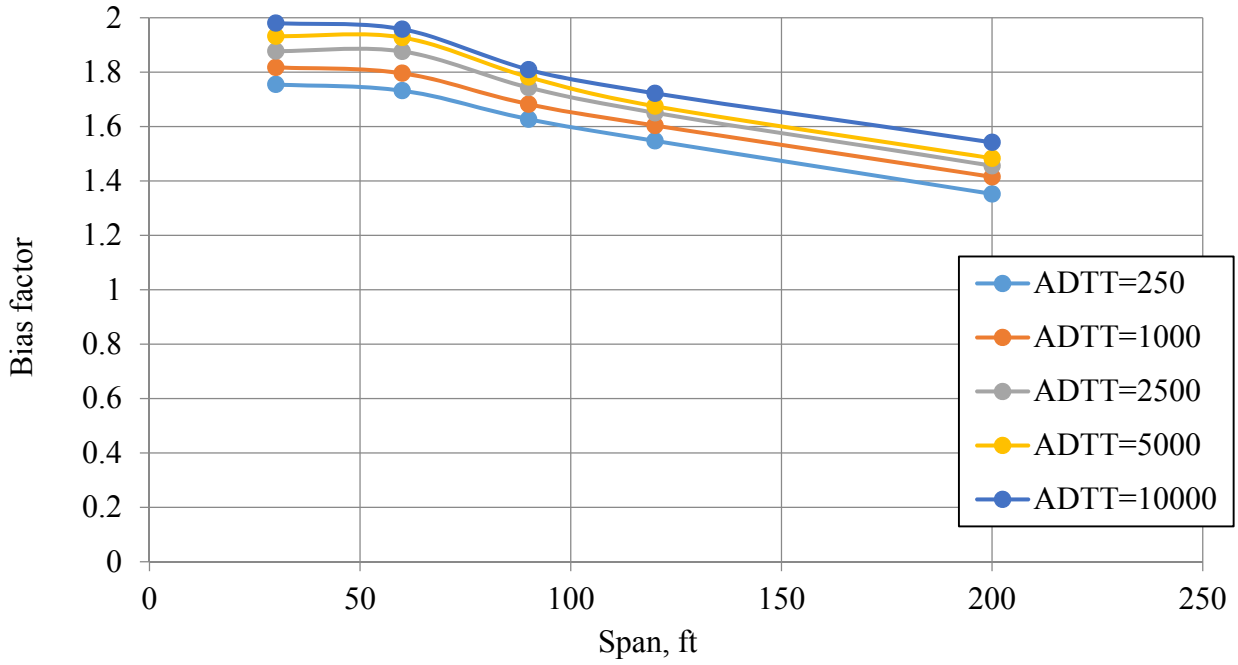

Figure 0-16. Bias Factors for Moment Ratios vs. Span Length for the Maximum 75 years using Monte Carlo Simulation

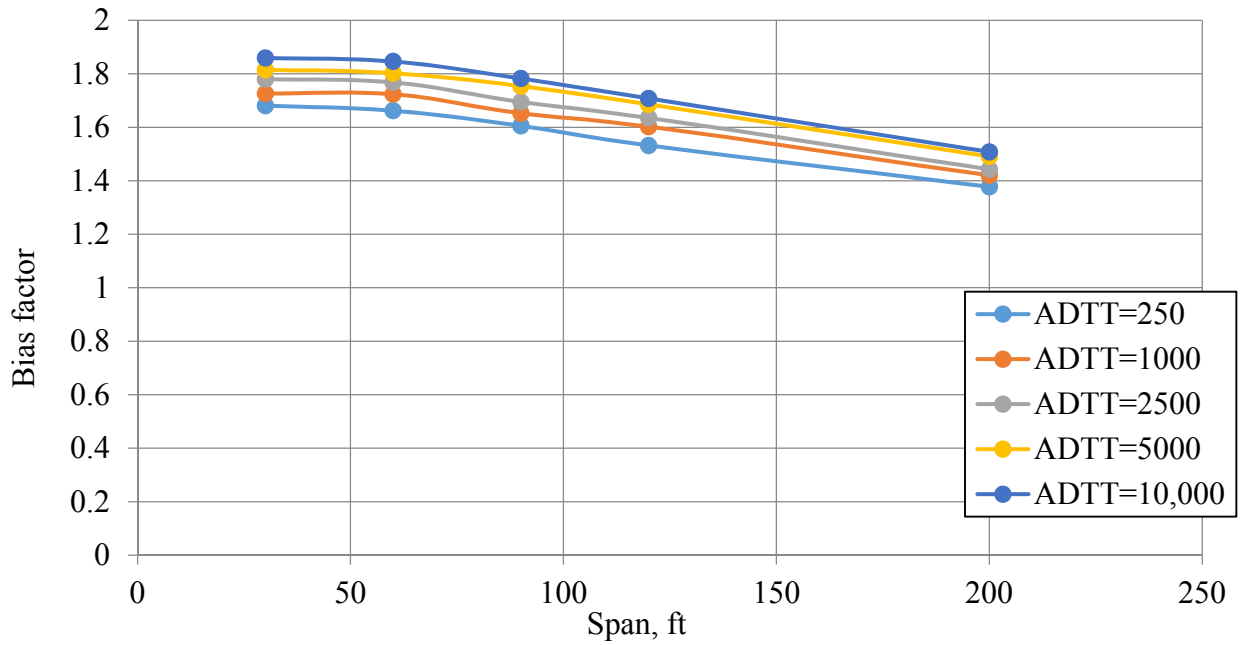

Figure 0-17. Bias Factors for Shear Force Ratios vs. Span Length for the Maximum 75 years using Monte Carlo Simulation

The 75-years maximum expected moment ($\lambda_{75years}$) varies from 1.35 to 1.95 times corresponding HL-93 moment for all considered spans and ADTT. For comparison, the results obtained by the extrapolation and MC simulation for ADTT=1000 are summarized in Table 0-13. The distribution is mostly similar to the results of linear extrapolation for medium (90ft) and long (120-200ft) spans. However, the moment ratios for 30-60ft span substantially outlay from the rest of the results. While the mean values are close to the corresponding results of extrapolation, the coefficients of variation are higher (up to 20%). On average, the MC simulation produces 20% more conservative results than the linear extrapolation results.

Similarly, the resultant shear force ratios were plotted versus span length as it is shown in Figure 0-18. The statistical parameters (bias factor, mean and standard deviation) calculated for ADTT=1000 are summarized in Table 0-14. Bias factors for shear force ratios vary from 1.39 to

1.90 for all considered cases. In comparison to the extrapolated statistical parameters, the bias factors obtained using MC simulation are 15-20% higher and therefore more conservative. However, the average coefficient of variation is 0.13, which is close to corresponding values obtained by linear extrapolation.

Table 0-13. Comparison of Bias Factors for Moment Ratios (WIM Truck/HL-93 Truck)

Span	30ft			60ft			90ft			120ft			200ft		
	λ	μ	V	λ	μ	V	λ	μ	V	λ	μ	V	λ	μ	V
Nowak and	1.60	1.41	0.11	1.50	1.30	0.11	1.50	1.27	0.12	1.48	1.30	0.09	1.45	1.23	0.12
Monte Carlo	1.93	1.44	0.20	1.93	1.43	0.18	1.78	1.37	0.15	1.68	1.30	0.14	1.48	1.13	0.14

Although the applied method produces substantially

Table 0-14. Comparison of Bias Factors for Shear Force Ratios (WIM Truck/HL-93 Truck)

Span	30ft			60ft			90ft			120ft			200ft		
	λ	μ	V	λ	μ	V	λ	μ	V	λ	μ	V	λ	μ	V
Nowak and	1.57	1.34	0.11	1.47	1.26	0.11	1.57	1.31	0.13	1.58	1.31	0.14	1.48	1.21	0.15
Monte Carlo	1.72	1.50	0.13	1.72	1.46	0.13	1.65	1.40	0.13	1.60	1.35	0.13	1.42	1.18	0.15

4.5. Design Tandem Load Model for Short

Bias factors for 75-year maximum bending moments are substantially higher than corresponding values for 60-200ft spans for all considered ADTTs. Since the maximum bending moment for short span bridges (11-40ft) is controlled by the HL-93 tandem load along with the lane load, it

may no longer reflect the actual traffic load. Thus, it is reasonable to increase the current HL-93 tandem load combination (Figure 0-12) to efficiently count for the time-dependent changes in short span live load effects.

There are three tandem combinations considered in

- Tandem (25kips-25kips) + Lane Load (0.64klf) - Figure 0-12(*AASHTO LRFD* 2014).
- Tandem (30kips-30kips)
- Tandem (30kips-30kips) + Lane Load (0.64klf).

CDF's of WIM truck moments caused divided by corresponding moment caused by the current and modified HL-93 loading combinations are shown in Figure 0-18.

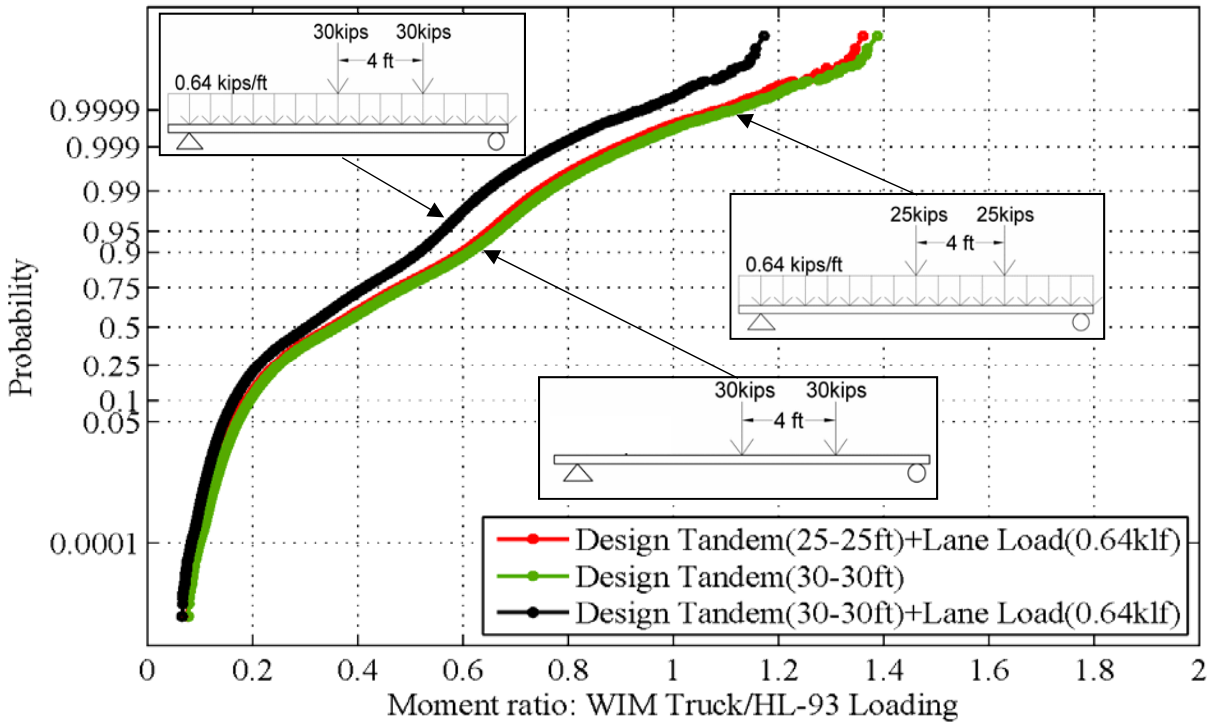

Figure 0-18. 30-ft Moment Ratio for WIM Site FL I-10 Using Different Tandem Load Combinations

There is no significant difference in the distribution of moment ratio using current and modified (30-30ft no Lane Load) Tandem (Figure 0-18). However, the 3rd combination (Tandem (30kips-30kips) + Lane Load (0.64klf) reduces the short span moment ratio by approximately 5-10%. The current HL-93 design tandem covers the range of simple spans from 10 to 40ft, as it is shown in Figure 0-19. The proposed design tandem controls for a broader range of short span bridges from 8 to 75ft (Figure 0-20). The bias factor for 75 years live load moment ratios (WIM Truck/30ft-30ft + Lane Load) is plotted in Figure 0-21 versus the bias factor based on the current AASHTO Tandem model for ADTT from 250 to 10,000. Similarly, the resultant moment ratios obtained by MC simulation for the current and newly proposed Tandem model are plotted versus span length in Figure 0-22.

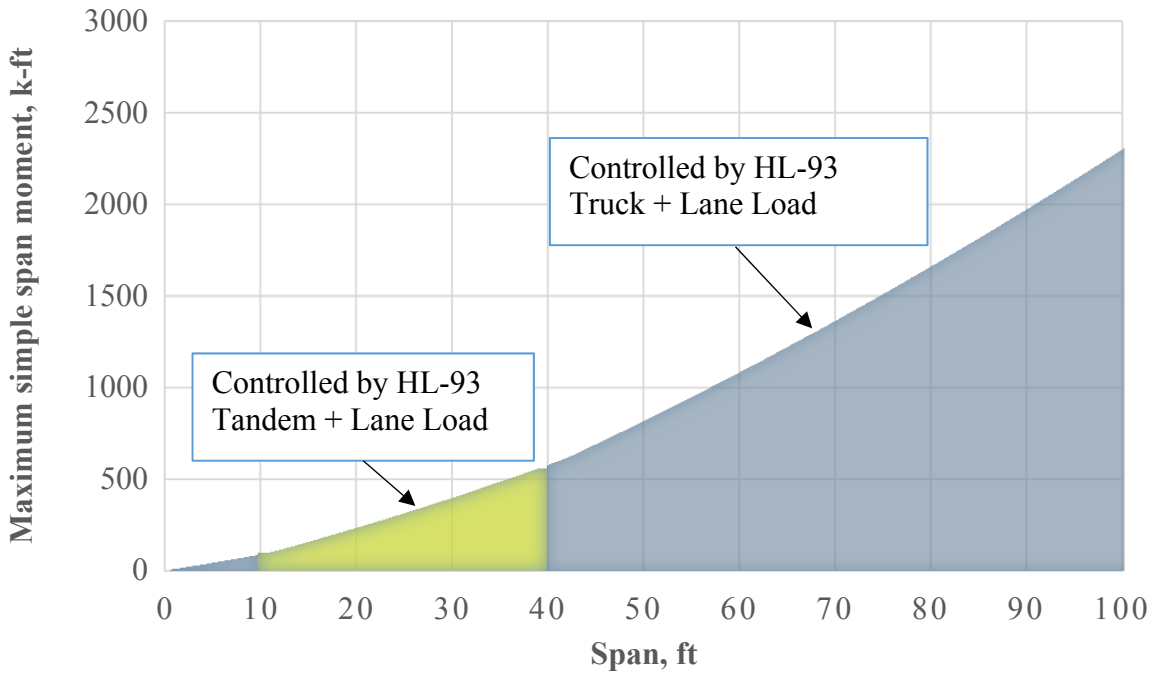

Figure 0-19. Maximum Simple Span Moment Based on Current HL-93 Design Load Model

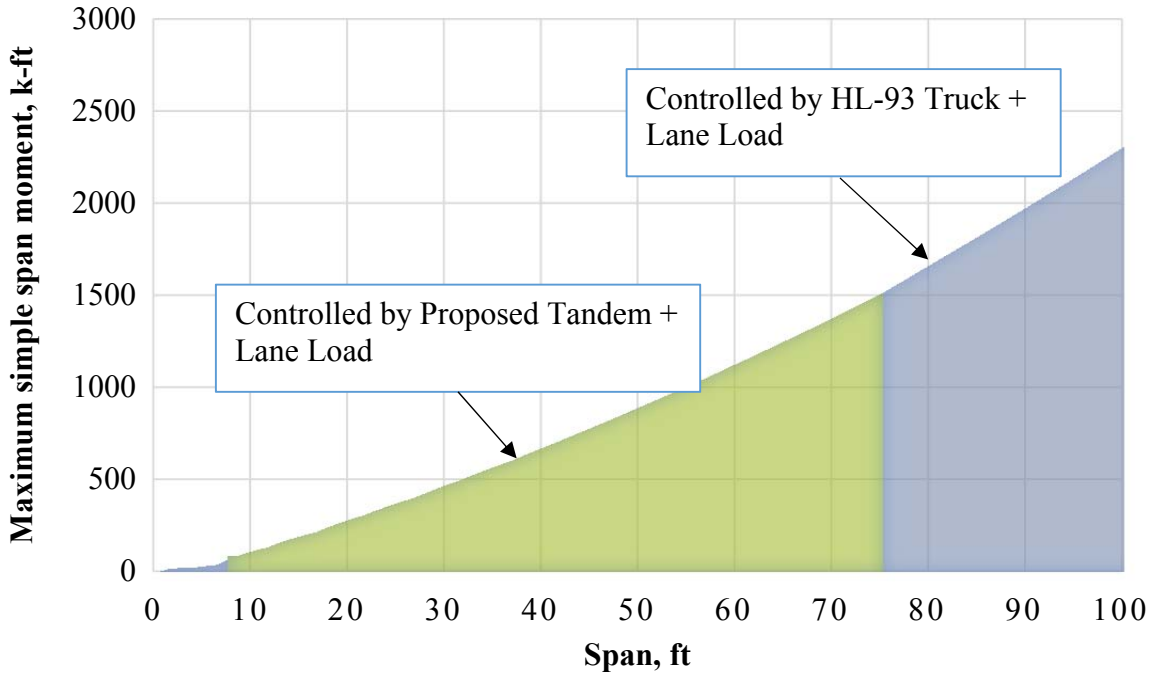

Figure 0-20. Maximum Simple Span Moment Based on Proposed Design Tandem Load

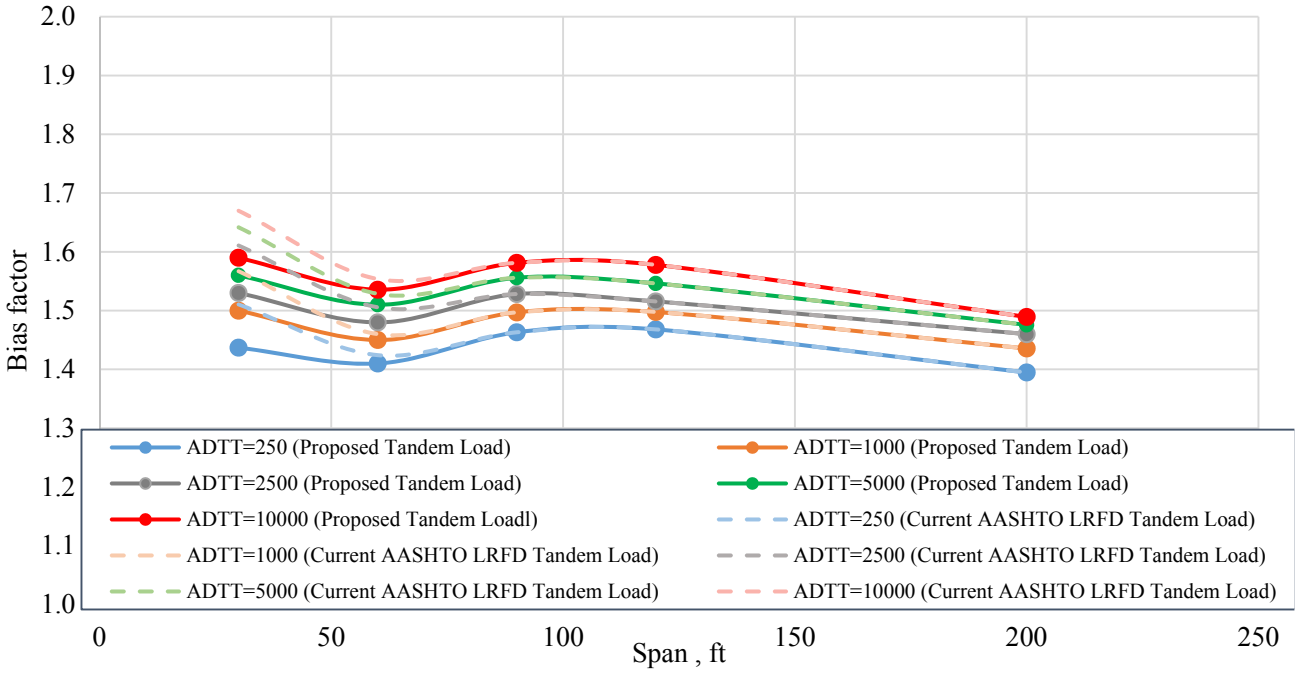

Figure 0-21. Bias Factor for Moment vs. Span Length for the Maximum 75-years for the Current and Proposed HL-93 Load Model Obtained Using Linear Extrapolation

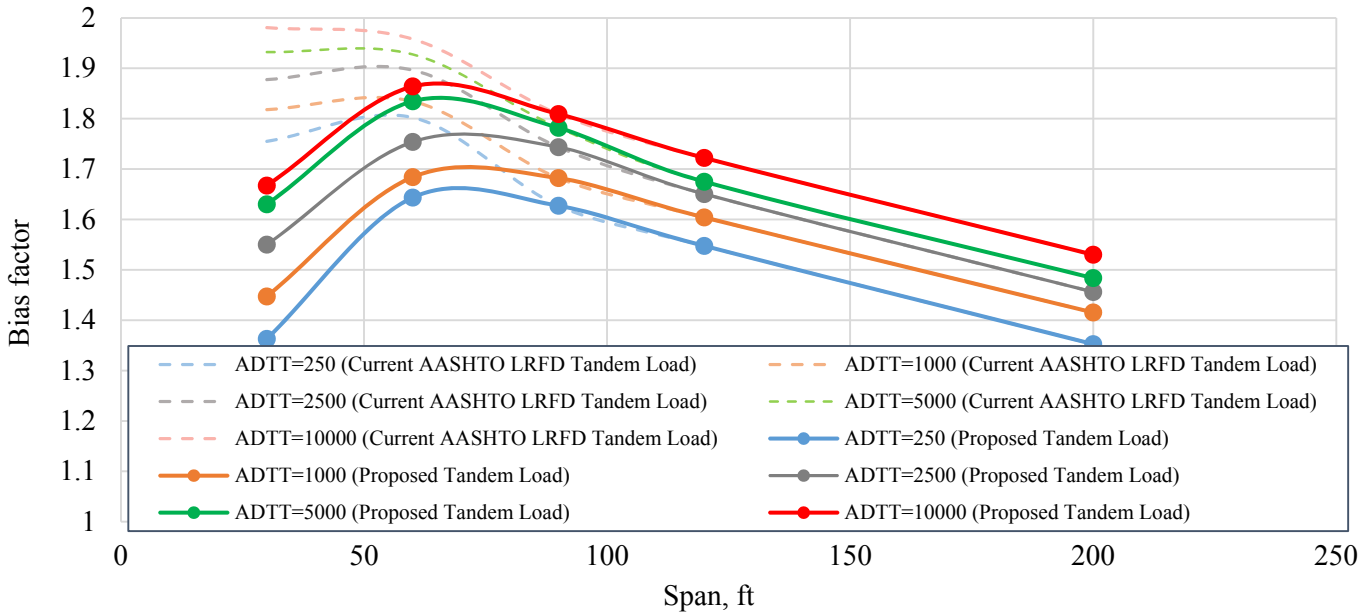

Figure 0-22. Bias Factor for Moment vs. Span Length for the Maximum 75-years for the Current and Proposed HL-93 Load Model (Monte Carlo Simulation)

Permit and Illegal Traffic Load in Alabama

5.1. Summary

Prediction of extreme live load involves

5.2. Background

Overloaded vehicles cause most of the damage to

Permit regulations and monitoring procedures were

The problem of overloading the trucks illegally

Knowledge of the actual loads including illegally

There is no exact method to distinguish permit and

The procedure to identify permits and illegally

5.3. Permit Database

The Maintenance Bureau of Alabama DOT issues

5.4. Legal vs. Overloaded Vehicles

In the United States, vehicles are allowed to operate without any permit and are considered as legal, as long as they satisfy the weight guidelines of Federal Bridge Formula Weights (Formula *LNN-1+12N+36* Equation 0-1) ("Bridge Formula Weights- FHWA Freight Management and Operations" n.d.). The primary purpose of the formula is to reduce the risk of damage to highway bridges by adequately distributed load by determining the optimum axle configuration and axle load distribution.

$$W=500\left\lceil\frac{LN}{N-1}+12N+36\right\rceil \qquad \textbf{Equation 0-1}$$

Where: W – Gross vehicle weight of a group of axles under consideration, lbs

L – The distance between the outer axles of any group of two consecutive axles, ft

N – The number of axles in considered group

However, this is applicable only to the Interstate network. For the state and local highway systems, each state has their set of weight guidelines. Many vehicles that do not obey the Federal Bridge Formula B but do obey the state's legal weight guidelines are commonly referred to as vehicles exempt with "grandfather rights" (Moses 2001). Weight limits that are in use now along with Formula B and state-specific "grandfather" exceptions were established in the mid-1970's (Federal Highway Administration and U.S. Department of Transportation 2015).

Each state has specific permit regulations for transportation of certain goods through the state. Figure 0-1 shows a graphical representation for sorting legal and permit vehicles (Iatsko et al. 2017). According to AASHTO LRFD (2014), the normal vehicular live load for bridges (Strength I limit state) includes all legal trucks, "grandfathered" exceptions and vehicles permitted by routine permits. Illegally overloaded vehicles without permits belong to an unanalyzed portion of bridge live load that is more likely to create an extreme lifetime stress condition.

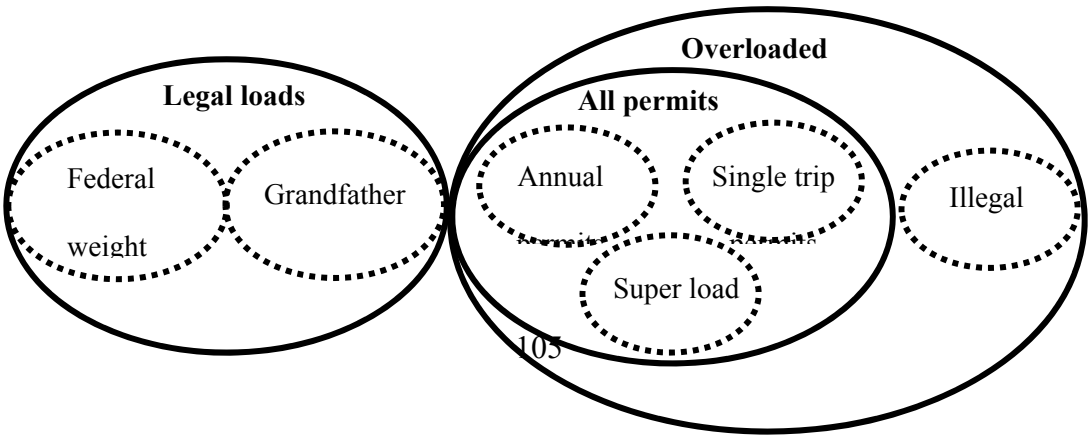

Figure 0-1.Vehicle categories (Iatsko et al. 2017 - prepared in cooperation with A. Ramesh Babu)

WIM records were checked for compliance with the State permit regulations. For example, Alabama's permit regulations("Alabama Code Title 32. Motor Vehicles and Traffic" n.d.) are summarized in Figure 0-2. Vehicles that satisfy Federal legal weight limit and "grandfathered rights" in Figure 0-2 are considered as "Legal loads." Otherwise, they require permits, either annual, single trip or "Super load" permit. Vehicles that require a permit but do not have it are considered as "Illegal Trucks." For example, in Table 0-1, for WIM sites in Alabama in the year 2014, there is a summary listing the total number of legal vehicles, number of vehicles that require a permit, and number of permits issued by the state.

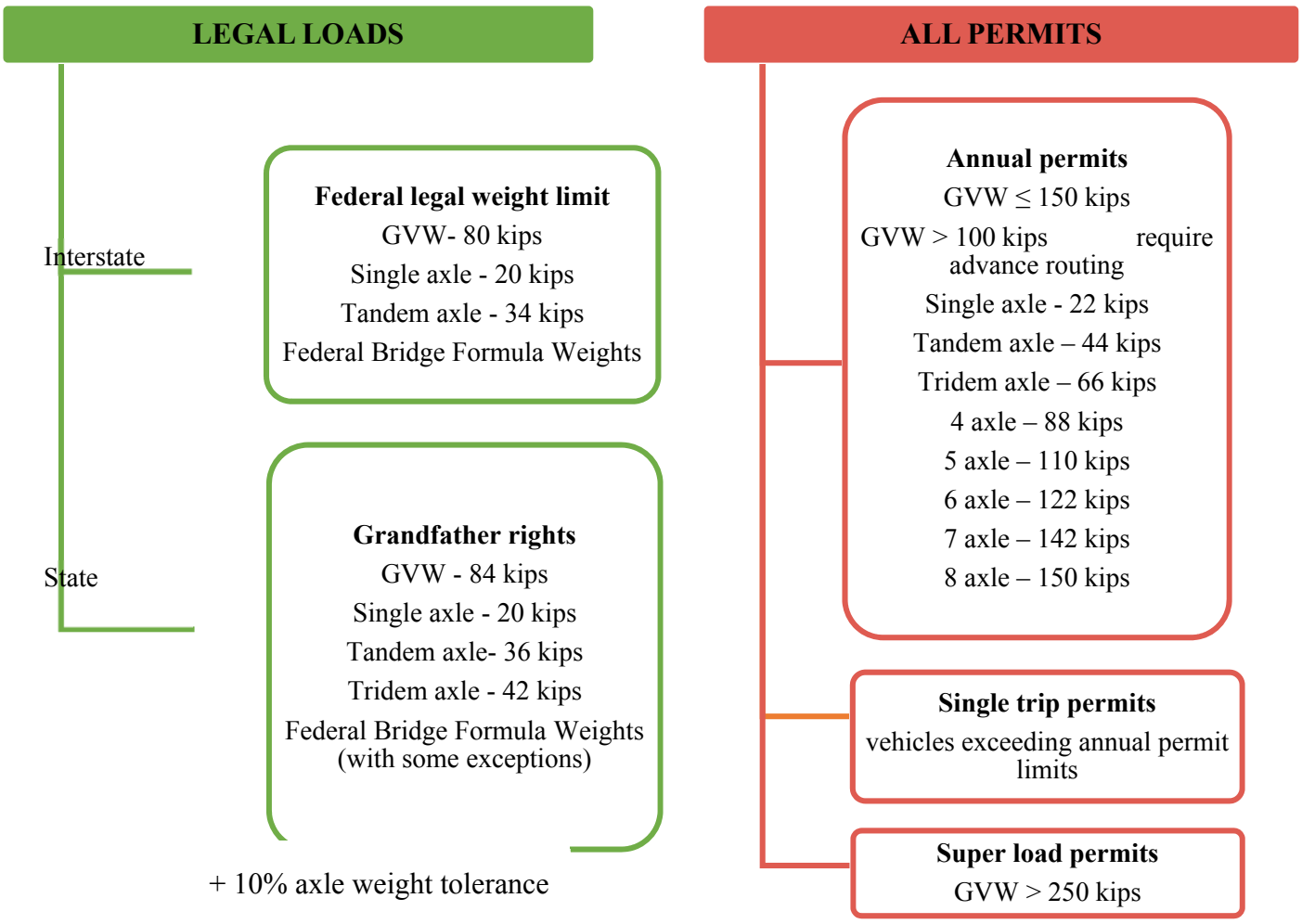

Figure 0-2.Filtering Criteria for Permit Vehicles based on Alabama's Permit Regulation (Iatsko et al. 2017 - prepared by A. Ramesh Babu)

Permits issued by Alabama DOT for the route, where a particular WIM station is located, were selected based on the permit category (weight, length, or width) and route description provided. The total number of WIM vehicles requiring permits (1,806,278 - Table 0-1), with regard to WIM locations, is substantially higher than the number of permits that were issued (89,775), even though the permit trucks often pass more than one WIM site. This disproportion can be greater since WIM data represents the traffic data collected from only 12 WIM sites, while the

database of issued permits includes all permitted vehicles operating in the State. It indicates a need to assess the percentage of illegal traffic operating on the state's bridges and roads.

Table 0-1.Summary of the Vehicles by Category for 2014

Station code	WIM Database			Database of issued permits	
	Legal vehicles	Vehicles that require permits	%	Permits issued by state	%
911 (US280)	334,793	25,222	7	2,510	1
915 (US43)	236,492	30,992	12	2,995	1
918 (I20)	Eliminated from analysis				
931 (I65)	939,109	636,555	40	24,421	2
933 (AL157)	394,988	33,507	8	1,108	0.3
934 (US78)	148,615	20,203	12	2,824	2
942 (US231)	726,121	37,966	5	4,448	1
960 (US84)	229,546	66,736	23	2,038	1
961 (I65)	638,383	171,138	21	24,421	3
963 (I10)	981,801	715,257	42	15,118	1
964 (US231)	571,105	53,538	9	4,448	1
965 (I85)	1,849,149	15,164	1	5,444	0.3
Total	7,050,102	1,806,278	Avg=20%	89,775	Avg=1%

5.5. Permit Vehicle Detection

The first step in a procedure to identify permit and illegal trucks in the WIM database is to determine if there is any relationship between the vehicle configuration and category of vehicle (Legal, Permit or Illegal). In other words, is there any feature in vehicle configuration that can be grouped under Permit or Illegal traffic group? The anomalies in vehicle configurations that do not comply with clusters of Permit or Legal databases were considered in this study (Fiorillo and Ghosn 2014). This approach was expected to help in determining when a truck is illegal.

The procedure of identifying illegal vehicles in the WIM database is complicated due to the absence of the configuration features that distinguish them from permitted trucks. For example, Class 9 (5-axle, single trailer) is dominating for GVW permit criteria covering 897,863 or 50% of all WIM overloaded permit trucks in 2014. However, for the same period, only 6,666 permits were issued in Alabama for 5-axle trucks with Class 9 configuration. Therefore, 99% of Class 9 trucks that require a permit because of GVW operate without it.

To determine the distribution of issued permits and overloaded WIM trucks, both groups/databases were categorized depending on the permit limit they exceeded (Figure 0-2). The histogram representing the percentage of vehicles selected by each permit criterion is shown in Figure 0-3(a) and Figure 0-3(b) for each WIM site. Over 99% of State DOT permits were issued to the trucks exceeding legal GVW limit, while permits for exceeding individual axle limit or Formula B is not issued. From Figure 0-3(b), only about two-thirds (66%) of overloaded WIM trucks require permits due to the GVW. Thus, the remaining WIM trucks with overloaded individual, tandem or tridem axles or violating Formula B are mostly operating illegally.

Another aspect indicating the illegal trucks in the WIM database is GVW and axle weight distribution. There are weight distribution features that can help to recognize an illegal vehicle in the WIM database. For example, the total weight of WIM overloaded trucks of Class 9 varies from 40 to 220kips, while ALDOT issued permits for the same Class with the maximum GVW of 110kips. Similarly, according to WIM records, permit truck axles are loaded in the range up to 70 kips, while the maximum permitted axle load is 25 kips. These limitations can serve as exceptions in the procedure of identification of illegal trucks.

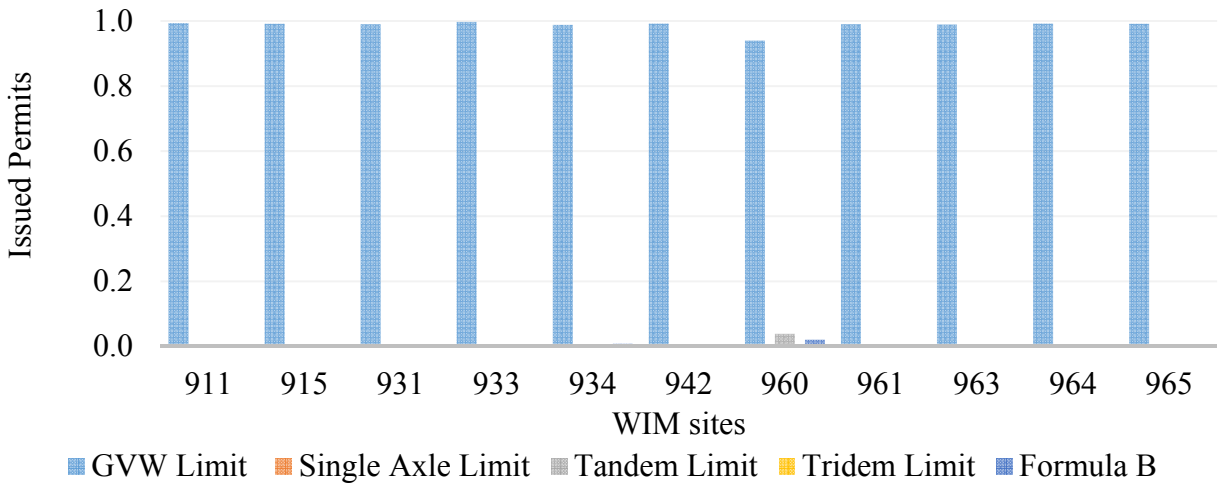

a)

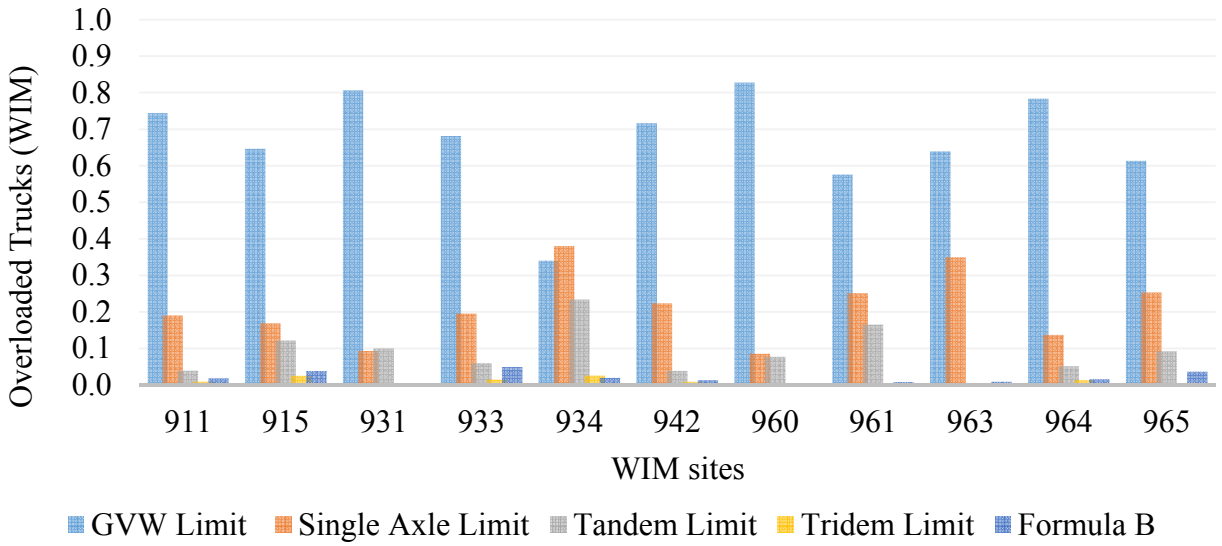

b)

Figure 0-3. Distribution of Overloaded WIM Trucks based on Legal Load regulations for (a) State Issued Permits (b) Overloaded trucks sorted in WIM

The database of WIM overloaded trucks was further analyzed with the procedure developed to determine compliance of the WIM truck with the corresponding issued permit. The proposed matching algorithm is based on the available information: detailed route, a period of permit

validity, the number of axles and axle configuration. Bending plate measurement tolerance (*ASTM E1318 - 09 Standard Specification for Highway Weigh-in-Motion (WIM) Systems with User Requirements and Test Methods* 2009) is also included in the procedure. The position of a truck, lane, and direction of travel are not considered. Axle weight and GVW illegal exceptions discussed in the earlier section are applied before the matching procedure to eliminate obviously illegal vehicles, even though these criteria can detect only 1-2% of violators. All cases of matching are recorded as separate matrices containing the information of GVW, weight distribution, and axle spacing configuration.

5.5.1. Gross Vehicle Weight

Comparisons of GVW were made for three cases: permits issued, permit trucks identified in the WIM data, and illegal trucks. As an example, the cumulative distribution functions (CDF's) of GVW are plotted on normal probability paper for WIM site 933 (Figure 0-4 (a) and (b)). The construction and application of the normal probability paper is described in Chapter2.2. .

The analysis of the plotted data indicates that the shapes of the cumulative distribution functions (CDF's) of the WIM and ALDOT permit data are not similar. Distribution of GVW for the issued permits demonstrates a more severe pattern than the corresponding WIM records. In Figure 0-4(a), the CDF's for GVW are shown for permit trucks in WIM data and issued permits. The highest GVW in WIM is 160 kips and for issued permits it is 400kips. From Figure 0-4(b) it is clear that permit regulations do not cover overloaded vehicles with GVW below 80kips.

The upper tails of the CDF's demonstrate a significant difference between WIM and permit data. According to ALDOT permit reports, 5% of the heaviest permitted vehicles have GVW in the range from 200 to 400 kips for WIM site 933.

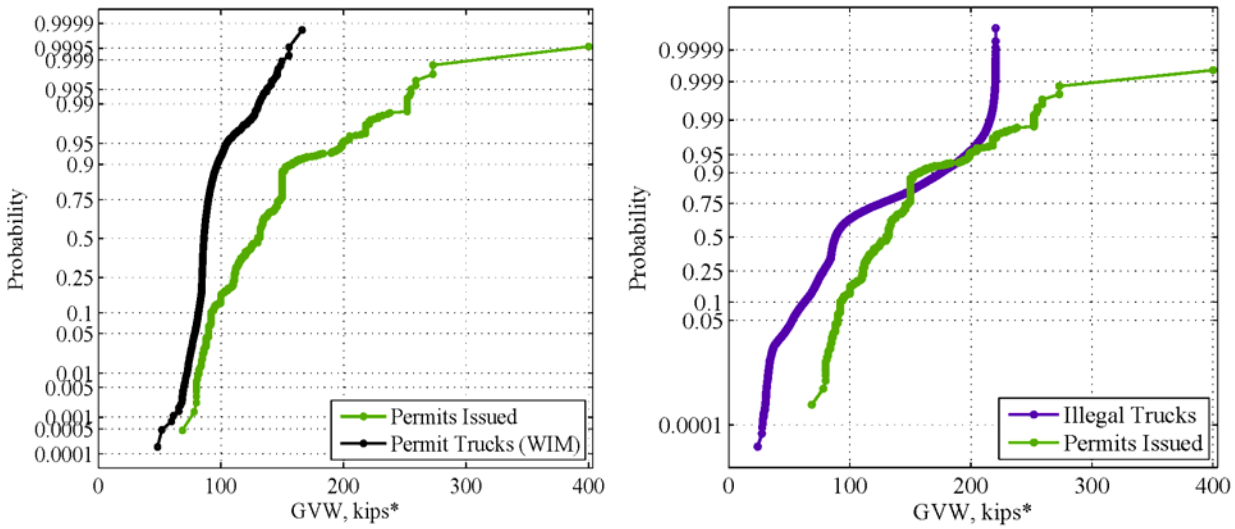

a) b)

Figure 0-4. CDF's of GVW for location 933 (a) ALDOT vs. WIM-based permits and (b) ALDOT permits vs. detected illegals in WIM data.

5.5.2. Load effects

Repeatable load effects caused by moving trucks often lead to progressive damage to the road and structural components of bridges. To assess the magnitude of the load effect, each truck in WIM and ALDOT permit databases were run over influence lines and the maximum values of bending moment and shear force were calculated before the matching procedure is applied. The calculations were performed for simple spans of 30, 60, 90, 120 and 200ft. The resulting moments and shear forces were divided by the corresponding HL-93 moments and shear forces. The CDF's of these nondimensional ratios are plotted on normal probability paper. In Figure 0-5 and Figure 0-6 the CDF's of moment ratios are plotted for the same location 933 for 30, and 200ft spans, respectively.

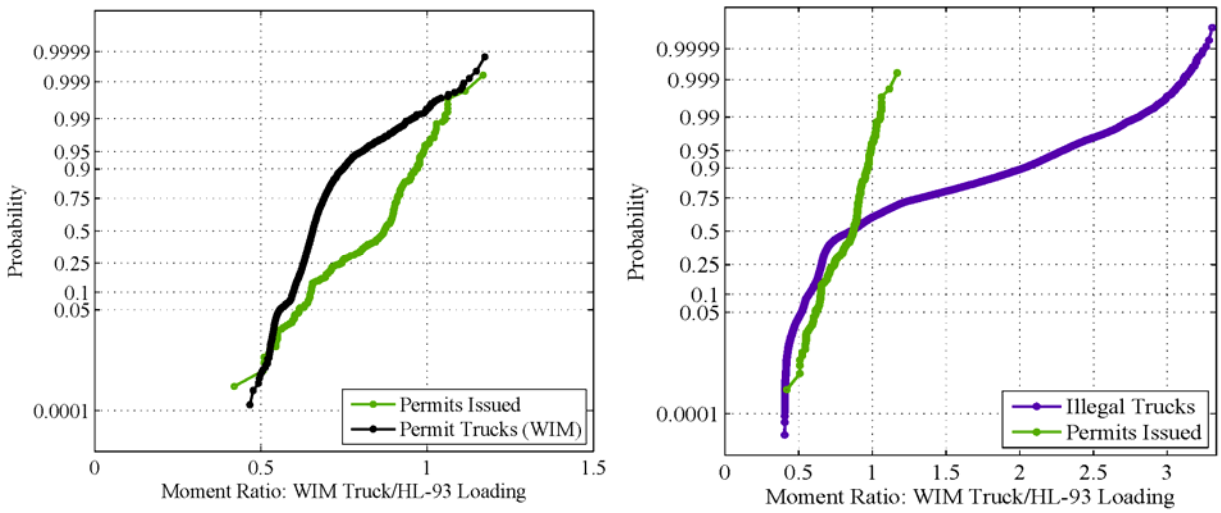

a) b)

Figure 0-5.CDF's of Moment Ratios of 30ft (9 m) for Location 933 (a) for ALDOT vs. WIM Permit Vehicles and (b) ALDOT Permits and Detected Illegals

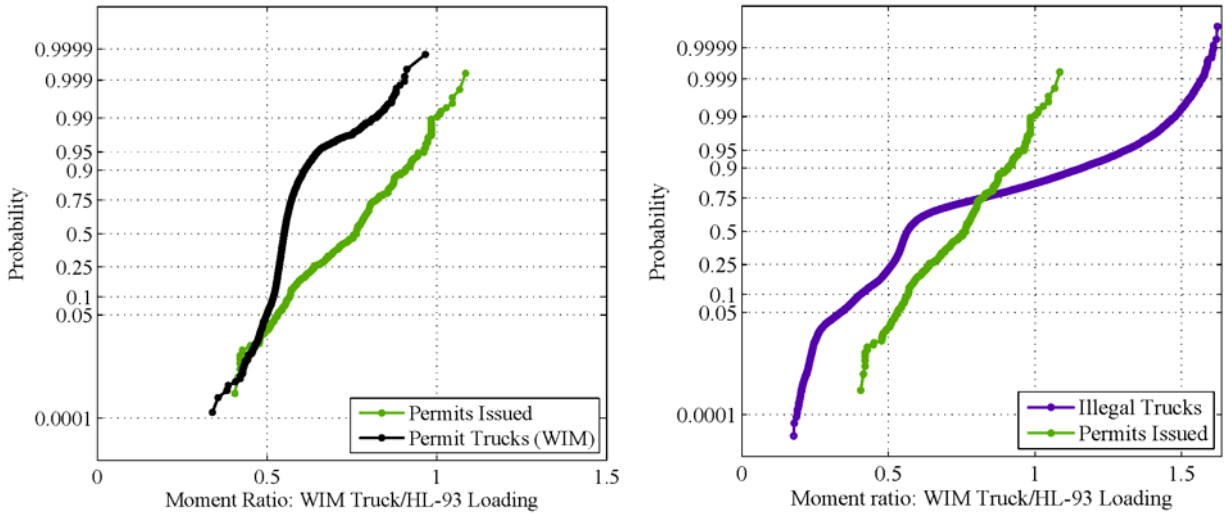

a) b)

Figure 0-6.CDF's of Moment Ratios of 200ft (60m) for Location 933 (a) ALDOT vs. WIM Permit Vehicles and (b) ALDOT Permits and Detected Illegals.

The overall shapes of CDF's representing load effects caused by the trucks and WIM-based permits are not consistent with all cases. The mean value of the moment ratio for the 30ft span

varies from 0.7 to 0.9 for both: the issued permits and corresponding permit trucks identified in the WIM data (Figure 0-5 (a)). Although vehicle configurations listed in permit applications have more severe effects for 200ft span than the corresponding WIM records, the maximum value hardly exceeds 1 (Figure 0-6 (a)).

From Figure 0-5 (b) and Figure 0-6 (b), the upper tail of CDF representing the illegal vehicles identified in WIM data significantly overlaps issued permits. The maximum short span effect caused by illegal trucks is 3.5 while the maximum expected from permits issued is 1.1. The similar but less critical pattern is shown in Figure 0-6 (b); for the 200ft span the moment ratio caused by illegal trucks is 1.6 while maximum permitted is 1.1.

5.5.3. Axle Weight Distribution Pattern

Application of the matching procedure detected a pattern of inconsistency in axle weight distribution recorded by WIM sensors and described in the permit applications. For many records, the axle load distribution in the permit database is uniformly distributed among axles, whereas in the WIM database it is not uniformly distributed. The actual axle weight distribution recorded by the WIM site is more severe even if the GVW is lower, as it is shown in Figure 0-7. In this case, the load effect created by the WIM truck is higher due to concentrated 3^{rd} and 4^{th} axle loads that exceed the permitted pattern. In average, 3^{rd}, $4^{th,}$ and 5^{th} axle load is up to 20% greater than it is declared in the corresponding permit application. This is possible because a permit is issued without the truck being weighed. This indicates a shortcoming of current permitting procedure that may control GVW but not axle weight.

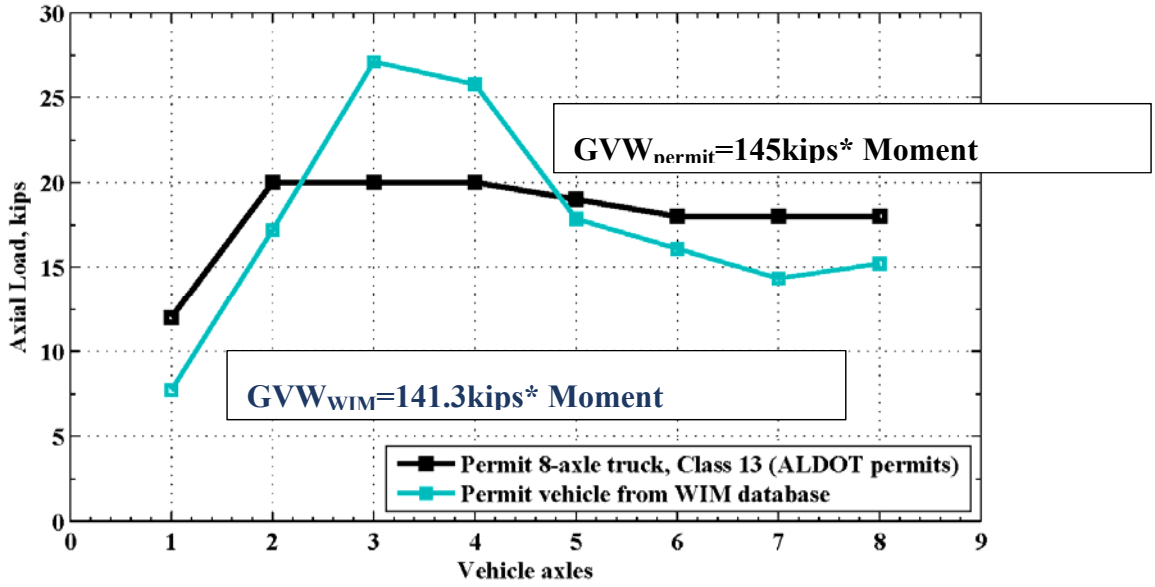

Figure 0-7. Axle Weight Distribution for 8-axle Permitted Truck vs. Corresponding WIM Record.

Calibration of Load and Resistance Factors for Bridge Design Specification

6.1. Summary

Current AASHTO LRFD Bridge Design Specification was calibrated using statistical parameters of load and resistance from the 1970's and early 1980's. In the original reliability-based procedure the load factors were calculated assuming that the design factored resistance is located two standard deviations below the mean value. The resistance parameters were calculated using the Rackwitz-Fiesler procedure and previously determined load factors. The acceptability criterion was closeness to the target reliability index (β=3.5). To count for the recent updates in the reliability-based code development procedures, load and resistance statistics, the original calibration of AASHTO LRFD design formula for Strength I Limit state has been re-visited in this study. The new load and resistance factors were determined as coordinates of the so-called "design point" for reinforced concrete T-beams, prestressed concrete and steel girder bridges as in the original calibration. The new load and resistance factors, along with the updated design formula is proposed in this chapter.

6.2. Design Formula

This study is focused on updating the load and resistance factors for the design of structural components of new bridges. The current version of AASHTO LRFD Bridge Design Specification was based on the Standard Specification for Highway Bridges (AASHTO 2002).

The basic design formula for structural components in the Standard Specifications (AASHTO 2002) is:

$$1.3\,D+2.17\,(LL+I) < \phi\,R \qquad \textbf{Equation 0-1}$$

where: D – dead load effect

LL – live load effect (HS-20 truck)

I – dynamic impact

R – carrying capacity (structural resistance)

ϕ – resistance factor

Transitioning from the Standard Specifications (AASHTO, 2002) to AASHTO LRFD four types of the limit state were introduced and corresponding load and resistance factors developed (Table 3.10.1.1-1, (*AASHTO LRFD* 2014). The AASHTO LRFD design formula for bridge structural components is:

$$\mathbf{1.25}\,\boldsymbol{D} + \mathbf{1.50}\,\boldsymbol{D_w} + \mathbf{1.75}\,(\boldsymbol{LL} + \boldsymbol{I}) < \boldsymbol{\phi}\,\boldsymbol{R} \qquad \textbf{Equation 0-2}$$

where: D_w – dead load effect due to wearing surface

LL – live load effect (HL-93 loading)

ϕ – resistance factor

From $\mathbf{1.25}\,\boldsymbol{D} + \mathbf{1.50}\,\boldsymbol{D_w} + \mathbf{1.75}\,(\boldsymbol{LL} + \boldsymbol{I}) < \boldsymbol{\phi}\,\boldsymbol{R}$ Equation 0-2 the significant changes were done to the load side of the design formula, i.e. load components and load factors. This means that the safety margin is mostly assured by the load factors, which increase the design load. Thus, the probability of exceedance is acceptably lower. The role of the resistance

factor is to decrease the design load carrying capacity, to result in an acceptably low probability of exceeding the critical level.

Over the last few decades, there are considerable changes observed in the magnitude and variability of the load and resistance components (Szerszen and Nowak 2003), (Nowak and Szerszen 2003), (SHRP 2 Research Reports 2015). Thus, it is important to revisit the original calibration and update the existing load and resistance factors accordingly. The re-calibration process involves the reliability-based analysis and defining the position of the so-called "design point" at the failure surface (Nowak and Collins 2012).

6.3. Reliability Analysis Procedure

There are a few methods available for reliability analysis (Thoft-Christensen and Baker 1982), (Rackwitz and Flessler 1978), (Melchers 1988), (Nowak and Collins 2012). In this study, the reliability index β, type of distribution of load Q (Figure 0-1) and resistance R (Figure 0-2), and coordinates of the "design point" Q^* and R^* are unknown, and the limit state function is linear. Thus, the calibration procedure is developed based on iterative Rackwitz-Fiessler method (Rackwitz and Flessler 1978).

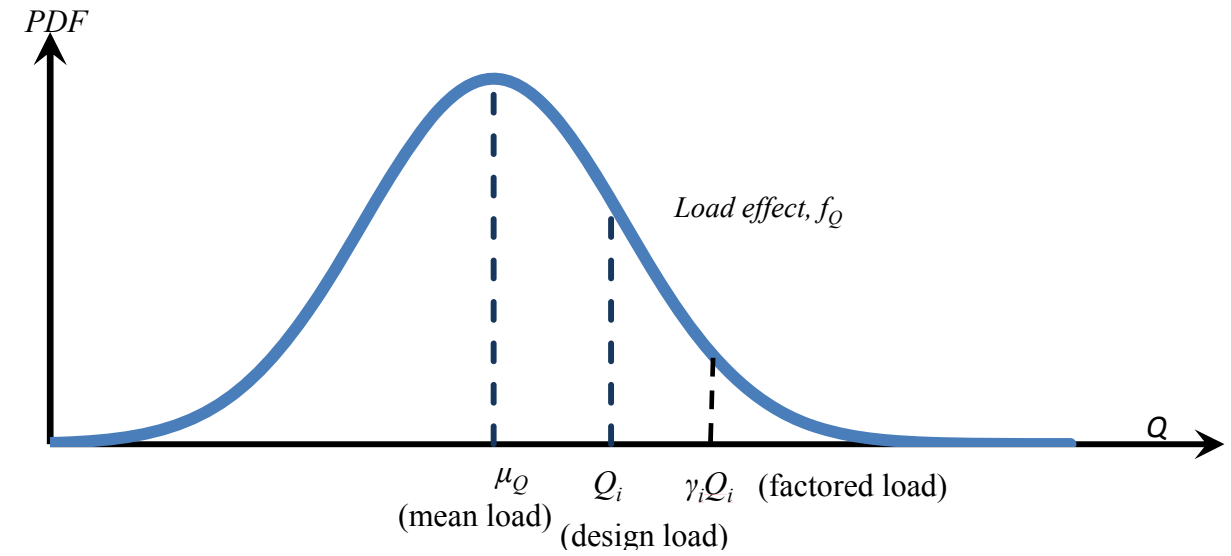

Figure 0-1. Location of the Factored Load Effect

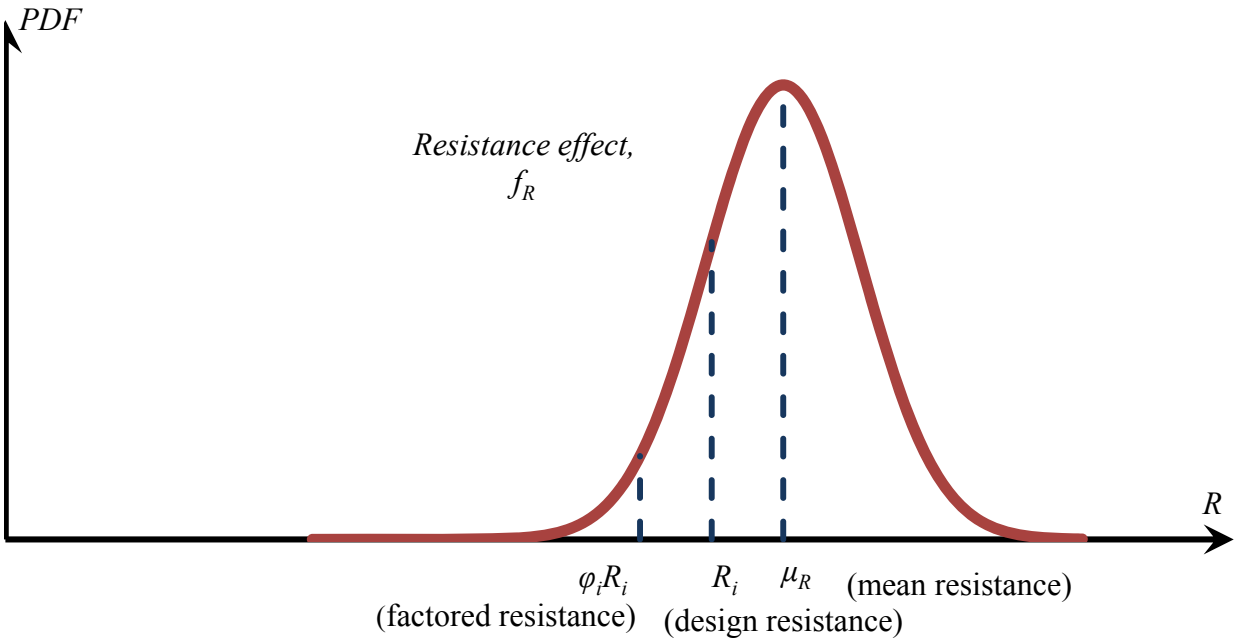

Figure 0-2. Location of the Factored Resistance Effect

In the description of calibration procedure, the design formula is presented in basic format:

$$\sum_{i=1}^{n}(\gamma_i Q_i) = \phi R \qquad \textbf{Equation 0-3}$$

Where: n – number of load components in the design formula

Q_i – nominal value load component

γ_i – load factor of Q_i

R – nominal resistance of the structural component

ϕ – resistance factor

The coordinates of the "design point" Q_i^* and R^* are unknown. Thus for the first iteration, the design point is located on the failure boundary ($R^* = Q^*$), where $R^* = \phi R$ (Figure 0-2) and $Q_i^* = \gamma_i Q_i$ (Figure 0-1). In this study, the initial factors of load and resistance were taken from the current design formula ($\mathbf{1.25\,D + 1.50\,D_w + 1.75\,(LL + I) < \phi\,R}$ Equation 0-2).

The reliability analysis was performed for the selected design cases. For each design case, the statistical parameters of the load Q_i and resistance R_i components were determined based on available WIM databases and literature.

For the given statistics of n load components, such as mean μ_{Qi} and standard deviation σ_{Qi} the resultant parameters can be determined as follows :

$$\boldsymbol{\mu_Q = \sum_{i=1}^{n} (\mu_{Q_1} \ldots, \mu_{Q_n})} \qquad \textbf{Equation 0-4}$$

Where: μ_{Qi} – mean value of Q_i

n – the number of load components in the design formula

$$\boldsymbol{\sigma_Q = \sqrt{\sum (\sigma_i)^2 \ldots, (\sigma_n)^2}} \qquad \textbf{Equation 0-5}$$

Where: σ_{Qi} – standard deviation of Q_i

If the statistical parameters (bias factor λ_R and coefficient of variation V_R) of resistance are known, the value of nominal (design) value of resistance R_n can be determined from $\sum_{i=1}^{n}(\gamma_i Q_i) = \phi R$ Equation 0-3. The corresponding reliability index computed based on the $\beta = \frac{\mu_R - \mu_Q}{\sqrt{\sigma_R^2 + \sigma_Q^2}}$ Equation 0-24. Knowing the value of β, the coordinates of the design point for the next iteration can be calculated using $R^* = \mu_R - \frac{\beta \sigma_R^2}{\sqrt{\sigma_R^2 + \sigma_Q^2}}$ Equation 0-18 and $Q^* = \mu_Q + \frac{\beta \sigma_Q^2}{\sqrt{\sigma_R^2 + \sigma_Q^2}}$ Equation 0-19.

For each load component, Q_i, the optimum load factor, γ_i, is determined as a ratio between the initially assumed design point and calculated in the new one ($\gamma_i = \frac{\lambda_{Q_i} Q_i^*}{\mu_{Q_i}}$ Equation 0-6):

$$\gamma_i = \frac{\lambda_{Q_i} Q_i^*}{\mu_{Q_i}} \qquad \textbf{Equation 0-6}$$

where: λ_{Qi} – bias factor of Q_i

Q_i^* - coordinate of the design point

and for resistance ($\phi = \frac{\lambda_R R^*}{\mu_R}$ Equation 0-7):

$$\phi = \frac{\lambda_R R^*}{\mu_R} \qquad \textbf{Equation 0-7}$$

To be conservative in the actual re-calibration, the resistance is assumed to be normally distributed, while load components are considered to be lognormal.

6.4. Calibration Procedure

The calibration procedure applied in this study included the following steps:

- Selection of representative design cases
- Determination of the statistical parameters of load components
- Determination of the statistical parameters of resistance
- Development of the reliability-based calibration procedure
- Calculation of the load and resistance factors for new design formula

6.5. Representative Design Cases

To be consistent, the reliability analysis is performed for the same design cases as in the original NCHRP Report 368. Representative design cases were selected based on the analysis of about 200 bridges designed according to AASHTO (1989) from different regions of the United States, provided by State DOTs (Nowak 1999). These structures were selected based on types, materials, and span lengths representative for a particular region.

Different types and configurations of girder bridges were considered: prestressed concrete, reinforced concrete T-beams and steel (composite and non-composite). For each material, the analysis is performed for spans: 30, 60, 90, 120 and 200 ft and girder spacing 4, 6, 8, 10 and 12ft. For reinforced concrete T-beams the span length was limited to 60 ft. The analysis was performed for ADTT from 250 to 10,000. For each selected bridge, load effects, as well as load carrying capacity of the structural components were determined. The load components calculated

for the considered design cases for flexure and shear are summarized in **Error! Reference source not found.**.

6.6. Statistical Parameters for Resistance

The parameters of bridge resistance, *R,* depend on the capacity of each structural component. The resistance of a particular bridge component is determined by the strength of material, component geometry, and quality of fabrication. These three quantities are not deterministic and thus define the statistics of the total carrying capacity of a structure. Mathematically, the total capacity of the structural member can be computed as a product of the following random variables:

$$\boldsymbol{R = M\,F\,P\,R_n} \qquad \textbf{Equation 0-8}$$

Where: R_n – Nominal resistance

M – material factor (strength, toughness, modulus of elasticity, etc.)

F – fabrication factor (area of cross-section, modulus of inertia, section modulus, etc.)

P – analysis factor that includes inaccuracy of analysis technique (assumptions, approximations, etc.)

Since the objective of this study is to update the existing load and resistance factors (*AASHTO LRFD* 2014) the reliability analysis was performed for the same design cases as the original calibration (Nowak 1999). The statistical parameters of resistance were developed using test data and simulation for the following cases: prestressed and reinforced concrete girders, composite and non-composite steel girders. For each material, the bias factor λ_R was determined as:

$$\boldsymbol{\lambda_R = \lambda_M \lambda_F \lambda_P}$$ **Equation 0-9**

Where: λ_M – Bias factor of M

λ_F – Bias factor of F

λ_P - Bias factor of P

Similarly the coefficient of variation for the resistance of a structural component, V_R is:

$$\boldsymbol{V_R = \sqrt{V_M^2 + V_F^2 + V_P^2}}$$ **Equation 0-10**

Where: V_M – Coefficient of variation of M

V_F – Coefficient of variation of F

V_P - Coefficient of variation of P

The statistical parameters, the corresponding resultant bias factors and coefficients of variation from the original calibration are listed in Table 0-1.

Table 0-1. Statistical Parameters of Resistance from NCHRP Report 368 (Nowak 1999)

Material	Moment		Shear	
	λ	V	λ	V
Steel – Non-composite	1.12	0.1	1.14	0.105
Steel – Composite	1.12	0.1	1.14	0.105
Reinforced Concrete	1.14	0.13	1.2	0.155
Prestressed Concrete	1.05	0.075	1.15	0.14

Since the 1970's, steel and concrete technology and associated regulations have changed considerably. Substantial research was conducted in order to revise the ACI 318 Code with updated statistics for compressive strength of concrete, the yield strength of reinforcing bars and

tensile strength of prestressing strands (Nowak and Szerszen 2003), (Szerszen and Nowak 2003) and (Nowak et al. 2012b). It was observed that the coefficient of variation of f_c' had been reduced due to more efficient quality control procedures. The compressive strength of concrete has a bias factor, $\lambda_{fc'}$, is equal to 1.3 and 1.1 for f_c'= 3000 psi and f_c'= 12,000 psi respectively. The corresponding coefficients of variation, $V_{fc'}$, varies from 0.17 to 0.10 for the same concrete strength.

In the original calibration grade A36 steel was used. Nowadays, the most common steel grade is ASTM A992 which meets or exceeds the A36 and A572 grade 50 (yielding stress increased more than 38%; ultimate stress increased about 12%). These material parameters can serve as a basis for revising the resistance models for bridge components. It is estimated that the mean load carrying capacity of bridge girders is higher by 5 to 10% compared to what was considered in the original calibration. Some newer data is now available as it is shown in Figure 0-3 and Figure 0-4 and can be used to update the statistical database for the development of the new resistance factors. However, since additional data collection is required to develop updated statistical parameters for the resistance of bridge components, the reliability analysis is carried out using the parameters from Table 0-1.

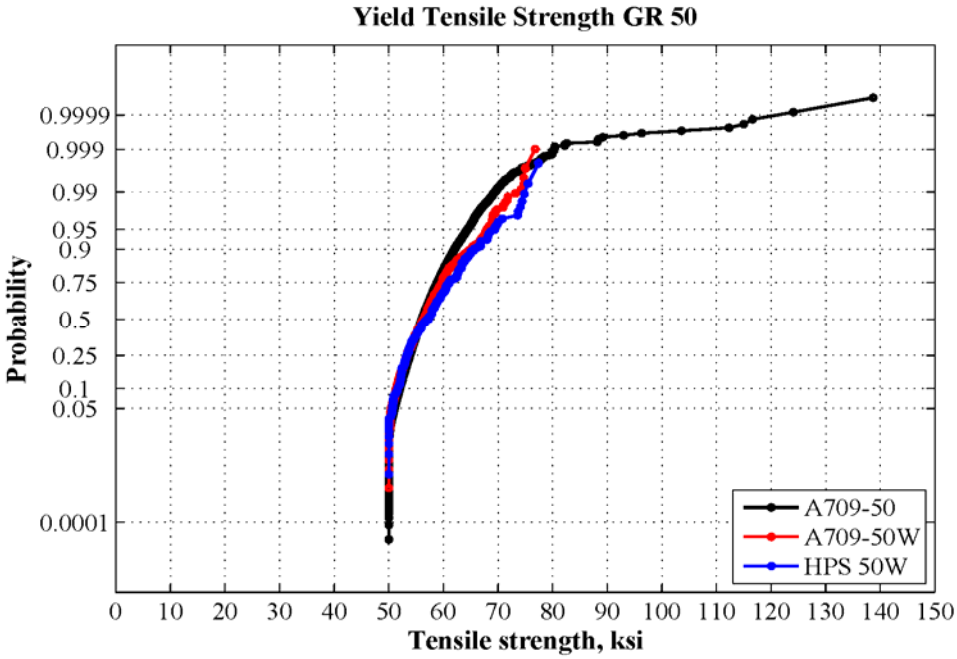

Figure 0-3. Yield Tensile Strength GR 50

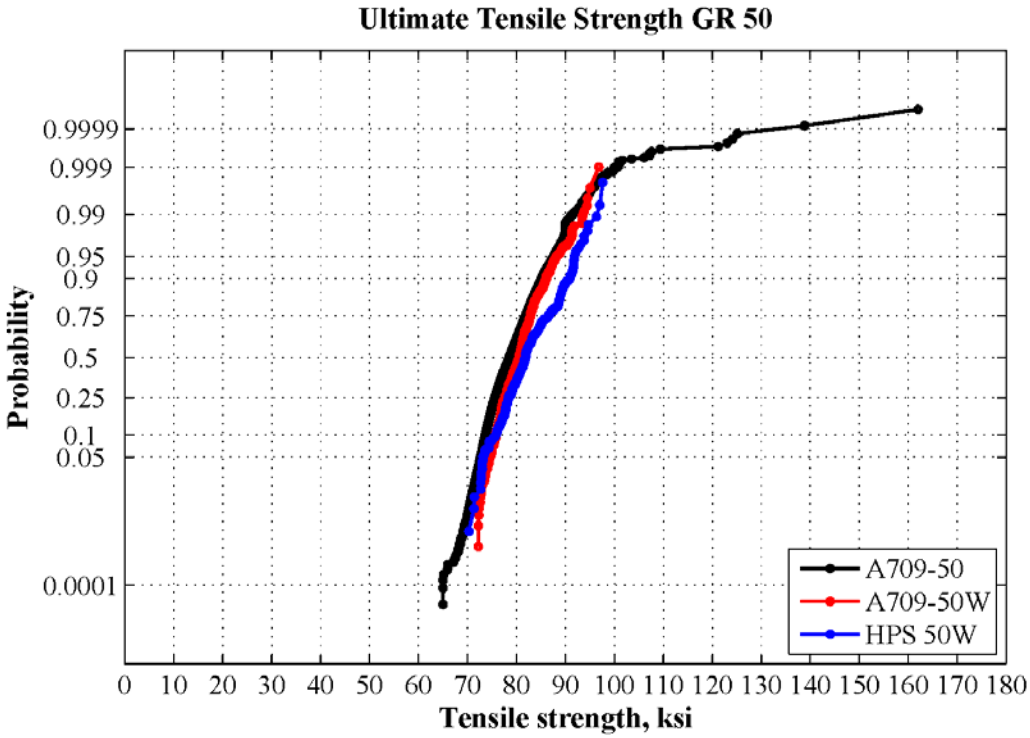

Figure 0-4. Ultimate Tensile Strength GR 50

6.7. Statistical Parameters of Load Components

The basic load combination for bridge components includes the dead load, dead load due to the wearing surface, live load, and dynamic load. Most of the load components contain several subcomponents. Each component is considered as a random variable since it varies depending on condition, type, and parameters of the bridge. It can be described with a type of CDF (normal, log-normal, extreme type, etc.) and corresponding mean and standard deviation. It is also convenient to use the non-dimensional bias factor, which is the ratio of mean-to-nominal value, and the coefficient of variation, equal to the ratio of the standard deviation and the mean. The detailed description of the statistical parameters can be found in 0.

6.7.1. Dead Load

By definition, the dead load, denoted with D, is usually a combination of the gravity loads due to a self-weight of all considered structural and non-structural components. In practice, elements of the structure have different variability. Thus, in bridge engineering the total dead load is divided into several components:

- dead load, D_1, due to the weight of factory-made elements (precast concrete members, steel elements).
- dead load, D_2, due to the weight of cast-in-place concrete members.
- dead load, D_w, due to the weight of the wearing surface (concrete, asphalt).

Since there is no study, similar to NCHRP 368 (Nowak 1999 p. 368), conducted for the recent decades, the statistical parameters of dead load component are assumed to remain unchanged. The bias factors and coefficients of variation are summarized in Table 0-2.

Table 0-2. Statistical Parameters of the Dead Load Components (Nowak 1999)

Component of dead load	Bias factor, λ	Coefficient of variation, V
D_1, weight of factory-made elements	1.03	0.08
D_2, weight of cast-in-place concrete members.	1.05	0.10
D_w, weight of the wearing surface	1.00 (3.5in)	0.25

There are different opinions regarding the accuracy of the statistical parameters for dead load. In 1972, E. (Rosenblueth 1972) raised a concern about the dead load effects being underestimated by designers due to a number of human errors. These errors are mostly related to the geometry of structural members and material properties which are often different than specified in the design documentation. Thus, it is often recommended to apply the coefficient of variation V_D equal to 0.1.

At the same time, the dimensions of bridge structural components are much larger than in buildings. Therefore, the dead load components are less sensitive to a possible variation of weight. According to Galambos (1979) the appropriate bias factor and coefficient of variation for total bridge dead load are 1.05 and 0.08 respectively.

Later on, Nowak and Zhou (1985) performed the study to derive more precise statistical parameters for each dead load component based on the data for (*Ontario Highway Bridge Design Code* 1983). From cumulative distribution functions (CDFs) the statistical parameters for each component of *D* were determined (Table 0-2). The highest uncertainty was associated with the weight of the wearing surface since it is often hard to estimate the actual thickness of asphalt layered one on the top of another. Thus, the thickness of asphalt was simulated based on the data obtained from Ontario Ministry of Transportation. From the CDF plot, the average value was 3.5

in Table 0-2. Based on the shapes of CDFs for D_1, D_2, and D_w, all components were treated as normally distributed random variables.

6.7.2. Static Live Load

For bridges, the live load component includes the effect of forces caused by the traffic flow. This depends on the following factors: bridge configuration, average annual track traffic (ADTT), vehicle axle load distribution and spacing configuration, number of vehicles moving side-by-side (multiple presence) and position of the vehicle on a bridge in longitudinal and transverse direction. To count for these impacts, AASHTO Specifications recommended using live load distribution factors (LLDFs) (U.S. Department of Transportation, FHWA 2015). Live load affects also consists of two components: static, denoted as *LL*, and dynamic, denoted as *I*. The updated statistical parameters for the static component of the live load effect for one lane simple span bridges were developed and presented in 0.

Most of the bridges located on state or interstate roads are multilane bridges. Therefore, the governing live load effect can be a created by some trucks moving side-by-side. The initial line load distribution factors were developed within NCHRP 368 Project (Nowak 1999) using simulation techniques. The maximum live load effect was calculated for a number of lanes from 1 to 4, taking into account the GVW of the vehicles, and the correlation between vehicles moving in parallel. For example, according to simulation results for the two-lane bridge, the probability of occurrence of a single heavy truck is much higher than the probability of occurrence of two very heavy trucks. Thus, for this case, the maximum moment is caused by two fully correlated trucks moving side-by-side in adjacent lanes with the average weight (two-month maximum GVW). The ratio between, two month and 75-years maximum truck is 0.85 for all

considered span lengths. Based on the assumption that for the two-lane bridge the multilane factor for ADTT=1,000 is equal to 1.00, for the one-lane bridge, this factor is equal to the inverse of 0.85. The summary of multilane distribution factors is shown in Table 0-3 for ADTT from 100 to 5,000.

These factors were determined using the Ontario truck survey as a basis for simulation. With the availability of new traffic data, multiple presence statistics was re-visited (Gindy and Nassif 2007), (Fu Gongkang et al. 2013), (SHRP 2 Research Reports 2015). Authors considered different cases of correlation and position of vehicles in adjacent lanes. However, the current design code refers to the values obtained by (Nowak 1999), (*AASHTO LRFD* 2014). Thus, in this analysis, the multiple presence factors listed in Table 0-3 are applied.

Table 0-3. Multilane live load distribution factors (Nowak 1999)

ADTT in one direction	Number of lanes			
	1	2	3	4 or more
100	1.15	0.95	0.65	0.55
1,000	1.20	1.00	0.85	0.60
5,000	1.25	1.05	0.90	0.65

For girder bridges, the lane live load effect transferred to each particular girder through the complex floor system is usually determined by empirical or semi-empirical techniques. These methods are called to determine the girder distribution factor (GDF) that converts the effect caused by one lane of wheels into a bending moment for a particular girder. This factor depends primarily on bridge geometry parameters: span length, number of lanes and girder spacing.

One of the first empirical formulas recommended by AASHTO Standard (AASHTO 2002) remained unchanged since the 1st edition of (AASHTO 1931). It was developed for the short spacing of straight(no skew) girders common in the 1930s. Due to small overlaps typical for that period, the interior girders controlled the design. Thus, for regular steel or concrete girder, the value of GDF is:

$$\boldsymbol{GDF = \frac{S}{D}} \qquad \textbf{Equation 0-11}$$

Where: S – Spacing between girders (center-to-center), ft;

D – Constant equal to 7 and 5.5 for one lane and two lanes respectively.

Although the $\boldsymbol{GDF = \frac{S}{D}}$ Equation 0-11 is simple, the corresponding GDFs were not always accurate.

Current *AASHTO LRFD* (2014) regulates the value of GDF depending on the number of lanes and bridge span length. The empirical formulas were developed separately for flexure and shear in order capture the effects of bridge geometry and stiffness parameters. The provisions defining GDF for 12 different bridge types are available in *AASHTO LRFD* (2014) - Table 4.6.2.2.1-1. The approach was developed as a part of NCHRP Report 12-26 (Zokaie et al. 1991) based on analysis of over 800 random bridges from different locations across the US. The impact of each parameter was approximated using exponential functions. Finally, the formulas presented in the AASHTO Specifications were modified to account for a multiple presence.

The following provisions are applicable for girder bridges with constant width of the deck, girders with approximately the same stiffness, deck overhang below 3.0ft and number of girders

higher than four. For example, the GDF for flexure of I-shape steel interior girder is defined as the maximum of two:

One lane loaded:

$$\mathbf{0.06} + \left(\frac{S}{14}\right)^{0.4}\left(\frac{S}{L}\right)^{0.3}\left(\frac{K_g}{12\,L\,t_s^3}\right)^{0.1} \qquad \textbf{Equation 0-12}$$

Two lanes loaded:

$$\mathbf{0.075} + \left(\frac{S}{9.5}\right)^{0.6}\left(\frac{S}{L}\right)^{0.2}\left(\frac{K_g}{12\,L\,t_s^3}\right)^{0.1} \qquad \textbf{Equation 0-13}$$

Where: L – Span length, ft

t_s – Depth of the concrete slab, in

K_g – Longitudinal stiffness parameter that can be obtained as follows *AASHTO LRFD* (2014), Eq. 4.6.2.2.1-1):

$$\boldsymbol{K_g = n(I + Ae_g^2)} \qquad \textbf{Equation 0-14}$$

Where: A – the area of girder cross-section, in

e_g – distance between the gravity centers of the girder and bridge deck, in

I – moment of inertia of the girder, in^4

n – ratio of modulus of elasticity of the girder(E_B) to modulus of elasticity of bridge deck (E_D):

$$\boldsymbol{n = \frac{E_B}{E_D}} \qquad \textbf{Equation 0-15}$$

Similarly, for shear the GDF for internal girder is a maximum of two:

One lane loaded:

$$\mathbf{0.36 + \frac{S}{25}} \qquad \textbf{Equation 0-16}$$

Two lanes loaded:

$$\mathbf{0.2 + \frac{S}{12} - \left(\frac{S}{35}\right)^2} \qquad \textbf{Equation 0-17}$$

6.7.3. Dynamic Live Load

As it was mentioned before (0. 6.7.2. Static Live Load0) the total live load consists of two components: static and dynamic live load. The latter mainly depends on vehicle suspension system, bridge frequency of vibration and road roughness. The (AASHTO 2002) specified the dynamic impact as a function of a bridge span length, formulated in 1944:

$$\boldsymbol{I = \frac{50}{L+125}} \qquad \textbf{Equation 0-18}$$

Where: L – Span length, ft.

According to $\boldsymbol{I=\frac{50}{L+125}}$ Equation 0-18, the maximum value of the dynamic factor is 0.3.

The statistical model for dynamic impact used in current (*AASHTO LRFD* 2014) was developed based on field tests conducted for the NCHRP Project 368 (Nowak 1999). In this model, the dynamic load factor (DLF) was considered as a fraction of a static load component (*I/L)*, measured in terms of deflection. The results show, that while the static component increases for

the heavier trucks, the dynamic component remains constant (Nassif and Nowak 1995). Therefore, the dynamic load factor decreases for heavier trucks.

The results of simulations indicate that dynamic deflections are almost constant while static deflections increase for heavier trucks. Therefore, the dynamic load factors (DLF), are lower for two trucks than for one truck.

The statistics of the dynamic impact was obtained by applying the DLF to the 75-years maximum static live load effect. According to the results, the 75-years maximum dynamic load is close to the mean value of DLF (Nowak 1999). Since the simultaneous occurrence of two trucks controls in case of longer span bridges, the DLF for two trucks side-by-side is lower. Therefore, the mean value of DLF is equal to 0.15 and 0.1 for a single truck and two trucks respectively. The coefficient of variation is equal to 0.8. The value of DLF applied in the current (*AASHTO LRFD* 2014) is 0.3.

Since a multiple presence of trucks is considered for reliability analysis as a more severe event, the mean value (μ_I) and coefficient of variation (V_I) of the dynamic load factor are taken as 0.10 and 0.8 respectively.

From 0, the average coefficient of variation for 75-years maximum static live load effect, V_L, is approximately equal to 0.12. Thus, the coefficient of variation of the sum of static and dynamic components, V_{L+I} can be determined by the total standard deviation, σ_{LL+I}:

$$\boldsymbol{\sigma_{L+I} = \mu_{LL+I}\, V_{LL+I} = \sqrt{\sigma_{LL}^2 + \sigma_I^2}} \qquad \textbf{Equation 0-19}$$

Where: $\sigma_{LL} = (0.12)\mu_{LL}$ – Standard deviation of the static component of live load effect

$\sigma_{LL} = (0.8)\ (0.1)\mu_{LL}$– Standard deviation of the dynamic component of live load effect

$\mu_{LL+I} = (1.1)\mu_{LL}$ – Mean value of static and dynamic components of live load effect

From $\boldsymbol{\sigma_{L+I} = \mu_{LL+I}\, V_{LL+I} = \sqrt{\sigma_{LL}^2 + \sigma_I^2}}$ Equation 0-19:

$$\sigma_{L+I} = \mu_L\sqrt{(0.12)^2 + (0.08)^2} = 0.144\mu_L$$

Thus, the resultant coefficient of variation, V_{L+I}, for static and dynamic live load is:

$$V_{L+I} = \frac{\sigma_{L+I}}{\mu_{L+I}} \approx 0.14$$

The total load as a sum of several components can

6.8. Updated Load and Resistance Factors

The reliability-based calibration procedure was applied to the design cases described in Chapter 0.

6.8.1. Recommended Load and Resistance

The resultant reliability indices for prestressed concrete AASHTO girder, reinforced concrete T-girder, and steel girder bridges are shown in Figure 0-5, Figure 0-6 and Figure 0-7 for flexure (a) and shear (b). In average, the reliability index is close to 3.5, which is considered as a target reliability index, β_T, for structural bridge components. A small degree of variation indicates that the code is consistent.

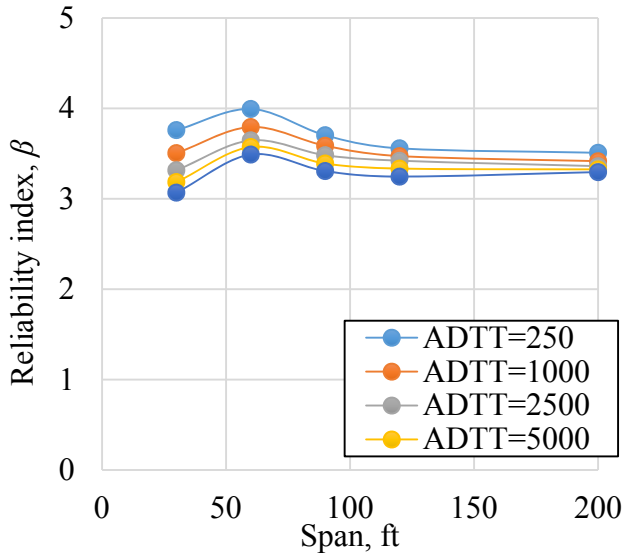

a) b)

Figure 0-5. Reliability Index vs. Span Length for (a) Moment and (b) Shear, for Prestressed Concrete Girders

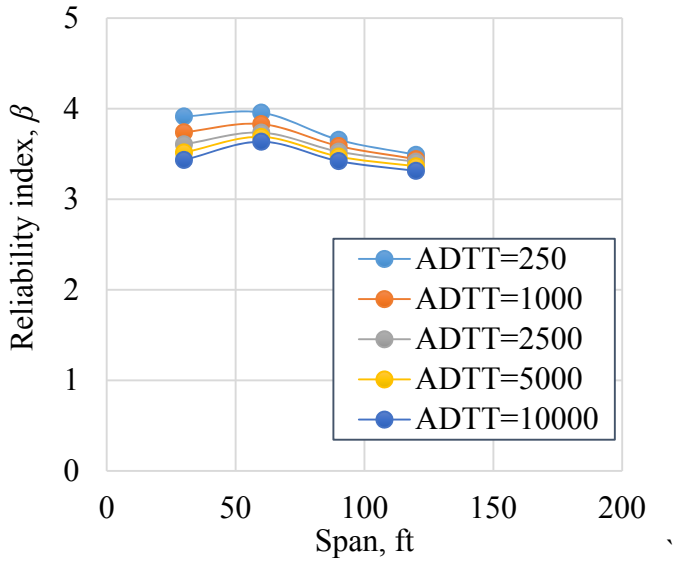

a) b)

Figure 0-6. Reliability Index vs. Span Length for (a) Moment and (b) Shear, for Reinforced Concrete T-Beams

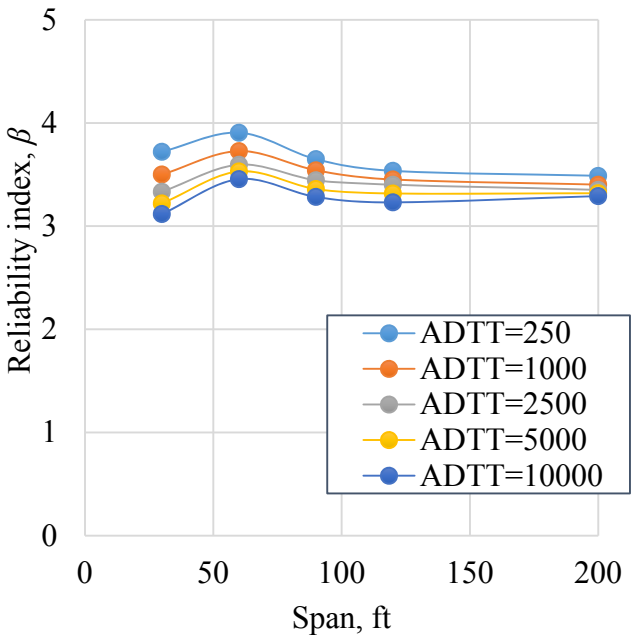

a) b)

Figure 0-7. Reliability Index vs. Span Length for (a) Moment and (b) Shear, for Steel Girders

For these design cases, the coordinates of the design point were also calculated for the current

$R^*=\mu R-\beta\,\sigma R2\sigma R2+\sigma Q2$ Equation 0-18 $Q^*=\mu Q+\beta\,\sigma Q2\sigma R2+\sigma Q2$

Equation 0-19. For each load component, X, the location of the design point is defined by the optimum load factor, γ_X, using the equation:

$$\gamma_X=\frac{\lambda_X X^*}{\mu_X}$$ **Equation 0-20**

where: λ_X - bias factor of X

X^* - coordinate of the design point

μ_x = mean value of X

The updated dead load factors are summarized in Table 0-4 and

Table 0-5 for flexure and shear respectively. The value of optimum load factor corresponds to the target reliability, β_T=3.5.

Table 0-4. Updated Load Factors for Dead Load Components - Flexure

Dead Load Component	Calculated	Optimum	Recommended
γ_{D1}, (weight of factory	1.05-	1.15	1.20
γ_{D2}, (weight of cast-in-	1.10-		
γ_{Dw}, (weight of the wearing	1.03-		

Table 0-5. Updated Load Factors for Dead Load Components - Shear

Dead Load Component	Calculated	Optimum	Recommended
γ_{D1}, (weight of factory	1.07-	1.15	1.20
γ_{D2}, (weight of cast-in-place	1.05-		
γ_{Dw}, (weight of the wearing	1.03-		

As an example, the dead load factors γ_{D2} load factors are shown in Figure 0-8, Figure 0-9 and Figure 0-10 for bending moment (a) and shear (b) for different span prestressed concrete girders, reinforced concrete T-beams and steel girders respectively.

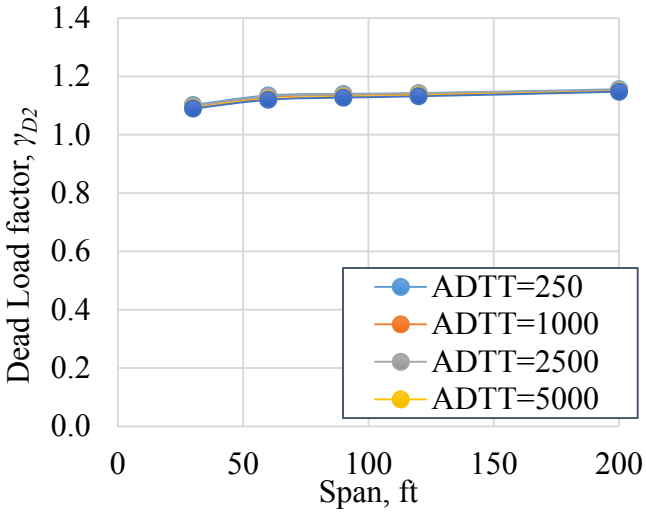

a)

Figure 0-8. Dead Load Factors vs. Span Length for (a) Moment and (b) Shear, for Prestressed Concrete Girders

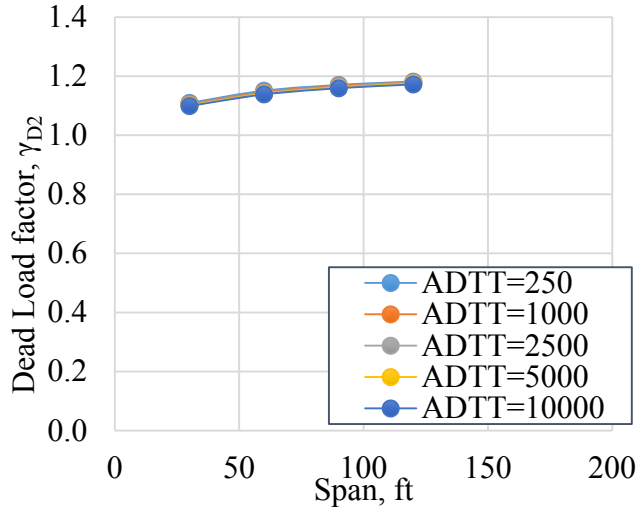

a)

Figure 0-9. Dead Load Factors vs. Span Length for (a) Moment and (b) Shear, for Reinforced Concrete T-Beams Girders

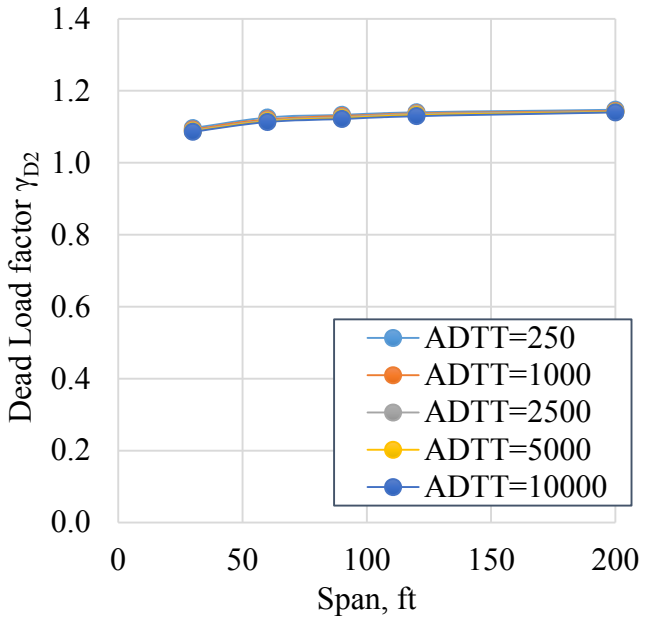

a)

Figure 0-10.Dead Load Factors vs. Span Length for (a) Moment and (b) Shear, for Steel Girders

From Figure 0-8, Figure 0-9 and Figure 0-10 it is clear that the values of the dead load factors are mostly consistent with regard to different span lengths and ADTT. The distribution of the live load factor, in its turn, is substantially more sensitive to the ADTT, material, and length of the girder. Based on the $\gamma X=\frac{\lambda_X X^*}{\mu_X}$ Equation 0-20 the factor defining the position of the "design point" for live load component, γ_{LL}, is:

$$\gamma_{LL}=\frac{\lambda_{LL}\, LL^*}{\mu_{LL}} \qquad \textbf{Equation 0-21}$$

$\gamma LL=\lambda LL\ LL^*\mu LL$ Equation 0-21 are plotted in versus span length for ADTT=250 … 10,000 and prestressed concrete girders, reinforced concrete T-beams and steel girders respectively.

Table 0-6. Updated Load Factors for Live Load Component - Flexure

Material	Live Load	Calculated	Optimum	Recommended
Composite and	1.75	1.35-1.65	1.55	1.60
Prestressed		1.35-1.60		
Reinforced		1.30-1.55		

Table 0-7. Updated Load Factors for Live Load Component - Shear

Material	Live Load	Calculated	Optimum	Recommended
Composite and	1.75	1.4-1.60	1.55	1.60
Prestressed		1.45-1.60		
Reinforced		1.30-1.50		

The optimum live load factor, γ_{LL} falls into the

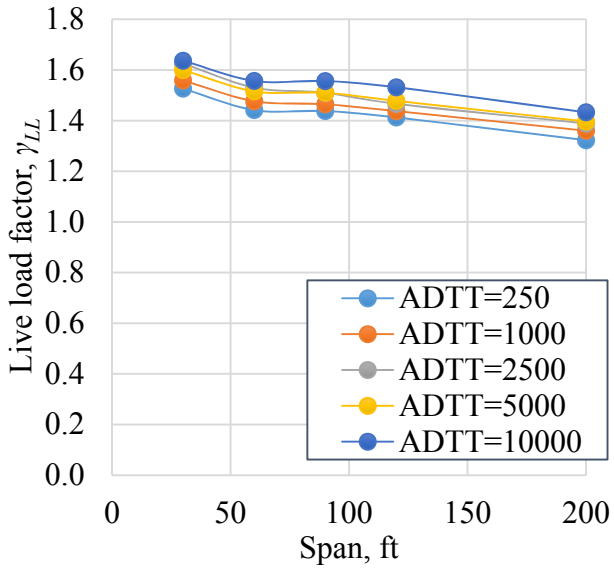

a) b)

Figure 0-11. Live load factor vs. Span Length for (a) Moment and (b) Shear, for Prestressed Concrete Girders

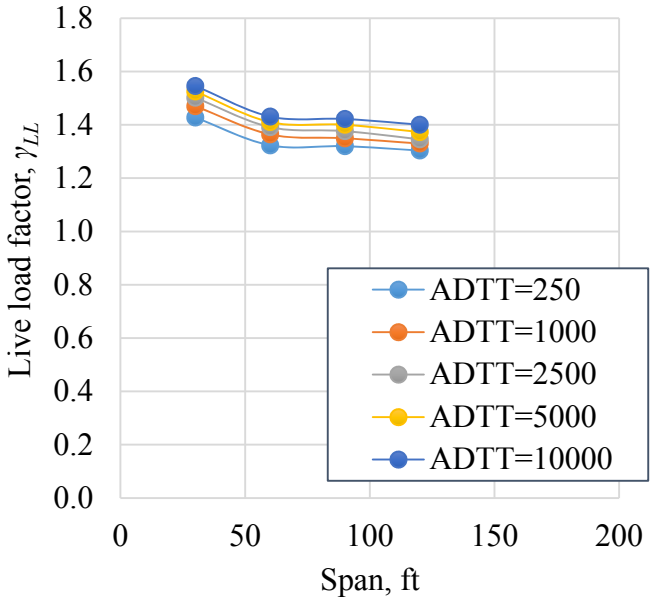

a) b)

Figure 0-12. Live load factor vs. Span Length for (a) Moment and (b) Shear, for Reinforced Concrete T-Beams

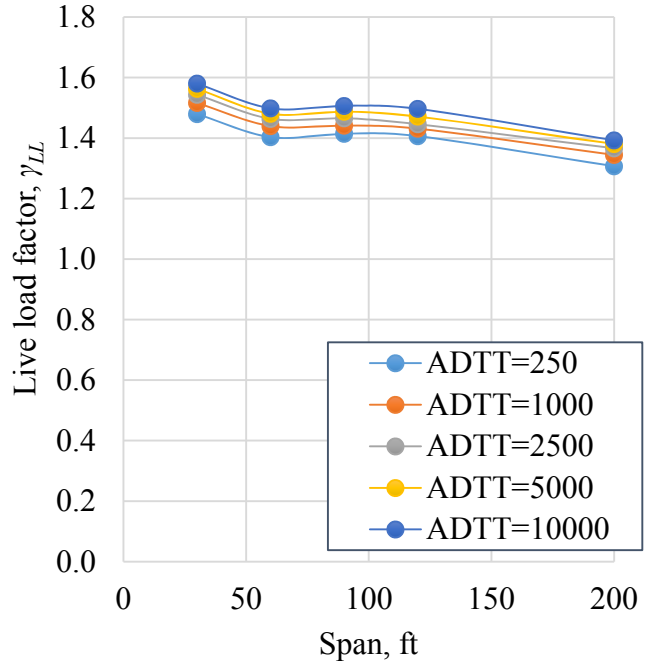

a) b)

Figure 0-13.Live load factor vs. Span Length for (a) Moment and (b) Shear, for Steel Girders

$\lambda RR^{*}\mu R$ Equation 0-7 for the same design cases as factors for the load components. The results are presented in Figure 0-14, **Error! Reference source not found.** and Figure 0-16 for prestressed concrete girders, reinforced concrete T-beams, and steel girders respectively. The results are also summarized in Table 0-8 for flexure and Table 0-9 for shear.

Table 0-8. Resistance factors for flexure according to the current (*AASHTO LRFD* 2014)

Material	Resistance Factor ϕ in Current AASHTO LRFD	Calculated Resistance Factor ϕ	Optimum Resistance Factor ϕ	Recommended Resistance Factor ϕ
Composite and Non-composite steel	1.00	0.85-0.90	0.85	0.9
Prestressed concrete	1.00	0.75-0.80	0.85	0.9
Reinforced concrete	0.90	0.85-0.90	0.75	0.8

Table 0-9. Resistance factors for shear according to the current (*AASHTO LRFD* 2014)

Material	Resistance Factor ϕ in Current AASHTO LRFD	Calculated Resistance Factor ϕ	Recommended Resistance Factor ϕ
Composite and Non-composite steel	1.00	0.85	0.9
Prestressed concrete	0.9	0.75	0.8
Reinforced concrete	0.85	0.70	0.75

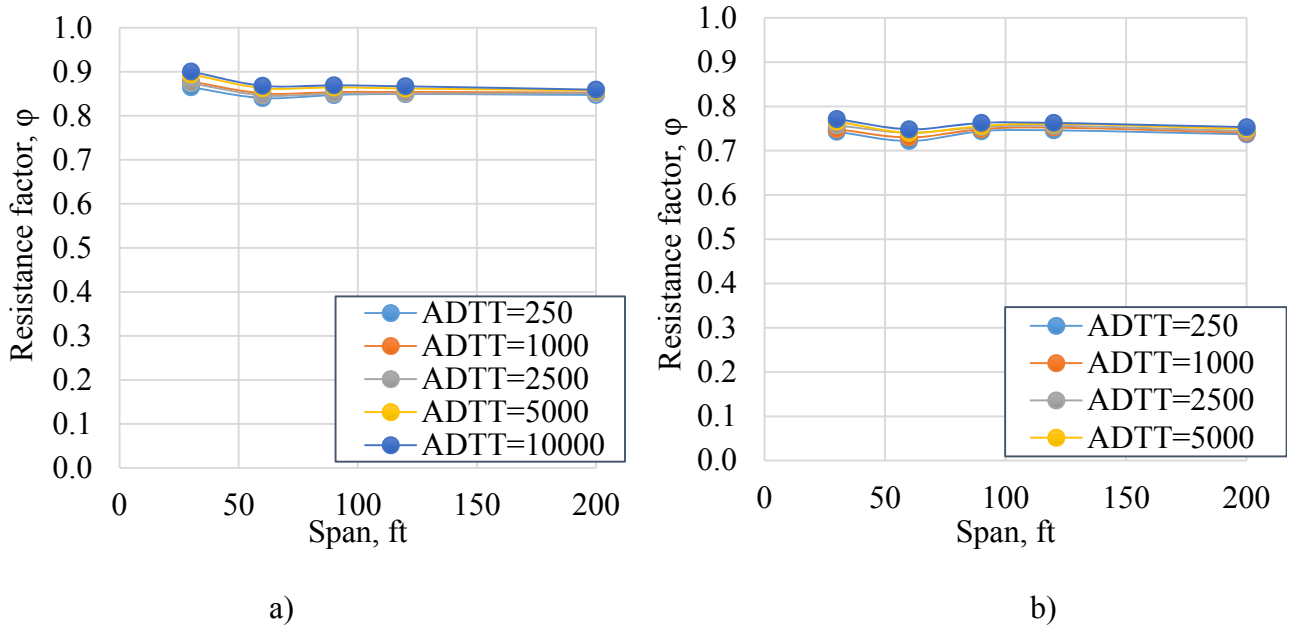

Figure 0-14.Resistance Factor vs. Span Length for (a) Moment and (b) Shear, for Prestressed Concrete Girders

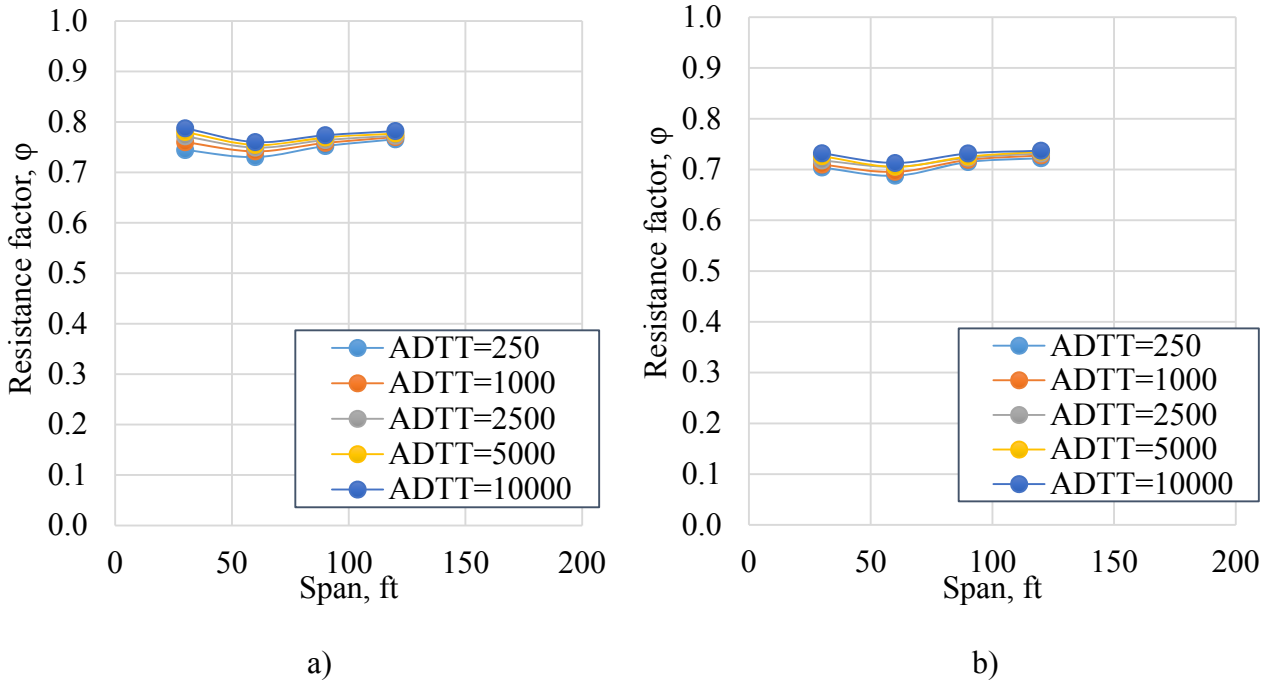

Figure 0-15.Resistance Factor vs. Span Length for (a) Moment and (b) Shear, for Reinforced Concrete T-Beams

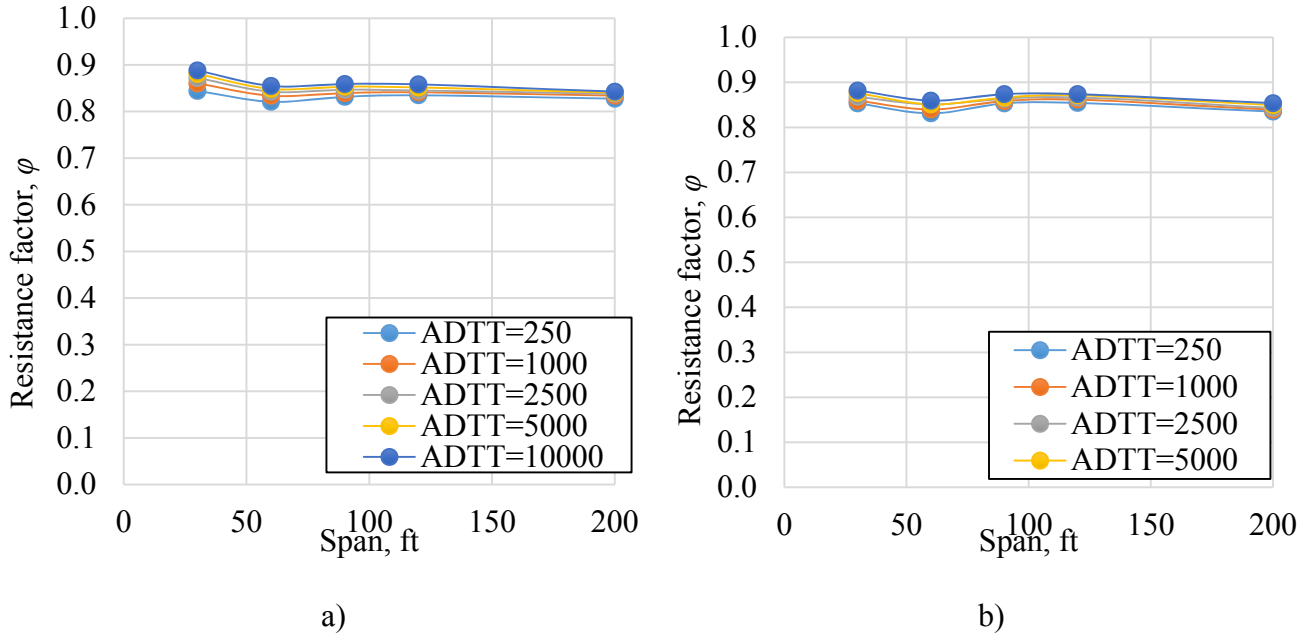

Figure 0-16. Resistance Factor vs. Span Length for (a) Moment and (b) Shear, for Steel Girders

The results indicate that the optimum load and resistance factors corresponding to the coordinates of the design point are about 10-15% lower than what is in the current AASHTO LRFD Specifications (AASHTO 2014). The reliability indices are consistent at about 3.5 level that corresponds to the target reliability index, β_T. The calculated values of live load factor γ_{LL} are between 1.40 and 1.65. Higher value shows only for short span, and it is due to the design tandem load being inadequately low. The calculated dead load factor for three components D_1, D_2 and D_w varies from 1.03 to 1.17 depending on girder material and span length. For simplicity is was decided to consider a single load factor for all components of the dead load. Therefore, the design formula updated with the optimum developed load and resistance factors is:

$$1.15(D_1+D_2+D_W) + 1.55\,(LL + I) \leq 0.85\,R \qquad \textbf{Equation 0-22}$$

As it was mentioned before, the optimum values of load and resistance factors correspond to the same target reliability index, as in the original calibration (Nowak 1999). This location of the "design point" corresponds to the same safety margin as the current design. In order to be more conservative and increase the safety of the new design the more conservative factors 1.20 and 1.60 for dead and live load components respectively are recommended. It is also recommended to increase the optimum resistance factor by 0.05, which is justified because of conservatism in the dead load factor and live load factor. Therefore, the recommended new design formula is:

$$1.20\ (D+D_w) + 1.6\ (LL+I) < \phi R \qquad \textbf{Equation 0-23}$$

The reliability indices are calculated for the recommended load and resistance factors (*1.20 (D+D_w) + 1.6 (LL+I)<ϕR*

Equation

0-23) and compared to the corresponding reliability indices from the current AASHTO LRFD ($\mathbf{1.25\,D + 1.50\,D_w + 1.75\,(LL + I) < \phi\,R}$

Equation 0-2). The results are shown as scatter plot in Figure 0-17(a) for the bending moments and Figure 0-17(b) for shear. The required moment and shear carrying capacity corresponding to the recommended load and resistance factors are about 3-5% higher than for the current (*AASHTO LRFD* 2014).

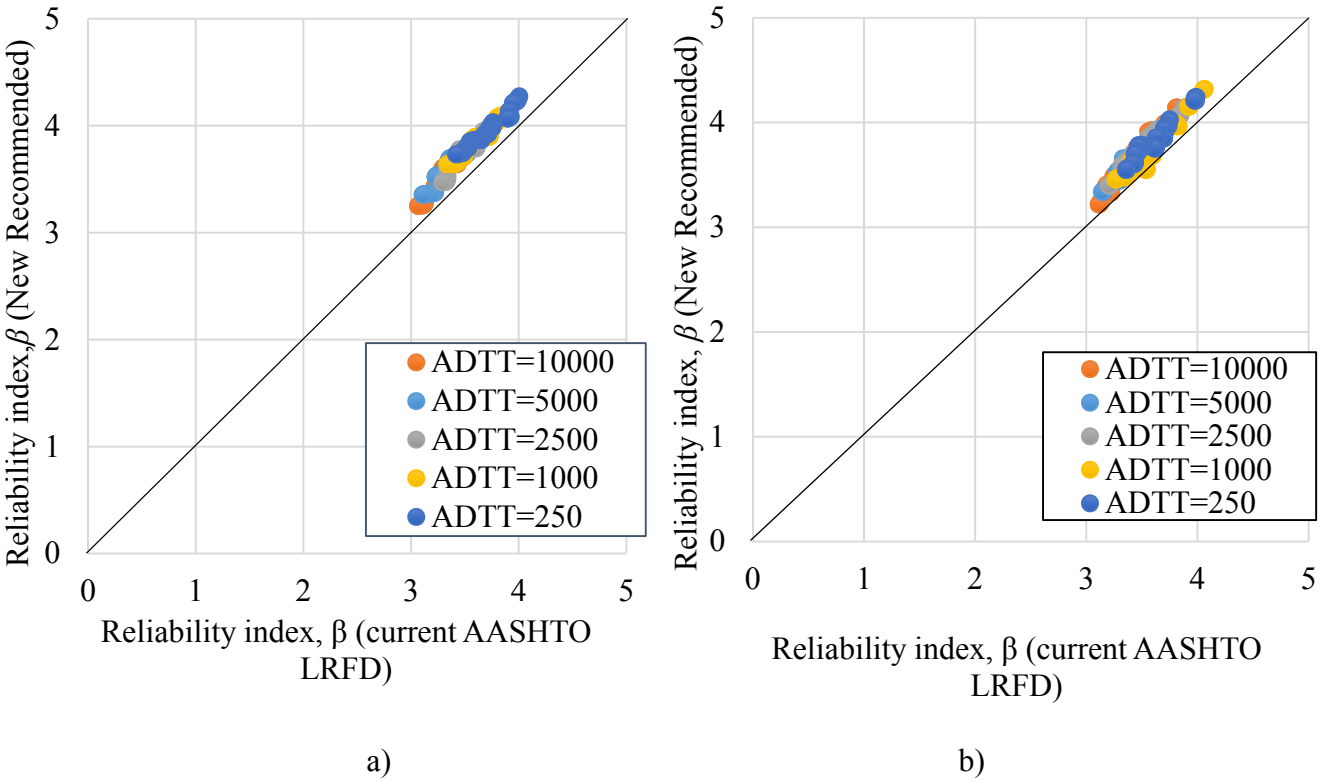

Figure 0-17. Reliability indices for New Recommended Load and Resistance Factors vs. Current AASHTO Code, (a) moment and (b) shear.

The recommended factors are equal to 1.20 for dead load, 1.60 for live load and 0.90 for resistance of steel and P/C girders. Incidentally, these load and resistance factors would then be the same as in American Society of Civil Engineers (2016), American Concrete Institute (2014), American Institute of Steel Construction (2011) and American Wood Council (2015).

The higher value of the live load factor for short spans corresponds to the higher bias factors for the same span length (Figure 0-10). Thus, there is a need to include the effect of the proposed design tandem on the short span live load factors for flexure (Figure 0-18).

6.8.2.Updated Load and Resistance Factors for Flexure using Proposed Tandem Model

According to the current design code (*AASHTO LRFD* 2014), the design live load effect for flexure is controlled by HL-93 design tandem for short span bridges (10-40ft - Figure 0-19). The load and resistance factors, recommended in the previous section, were conservatively selected based on the maximum ADTT and minimum span length. It was concluded (Chapter 0) that the higher bias for short span compared to other span lengths is an indication that the design live load for short spans should be increased. The effect of the proposed design tandem (Figure 0-18) on the location of the design point is analyzed in this Chapter.

The reliability indices were determined for the same design cases using the procedure described in Section 0. The resultant values of β were compared with corresponding reliability indices for prestressed concrete AASHTO girders (Figure 0-18), reinforced concrete T-girders (Figure 0-19) and steel girders (Figure 0-20) obtained using the current HL-93 design tandem.

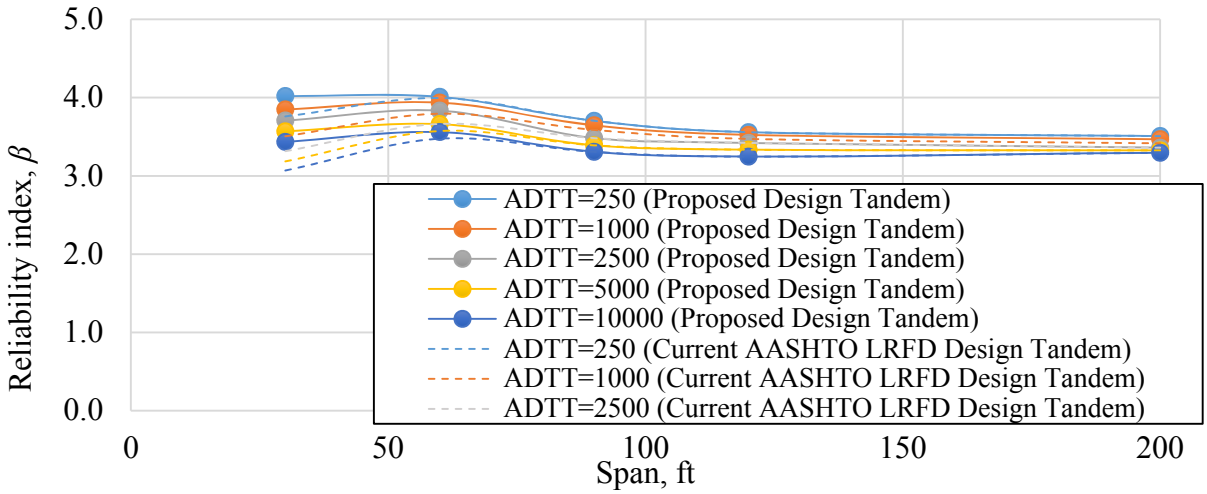

Figure 0-18. Reliability Index vs. Span Length for Moment and Prestressed Concrete Girders (New Design Tandem)

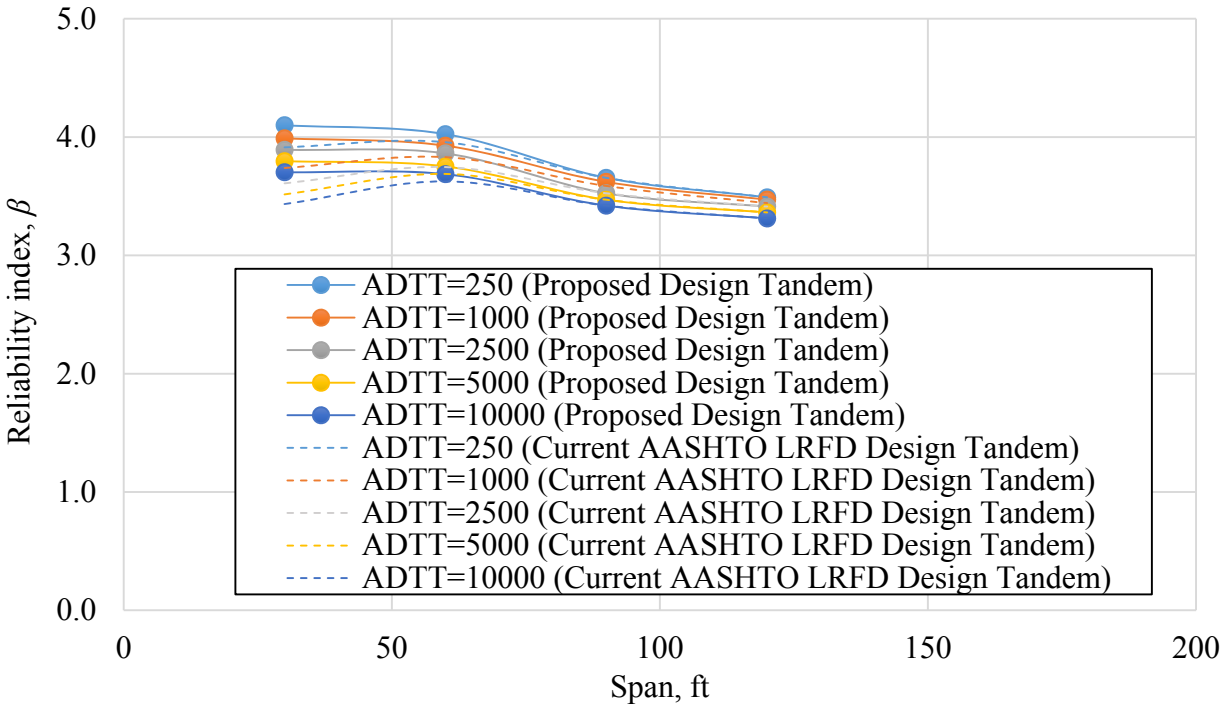

Figure 0-19. Reliability Index vs. Span Length for Moment and Reinforced Concrete Girders (New Design Tandem)

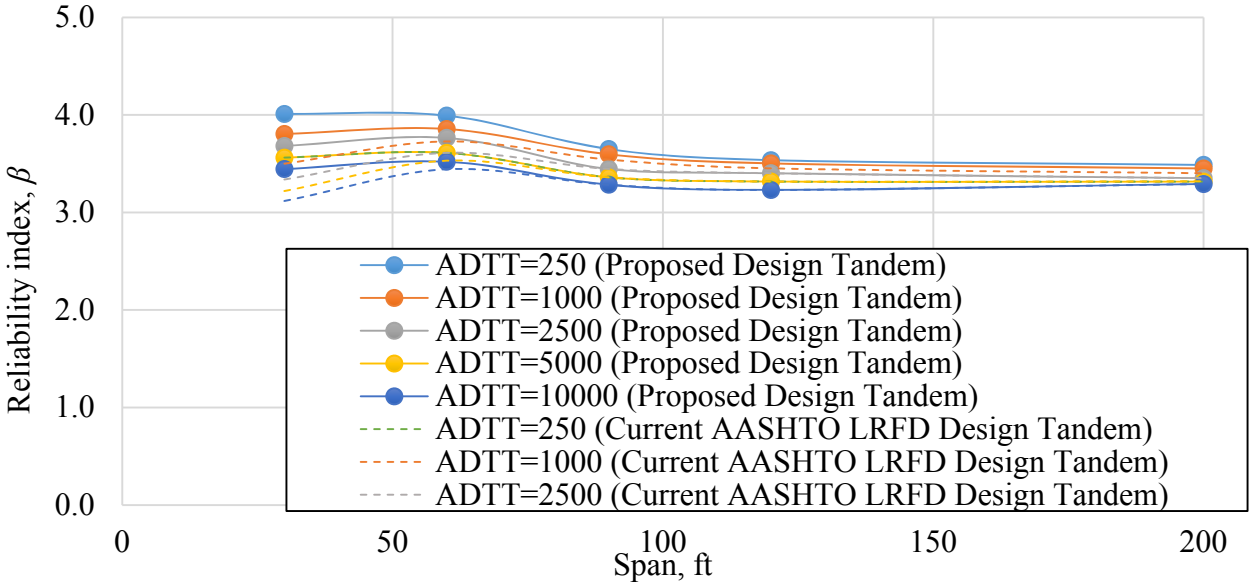

Figure 0-20. Reliability Index vs. Span Length for Moment and Steel Girders (New Design Tandem)

The resultant reliability indices vary from 3.5 (ADTT=10,000) to 4.2. (reinforced concrete T-girders and ADTT=250). On average, the reliability index for 30ft span bridge is 5-7% higher with the new design tandem for all considered design cases.

Due to the natural low variation of the dead load components, there was also no significant effect on the dead load factors (<1%) observed. The resultant dead load factors remain in the same range as shown in Table 0-4 and

Table 0-5. Thus, the results are not presented herein.

The live load factors are more sensitive to variation in nominal live load, than dead load components. The increase in design tandem directly affects the bias factors for static live load components and, therefore, the coordinates of the design point for live load. The live load factors determined using the $\gamma_{LL}=\frac{\lambda_{LL}\ LL^*}{\mu_{LL}}$ Equation 0-21 are summarized in Table 0-10 and plotted versus span length in Figure 0-21Figure 0-22Figure 0-23 for prestressed concrete girders, reinforced concrete T-beams, and steel girders respectively. The resultant live load factor γ_{LL} varies from 1.3 (ADTT=250) to 1.57 (ADTT=10,000), while the optimum factor that corresponds to β_T=3.5 is 1.50. The increase in each axle load of the recommended tandem by 5 kips resulted in 3% lower for 30ft span and 1% for 60ft span (**Error! Reference source not found.**).

Table 0-10. Updated live load factors for new design tandem

Material	Live Load Factor γ_{LL} in Current AASHTO LRFD	Calculated Live Load Factor, γ_{LL}	Optimum Live Load Factor, γ_{LL}	Recommended Live Load Factor, γ_{LL}

Composite and Non-composite steel	1.75	1.35-1.50	1.50	1.55
Prestressed concrete		1.35-1.57		
Reinforced concrete		1.30-1.50		

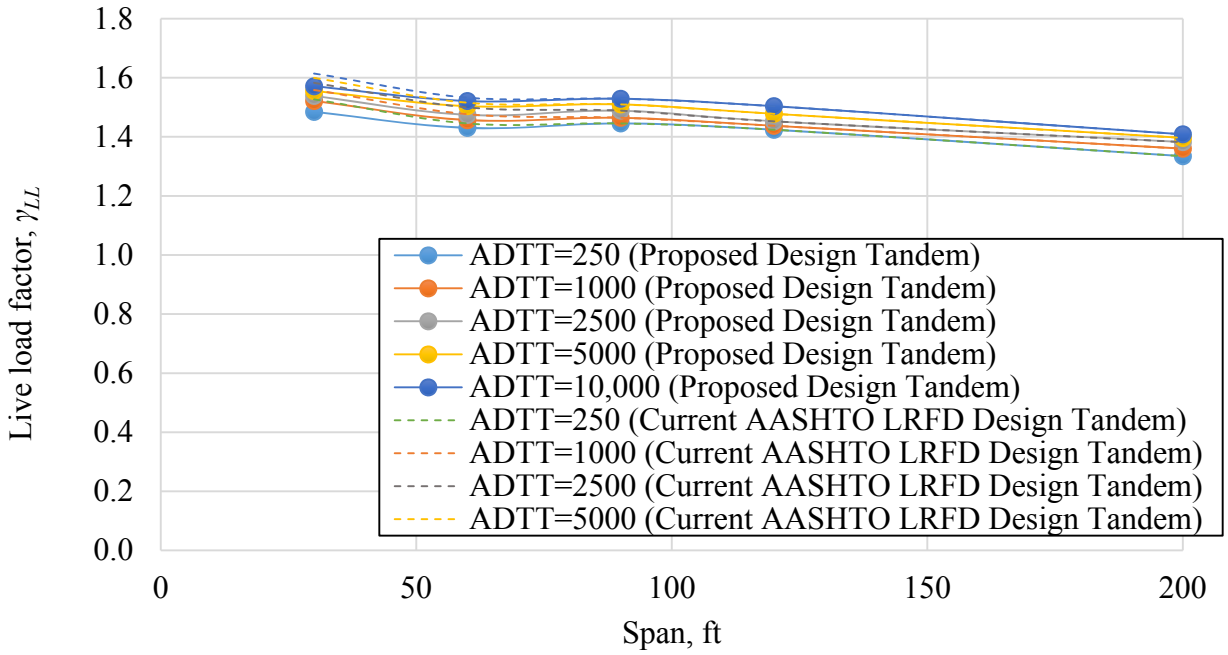

Figure 0-21. Resistance Factor vs. Span Length for Moment and Prestressed Concrete Girders (New Design Tandem)

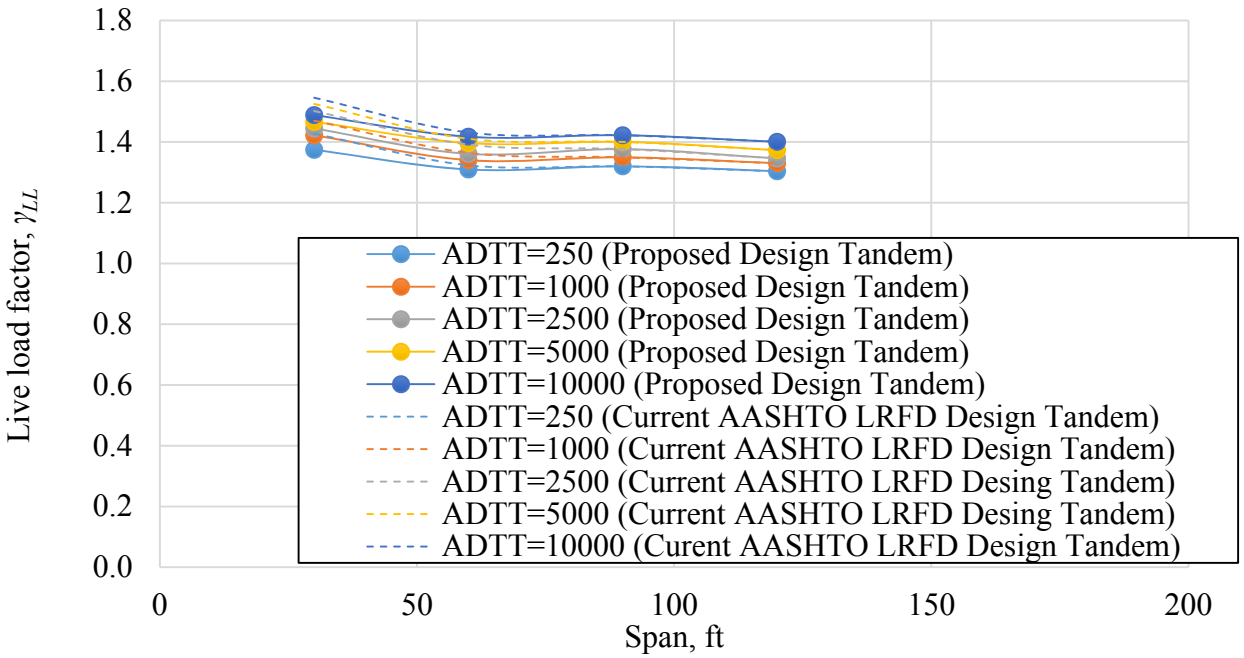

Figure 0-22.Resistance Factor vs. Span Length for Moment and Reinforced Concrete Girders (New Design Tandem)

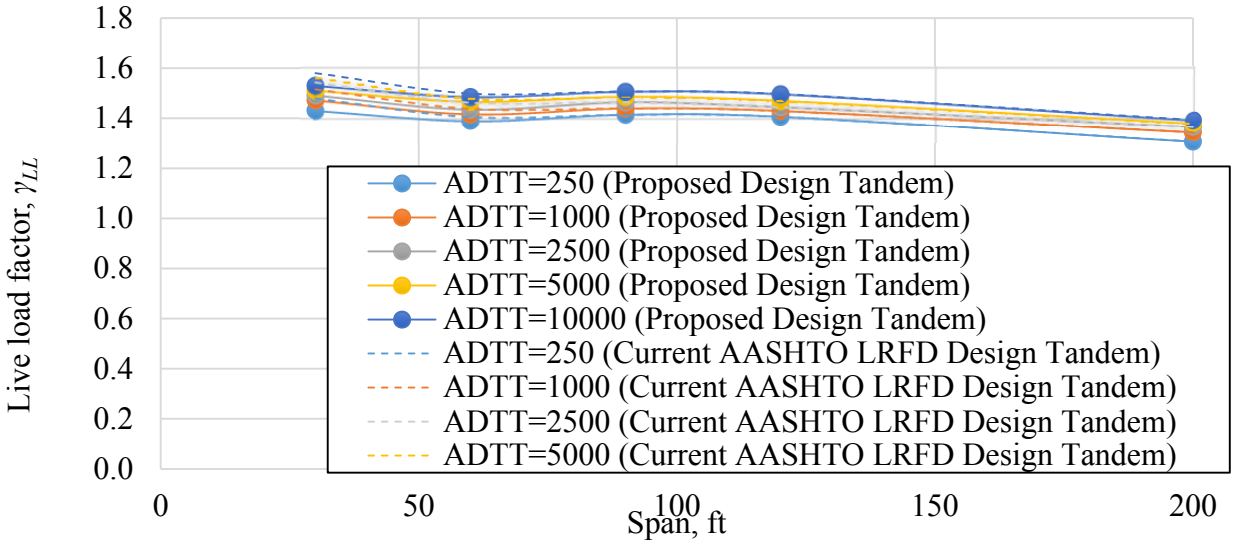

Figure 0-23. Resistance Factor vs. Span Length for Moment and Steel Girders (New Design Tandem)

Applying the same procedure as in the previous chapter, the resistance factors, φ, were calculated for prestressed concrete girders, reinforced concrete T-beams, and steel girders. The results are summarized in Table 0-11 and plotted in Figure 0-24, Figure 0-25 and Figure 0-26. With the 3% decrease, the resistance factor became more consistent with regard to the span length. While the resultant value of φ varies from 0.75 to 0.8 depending on ADTT and material properties, it is conservatively recommended to remain the resistance factors unchanged (Table 0-11).

Table 0-11. Resistance Factors for Flexure According to the Current *AASHTO LRFD* 2014)

Material	Resistance Factor ϕ in Current AASHTO LRFD	Calculated Resistance Factor ϕ	Optimum Resistance Factor ϕ	Recommended Resistance Factor ϕ
Composite and Non-composite steel	1.00	0.85	0.85	0.9
Prestressed concrete	1.00	0.85	0.85	0.9
Reinforced concrete	0.90	0.75-0.80	0.75	0.8

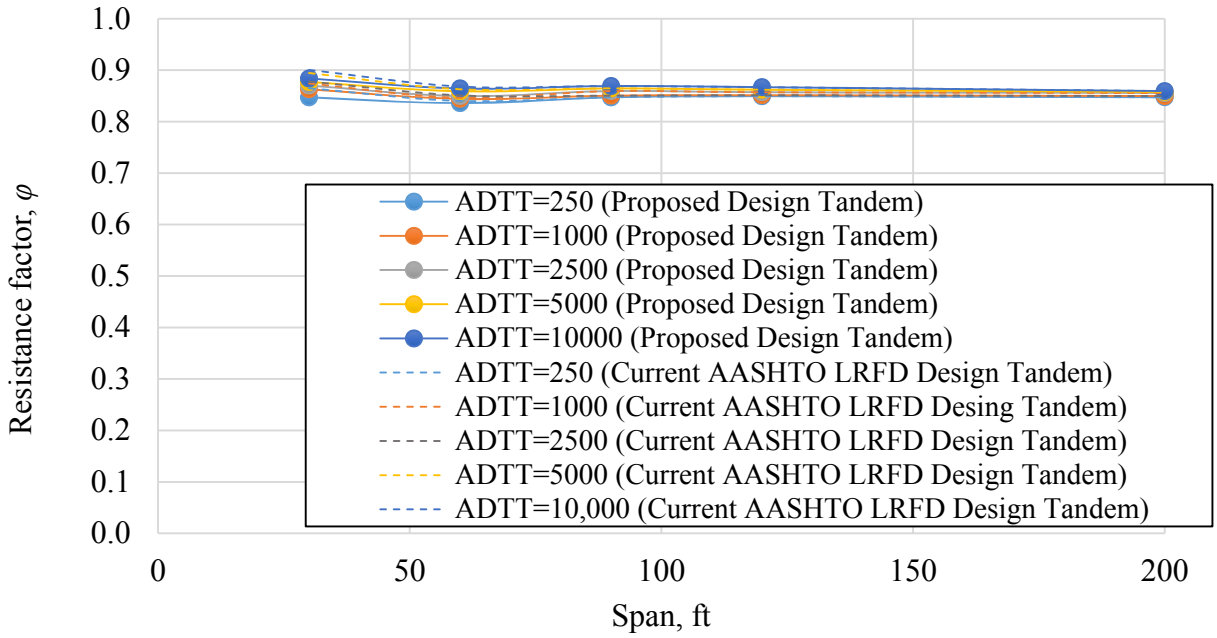

Figure 0-24. Resistance Factor vs. Span Length for Moment and Prestressed Concrete Girders (New Design Tandem)

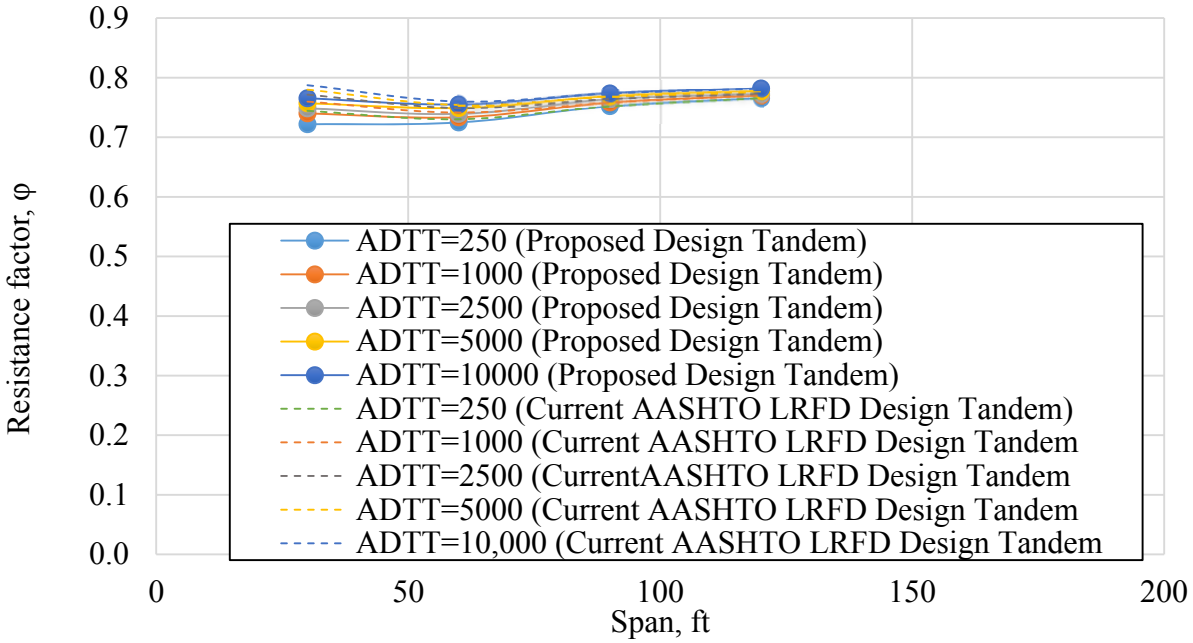

Figure 0-25. Resistance Factor vs. Span Length for Moment and Reinforced Concrete Girders (New Design Tandem)

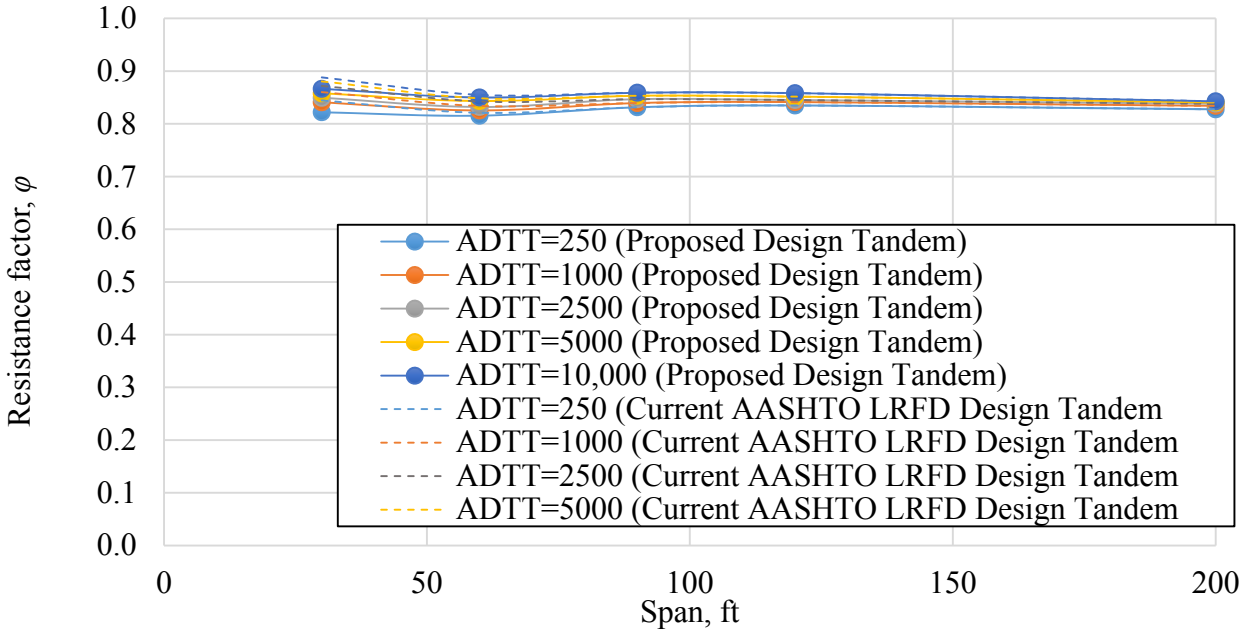

Figure 0-26. Resistance Factor vs. Span Length for Moment and Steel Girders (New Design Tandem)

The application of the new design tandem resulted in 3-5% decrease of calculated load and resistance factors for short span girders. This lead to the additional 5-7% increase of the reliability index for all considered cases in comparison to the current design formula ($\mathbf{1.25}\,\boldsymbol{D} + \mathbf{1.50}\,\boldsymbol{D_w} + \mathbf{1.75}\,(\boldsymbol{LL} + \boldsymbol{I}) < \boldsymbol{\phi}\,\boldsymbol{R}$ Equation 0-2, (*AASHTO LRFD* 2014)). The reliability indices are now higher (4.0-4.2) for the short spans (40-60ft), which are now controlled by the proposed tandem (Figure 0-20). The calculated values of the live load factor γ_{LL} vary in range from 1.3 and 1.57(prestressed AASHTO girders). The calculated dead load factors remain unchanged 1.03-1.17 for all girder materials and span lengths. Therefore, the design formula including the effect of the proposed design tandem is:

$$1.15(D_1+D_2+D_W) + 1.50\,(LL + I) \leq 0.85\,R \qquad \textbf{Equation 0-24}$$

This design formula includes the optimum load and resistance factors that define the coordinates of the design point at the same location as current *AASHTO LRFD* (2014). In Chapter 0 it was recommended to use the load factors rounded up to 1.20 and 1.60 for dead and live load components respectively for conservative design. Similarly, to increase the safety margin, it was recommended to increase the resistance factor by 0.05.

The resultant reliability indices calculated based on the new design including the proposed design tandem are shown in the scatter plot versus the corresponding reliability indices calculated based on the current (*AASHTO LRFD* 2014) (Figure 0-27). The application of the updated design formula ($1.20\,(D+D_w) + 1.6\,(LL+I) < \phi R$ Equation 0-23) along

with the effect of a proposed design tandem results in about 10% of the reliability index, in comparison with the current design provisions (*AASHTO LRFD* 2014).

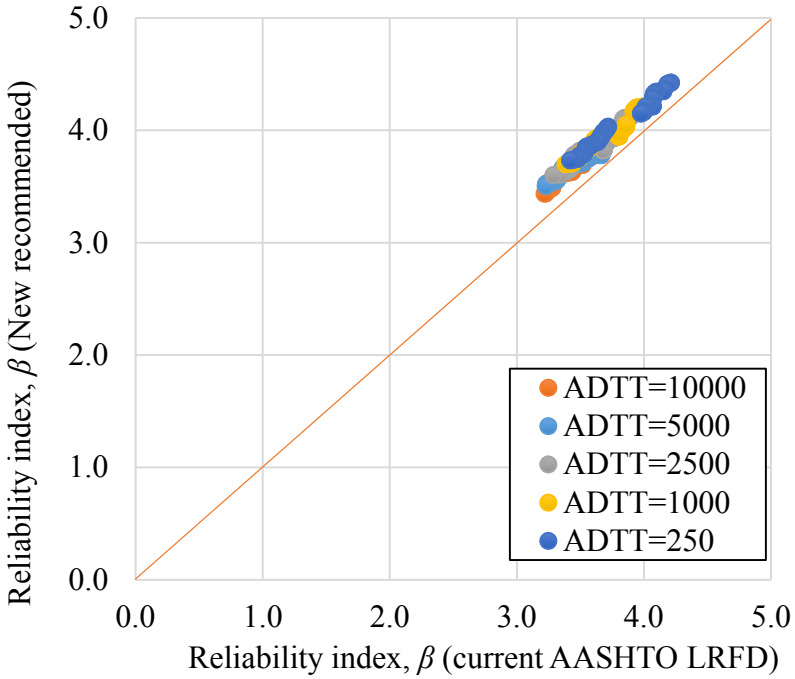

Figure 0-27. Reliability indices for New Recommended Load and Resistance Factors (including new design tandem) vs. Current AASHTO Specifications

Conclusions and Recommendations

7.1. Summary

The new load and resistance factors for Bridge Design Specifications have been developed in this study using new updated structural reliability analysis procedures and load and resistance parameters. The current AASHTO LRFD Specifications were developed based on the state-of-the art in 1990's, including a simplified reliability-based calibration procedure, live load statistics from Ontario Truck Survey (Agarwal and Wolkowicz 1976) and resistance statistics from 1970's

The background study was performed to review the previous research and current practices regarding the selected topic. In the reliability analysis, each design parameter is treated as a random variable with the specific statistical parameters and type of distribution.

The statistical model was developed for a static live load component based on recently collected WIM data. This database consists of individual truck records provided by the Federal Highway Administration, National Cooperative Highway Research Program and Alabama Department of Transportation and obtained using various WIM technologies. The available WIM database was processed using a specially developed computer program to obtain a consistent format . The analysis revealed a number of random and systematic errors in the traffic records due to various reasons, such as WIM system malfunction, irregular vehicle configuration, or position on the sensor. A special unique quality control procedure was developed based on the literature review and analysis of the available permit database to ensure the accuracy of the data for the further

steps of the analysis. The second set of filtering criteria was used to separate the truck data applicable for development of the live load model for the Strength I Limit State from special permit data (Strength II Limit State).

Gross vehicle weight and load effects were calculated and the corresponding CDFs were plotted on probability paper using probability scale for an easier examination and interpretation of the data. The live load effects were considered as non-dimensional mean-to-nominal ratios of bending moments and shear forces. Each vehicle in the database was run over the influence lines and the maximum envelope moment and shear force was then divided by corresponding tabulated value of HL-93 load effect. The moment and shear ratios were computed for simple spans ranging from 30 to 200 ft.

The statistical parameters depend on the considered period of time and limit state. The current AASHTO LRFD code specifies a 75-years service live for newly designed bridges. Therefore, the maximum expected live load effects were determined for a return period from 1 day to 100 years for each WIM site in the available database using a linear extrapolation and Monte Carlo simulation. The statistical parameters such as bias factor, mean value and coefficient of variation were derived from CDFs of the maximum ratios of the moment and shear for each considered time period, span length and ADTT from 250 to 10,000.

It was also observed that the bias factor for 75-years moment is larger for short span bridges (30-60ft). This is an indication that HL-93 design tandem is too low to represent the current traffic load for short spans. Therefore, a new tandem load combination is proposed that will control the design for spans from 8 to 75ft.

The design formula in the current AASHTO LRFD Bridge Design Specifications (2016) was re-calibrated using the statistical parameters of live load developed in 0. The revision of statistical parameters for resistance has not been completed yet and therefore, the resistance models are taken from the original calibration (Nowak 1999). The reliability-based calibration procedure was based on the concept of "design point" (Nowak and Collins 2013). Load and resistance factors were determined using iterative Rackwitz-Fiesler procedure for the same design cases as in the original calibration for reinforced concrete T-beams, prestressed concrete and steel girder bridges. The load and resistance were considered as a normal and a log-normal random variable, respectively. An additional study was conducted to assess the effect of the proposed design tandem on the reliability index. An updated design formula with new load and resistance factors is proposed.

7.2.Conclusions

Weigh-in-Motion data is a good basis to develop the design live load model that adequately reflects the traffic load on roads and bridges. The WIM sites located state-wide can provide sufficient information about the traffic density, weight, and configuration. About 100 million WIM records collected from 38 WIM sites located in 18 states across the US during 2005-2017 were analyzed in this study. The statistical parameters were determined for GVW and live load effects, such as moment and shear forces. Summarizing the results of the study, the following conclusions can be drawn:

1. The available WIM data is representative and can serve as a basis for the development of the national live load statistics. It contains about 50% (depending on WIM site) of

lightweight vehicles and incorrect records that have to be eliminated using a special quality control filtering procedure. Also,

2. 5-10% of the heaviest vehicles in the database belong to state-restricted "Super load" group, which is applicable to Strength II or Fatigue limit states.

3. Vehicle class 9 (five-axle, single trailer truck) is the most common type for most of the considered states. However, in some states, vehicles of the other classes create a substantial portion of the traffic mix. Class 5 (single unit, 2-axle trucks) is from 10 to 30 % of a total number of trucks in Delaware, Maryland, Florida, Mississippi and Virginia. Similarly, class 6 (single unit, 3-axle trucks) is 10% of a total number of trucks in Delaware and California, and class 10 (single trailer, 6 or more axle trucks) is 20% in Maryland.

4. The maximum value of moment ratio is below 1.6 for 30ft and below 1.4 for 200ft span for most states. Vehicles of class 7 (single-unit, 4 or more–axle truck) cause the highest bending moment for short (30ft) spans, while trucks of class 13 (multi-trailer, 6-axle) control longer spans. The changes in moment ratio distribution are mostly caused by changes in traffic mix over the years.

5. Live load statistics was developed based the extrapolation of the upper tail of the CDFs of the calculated moment and shear ratios. This approach allowed calculation of the maximum live load effect for different periods of time. The cumulative distribution functions of the extreme values are normal and therefore, accurate statistical parameters can be obtained directly from the CDF plot. The slope of the CDF's upper tail is sensitive to the number of records in the database.

6. The obtained 75-years maximum values were compared with the corresponding Ontario data, used for the original calibration of AASHTO LRFD (NCHRP 368). The results show that on average the Ontario trucks have greater GVW ($\mu_{GVW(Ontario)}$=80 kips, μ_{GVW_WIM}=50-60 kips). However, the maximum expected live load effects are 15% larger than Ontario.

7. The statistical parameters for moment and shear force ratio are strongly depending on the span length and ADTT. The 75-years bias factor for moment ratio varies from 1.67 (30ft span and ADTT=10,000) to 1.45 (200ft span and ADTT=250). The coefficient of variation decreases for the increased return time periods. On average, 75-years COV is 12%.

8. The 75-years bias factor for short spans (30ft) is higher than for other spans, which is an indication that HL-93 tandem load is too small and it does not represent the current traffic. Therefore, it is recommended to increase the design tandem to 30kips/axle in addition to lane load.

9. Illegal traffic and vehicles that do not follow the axle load limits as applied for in the permit application create a potential source of damage to the roads and bridges. The number of permits issued by the Alabama DOT is 1% of the truck traffic, which is substantially smaller than the number of WIM trucks requiring permits (20%). The permit vehicles are mostly underloaded (by about 50 kips). However, the bending moments caused by illegal WIM trucks are significantly larger than what can be expected based on issued permits, especially for short span bridges. On average, the WIM trucks with GVW below 80kips (355kN) that require a permit – operate without it.

10. The calculated load and resistance factors corresponding to the "design point" are about 10% lower than those specified in the AASHTO code (2014). The reliability indices calculated for design cases using the current and recommended new load and resistance factors show a 5% increase in the safety margin for newly developed design formula.

11. The proposed design tandem with proposed load and resistance factors result in about 10% increase of the reliability index, compared with the current (AASHTO LRFD 2016).

7.3. Future Research

1. Continuation of WIM data collection is needed for continuous updating of the actual traffic model. Traffic records are also needed for road planning, evaluation of existing bridges, damage accumulation models, etc.

2. The database considered in this study had some gaps, in some cases several years were missing. It is important to make sure the WIM data is collected without interruptions in the future.

3. The present study showed that there are considerable changes in truck traffic distribution and load effects. There is need for computer procedures for real-time processing of the raw WIM data.

4. Similarly to the live load model, the resistance model has to be revised using the new material test data.

5. There is a need for developing a procedure for assessment of the fatigue damage accumulation index based on the real-time WIM records.

References

1. AASHTO. (1931). “Standard Specifications for Highway Bridges and Incidental Structures.” AASHTO.
2. AASHTO. (1989). “AASHTO Standard Specifications for Hightway Bridges.”
3. AASHTO. (2002). “AASHTO Standard Specifications for Highway Bridges.” AASHTO.
4. AASHTO. (2011). “Manual for Bridge Evaluation.”
5. AASHTO. (2014). AASHTO LRFD Bridge Design Specifications, 7th Edition. Washington, D.C.
6. *AASHTO LRFD Bridge Design Specifications, 7th Edition*. (2014). Washington, D.C.
7. Abowd, G. D., Dey, A. K., Brown, P. J., Davies, N., Smith, M., and Steggles, P. (1999). “Comprehensive Truck Size and Weight Study.” *International Symposium on Handheld and Ubiquitous Computing*, Springer, 304–307.
8. Agarwal, A. C., and Wolkowicz, M. (1976). *Ontario Commercial Vehicle Survey*. Interim Report, Research and Development Branch, Ontario Ministry of Transportation and Communications, Downsview Ontario.
9. Akaike, H. (1973). *Information theory and an extension of the maximum likelihood principle*. 2nd International Symposium on Information Theory., 267–281.
10. “Alabama Code Title 32. Motor Vehicles and Traffic.” (n.d.). *Findlaw*, <http://codes.findlaw.com/al/title-32-motor-vehicles-and-traffic/> (Mar. 23, 2017).
11. Allen, T. M., Nowak, A. S., and Bathurst, R. J. (2005). *Calibration to Determine Load and Resistance Factors for Geotechnical and Structural Design*. Transportation Research Circular E-C079, Transportation Research Board, Washington D.C.

12. Al-Qadi, I., Wang, H., Ouyang, Y., Grimmelsman, K., and Purdy, J. (2016). *LTBP Program's Literature Review on Weigh-in-Motion Systems*.

13. American Concrete Institute. (2014). *ACI 318-14*. Farmington Hills, Michigan.

14. American Institute of Steel Construction. (2011). *Steel Construction Manual*. Amer Inst of Steel Construction, Chicago, Illinois.

15. American Society of Civil Engineers. (2016). *ASCE Standard 7*.

16. American Wood Council. (2015). *National Design Specification (NDS) for Wood Construction*. Leesburg, VA.

17. *ASCE's 2017 Infrastructure Report Card*. (n.d.). .

18. *ASTM E1318 - 09 - Standard Specification for Highway Weigh-in-Motion (WIM) Systems with User Requirements and Test Methods*. (2009). ASTM International, West Conshohocken, PA.

19. *ASTM E1318 - 09 Standard Specification for Highway Weigh-in-Motion (WIM) Systems with User Requirements and Test Methods*. (2009). ASTM International, West Conshohocken, PA.

20. Bailey, S. F., and Bez, R. (1999). "Site specific probability distribution of extreme traffic action effects." *Probabilistic Engineering Mechanics*, 14(1), 19–26.

21. Benjamin, J. R., Cornell, C. A. (1970). *Probability, Statistics, and Decisions for Civil Engineers*. McGraw-Hill, New York; Maidenhead.

22. Beyer, W. H. (Ed.). (1987). *CRC Standard Mathematical Tables*. CRC Press, Boca Raton, Fla.

23. "Bridge Formula Weights- FHWA Freight Management and Operations." (n.d.). <https://ops.fhwa.dot.gov/freight/publications/brdg_frm_wghts/> (Jun. 16, 2017).

24. Buch, N., Haider, S. W., Brown, J., and Chatti, K. (2009). "Characterization of truck traffic in Michigan for the new mechanistic empirical pavement design guide." *Final Report*, 1537, 68–76.

25. *Calibration of the Ontario Highway Bridge Design Code 1991 Edition*. (1994). Canada. national research council of canada.

26. “California Permit and Fatigue Truck Load Development and Calibration.” (n.d.). .

27. Cambridge Systematics, Inc. (2007). *MAG Internal Truck Travel Survey and Truck Model Development Study*. Maricopa Association of Governments, 128.

28. Caprani, C. C., OBrien, E. J., and McLachlan, G. J. (2008). “Characteristic traffic load effects from a mixture of loading events on short to medium span bridges.” *Structural Safety*, 30(5), 394–404.

29. Castillo, E. (1988). *Extreme Value Theory in Engineering*. Academic Press.

30. Coles, S. (2001). *An Introduction to Statistical Modeling of Extreme Values*. Springer-Verlag, London.

31. Commernet, 2011. (n.d.). “Part 650 - BRIDGES, STRUCTURES, AND HYDRAULICS, SUBCHAPTER G — ENGINEERING AND TRAFFIC OPERATIONS, CHAPTER I — FEDERAL HIGHWAY ADMINISTRATION, DEPARTMENT OF TRANSPORTATION, Title 23 - Highways, Code of Federal Regulations.” *CODE OF FEDERAL REGULATIONS & FEDERAL REGISTER*, <http://federal.elaws.us/cfr/title23.part650> (Jul. 28, 2017).

32. Cornell, C. A. (1967). “Bounds on the Reliability of Structural Systems.” *Journal of the Structural Division*, 93(1), 171–200.

33. “COST | Weighing in motion of road vehicles.” (1999). Laboratoire Central des Ponts et Chaussees.

34. Elkins, L., and Higgins, C. (2008). “Development of Truck Axle Spectra from Oregon Weigh-in-Motion Data for Use in Pavement Design and Analysis.”

35. Ellingwood, B. (1980). *Development of a Probability Based Load Criterion for American National Standard A58: Building Code Requirements for Minimum Design Loads in Buildings and Other Structures*. U.S. Department of Commerce, National Bureau of Standards.

36. Enright, B., and OBrien, E. (2012). “Monte Carlo Simulation of Extreme Traffic Loading on Short and Medium Span Bridges.” *Articles*.

37. Enright, B., OBrien, E. J., and Leahy, C. (2016). “Identifying and modelling permit trucks for bridge loading.” *Proceedings of the Institution of Civil Engineers - Bridge Engineering*, 169(4), 235–244.

38. Federal Highway Administration. (2015). “Deficient Bridges by Highway System.” *Bridge Inspection*, <https://www.fhwa.dot.gov/bridge/nbi/no10/defbr15.cfm> (Sep. 21, 2016).

39. Federal Highway Administration, and U.S. Department of Transportation. (2015). *Compilation of Existing State Truck Size and Weight Limit Laws - FHWA Freight Management and Operations*.

40. Fiorillo, G., and Ghosn, M. (2014). “Procedure for Statistical Categorization of Overweight Vehicles in a WIM Database.” *Journal of Transportation Engineering*, 140(5), 04014011.

41. Fiorillo, G., and Ghosn, M. (2016). “Minimizing Illegal Overweight Truck Frequencies through Strategically Planned Truck Inspection Operations.” *Journal of Transportation Engineering*, 142(9), 04016038.

42. Fisher, J., Mertz, D., and Zhong, A. (1983). “Steel bridge members under variable amplitude, long life fatigue loading, Final Report Draft, May 1983 83p.” *Fritz Laboratory Reports*.

43. Fu Gongkang, Liu Lang, and Bowman Mark D. (2013). “Multiple Presence Factor for Truck Load on Highway Bridges.” *Journal of Bridge Engineering*, 18(3), 240–249.

44. Galambos, C. F. (1979). “Highway bridge loadings.” Volume 1(Issue 5).

45. Ghosn, M., and Moses, F. (1984). “Reliability Calibratio of Bridge Design Code.” *ASCE*.

46. Ghosn, M., Sivakumar, B., and Miao, F. (2010). “Calibration of Load and Resistance Factor Rating Methodology in New York State.” *Transportation Research Record: Journal of the Transportation Research Board*, (2200).

47. Ghosn, M., Sivakumar, B., Moses, F., Transportation Research Board, National Cooperative Highway Research Program, and Transportation Research Board. (2011). *Protocols for Collecting and Using Traffic Data in Bridge Design*. NCHRP Project 12-76. National Academies Press, Washington, D.C.

48. Gindy, M., and Nassif, H. (2007). "Multiple Presence Statistics for Bridge Live Load Based on Weigh-in-Motion Data." *Transportation Research Record: Journal of the Transportation Research Board*, 2028, 125–135.

49. Hasofer, A. M., and Lind, N. (1974). "An Exact and Invariant First Order Reliability Format." *Journal of Engineering Mechanics*, 100.

50. Hellenbeck, M. (1994). "WIM Data Quality Assurance." *National Traffic Data Acquisition Conference*, Volume II, 251–266.

51. Iatsko, O., Ramesh Babu, A., and Nowak, A. S. (2017). "Load effects caused by permit and illegally overloaded vehicles." XXVIII Scientific and Practical Conference "Structural Failures" (Awarie Budowlane). *Conference Proceedings 2017*, Szczecin - Miedzyzdroje.

52. Jacoboni, C., and Reggiani, L. (1983). "The Monte Carlo method for the solution of charge transport in semiconductors with applications to covalent materials." *Reviews of Modern Physics*, 55(3), 645–705.

53. Jian Zhao, and Habib Tabatabai. (2012). "Evaluation of a Permit Vehicle Model Using Weigh-in-Motion Truck Records." *Journal of Bridge Engineering*, 17(2), 389–392.

54. Kwon, O.-S., Orton, S., Salim, H., Kim, E., and Hazlett, T. (2010). *Calibration of the live load factor in LRFD design guidelines*.

55. Laman, J. A., and Nowak, A. S. (1996). "Fatigue-Load Models for Girder Bridges." *Journal of Structural Engineering*, 122(7), 726–733.

56. Luskin, D. L., and Walton, C. M. (2001). *Synthesis Study of the Effects of Overweight/oversize Trucks*. Center for Transportation Research, Bureau of Engineering Research, University of Texas at Austin.

57. *MATLAB*. (2014). The MathWorks Inc, Natick, MA.

58. McCall, B., and Vodrazka, W. J. (1997). *Weigh-in-Motion Handbook*. Federal Highway Administration.

59. Melchers, R. E. (1988). "Structural reliability analysis and prediction." *Quality and Reliability Engineering International*, 4(3), 294–295.

60. Middleton, D. R., Li, Y., Le, J., Agrawal, A. K., Liu, H., Imbsen, R. A., and Zong, X. (2012). *Accommodating Oversize and Overweight Loads: Instructor and Student Guide*. Texas Transportation Institute, Texas A & M University System.

61. "Mike Sheppard - MATLAB Central." (n.d.). <https://www.mathworks.com/matlabcentral/profile/authors/2201006-mike-sheppard> (Jan. 31, 2018).

62. Moses, F. (2001). "Calibration of Load Factors for LRFR Bridge Evaluation." *NCHRP Report*, (454).

63. Nassif, H., and Nowak, A. S. (1995). "Dynamic Load Spectra for Girder Bridges." *Transportation Research Record*.

64. Norman, O. K., and Hopkins, R. C. (1952). "Weighing vehicles in motion." *Highway Research Board Bulletin*, (50).

65. Nowak, A. (1994). *Load model for bridge design code*.

66. Nowak, A., and Hong, Y. (1991). "Bridge Live□Load Models." *Journal of Structural Engineering*, 117(9), 2757–2767.

67. Nowak, A., Rakoczy, P., and Sheikh Ibrahim, F. I. (2012a). "Proposed load combination factors for bridges with high dead-to-live load ratios." *Bridge Structures*, 8, 61–66.

68. Nowak, A. S. (1993). "Live load model for highway bridges." *Structural Safety*, Special Issue on Combinations of Actions to Structures, 13(1), 53–66.

69. Nowak, A. S. (1999). "Calibration of Lrfd Bridge Design Code." *NCHRP Report*, (368).

70. Nowak, A. S., and Collins, K. R. (2012). *Reliability of Structures, Second Edition*. CRC Press, Boca Raton.

71. Nowak, A. S., and Grouni, H. N. (1994). “Calibration of the Ontario Highway Bridge Design Code 1991 Edition.”

72. Nowak, A. S., and Iatsko, O. (2017). “Revised load and resistance factors for the AASHTO LRFD Bridge Design Specifications.” PCI Journal. May 2017, 66, (3), 46–58.

73. Nowak, A. S., and Lind, N. C. (1979). “Practical Bridge Code Calibration.” *ASHRAE Journal*, 105(12).

74. Nowak, A. S., Rakoczy, A. M., and Szeliga, E. K. (2012b). “Revised Statistical Resistance Models for R/C Structural Components.” *Special Publication*, 284, 1–16.

75. Nowak, A. S., Rakoczy, P., and Kulicki, J. M. (2012c). “WIM-Based Live Load for Bridges.”

76. Nowak, A. S., and Szerszen, M. M. (2003). “Calibration of Design Code for Buildings (ACI 318): Part 1—Statistical Models for Resistance.” *Structural Journal*, 100(3), 377–382.

77. Nowak, A. S., and Tharmabala, T. (1988). “Bridge Reliability Evaluation Using Load Tests.” *Journal of Structural Engineering*, 114(10), 2268–2279.

78. Nowak, A. S., and Zhou, J. (1985). *Reliability Models for Bridge Analysis*. Department of Civil Engineering, University of Michigan.

79. O’Brien, E. J., Caprani, C. C., and O’Connell, G. J. (2006). “Bridge assessment loading: a comparison of West and Central/East Europe.” *Bridge Structures*, 2(1), 25–33.

80. OBrien, E. J., Leahy, C., Enright, B., and Caprani, C. C. (2016). “Validation of scenario modelling for bridge loading.” *The Baltic Journal of Road and Bridge Engineering*, 11(3), 233–241.

81. O’Brien;, E. J., Znidaric, A., and Dempsey, A. T. (1999). “Comparison of two independently developed bridge weigh-in-motion systems.” *International Journal of Heavy Vehicle Systems*, 6(1/2/3/4), 147.

82. O’Connor, A., and Enevoldsen, I. (2009). “Probability-based assessment of highway bridges according to the new Danish guideline.” *Structure and Infrastructure Engineering*, 5(2), 157–168.

83. O'Connor, A., and O'Brien, E. J. (2005). "Traffic load modelling and factors influencing the accuracy of predicted extremes." *Canadian Journal of Civil Engineering*, 32(1), 270–278.

84. Office of Freight Management and Operations. (2017). "Concept of Operations for Virtual Weigh Station: 4.0 Concept of Operations." Federal Highway Administration.

85. *Ontario Highway Bridge Design Code*. (1983). Ontario Ministry of Transportation and Communications, Highway Engineering Division.

86. Pigman, J., Graves, C., Hunsucker, D., and Cain, D. (2012). "WIM Data Collection and Analysis." *Kentucky Transportation Center Research Report*.

87. Qu, T., Lee, C. E., and Huang, L. (1997). "Traffic-load forecasting using weigh-in-motion data." *Work*, 987, 6.

88. Quinley, R. (2010). *WIM Data Analyst's Manual*. FHWA Office of Pavement Technology, Washington, D.C.

89. Rackwitz, R. (2001). "Reliability analysis—a review and some perspectives." *Structural Safety*, 23(4), 365–395.

90. Rackwitz, R., and Flessler, B. (1978). "Structural reliability under combined random load sequences." *Computers & Structures*, 9(5), 489–494.

91. Ramachandran, A. N., Taylor, K. L., Stone, J. R., and Sajjadi, S. S. (2011). "NCDOT Quality Control Methods for Weigh-in-Motion Data." *Public Works Management & Policy*, 16(1), 3–19.

92. Rosenblueth, E. (1972). "Point estimates for probability moments." pp 3812-3814.

93. Schwarz, G. E. (1978). "Schwartz_complexitycontrol.pdf." 461–464.

94. SHRP 2 Research Reports. (2015). *Bridges for Service Life Beyond 100 Years: Service Limit State Design*. Transportation Research Board, Washington D.C.

95. Sivakumar, B. (2007). *Legal Truck Loads and AASHTO Legal Loads for Posting*. Transportation Research Board.

96. *SiWIM Bridge Weigh-in-Motion Manual: 4th Edition*. (2011). ZAG Ljubljana, Trzin, Slovenia.

97. Southgate, H. F. (1990). "Estimation of Equivalent Axleloads Using Data Collected by Automated Vehicle Classification and Weigh-in-motion Equipment."

98. Stern, R., Dale, I., and Leidi, S. (2000). *Glossary of statistical terms*.

99. Stith, P. (2006). "Legal Load Limits, Overweight Loads and Pavements and Bridges."

100. Systematics, C. (2007). "MAG internal truck travel survey and truck model development study."

101. Szerszen, M., and Nowak, A. (2003). "Calibration of design code for buildings (ACI 318): Part 2 - Reliability analysis and resistance factors." *ACI Structural Journal*, 100, 383–391.

102. Tabsh, S. (1990). *Reliability-based sensitivity analysis of girder bridges.*

103. Taylor, B., Bergan, A., Lindgren, N., and Eng, C. B. P. D. P. (2000). "The importance of commercial vehicle weight enformcement in safety and road asset management." *Annual Review pp*, 234, 237.

104. Thoft-Christensen, P., and Baker, M. J. (1982). *Structural Reliability Theory and Its Applications*. Springer.

105. "Title 32. Motor Vehicles and Traffic." (2015). *Code of Alabama*, Legislative Reference Service, Montgomery, AL, USA.

106. *Traffic Monitoring Guide*. (2001a). U.S. Department of Transportation, Federal Highway Administration, Office of Highway Policy Information.

107. Traffic Monitoring Guide. (2001). U.S. Department of Transportation, Federal Highway Administration, Office of Highway Policy Information.

108. *Traffic Monitoring Guide*. (2016). Federal Highway Administration.

109. Treacy, M., and Brühwiler, E. (2012). "Fatigue Loading Estimation for Road Bridges Using Long Term Wim Monitoring."

110. Turkstra, C. J. (1970). *Theory of structural design decisions*. Solid Mechanics Division, University of Waterloo.

111. Turochy, R. E., Timm, D. H., and Mai, D. (2015). "Development of Alabama Traffic Factors for use in Mechanistic-Empirical Pavement Design." Research Report for ALDOT Project 930-793.

112. Turochy, R. E., Timm, D. H., and Mai, D. (2015b). "Development of Alabama Traffic Factors for use in Mechanistic-Empirical Pavement Design."

113. U.S. Department of Transportation, FHWA. (2015). *Load and Resistance Factor Design (LRFD) for Highway Bridge*. FHWA, Washington D.C.

114. White, R., Song, J., Haas, C., and Middleton, D. (2006). "Evaluation of Quartz Piezoelectric Weigh-in-Motion Sensors." *Transportation Research Record: Journal of the Transportation Research Board*, 1945, 109–117.

115. Zokaie, T., Osterkamp, T. A., and Imbsen, R. A. (1991). *Distribution of Wheel Loads on Highway Bridges*. NCHRP Project 12-16, Transportation Research Board, Washington, D.C.

Appendix A

The reliability analysis was performed for the design cases considered in Chapter 0. The calculated values of load (D_1, D_2, D_w, LL and I) components for flexure presented in **Error! Reference source not found.**,

,

Error! Reference source not found. for the prestressed concrete, reinforced concrete T-beams and steel (composite and non-composite) girder bridges respectively.

Table A-1. Load Components for Flexure Design of Prestressed AASHTO Girder Bridges

# Bridge	Parameters of bridge, ft		Dead load, kip-ft			Live load HL 93, kip-ft		
	L	*S*	D_1	D_2	D_3	$GDF_{HL\text{-}93}$	*LL*	*I*
1	30	4	43.00	61.31	12.15	0.473	187.67	50.70
2	30	6	43.00	83.81	18.23	0.625	248.18	67.04
3	30	8	43.00	103.50	24.30	0.767	304.69	82.31
4	30	10	43.00	130.22	30.38	0.903	358.42	96.83
5	30	12	43.00	159.75	36.45	1.033	410.03	110.77
6	60	4	262.00	245.25	48.60	0.421	458.31	111.21
7	60	6	262.00	335.25	72.90	0.554	602.66	146.23
8	60	8	262.00	414.00	97.20	0.678	737.50	178.95
9	60	10	262.00	520.88	121.50	0.796	865.69	210.06
10	60	12	262.00	639.00	145.80	0.909	988.81	239.93
11	90	4	832.00	551.81	109.35	0.394	783.82	174.35
12	90	6	832.00	754.31	164.03	0.517	1027.02	228.44
13	90	8	832.00	931.50	218.70	0.631	1254.21	278.98
14	90	10	832.00	1171.97	273.38	0.740	1470.19	327.02
15	90	12	832.00	1437.75	328.05	0.844	1677.65	373.17
16	120	4	1899.00	981.00	194.40	0.376	1141.32	233.53
17	120	6	1899.00	1341.00	291.60	0.492	1491.50	305.19
18	120	8	1899.00	1656.00	388.80	0.600	1818.62	372.12
19	120	10	1899.00	2083.00	486.00	0.702	2129.61	435.76
20	120	12	1899.00	2556.00	583.20	0.801	2428.32	496.88
21	200	4	5650.00	2725.00	540.00	0.347	2263.42	380.34
22	200	6	5650.00	3725.00	810.00	0.451	2943.30	494.58
23	200	8	5650.00	4600.00	1080.00	0.549	3578.44	601.31
24	200	10	5650.00	5787.50	1350.00	0.641	4182.24	702.77
25	200	12	5650.00	7100.00	1620.00	0.730	4762.19	800.22

Table A-2. Load Components for Flexure Design of Reinforced T-girder Bridges

# Bridge	Parameters of bridge, ft		Dead load, kip-ft			Live load HL 93, kip-ft		
	L	S	D_1	D_2	D_3	$GDF_{HL\text{-}93}$	LL	I
1	30	4	0.00	107.00	12.15	0.521	187.67	50.70
2	30	6	0.00	129.00	18.23	0.672	248.18	67.04
3	30	8	0.00	150.00	24.30	0.817	304.69	82.31
4	30	10	0.00	174.00	30.38	0.956	358.42	96.83
5	30	12	0.00	236.00	36.45	1.089	410.03	110.77
6	60	4	0.00	460.00	48.60	0.521	458.31	111.21
7	60	6	0.00	630.00	72.90	0.672	602.66	146.23
8	60	8	0.00	720.00	97.20	0.817	737.50	178.95
9	60	10	0.00	878.00	121.50	0.956	865.69	210.06
10	60	12	0.00	1035.00	145.80	1.089	988.81	239.93
11	90	4	0.00	1420.00	109.35	0.521	783.82	174.35
12	90	6	0.00	1720.00	164.03	0.672	1027.02	228.44
13	90	8	0.00	1923.00	218.70	0.817	1254.21	278.98
14	90	10	0.00	2278.00	273.38	0.956	1470.19	327.02
15	90	12	0.00	2683.00	328.05	1.089	1677.65	373.17
16	120	4	0.00	2790.00	194.40	0.521	1141.32	233.53
17	120	6	0.00	3330.00	291.60	0.672	1491.50	305.19
18	120	8	0.00	3870.00	388.80	0.817	1818.62	372.12
19	120	10	0.00	4590.00	486.00	0.956	2129.61	435.76
20	120	12	0.00	5400.00	583.20	1.089	2428.32	496.88

Table A-3. Load Components for Flexure Design of Composite Steel Girders

# Bridge	Parameters of bridge, ft		Dead load, kip-ft			Live load HL 93, kip-ft		
	L	S	D_1	D_2	D_3	$GDF_{HL\text{-}93}$	LL	I
1	30	4	7.00	61.31	12.15	0.521	187.67	50.70
2	30	6	7.00	83.81	18.23	0.672	248.18	67.04
3	30	8	8.00	103.50	24.30	0.817	304.69	82.31
4	30	10	9.00	130.22	30.38	0.956	358.42	96.83
5	30	12	10.00	159.75	36.45	1.089	410.03	110.77
6	60	4	39.00	245.25	48.60	0.521	458.31	111.21
7	60	6	48.00	335.25	72.90	0.672	602.66	146.23
8	60	8	70.00	414.00	97.20	0.817	737.50	178.95
9	60	10	84.00	520.88	121.50	0.956	865.69	210.06
10	60	12	103.00	639.00	145.80	1.089	988.81	239.93
11	90	4	258.00	551.81	109.35	0.521	783.82	174.35
12	90	6	268.00	754.31	164.03	0.672	1027.02	228.44
13	90	8	286.00	931.50	218.70	0.817	1254.21	278.98
14	90	10	303.00	1171.97	273.38	0.956	1470.19	327.02
15	90	12	339.00	1437.75	328.05	1.089	1677.65	373.17
16	120	4	502.00	981.00	194.40	0.521	1141.32	233.53
17	120	6	607.00	1341.00	291.60	0.672	1491.50	305.19
18	120	8	650.00	1656.00	388.80	0.817	1818.62	372.12
19	120	10	681.00	2083.00	486.00	0.956	2129.61	435.76
20	120	12	773.00	2556.00	583.20	1.089	2428.32	496.88
21	200	4	2780.00	2725.00	540.00	0.521	2263.42	380.34
22	200	6	3303.00	3725.00	810.00	0.672	2943.30	494.58
23	200	8	3790.00	4600.00	1080.00	0.817	3578.44	601.31
24	200	10	4190.00	5787.50	1350.00	0.956	4182.24	702.77
25	200	12	4875.00	7100.00	1620.00	1.089	4762.19	800.22

Table A-4. Load Components for Flexure Design of Non-composite Steel Girders

# Bridge	Parameters of bridge, ft		Dead load, kip-ft			Live load HL 93, kip-ft		
	L	S	D_1	D_2	D_3	$GDF_{HL\text{-}93}$	LL	I
1	30	4	7.88	61.31	12.15	0.521	187.67	50.70
2	30	6	8.44	83.81	18.23	0.672	248.18	67.04
3	30	8	9.00	103.50	24.30	0.817	304.69	82.31
4	30	10	10.13	130.22	30.38	0.956	358.42	96.83
5	30	12	11.25	159.75	36.45	1.089	410.03	110.77
6	60	4	40.50	245.25	48.60	0.521	458.31	111.21
7	60	6	54.00	335.25	72.90	0.672	602.66	146.23
8	60	8	76.50	414.00	97.20	0.817	737.50	178.95
9	60	10	94.50	520.88	121.50	0.956	865.69	210.06
10	60	12	112.50	639.00	145.80	1.089	988.81	239.93
11	90	4	263.25	551.81	109.35	0.521	783.82	174.35
12	90	6	283.50	754.31	164.03	0.672	1027.02	228.44
13	90	8	303.75	931.50	218.70	0.817	1254.21	278.98
14	90	10	324.00	1171.97	273.38	0.956	1470.19	327.02
15	90	12	354.38	1437.75	328.05	1.089	1677.65	373.17
16	120	4	540.00	981.00	194.40	0.521	1141.32	233.53
17	120	6	630.00	1341.00	291.60	0.672	1491.50	305.19
18	120	8	684.00	1656.00	388.80	0.817	1818.62	372.12
19	120	10	720.00	2083.00	486.00	0.956	2129.61	435.76
20	120	12	810.00	2556.00	583.20	1.089	2428.32	496.88
21	200	4	3000.00	2725.00	540.00	0.521	2263.42	380.34
22	200	6	3500.00	3725.00	810.00	0.672	2943.30	494.58
23	200	8	4000.00	4600.00	1080.00	0.817	3578.44	601.31
24	200	10	4500.00	5787.50	1350.00	0.956	4182.24	702.77
25	200	12	5000.00	7100.00	1620.00	1.089	4762.19	800.22

The load components (D_1, D_2, D_w, L and I) for shear are presented in **Error! Reference source not found.**, **Error! Reference source not found.**,**Error! Reference source not found.Error! Reference source not found.** for the prestressed concrete, reinforced concrete T-beams and steel (composite and non-composite) girder bridges respectively.

Table A-5. Load Components for Shear Design of Prestressed AASHTO Girder Bridges

# Bridge	Parameters of bridge, ft		Dead load, kip-ft			Live load HL 93, kip-ft		
	L	S	D_1	D_2	D_3	GDF_{HL-93}	LL	I
1	30	4	5.73	8.17	1.62	0.473	30.84	8.53
2	30	6	5.73	11.17	2.43	0.625	39.80	11.00
3	30	8	5.73	13.80	3.24	0.767	48.38	13.38
4	30	10	5.73	17.36	4.05	0.903	56.61	15.65
5	30	12	5.73	21.30	4.86	1.033	64.46	17.82
6	60	4	17.47	16.35	3.24	0.421	41.68	10.45
7	60	6	17.47	22.35	4.86	0.554	53.78	13.49
8	60	8	17.47	27.60	6.48	0.678	65.38	16.40
9	60	10	17.47	34.73	8.10	0.796	76.49	19.18
10	60	12	17.47	42.60	9.72	0.909	87.11	21.85
11	90	4	36.98	24.52	4.86	0.394	48.61	11.09
12	90	6	36.98	33.52	7.29	0.517	62.72	14.31
13	90	8	36.98	41.40	9.72	0.631	76.25	17.40
14	90	10	36.98	52.09	12.15	0.740	89.21	20.35
15	90	12	36.98	63.90	14.58	0.844	101.59	23.18
16	120	4	63.30	32.70	6.48	0.376	54.60	11.42
17	120	6	63.30	44.70	9.72	0.492	70.45	14.73
18	120	8	63.30	55.20	12.96	0.600	85.65	17.91
19	120	10	63.30	69.43	16.20	0.702	100.21	20.95
20	120	12	63.30	85.20	19.44	0.801	114.12	23.86
21	200	4	113.00	54.50	10.80	0.347	69.08	11.79
22	200	6	113.00	74.50	16.20	0.451	89.14	15.22
23	200	8	113.00	92.00	21.60	0.549	108.37	18.50
24	200	10	113.00	115.75	27.00	0.641	126.79	21.65
25	200	12	113.00	142.00	32.40	0.730	144.39	24.65

Table A-6. Load Components for Shear Design of Reinforced Concrete T-girder Bridges

# Bridge	Parameters of bridge, ft		Dead load, kip-ft			Live load HL 93, kip-ft		
	L	S	D_1	D_2	D_3	$GDF_{HL\text{-}93}$	LL	I
1	30	4	0.00	14.27	1.62	0.473	30.84	8.53
2	30	6	0.00	17.20	2.43	0.625	39.80	11.00
3	30	8	0.00	20.00	3.24	0.767	48.38	13.38
4	30	10	0.00	23.20	4.05	0.903	56.61	15.65
5	30	12	0.00	31.47	4.86	1.033	64.46	17.82
6	60	4	0.00	30.67	3.24	0.421	41.68	10.45
7	60	6	0.00	42.00	4.86	0.554	53.78	13.49
8	60	8	0.00	48.00	6.48	0.678	65.38	16.40
9	60	10	0.00	58.53	8.10	0.796	76.49	19.18
10	60	12	0.00	69.00	9.72	0.909	87.11	21.85
11	90	4	0.00	63.11	4.86	0.394	48.61	11.09
12	90	6	0.00	76.44	7.29	0.517	62.72	14.31
13	90	8	0.00	85.47	9.72	0.631	76.25	17.40
14	90	10	0.00	101.24	12.15	0.740	89.21	20.35
15	90	12	0.00	119.24	14.58	0.844	101.59	23.18
16	120	4	0.00	93.00	6.48	0.376	54.60	11.42
17	120	6	0.00	111.00	9.72	0.492	70.45	14.73
18	120	8	0.00	129.00	12.96	0.600	85.65	17.91
19	120	10	0.00	153.00	16.20	0.702	100.21	20.95

Table A-7. Load Components for Shear Design of Composite Steel Girder Bridges

# Bridge	Parameters of bridge, ft		Dead load, kip-ft			Live load HL 93, kip-ft		
	L	*S*	D_1	D_2	D_3	$GDF_{HL\text{-}93}$	*LL*	*I*
1	30	4	0.93	8.17	1.62	0.473	30.84	8.53
2	30	6	0.93	11.17	2.43	0.625	39.80	11.00
3	30	8	1.07	13.80	3.24	0.767	48.38	13.38
4	30	10	1.20	17.36	4.05	0.903	56.61	15.65
5	30	12	1.33	21.30	4.86	1.033	64.46	17.82
6	60	4	2.60	16.35	3.24	0.421	41.68	10.45
7	60	6	3.20	22.35	4.86	0.554	53.78	13.49
8	60	8	4.67	27.60	6.48	0.678	65.38	16.40
9	60	10	5.60	34.73	8.10	0.796	76.49	19.18
10	60	12	6.87	42.60	9.72	0.909	87.11	21.85
11	90	4	11.47	24.52	4.86	0.394	48.61	11.09
12	90	6	11.91	33.52	7.29	0.517	62.72	14.31
13	90	8	12.71	41.40	9.72	0.631	76.25	17.40
14	90	10	13.47	52.09	12.15	0.740	89.21	20.35
15	90	12	15.07	63.90	14.58	0.844	101.59	23.18
16	120	4	16.73	32.70	6.48	0.376	54.60	11.42
17	120	6	20.23	44.70	9.72	0.492	70.45	14.73
18	120	8	21.67	55.20	12.96	0.600	85.65	17.91
19	120	10	22.70	69.43	16.20	0.702	100.21	20.95
20	120	12	25.77	85.20	19.44	0.801	114.12	23.86
21	200	4	55.60	54.50	10.80	0.347	69.08	11.79
22	200	6	66.06	74.50	16.20	0.451	89.14	15.22
23	200	8	75.80	92.00	21.60	0.549	108.37	18.50
24	200	10	83.80	115.75	27.00	0.641	126.79	21.65
25	200	12	97.50	142.00	32.40	0.730	144.39	24.65

Table A-8. Load Components for Shear Design of Non-composite Girder Bridges

# Bridge	Parameters of bridge, ft		Dead load, kip-ft			Live load HL 93, kip-ft		
	L	*S*	D_1	D_2	D_3	$GDF_{HL\text{-}93}$	*LL*	*I*
1	30	4	1.05	8.17	1.62	0.473	30.84	8.53
2	30	6	1.13	11.17	2.43	0.625	39.80	11.00
3	30	8	1.20	13.80	3.24	0.767	48.38	13.38
4	30	10	1.35	17.36	4.05	0.903	56.61	15.65
5	30	12	1.50	21.30	4.86	1.033	64.46	17.82
6	60	4	2.70	16.35	3.24	0.421	41.68	10.45
7	60	6	3.60	22.35	4.86	0.554	53.78	13.49
8	60	8	5.10	27.60	6.48	0.678	65.38	16.40
9	60	10	6.30	34.73	8.10	0.796	76.49	19.18
10	60	12	7.50	42.60	9.72	0.909	87.11	21.85
11	90	4	11.70	24.52	4.86	0.394	48.61	11.09
12	90	6	12.60	33.52	7.29	0.517	62.72	14.31
13	90	8	13.50	41.40	9.72	0.631	76.25	17.40
14	90	10	14.40	52.09	12.15	0.740	89.21	20.35
15	90	12	15.75	63.90	14.58	0.844	101.59	23.18
16	120	4	18.00	32.70	6.48	0.376	54.60	11.42
17	120	6	21.00	44.70	9.72	0.492	70.45	14.73
18	120	8	22.80	55.20	12.96	0.600	85.65	17.91
19	120	10	24.00	69.43	16.20	0.702	100.21	20.95
20	120	12	27.00	85.20	19.44	0.801	114.12	23.86
21	200	4	60.00	54.50	10.80	0.347	69.08	11.79
22	200	6	70.00	74.50	16.20	0.451	89.14	15.22
23	200	8	80.00	92.00	21.60	0.549	108.37	18.50
24	200	10	90.00	115.75	27.00	0.641	126.79	21.65
25	200	12	100.00	142.00	32.40	0.730	144.39	24.65

Appendix B

The new design tandem for short spans was introduced in Chapter 0. The corresponding the load components (D_1, D_2, D_w, L and I) for flexure presented in **Error! Reference source not found.**, **Error! Reference source not found.**, **Error! Reference source not found.** and **Error! Reference source not found.** for the prestressed concrete, reinforced concrete T-beams and steel (composite and non-composite) girder bridges respectively.

Table B-1. Load Components for Flexure Design of Prestressed AASHTO Girder Bridges (New Design Tandem)

# Bridge	Parameters of bridge, ft		Dead load, kip-ft			Live load HL 93, kip-ft		
	L	S	D_1	D_2	D_3	$GDF_{HL\text{-}93}$	LL	I
1	30	4	43.00	61.31	12.15	0.473	219.35	61.15
2	30	6	43.00	83.81	18.23	0.625	290.06	80.87
3	30	8	43.00	103.50	24.30	0.767	356.12	99.28
4	30	10	43.00	130.22	30.38	0.903	418.91	116.79
5	30	12	43.00	159.75	36.45	1.033	479.23	133.61
6	60	4	262.00	245.25	48.60	0.421	475.59	116.91
7	60	6	262.00	335.25	72.90	0.554	625.37	153.73
8	60	8	262.00	414.00	97.20	0.678	765.29	188.12
9	60	10	262.00	520.88	121.50	0.796	898.31	220.82
10	60	12	262.00	639.00	145.80	0.909	1026.08	252.23
11	90	4	832.00	551.81	109.35	0.394	783.82	174.35
12	90	6	832.00	754.31	164.03	0.517	1027.02	228.44
13	90	8	832.00	931.50	218.70	0.631	1254.21	278.98
14	90	10	832.00	1171.97	273.38	0.740	1470.19	327.02
15	90	12	832.00	1437.75	328.05	0.844	1677.65	373.17
16	120	4	1899.00	981.00	194.40	0.376	1141.32	233.53
17	120	6	1899.00	1341.00	291.60	0.492	1491.50	305.19
18	120	8	1899.00	1656.00	388.80	0.600	1818.62	372.12
19	120	10	1899.00	2083.00	486.00	0.702	2129.61	435.76
20	120	12	1899.00	2556.00	583.20	0.801	2428.32	496.88
21	200	4	5650.00	2725.00	540.00	0.347	2263.42	380.34
22	200	6	5650.00	3725.00	810.00	0.451	2943.30	494.58
23	200	8	5650.00	4600.00	1080.00	0.549	3578.44	601.31
24	200	10	5650.00	5787.50	1350.00	0.641	4182.24	702.77

25	200	12	5650.00	7100.00	1620.00	0.730	4762.19	800.22

Table B-2. Load Components for Flexure Design of Reinforced T-girder Bridges (New Design Tandem)

# Bridge	Parameters of bridge, ft		Dead load, kip-ft			Live load HL 93, kip-ft		
	L	*S*	D_1	D_2	D_3	$GDF_{HL\text{-}93}$	*LL*	*I*
1	30	4	0.00	107.00	12.15	0.521	219.35	61.15
2	30	6	0.00	129.00	18.23	0.672	290.06	80.87
3	30	8	0.00	150.00	24.30	0.817	356.12	99.28
4	30	10	0.00	174.00	30.38	0.956	418.91	116.79
5	30	12	0.00	236.00	36.45	1.089	479.23	133.61
6	60	4	0.00	460.00	48.60	0.521	475.59	116.91
7	60	6	0.00	630.00	72.90	0.672	625.37	153.73
8	60	8	0.00	720.00	97.20	0.817	765.29	188.12
9	60	10	0.00	878.00	121.50	0.956	898.31	220.82
10	60	12	0.00	1035.00	145.80	1.089	1026.08	252.23
11	90	4	0.00	1420.00	109.35	0.521	783.82	174.35
12	90	6	0.00	1720.00	164.03	0.672	1027.02	228.44
13	90	8	0.00	1923.00	218.70	0.817	1254.21	278.98
14	90	10	0.00	2278.00	273.38	0.956	1470.19	327.02
15	90	12	0.00	2683.00	328.05	1.089	1677.65	373.17
16	120	4	0.00	2790.00	194.40	0.521	1141.32	233.53
17	120	6	0.00	3330.00	291.60	0.672	1491.50	305.19
18	120	8	0.00	3870.00	388.80	0.817	1818.62	372.12
19	120	10	0.00	4590.00	486.00	0.956	2129.61	435.76
20	120	12	0.00	5400.00	583.20	1.089	2428.32	496.88

Table B-3. Load Components for Flexure Design of Composite Steel Girders (New Design Tandem)

# Bridge	Parameters of bridge, ft		Dead load, kip-ft			Live load HL 93, kip-ft		
	L	*S*	D_1	D_2	D_3	$GDF_{HL\text{-}93}$	*LL*	*I*
1	30	4	7.00	61.31	12.15	0.521	219.35	61.15
2	30	6	7.00	83.81	18.23	0.672	290.06	80.87
3	30	8	8.00	103.50	24.30	0.817	356.12	99.28
4	30	10	9.00	130.22	30.38	0.956	418.91	116.79
5	30	12	10.00	159.75	36.45	1.089	479.23	133.61
6	60	4	39.00	245.25	48.60	0.521	475.59	116.91
7	60	6	48.00	335.25	72.90	0.672	625.37	153.73
8	60	8	70.00	414.00	97.20	0.817	765.29	188.12
9	60	10	84.00	520.88	121.50	0.956	898.31	220.82
10	60	12	103.00	639.00	145.80	1.089	1026.08	252.23
11	90	4	258.00	551.81	109.35	0.521	783.82	174.35
12	90	6	268.00	754.31	164.03	0.672	1027.02	228.44
13	90	8	286.00	931.50	218.70	0.817	1254.21	278.98
14	90	10	303.00	1171.97	273.38	0.956	1470.19	327.02
15	90	12	339.00	1437.75	328.05	1.089	1677.65	373.17
16	120	4	502.00	981.00	194.40	0.521	1141.32	233.53
17	120	6	607.00	1341.00	291.60	0.672	1491.50	305.19
18	120	8	650.00	1656.00	388.80	0.817	1818.62	372.12
19	120	10	681.00	2083.00	486.00	0.956	2129.61	435.76
20	120	12	773.00	2556.00	583.20	1.089	2428.32	496.88
21	200	4	2780.00	2725.00	540.00	0.521	2263.42	380.34
22	200	6	3303.00	3725.00	810.00	0.672	2943.30	494.58
23	200	8	3790.00	4600.00	1080.00	0.817	3578.44	601.31
24	200	10	4190.00	5787.50	1350.00	0.956	4182.24	702.77
25	200	12	4875.00	7100.00	1620.00	1.089	4762.19	800.22

Table B-4. Load Components for Flexure Design of Non-composite Steel Girders (New Design Tandem)

# Bridge	Parameters of bridge, ft		Dead load, kip-ft			Live load HL 93, kip-ft		
	L	*S*	D_1	D_2	D_3	$GDF_{HL\text{-}93}$	*LL*	*I*
1	30	4	7.88	61.31	12.15	0.521	219.35	61.15
2	30	6	8.44	83.81	18.23	0.672	290.06	80.87
3	30	8	9.00	103.50	24.30	0.817	356.12	99.28
4	30	10	10.13	130.22	30.38	0.956	418.91	116.79
5	30	12	11.25	159.75	36.45	1.089	479.23	133.61
6	60	4	40.50	245.25	48.60	0.521	475.59	116.91
7	60	6	54.00	335.25	72.90	0.672	625.37	153.73
8	60	8	76.50	414.00	97.20	0.817	765.29	188.12
9	60	10	94.50	520.88	121.50	0.956	898.31	220.82
10	60	12	112.50	639.00	145.80	1.089	1026.08	252.23
11	90	4	263.25	551.81	109.35	0.521	783.82	174.35
12	90	6	283.50	754.31	164.03	0.672	1027.02	228.44
13	90	8	303.75	931.50	218.70	0.817	1254.21	278.98
14	90	10	324.00	1171.97	273.38	0.956	1470.19	327.02
15	90	12	354.38	1437.75	328.05	1.089	1677.65	373.17
16	120	4	540.00	981.00	194.40	0.521	1141.32	233.53
17	120	6	630.00	1341.00	291.60	0.672	1491.50	305.19
18	120	8	684.00	1656.00	388.80	0.817	1818.62	372.12
19	120	10	720.00	2083.00	486.00	0.956	2129.61	435.76
20	120	12	810.00	2556.00	583.20	1.089	2428.32	496.88
21	200	4	3000.00	2725.00	540.00	0.521	2263.42	380.34
22	200	6	3500.00	3725.00	810.00	0.672	2943.30	494.58
23	200	8	4000.00	4600.00	1080.00	0.817	3578.44	601.31
24	200	10	4500.00	5787.50	1350.00	0.956	4182.24	702.77
25	200	12	5000.00	7100.00	1620.00	1.089	4762.19	800.22